technische universität
dortmund

Probing Flavor and CP in Decays of Beauty and Charm

Dissertation zu Erlangung des Grades Dr. rer. nat.

im Fach Physik

eingereicht an der Fakultät Physik der

Technischen Universität Dortmund

vorgelegt von
Stefan Schacht
aus Oer-Erkenschwick

Dortmund, Juni 2013

1. Gutachter: Prof. Dr. G. Hiller
2. Gutachter: Prof. Dr. H. Päs
Datum der mündlichen Prüfung: 10. Juli 2013
Vorsitzender des Promotionsausschusses: Prof. Dr. T. Weis

Parts of the results presented in this thesis were previously published or are planned to be published in the following articles and proceedings:

- G. Hiller, M. Jung, and S. Schacht, *Tracing QCD Factorization in $D \to P_8 P_8$*, in preparation.
- C. Hambrock, G. Hiller, S. Schacht and R. Zwicky, *$B \to K^*$ Form Factors from Flavor Data to QCD and Back*, DO-TH 13/13, in preparation.
- G. Hiller, M. Jung, and S. Schacht, *SU(3)-Flavor Anatomy of Non-Leptonic Charm Decays*, *Phys.Rev.* **D87** (2013) 014024, [arXiv:1211.3734].
- S. Schacht, *Squark Flavor Implications from $\bar{B} \to \bar{K}^{(*)} l^+ l^-$*, in *Proceedings of the 2nd Workshop on Flavor Symmetries and Consequences in Accelerators and Cosmology (FLASY12)* (I. M. Varzielas, C. Hambrock, G. Hiller, M. Jung, P. Leser, et al., eds.), 2012. arXiv:1210.6239.
- A. Behring, C. Gross, G. Hiller, and S. Schacht, *Squark Flavor Implications from $\bar{B} \to \bar{K}^{(*)} l^+ l^-$*, *JHEP* **1208** (2012) 152, [arXiv:1205.1500].

Abstract

In order to probe for new physics beyond the Standard Model of particle physics, we explore decays of beauty and charm mesons. In the b sector we find ourselves in the realm of precision physics so that we can improve significantly the bounds on supersymmetric flavor violation from new theoretical and experimental progress in $\bar{B} \to \bar{K}^{(*)} l^+ l^-$. From these bounds we derive several phenomenological implications, as bounds on Radiative Flavor Violation models that are partly even sharper than the ones from Kaon physics. In order to improve the bounds on new physics models from $\bar{B} \to \bar{K}^{(*)} l^+ l^-$ even more in the future, we extract subsequently $\bar{B} \to \bar{K}^*$ form factor ratios from data at high invariant lepton pair masses. These are the current bottleneck for the advancement in precision.

In the charm sector unexpectedly large CP violation was measured recently. Currently, the experimental situation is unsettled. We work here on the main problem that one cannot reliably calculate the hadronic part from first principles, *i.e.*, cannot exclude possible enhancements from this source. We perform for the first time a comprehensive $\mathrm{SU}(3)_F$ analysis of $D \to P_8 P_8$ decays including linear breaking in full generality. We find the $\mathrm{SU}(3)_F$ expansion to be indeed working. Furthermore, the fit shows a large triplet matrix element enhancement that cannot be excluded for sure without having a dynamical theory at hand. We show as a proof of principle that with significantly improved data we could disentangle the triplet model including the Standard Model from other new physics models. Using reasonable theoretical input from QCD factorization we can eliminate some of the many degrees of freedom of the pure $\mathrm{SU}(3)_F$ analysis. This can sharpen partially the correlation between D-decay CP asymmetries and branching ratios.

Zusammenfassung

Auf der Suche nach neuer Physik jenseits des Standardmodells erforschen wir Zerfälle von Beauty- und Charm-Mesonen. Im b-System befinden wir uns um Bereich der Präzisionsphysik, so dass wir die Schranken an supersymmetrische Flavorverletzung durch theoretischen als auch experimentellen Fortschritt bzgl. des Zerfalls $\bar{B} \to \bar{K}^{(*)} l^+ l^-$ signifikant verbessern können. Aus diesen Schranken leiten wir mehrere phänomenologische Implikationen ab, z.B. an Modelle mit radiativer Flavorverletzung, die teilweise sogar stärker sind als diejenigen aus der Kaon-Physik. Um die Schranken an Modelle neuer Physik in der Zukunft noch weiter zu verbessern, extrahieren wir anschließend $\bar{B} \to \bar{K}^*$-Formfaktorenverhältnisse aus Daten bei hohen invarianten Massen des Lepton-Paars. Diese sind momentan der Flaschenhals für Fortschritte in der Präzision.

Im Charm-System wurde unlängst unerwartet hohe CP-Verletzung gemessen. Gegenwärtig ist die experimentelle Situation nicht endgültig geklärt. Wir arbeiten hier an dem Hauptproblem, dass der hadronische Part nicht verlässlich aus ersten Prinzipien berechnet werden kann, sodass mögliche Erhöhungen von dieser Quelle nicht ausgeschlossen werden können. Wir führen das erste Mal eine vollständige $\mathrm{SU}(3)_F$-Analyse von $D \to P_8 P_8$-Zerfällen durch, die lineare $\mathrm{SU}(3)_F$-Brechung in voller Allgemeinheit einbezieht. Wir erhalten das Ergebnis, dass die $\mathrm{SU}(3)_F$-Entwicklung in der Tat funktioniert. Weiterhin zeigt der Fit eine große Erhöhung der Triplett-Matrixelemente, die nicht mit Sicherheit ausgeschlossen werden kann, ohne eine dynamische Theorie zu besitzen. Wir zeigen, dass grundsätzlich mit signifikant verbesserten Daten das Triplett-Modell inklusive dem Standardmodell von anderen Modellen neuer Physik unterschieden werden kann. Unter Verwendung von annehmbarem theoretischen Input aus QCD-Faktorisierung können wir einige der vielen Freiheitsgrade der reinen $\mathrm{SU}(3)_F$-Analyse eliminieren. Dies kann die Korrelation von CP-Asymmetrien und Verzweigungsverhältnissen von D-Zerfällen teilweise verschärfen.

“Three quarks for Muster Mark!”
(James Joyce, Finnegans Wake)

Contents

1. Introduction

From the perspective of theoretical particle physics, in contrast to experimental findings, in 2013 there is much pointing towards physics beyond what we call the Standard Model of the strong and electroweak interactions (SM). The most exciting news in 2012 was the detection of a new scalar boson [1, 2] which is seemingly the last important ingredient of the SM, predicted back in the 1960s: the Higgs boson [3–8]. In the Higgs mechanism the gauge symmetry is broken locally, in contrast to the breaking of global symmetries that has been studied previously [9–11]. The Higgs mass is measured consistently at ATLAS as $m_h = 125.5 \pm 0.2^{+0.5}_{-0.6}$ GeV [12] and at CMS as $125.8 \pm 0.4 \pm 0.4$ GeV [13]. The Higgs mass is consistent at 1.3σ with electroweak precision fits [14, 15], which is a great accomplishment of the SM at the loop level. One of the big programs of the Large Hadron Collider (LHC), the task to investigate the electroweak symmetry breaking, is thus in the beginning of its success.
On the other hand, the SM has no explanation for the vast separation of the scales of electroweak and gravitational physics. The same holds for the phenomena of the baryon asymmetry, dark matter and dark energy: We have no knowledge of about 95% of the energy density of the universe, although also in cosmology we have reached the precision era by the recent results from the Planck satellite [16].

A key puzzle in the SM is furthermore given by the hierarchies in the flavor sector. It is a deep gap in our knowledge that we do not have knowledge about the mechanism that determines the masses and mixing matrices of both quarks and leptons. Intrinsically connected to this issue is our ignorance of the mechanism which determines the common area of the unitarity triangles, *i.e.*, the size of CP violation. Although we know that in the SM CP violation is linked to three generations of matter being present [17] we do not know where these replicas come from. In the SM we write down nothing more than a mere parametrization for the whole flavor sector, with numbers extracted from experiment instead of being explained.
Consequently, every ansatz for an explanation of flavor is going beyond the SM and leads to the search for new physics (NP). In this thesis we concentrate on the quark sector of flavor physics. Experimentally, there are two complementary strategies: The direct production of new particles at the intensity frontier and the precision measurements at "low" energies where one carefully inspects the quantum corrections of rare decays. However, at the LHC, being a hadron machine, the data analysis also of direct searches is so involved that partly also this method seems quite "indirect" – of course in a different sense.

Historically, the way of exploring flavor physics and the violation of discrete symmetries led across many milestones. The quantum mechanical mixing of neutral mesons is now

observed for K mesons (first theoretical description by Gell-Mann and Pais 1955 [18], first observation of K_L states by Lande et al. 1956 [19]), B_d mesons (ARGUS 1987 [20]), B_s mesons (CDF 2006 [21]) and D mesons (BaBar [22–25], Belle [26], CDF [27], 2007-2009). The first 5σ observation of D mixing in a single experiment was only in 2012 by LHCb [28]. A great success of flavor physics was the prediction of the mass of the charm quark [29–32] which was possible due to its important contributions in quantum corrections, *i.e.*, loop diagrams.
A similar track record goes for the investigation of discrete symmetries: In 1957, parity violation has been observed in the β decay of polarized ^{60}Co [33, 34]. The violation of CP was for the first time measured 1964 in Kaon decays [35]. A mixture of T and CP violation has been observed 1998 in Kaon decays [36]. Only very recently, again in 2012, it was observed for the first time pure T violation in B decays [37] which is expected from the theory side due to the CPT theorem [38–41]. Right after the first observation of CP violation it was realized that the breaking of this combination of discrete symmetries is a necessary condition in order to explain the baryon-antibaryon asymmetry of the universe [42]. Still, the SM CP violation is far too small in order to explain the observed asymmetry, for a discussion and further references see the review given in Ref. [43]. It took some more years after the first observation of CP violation in order to realize in 1973 that three generations of matter are needed in order to explain its occurrence [17]—before even the beauty quark was observed. For that Kobayashi and Maskawa got one half of the 2008 noble prize. The beauty quark was observed in 1977 [44], the top quark only in 1995 [45, 46].

In conflict with theoretical expectation, in the beginning of 2013 NP keeps hiding away. The SM is still working better than anyone would have expected when it was invented more than 30 years ago. Most recently this has been exemplified again by the evidence for the very rare decay $B_s \to \mu^+\mu^-$ with a branching ratio near its SM value at the 10^{-9} level [47]. Additionally, in most simple and minimal scenarios of Supersymmetry (SUSY), an extension of the Poincaré symmetry that links bosonic and fermionic degrees of freedom, the mass spectrum of SUSY particles is pushed up by direct searches [48–53].

Nevertheless, there are several unresolved tensions of the SM with experiment, however below a statistical significance of 5σ. Just to name a few: the $t\bar{t}$ forward backward asymmetry at Tevatron [54], the different results for V_{ub} from inclusive/exclusive modes, see *e.g.* [55], the $B \to \pi K$ puzzle (for a brief status report see [56]), the enhancement in ratios of $b \to c\tau^-\bar{\nu}_\tau$ branching ratios [57–59] and the evidence for large CP violation ΔA_{CP} in charm decays that was found recently [60–63]. Statistically consistent with the precedent ones, newest results at LHCb presented at Moriond 2013 indicate now a smaller value for ΔA_{CP} with a small tension of 2.2σ between somewhat differing results from two distinct channels [64, 65]. The current experimental situation in charm CP violation remains to be settled and we are awaiting future experimental results with eager expectation. Furthermore, at ATLAS there is measured an enhancement of the branching ratio $\mathcal{B}(H \to \gamma\gamma)$ at $\sim 2.3\sigma$, including the full 2012 data set at 8 TeV [66]. Explanation for such enhancements can for example be provided in extensions of minimal forms of SUSY [67]. However, at CMS no enhancement of $\mathcal{B}(H \to \gamma\gamma)$ is visible [68].

A general problem in the search for NP in flavor physics is the control of the "old" physics, namely Quantum Chromomagnetics (QCD) at long distances.
It is instructive to compare here with another part of precision quantum correction physics, besides the already mentioned successful prediction of the Higgs mass. In the part of the SM where the gauge couplings are small, we can apply perturbative expansions and test the SM with never-seen precision. Quantum Electrodynamics (QED) is consequently one of the best tested theories mankind has invented so far. This is exemplified by the incredible precision of both theoretical and experimental results for the anomalous magnetic moment of the electron a_e [69]. The deviation of the QED four loop calculation from the experimental value has an absolute value of only $(10.5 \pm 8.1) \cdot 10^{-13}$ [70]. However, as can be seen from this number, the progress in precision is so far, that this corresponds to a deviation of 1.3σ. The latter can thus be used again as a probe of NP similar to the muon anomalous magnetic moment that shows a long-known discrepancy of $\sim 3.5\sigma$ [70–77].

Now, in meson decays on the other hand, we have a completely different starting point. Here, at the heart of the calculation appears the strong coupling constant of QCD, being evaluated at energies not much above Λ_{QCD}, where Λ_{QCD} is the scale of QCD where the strong interaction becomes nonperturbative. In charm meson decays the situation is especially complicated because m_c is close to Λ_{QCD}. The known methods from b physics like the systematic treatment of the factorization of long and short distance physics, so-called QCD factorization (QCDF) and likewise the heavy quark expansion cannot reliably be applied for charm physics—or only to a certain limited extent, that we analyze further in this work.

The plan of this thesis is as follows: In Ch. 2 we give an introduction to the SM Lagrangian, flavor physics and CP violation as well as to the minimal supersymmetric extension of the SM. We study how to parametrize flavor and look at minimal models of flavor violation. Furthermore, we discuss the approximate $\text{SU}(3)_F$ symmetry of QCD that will be used later on.

In Ch. 3 we analyze the implications of semileptonic decays $\bar{B} \to \bar{K}^{(*)} l^+ l^-$ for SUSY flavor. From the strong bounds that we extract from the data we derive various phenomenological consequences for b and top physics as well as for SUSY model building. In order to improve the bounds from $\bar{B} \to \bar{K}^{(*)} l^+ l^-$ on NP models even further, progress on $\bar{B} \to \bar{K}^{(*)}$ form factors is mandatory. Therefore, in Ch. 4 we fit form factor ratios from data at high invariant lepton masses q^2. We make use here of the cancellation of short distance physics in certain observables in this kinematic region [78]. Additionally, we study the constraints that follow from the data in connection with theoretical input from Light Cone Sum Rules (LCSRs) and perturbative Helicity Conservation (HC) at low q^2.

In Ch. 5 we continue to extract hadronic physics from data, going from the down to the up sector of quark flavor physics. We use the approximate $\text{SU}(3)_F$ symmetry of QCD in order to describe nonleptonic charm decays. We do so by including for the first time the linear breaking of $\text{SU}(3)_F$ in a comprehensive way without any theoretical bias for a global fit of $D \to P_8 P_8$ observables. We ask for the consequences of the recent measurements of enhanced CP violation. We furthermore analyze if NP models can be disentangled

from the SM now and in the future and account briefly for the very new results that were presented by LHCb at Moriond 2013.

In Ch. 6 we search for traces of QCDF that could be left in $D \to P_8 P_8$ decays. We find that certain elements of QCDF can be incorporated into the $SU(3)_F$ approach in order to reduce the number of unknown hadronic matrix elements. Including this information in the $SU(3)_F$ fits can considerably sharpen the patterns for some observables.

In Ch. 7 we summarize prospects for future measurements and experiments that are relevant to our predictions.
After concluding, in Appendix A we demonstrate the universality of the $SU(3)_F$ approach. For various decays, we give a tool box of $SU(3)_F$ decompositions including linear breaking. These decompositions will prove useful for further phenomenological analyses in the future.

2. Flavor and CP Probes of Physics Beyond the Standard Model

2.1. The Standard Model of Particle Physics

The Standard Model Lagrangian The Standard Model (SM) of particle physics is a renormalizable anomaly-free quantum field theory with gauge group $\mathrm{SU}(3)_C \times \mathrm{SU}(2)_L \times \mathrm{U}(1)_Y$. Its $\mathrm{SU}(2)_L \times \mathrm{U}(1)_Y$ part is spontaneously broken to $\mathrm{U}(1)_{\mathrm{QED}}$, *i.e.*, the SM has a non-trivial vacuum that does not respect the symmetry of the Lagrangian. The SM describes our present commonly accepted knowledge of the fundamental structures of nature. The electroweak part of the SM that is governed by the gauge groups $\mathrm{SU}(2)_L \times \mathrm{U}(1)_Y$ is called the "Glashow-Salam-Weinberg" model, after its noble prize (1979) winning architects [79–81]. The milestone of the exploration of the electroweak theory at the quantum level has been achieved by t'Hooft and Veltman [82] (noble prize 1999). In the QCD part of the SM the most important steps were the realization of the phenomena of confinement and asymptotic freedom. The greatest achievements were accomplished here by Gross, Politzer and Wilczeck [83, 84] (noble prize 2004).

Adapting the notation and conventions of [85–88] the SM Lagrangian reads as follows. It is decomposed as

$$\mathcal{L} = \mathcal{L}_{\mathrm{YM}}^{\mathrm{SU}(3)_C} + \mathcal{L}_{\mathrm{YM}}^{\mathrm{SU}(2)_L \otimes \mathrm{U}_Y(1)} + \mathcal{L}_{\mathrm{H}} + \mathcal{L}_{\mathrm{F}}\,, \tag{2.1}$$

with the Yang-Mills parts $\mathcal{L}_{\mathrm{YM}}^{\mathrm{SU}(3)_C}$ and $\mathcal{L}_{\mathrm{YM}}^{\mathrm{SU}(2)_L \otimes \mathrm{U}_Y(1)}$, the Higgs part $\mathcal{L}_{\mathrm{H}}$ and the Fermion part $\mathcal{L}_{\mathrm{F}}$. The Yang-Mills parts are given as

$$\mathcal{L}_{\mathrm{YM}}^{\mathrm{SU}(3)_C} = -\frac{1}{4}\left(\partial_\mu G_\mu^A - \partial_\nu G_\mu^A - g_s f^{ABC} G_\mu^B G_\nu^C\right)^2, \tag{2.2}$$

$$\mathcal{L}_{\mathrm{YM}}^{\mathrm{SU}(2)_L \otimes \mathrm{U}_Y(1)} = -\frac{1}{4}\left(\partial_\mu W_\nu^a - \partial_\nu W_\mu^a + g_2 \varepsilon^{abc} W_\mu^b W_\nu^c\right)^2 - \frac{1}{4}\left(\partial_\mu B_\nu - \partial_\nu B_\mu\right)^2. \tag{2.3}$$

Here, G_μ^A, $A, B, C = 1, 2, \ldots, 8$ are the octet gluon fields, g_s is the strong coupling and f^{ABC} are the structure constants of SU(3). Likewise, W_μ^a with $a, b, c = 1, 2, 3$ and B_μ are the fields of the electroweak interaction. For a concise notation one also uses the field strength tensor, which is for example in the case of QCD given as

$$G_{\mu\nu}^A = \partial_\mu G_\mu^A - \partial_\nu G_\mu^A - g_s f^{ABC} G_\mu^B G_\nu^C. \tag{2.4}$$

For brevity, we omit here the gauge-fixing and ghost parts. Furthermore, we omit the part of the Lagrangian that would induce CP violation in QCD through the non-trivial topology of the vacuum. This is further discussed briefly at the end of this section. The triplet fields W_μ^a are the gauge fields of $\mathrm{SU}(2)_L$, the singlet B_μ corresponds to the hypercharge $U(1)_Y$. The Higgs part of the Lagrangian is given as

$$\mathcal{L}_\mathrm{H} = \left(D_\mu \Phi\right)^\dagger \left(D^\mu \Phi\right) - V(\Phi), \qquad V(\Phi) = \frac{\lambda}{4}\left(\Phi^\dagger \Phi\right)^2 - \mu^2 \Phi^\dagger \Phi\,, \tag{2.5}$$

with a Higgs field $\Phi(x) = \left(\phi^+(x),\, \phi^0(x)\right)^\mathrm{T}$ that has a non-vanishing vacuum expectation value (vev)

$$|\langle \Phi \rangle| = \sqrt{\frac{2\mu^2}{\lambda}} = \frac{v}{\sqrt{2}}\,, \tag{2.6}$$

and the quantum numbers $\Phi(1,2)_{\frac{1}{2}}$. For a field ϕ in $\phi(n_{\mathrm{SU}(3)_C}, n_{\mathrm{SU}(2)_L})_{n_{U(1)_Y}}$ the numbers $n_{\mathrm{SU}(3)_C}$, $n_{\mathrm{SU}(2)_L}$ and $n_{U(1)_Y}$ indicate the dimension under the groups $\mathrm{SU}(3)_C$, $\mathrm{SU}(2)_L$ and the $U(1)_Y$ charge, respectively. Around its vev, the Higgs field exhibits excitations that can after $\mathrm{SU}(2)_L$ transformations without loss of generality be written as

$$\Phi = \frac{1}{\sqrt{2}}\left(0, v + H(x)\right)^\mathrm{T}\,, \tag{2.7}$$

where H is the physical Higgs particle. Note that the SM assumes ad hoc a minimal Higgs sector with only one doublet Φ.

The fermionic part of the Lagrangian $\mathcal{L}_\mathrm{F} = \mathcal{L}_\mathrm{int.} + \mathcal{L}_\mathrm{Yuk.}$ is divided into a part $\mathcal{L}_\mathrm{int.}$ that gives the interaction of the fermions with the gauge bosons and another part $\mathcal{L}_\mathrm{Yuk.}$ which consists of Yukawa terms and describes the couplings of the fermions to the Higgs boson. The first one reads

$$\mathcal{L}_\mathrm{int} = \bar{L}_L i \not{D} L_L + \bar{Q}_L i \not{D} Q_L + \bar{e}_R i \not{D} e_R + \bar{u}_R i \not{D} u_R + \bar{d}_R i \not{D} d_R\,, \tag{2.8}$$

where we used the notation $\psi_{R,L} = \frac{1 \pm \gamma_5}{2}\psi$. The covariant derivative is given by

$$D_\mu = \partial_\mu - i g_s G_\mu^A t^A - i g_2 T^a W_\mu^a + i g_1 \frac{Y_W}{2} B_\mu\,, \tag{2.9}$$

and it is understood that in the singlet terms $\bar{\psi}_R i \not{D} \psi_R$ the interaction term with $i g_2 T^a W_\mu^a$ is not there. After the rotation to the mass eigenstates of the gauge bosons the covariant derivative with physical $W^\pm$, Z and γ fields reads

$$D_\mu = \partial_\mu - i\frac{g_2}{\sqrt{2}}\left(\sigma^+ W_\mu^+ + \sigma^- W_\mu^-\right) - i\frac{g_2}{\cos\theta_W} Z_\mu (T^3 - \sin^2\theta_W Q) - ieA_\mu Q\,, \tag{2.10}$$

with the charge of the electron $e = g_1 g_2 / \sqrt{g_1^2 + g_2^2}$ and the Weinberg angle θ_W that changes the basis according to

$$\begin{pmatrix} Z^0 \\ A \end{pmatrix} = \begin{pmatrix} \cos\theta_w & -\sin\theta_w \\ \sin\theta_w & \cos\theta_w \end{pmatrix} \begin{pmatrix} W^3 \\ B \end{pmatrix}. \tag{2.11}$$

The linear combinations of Pauli matrices are given as $\sigma^{\pm} = \frac{1}{2}(\sigma_1 \pm i\sigma_2)$. In Eq. (2.8) one can read off the fermionic particle content of the SM. It is given as

$$Q_L(3,2)_{\frac{1}{6}} = (u_L, d_L)\,, \qquad U(3,1)_{\frac{2}{3}} = u_R\,, \qquad D(3,1)_{\frac{1}{3}} = d_R\,, \tag{2.12}$$

$$L_L(1,2)_{-\frac{1}{2}} = (\nu_L, e_L)\,, \qquad E(1,1)_1 = e_R. \tag{2.13}$$

As in this work we are mainly concerned with quark flavor we disregard the presence of right-handed neutrinos and a neutrino mass term in the particle content of the SM. Note also that the lepton sector does not interact directly with QCD. The non-vanishing mass of neutrinos is an experimental fact [89] which leaves however the nature of the mass term itself as an open question. We do not know if the neutrino has a Majorana and/or Dirac mass term. A natural explanation for the extreme smallness of the neutrino masses in comparison to the other elementary particles is provided by different variants of the seesaw mechanism of category I [90–94], II [94–99] or III [100].

In the SM, matter comes in three generations. All the so far specified terms of the Lagrangian, *i.e.*, $\mathcal{L}_{\mathrm{YM}}^{\mathrm{SU(3)}_C}$, $\mathcal{L}_{\mathrm{YM}}^{\mathrm{SU(2)}_C \otimes \mathrm{U}_Y(1)}$, $\mathcal{L}_{\mathrm{H}}$ and the $\mathcal{L}_{\mathrm{int}}$ part of $\mathcal{L}_{\mathrm{F}}$ are invariant under rotations in generation space:

$$G_F = U(3)^5 = U(3)_{Q_L} \otimes U(3)_U \otimes U(3)_D \otimes U(3)_{L_L} \otimes U(3)_E. \tag{2.14}$$

This symmetry is only broken by the Yukawa terms. These are given as

$$-\mathcal{L}_{\mathrm{Yuk.}} = \bar{L}_L Y_l l_R \Phi + \bar{Q}_L Y_u u_R \tilde{\Phi} + \bar{Q}_L Y_d d_R \Phi + \mathrm{h.c.} \tag{2.15}$$

Here, $\tilde{\Phi} = i\sigma_2 \Phi^*$ is the charge conjugated Higgs field and Y_i are the Yukawa matrices that have dimension 3×3 in generation space. In the case of n generations these would be promoted to $n \times n$ matrices and G_F would be a $U(n)^5$ symmetry. However, already the simplest extensions of the SM to four generations become more and more improbable [101].

When the Higgs particle gets its vev during spontaneous symmetry breaking Eq. (2.15) gives the mass terms for the fermions. This mechanism is necessary, as a mass term $m\bar{\psi}\psi$ would break the $\mathrm{SU(2)_L}$ gauge invariance (the right-handed fermions transform differently than the left-handed ones). Therefore, the SM needs and predicts at least one agent of electroweak symmetry breaking. And indeed recent spectacular results show the existence of a scalar boson that can be interpreted as the SM Higgs [1, 2]. However, there is no theoretical reason why there should be only one Higgs boson. Also, the found scalar

boson could be composite due to new strong forces beyond the SM, see recently [102, 103]. An important prediction of composite models is the alteration of the couplings of the Higgs particle to the SM fermions by higher dimensional operators [104]. The measurement of the Yukawa couplings is therefore of extraordinary importance.

The effective coupling measured in $gg \to H$ production [105] that probes the $H\bar{t}t$ vertex suggests $Y_t \sim O(1)$ [106] as expected in the SM. As is demonstrated in Ref. [106] for disentangling different flavor models it is especially useful to measure $\mathcal{B}(H \to \mu^+\mu^-)$ and $\mathcal{B}(H \to \tau^+\tau^-)$. The channel $H \to \tau^+\tau^-$ is found to exist at $\sim 2.9\sigma$ at CMS [107] and so far its couplings are measured to be consistent with the SM [107, 108].
Using the channel $H \to \gamma\gamma$, which is observed at 7.4σ [66], one can also show that the SM-like spin-0 is favored for the found new particle [109]. Although at ATLAS there is seen an enhancement of the branching ratio of $H \to \gamma\gamma$ in comparison to the SM at 2.3σ [66], this is nevertheless still consistent with the SM. Furthermore, CMS does not see a corresponding enhancement of this channel [68].

The Yukawa matrices in Eq. (2.15) have a non-trivial generational structure for that we currently do not have an experimentally supported explanation. Without loss of generality we can do unitary rotations and phase transformations $\in G_F$ in order to diagonalize the mass matrices $M_i = \frac{v}{\sqrt{2}} Y_i$ so that we obtain mass eigenstates with diagonal mass matrices

$$\mathrm{diag}(m_u, m_c, m_t) = \frac{v}{\sqrt{2}}\, U_L^u Y_u U_R^{u\dagger}\,, \qquad \mathrm{diag}(m_d, m_s, m_b) = \frac{v}{\sqrt{2}}\, U_L^d Y_d U_R^{u\dagger}. \tag{2.16}$$

These unitary transformations cancel out in all terms of the Lagrangian but the charged-current $W^\pm$ interactions that are implied in Eq. (2.10). There we get a term proportional to a unitary matrix $V^{\mathrm{CKM}} \equiv U_L^u U_L^{d\dagger}$ called the Cabibbo-Kobayashi-Maskawa (CKM) matrix [17, 110]:

$$\bar{Q}_L i \not{D} Q_L \supset -i\frac{g}{\sqrt{2}} (\bar{u}_L)_i \sigma^+ \not{W}^+ V_{ij}^{\mathrm{CKM}} (d_L)_j + \mathrm{h.c.}\,, \tag{2.17}$$

with generation indices $i, j = 1, 2, 3$. Due to $V^{\mathrm{CKM}} \neq \mathbb{1}$ there is flavor violation at the $W^\pm$ vertex in the SM. The non-trivial generational structure of the SM has important consequences for the discrete symmetries of the Lagrangian: It is the only source of CP violation in the perturbative part of the SM. Both flavor and CP violation are further elucidated in Sec. 2.2.1 and are the main topics of this work. Before we come to that, we introduce briefly the discrete symmetries of the SM Lagrangian and comment on potential CP violation through QCD.

Discrete Symmetries of QED and QCD In Eq. (2.2) we gave only the part of the Yang-Mills QCD-Lagrangian that is relevant for perturbation theory. This part conserves the following symmetries:

- C : charge symmetry. Invariance under particle–antiparticle transformation.
- P : parity symmetry. Invariance under $(t, \vec{x}) \mapsto (t, -\vec{x})$.

- T : time symmetry. Invariance under $(t, \vec{x}) \mapsto (-t, \vec{x})$.

The same is also true for QED, *i.e.*, the electroweak sector of the SM is the only one where the discrete symmetries C, P and T, respectively, are broken. Also gravitation respects them. The conservation of CPT, *i.e.*, invariance under the subsequent execution of all three operations is a fundamental theorem of quantum field theories [38–41]. For an introduction from the perspective of Axiomatic Quantum Field Theory see [111]. Therefore, in the SM there is by construction *a priori* no term that violates CPT. Nevertheless we can of course test it, *e.g.* in neutral kaon decays [89].

In addition to the term given in Eq. (2.2) there is in principle also a QCD-term that *violates* CP. It reads

$$\mathcal{L}^{\theta}_{\mathrm{YM}} = \frac{\theta}{64\pi^2}\varepsilon^{\mu\nu\rho\sigma}G^A_{\mu\nu}G^A_{\rho\sigma}. \tag{2.18}$$

A priori it is $\theta \neq 0$. The corresponding parameter that is invariant under rephasings of the fields in the Lagrangian is $\bar{\theta} = \theta - \mathrm{arg\,det} Y_u - \mathrm{arg\,det} Y_d$. As the term (2.18) can be written as a total divergence it does only contribute a surface term to the action $S = i\int \mathcal{L}\, \mathrm{d}^4x$. Therefore, it is not relevant to perturbation theory. However, the term (2.18) can have nonperturbative CP violating effects that affect the non-trivial topological structure of the vacuum of QCD [86, 112]. It is an open problem why this is experimentally not the case: The strongest reliable bounds on $\bar{\theta}$ stem from the ones on the neutron electric dipole moment and are given as $\bar{\theta} \leq 2.4 \cdot 10^{-10}$ [113–115]. The current bounds on $\bar{\theta}$ from the Schiff moment of ^{199}Hg are weaker by a factor ~ 2 [113]. This small value for $\bar{\theta}$ is not explained in the SM. However, there are theoretical ideas explaining it for example by an additional global U(1) symmetry, the so called Peccei-Quinn symmetry [116, 117], predicting an additional particle, the axion. Other ideas use the nonrenormalization theorems in SUSY [118].

In the following we will not be concerned with the strong CP problem but only with CP violating phenomena in the electroweak sector. In the SM, the latter have only flavor-dependent sources.

2.2. Flavor and CP Violation in the Standard Model

We return now to the electroweak sector of the SM. In Sec. 2.2.1 we have a closer look at the CKM matrix and parametrizations of flavor as well as its connection to CP violation. Reviews on the latter can be found, *e.g.*, in [119–121]. After that we turn from the electroweak to the strong sector and look in Sec. 2.2.2 at the role that especially the light quark flavors take in QCD.

2.2.1. Parametrizations of Flavor and CP Violation

CP Violation from the Cabibbo-Kobayashi-Maskawa Matrix

In 1956 the violation of parity in the weak interaction was observed [33, 34]. It was then believed that at least the combination CP would be conserved. But also this symmetry turned out to be violated as was for the first time observed in neutral Kaon decays in 1964 [35]. Up to now there is a long list of observables in which CP violation has been measured to $\geq 5\sigma$ [89]. It is a huge theoretical achievement that all of these different CP violating phenomena can be traced back to one single source, a single CP-odd phase in the CKM matrix which we introduce in the following. This can be taken as a classic example of theoretical reduction and simplification.

First of all, how many physical parameters does the matrix V_{CKM} of Eq. (2.17) actually contain? Putting it the other way around, how many of the 2×9 complex parameters of Y_u and Y_d can be rotated away after subtracting the six quark masses from the parameter budget? A general way to count the parameters of the Yukawa sector in any gauge theory is given by [122]

$$N_{\text{phys}} = N_{\text{Fl}} - N_{G_F} + N_{G^{\text{unbroken}}} \,. \tag{2.19}$$

The numbers N_i in Eq. (2.19) are given as follows, inserting always directly $n = 3$:

- N_{Fl}: Number of initial parameters of the Yukawa matrices, *i.e.*, $N_{\text{Fl}} = 4n^2 = 36$ real parameters, taking into account Y_u and Y_d. These are $2n^2 = 18$ moduli and $2n^2 = 18$ phases.
- N_{G_F}: Number of parameters of the flavor symmetry group that apply to the considered Yukawa matrices. For the quark sector according to Eq. (2.14) it is $G_F = U(3)_{Q_L} \otimes U(3)_U \otimes U(3)_D$. The number of parameters of a unitary matrix is given by $2n^2$ minus the number of constraints on its phases and moduli coming from the orthonormality constraints. We have thus $n^2 - n - \frac{n(n-1)}{2} = \frac{n(n-1)}{2} = 3$ moduli and $n^2 - \frac{n(n-1)}{2} = \frac{n(n+1)}{2} = 6$ phases for each unitary matrix. In total we have thus $N_{G_F} = 3n^2 = 27$ parameters of which $\frac{3n(n-1)}{2} = 9$ are moduli and $\frac{3n(n+1)}{2} = 18$ are phases.
- $N_{G^{\text{unbroken}}}$: Number of parameters of the subgroup $G^{\text{unbroken}} \subset G$ that is not broken by the Yukawa matrices. This subgroup is here given as $G^{\text{unbroken}} = U(1)_B$, *i.e.*, invariance under $N_{G^{\text{unbroken}}} = 1$ overall global phase transformation that corresponds to baryon number conservation.

The number of physical parameters in the quark sector is therefore altogether

$$N_{\text{phys}} = 4n^2 - 3n^2 + 1 = 1 + n^2 = 10 \,, \tag{2.20}$$

of which

$$N_{\text{moduli}} = 2n^2 - \frac{3n(n-1)}{2} = \frac{n(n+3)}{2} = 9 \tag{2.21}$$

are moduli and

$$N_{\text{phases}} = 2n^2 - \frac{3n(n+1)}{2} + 1 = \frac{2 - 3n + n^2}{2} = 1 \tag{2.22}$$

are phases in three generations. Using Eq. (2.22) for $n = 1, 2$ generations one obtains in both cases $N_{\text{phases}} = 0$. In this cases all phases can be rotated away using G_F transformations. On the contrary, for $n = 3$ this is not possible and one phase remains. Consequently, there is an important connection between the number of generations and CP violation: For one and two generations in the SM there is no CP violation. From the observation of CP violation, as in Kaon decays [35], or due to cosmological reasons, as given by the Sakharov rules [42], in the SM one could predict the presence of at least three generations [17]. All in all the 10 parameters of the quark flavor sector are thus decomposed into the six quark masses, the three mixing angles and the complex phase of V_{CKM}. All CP phenomena in the SM can be traced back to the latter.

Using these parameters, one can hence write the CKM matrix for example in the following "standard parametrization" [89, 123]

$$V_{\text{CKM}} \equiv \begin{pmatrix} V_{ud} & V_{us} & V_{ub} \\ V_{cd} & V_{cs} & V_{cb} \\ V_{td} & V_{ts} & V_{tb} \end{pmatrix} = \begin{pmatrix} c_{12}c_{13} & s_{12}c_{13} & s_{13}e^{-i\delta} \\ -s_{12}c_{23} - c_{12}s_{23}s_{13}e^{i\delta} & c_{12}c_{23} - s_{12}s_{23}s_{13}e^{i\delta} & s_{23}c_{13} \\ s_{12}s_{23} - c_{12}c_{23}s_{13}e^{i\delta} & -c_{12}s_{23} - s_{12}c_{23}s_{13}e^{i\delta} & c_{23}c_{13} \end{pmatrix}, \tag{2.23}$$

with the weak phase δ, $c_{ij} = \cos\theta_{ij}$, $s_{ij} = \cos\theta_{ij}$ and the three mixing angles θ_{12}, θ_{13} and θ_{23}. In the experiment, it turns out that the CKM matrix is a hierarchical matrix. This is easier visible if one writes the CKM matrix as [124–126]

$$V_{\text{CKM}} = \begin{pmatrix} 1 - \lambda^2/2 & \lambda & A\lambda^3(\rho - i\eta) \\ -\lambda & 1 - \lambda^2/2 & A\lambda^2 \\ A\lambda^3(1 - \rho - i\eta) & -A\lambda^2 & 1 \end{pmatrix} + \mathcal{O}(\lambda^4), \tag{2.24}$$

with $\lambda := s_{12} \ll 1$, $A := s_{23}/\lambda^2 \sim \mathcal{O}(1)$ and $(\rho + i\eta) := s_{13}e^{i\delta}/(A\lambda^3)$. Eq. (2.24) is the so called Wolfenstein expansion [124] of the CKM matrix and has the advantage that one can directly see the hierarchies while staying unitary order by order in the expansion in the small parameter λ. All other parameters in the Wolfenstein expansion could *a priori* be $\mathcal{O}(1)$. In actual fact it turns out that also ρ, η are small as well, of $\mathcal{O}(0.3)$.

Here, we concentrate on the mixing and CP violation in the quark sector. The mixing of neutrinos can be described in a way similar to the CKM matrix by the Pontecorvo-Maki-Nakagawa-Sakata (PMNS) matrix V_{PMNS} [127, 128]. A current global fit of neutrino

masses and mixing parameters of the PMNS matrix is given in [129]. $V_{\rm CKM}$ is strongly hierarchical and has small mixing angles, *i.e.*, $V_{\rm CKM} \approx \mathbb{1}$. In contrast to $V_{\rm CKM}$, $V_{\rm PMNS}$ consists of $O(1)$ numbers and incorporates large mixing angles. CP violation in the lepton sector is not measured at present.
In recent measurements the Daya Bay [130] and RENO [131] experiments obtained the result $\theta_{13}^{\rm PMNS} \neq 0$ at 5σ, therefore excluding the most simple ansätze and models for neutrino mixing like tribimaximal mixing [132]. However, this does not mean that approaches using discrete symmetries are not valid anymore. For example, the description in the framework of A_4 is even easier now and predicts large leptonic CP violation [133]. A possible alternative in light of $\theta_{13} \sim O(1)$ is the anarchical picture of neutrino mixing [134].

The parametrizations of flavor and CP violation in Eqs. (2.23) and (2.24) have the disadvantage that they are not invariant under G_F transformations and are therefore more or less ad hoc. Consequently, we consider next if and how one can parametrize flavor and CP violation in an invariant way, similar to the use of Mandelstam variables in kinematics, which are the corresponding invariants under the Lorentz group. In much the same way it is desirable to not depend on a "flavor coordinate system"—a point especially Jarlskog emphasizes [135], for example in discussions of the quark-lepton complementarity [136]. Bjorken and Dunietz introduced rephasing invariant "plaquette" invariants [137]. Due to their intuitive and natural geometric meaning, the plaquette invariants, namely the angles of the unitarity triangle α, β and γ specified below in Eqs. (2.36)–(2.38) are subject to extensive fits [126, 138, 139].

Invariant Parametrizations of Flavor and CP Violation

In a series of papers Jarlskog *et al.* found a flavor projection formalism in which one can express all masses, mixing angles and the phase of the CKM matrix using trace invariants of the Yukawa matrices, which works also for n generations [140–144]. The expressions for the invariant phase of the CKM matrix were identified in [140, 141, 145, 146]. It was discovered furthermore, that the Jarlskog invariant, the invariant measure of CP violation in the SM, has a geometric meaning, a fact that can also be generalized to *e.g.* four generations using quadrangles [147].
As we review below following [148–150], this program can be pursued by using the structure of the algebra of traces of all combinations of two three by three matrices C_{32} [151], where "3" stands for 3×3 matrices and "2" for two different matrices. Here these two matrices are given by the hermitian products $U \equiv Y_u Y_u^\dagger$ and $D \equiv Y_d Y_d^\dagger$ which form the representations $\mathbf{1} \oplus \mathbf{8}$ under $U(3)_{Q_L}$.

Sets of Generators of Flavor Trace Invariants The key point is that the algebra C_{32} is generated by a finite number of a few different traces. All other arbitrary traces can be reduced to algebraic combinations of a basis set using the Cayley-Hamilton theorem

[149]

$$X^3 = X^2\,\mathrm{Tr}(X) - \frac{1}{2}X\left[\mathrm{Tr}^2(X) - \mathrm{Tr}(X^2)\right] + \frac{1}{6}\left[\mathrm{Tr}^3(X) - 3\mathrm{Tr}(X^2)\mathrm{Tr}(X) + 2\mathrm{Tr}^3(X)\right]\mathbb{1}\,, \tag{2.25}$$

which is stated here for an arbitrary 3×3 matrix X. This fact can be used for a description of flavor in a completely trace invariant way: There are 11 trace invariant generators of C_{32}, however for one of these the square is not independent of the others but determined by the so called "defining relation" of the algebra. So for the 11th generator, only its sign is an independent information. These 10+1 trace invariant generators correspond to the six masses, three mixing angles c_{12}, c_{23}, c_{13} as well as $\cos\delta$ and the sign of δ for three generations of Dirac fermions [149].
In order to count the independent parameters of the Yukawa sector one can just count the number of generators of the algebra C_{32}. As we demonstrate in the following by compiling different sets of generators of C_{32}, also in a description of flavor that is invariant under the flavor symmetry group G_F there are nevertheless several ways to define the basic parameters. For that reason there is actually no "unique" choice for the parametrization of flavor. The notion of the "trace invariant" subsumes masses, angles and phases to just one concept. Note however, that this does not mean at all that the flavor problem is "solved". The usage of the trace invariant algebra as discussed in this paragraph is only an elegant reparametrization of flavor. Phenomenological implications are yet to be seen, so that in the main part of this work we do not utilize further the formalism outlined here.

- **Teranishi set.** The generators of the algebra C_{32} were for the first time given in 1986, however without reference to flavor, as [152]

$$\begin{aligned}&\mathrm{Tr}(U)\,, \quad \mathrm{Tr}(U^2)\,, \quad \mathrm{Tr}(U^3)\,, \quad \mathrm{Tr}(D)\,, \quad \mathrm{Tr}(D^2)\,, \quad \mathrm{Tr}(D^3)\,,\\ &\mathrm{Tr}(UD)\,, \quad \mathrm{Tr}(UD^2)\,, \quad \mathrm{Tr}(U^2D)\,, \quad \mathrm{Tr}(U^2D^2)\,, \quad \mathrm{Tr}(UDU^2D^2).\end{aligned} \tag{2.26}$$

- **Aslaksen Drensky Sadikova set.** Another two sets of generators of C_{32} that use traceless matrices and that have a much simpler defining relation than the Teranishi set are found in [153]. The first set is

$$\begin{aligned}&\mathrm{Tr}(U)\,, \quad \mathrm{Tr}(D)\,, \quad \mathrm{Tr}(u^2)\,, \quad \mathrm{Tr}(ud)\,, \quad \mathrm{Tr}(d^2)\,, \quad \mathrm{Tr}(u^3)\,,\\ &\mathrm{Tr}(u^2d)\,, \quad \mathrm{Tr}(ud^2)\,, \quad \mathrm{Tr}(d^3)\,, \quad \mathrm{Tr}(u^2d^2)\,, \quad \mathrm{Tr}(u^2d^2ud)\,,\end{aligned} \tag{2.27}$$

  where

$$U = \frac{1}{3}\mathrm{Tr}(U)\mathbb{1} + u\,, \qquad D = \frac{1}{3}\mathrm{Tr}(D)\mathbb{1} + d. \tag{2.28}$$

  The second set is given as

$$\begin{aligned}&\mathrm{Tr}(U)\,, \quad \mathrm{Tr}(D)\,, \quad \mathrm{Tr}(u^2)\,, \quad \mathrm{Tr}(ud)\,, \quad \mathrm{Tr}(d^2)\,, \quad \mathrm{Tr}(u^3)\,,\\ &\mathrm{Tr}(u^2d)\,, \quad \mathrm{Tr}(ud^2)\,, \quad \mathrm{Tr}(d^3)\,, \quad v\,, \quad w\,,\end{aligned} \tag{2.29}$$

  with

$$v = \mathrm{Tr}(u^2d^2) - \mathrm{Tr}(udud)\,, \qquad w = \mathrm{Tr}(u^2d^2ud) - \mathrm{Tr}(d^2u^2du). \tag{2.30}$$

- **Jenkins Manohar set.** In Ref. [149] the connection of the trace invariant generators to flavor physics is given. The trace invariants are in agreement with the Teranishi set while replacing $\mathrm{Tr}(UDU^2D^2)$ by the Jarlskog determinant [140, 141]

$$\frac{1}{3}\mathrm{Tr}\left([U,D]^3\right) = \mathrm{Tr}\left(U^2D^2UD - D^2U^2DU\right) = \det\left([U,D]\right). \tag{2.31}$$

  The first six trace invariants in Eq. (2.26) specify the masses of the particles, the next four the mixing. CP violation is characterized by the Jarlskog determinant. Only the sign of the latter is independent as the absolute value is determined by the other trace invariant generators due to the defining relation [149].

In the next paragraph, we discuss geometric interpretations of flavor invariants.

Geometric Interpretation I: Unitarity Polygons with Plaquette Invariant Angles Due to the unitarity of the CKM matrix, its columns and rows are mutually orthonormal: There are six unitarity conditions. For the rows and columns, respectively, these are given as (with fixed $i \neq j$)

$$\sum_k V_{ik}V_{jk}^* = 0\,, \qquad\qquad \sum_k V_{ki}V_{kj}^* = 0. \tag{2.32}$$

Each of these six relations give one unitarity triangle in the complex plane [147]. This picture is very useful as both the angles of these triangles as well as the area are invariant under G_F. When one speaks of *the* unitarity triangle one commonly means the one that is connected to most of the experimental measurements. This is specified by the relation

$$V_{ud}V_{ub}^* + V_{cd}V_{cb}^* + V_{td}V_{tb}^* = 0. \tag{2.33}$$

The area of each unitarity triangle is given by the same value, namely $1/2$ times the absolute value of the Jarlskog invariant J, which is defined by

$$\mathrm{Im}\left(V_{ij}V_{kl}V_{il}^*V_{kj}^*\right) = J\sum_{m,n}\varepsilon_{ikm}\varepsilon_{jln}\,, \tag{2.34}$$

and relates as follows to the Jarlskog determinant:

$$\det\left([U,D]\right) = 2iJ(m_c^2-m_u^2)(m_t^2-m_c^2)(m_t^2-m_u^2)(m_s^2-m_d^2)(m_b^2-m_s^2)(m_b^2-m_d^2). \tag{2.35}$$

The equality of the area of the triangles can be shown from the fact that the square of the Jarlskog invariant can be written by only four absolute values of CKM matrix elements using the Källen lambda function [147]. The non-vanishing of these areas is equivalent to CP violation. Instead of the three angles + one phase + its sign in the standard parametrization one can thus also choose four absolute values of the CKM matrix plus the sign of the Jarlskog determinant as fundamental parametrization. The relation of the Jarlskog invariant to the four absolute values of CKM matrix elements corresponds to the defining relation of the algebra C_{32}. From the latter it can likewise be seen that only the

sign of the Jarlskog determinant is an independent information. Its absolute value is then determined by the masses and four independent mixing trace invariants. Thus, we have a full understanding of the correspondence of the different ways of parameter counting.

The invariant angles of *the* unitarity triangle are given as

$$\alpha = \mathrm{Arg}\left(-\frac{V_{td}V_{tb}^*}{V_{ud}V_{ub}^*}\right) = \mathrm{Arg}\left(-V_{td}V_{tb}^*V_{ud}^*V_{ub}\right) , \tag{2.36}$$

$$\beta = \mathrm{Arg}\left(-\frac{V_{cd}V_{cb}^*}{V_{td}V_{tb}^*}\right) = \mathrm{Arg}\left(-V_{cd}V_{cb}^*V_{td}^*V_{tb}\right) , \tag{2.37}$$

$$\gamma = \mathrm{Arg}\left(-\frac{V_{ud}V_{ub}^*}{V_{cd}V_{cb}^*}\right) = \mathrm{Arg}\left(-V_{ud}V_{ub}^*V_{cd}^*V_{cb}\right) , \tag{2.38}$$

where we used the "plaquette" product invariants that were introduced in [137] in analogy to gauge theory. In global fits to data [126, 138, 139] the invariant triangle construction by Jarlskog and Bjorken (see [147] and references therein) can be overconstrained. This gives an important test of the SM.

Having by the area of the unitarity triangle a very intuitive geometrical picture and measure of CP violation at hand, how big actually is the CP violation in the SM? In order to answer this question, Jarlskog introduced a normalized version of her determinant that lies a priori in the range $-1 \leq a_{CP} \leq 1$ [144]

$$a_{\mathrm{CP}} \equiv 3\sqrt{6}\frac{\det C}{\mathrm{Tr}^{3/2}(C^2)} = -\sqrt{6}\frac{\mathrm{Tr}\left([U,D]^3\right)}{\mathrm{Tr}^{3/2}\left([U,D]\right)} \approx 3\sqrt{3}\frac{m_c^2}{m_t^2}\frac{m_s^2}{m_b^2}\frac{\eta}{A} \sim 10^{-8}. \tag{2.39}$$

Here, it is $iC = [U,D]$. Using the measure Eq. (2.39), CP violation seems to be quite "small". At any rate, it is several orders of magnitude too small to explain the observed matter-antimatter asymmetry, see the review [43]. Nevertheless, in b decays CP violation can be sizable as it is proportional to the large invariant angles of *the* unitarity triangle.

Geometric Interpretation II: Abstract angles between Yukawa matrices In this paragraph we briefly inspect whether normalized measures as the one in Eq. (2.39) do exist also for the other trace invariant generators besides the Jarlskog determinant. This leads to yet another invariant geometric picture of flavor.

Already Jarlskog has defined an abstract angle between mass matrices that measures their misalignment [154]

$$\cos\theta = \frac{\mathrm{Tr}(UDUD)}{\mathrm{Tr}(U^2D^2)}, \tag{2.40}$$

with $\theta = 0$ if and only if $[U,D] = 0$. A similar angle has been recently defined in [155–157]. For the traceless matrices u and d that correspond to U and D as in Eq. (2.28) it is

given as [155]

$$\cos\theta_{ud} = \frac{\mathrm{Tr}(ud)}{\sqrt{\mathrm{Tr}(u^2)\mathrm{Tr}(d^2)}}. \tag{2.41}$$

In [155–157] it is shown that analogous angles are especially useful in the analysis and classification of NP flavor structures. Furthermore, it is found that in two generations [155]

$$\cos 2\theta_C = \cos\theta_{ud}\,, \tag{2.42}$$

i.e., the abstract angle between Yukawa matrices and the Cabibbo angle are directly connected. Eq. (2.42) can also be obtained using Jarlskog's projection formalism which shows the other way around that all invariant approaches hang together: In [142] the general formula for expressing the CKM matrix elements by trace invariants is applied to two generations. Using additionally $\cos 2\theta = -1 + 2\cos^2\theta$ one obtains

$$\cos 2\theta = -1 + 2\frac{\mathrm{Tr}(UD) - 2(m_c^2 m_d^2 + m_u^2 m_s^2)}{(m_c^2 - m_u^2)(m_s^2 - m_d^2)}. \tag{2.43}$$

Plugging now $U = \frac{1}{3}\mathrm{Tr}(U)\mathbb{1} + u$ and $D = \frac{1}{3}\mathrm{Tr}(D)\mathbb{1} + d$ into Eq. (2.43) one obtains again Eq. (2.42).

But now, which and how many *independent* of such abstract angles between Yukawa matrices can be defined in three generations? This can be answered easily, knowing the structure of the algebra C_{32}. From the trace invariant formalism we see that only four such abstract angles suffice to determine the mixing in the quark sector of the SM:

$$\cos\theta_1 = \frac{\mathrm{Tr}(UD)}{\sqrt{\mathrm{Tr}(U^2)\mathrm{Tr}(D^2)}}\,, \qquad \cos\theta_2 = \frac{\mathrm{Tr}(U^2D)}{\sqrt{\mathrm{Tr}(U^4)\mathrm{Tr}(D^2)}}\,, \tag{2.44}$$

$$\cos\theta_3 = \frac{\mathrm{Tr}(UD^2)}{\sqrt{\mathrm{Tr}(U^2)\mathrm{Tr}(D^4)}}\,, \qquad \cos\theta_4 = \frac{\mathrm{Tr}(U^2D^2)}{\sqrt{\mathrm{Tr}(U^4)\mathrm{Tr}(D^4)}}. \tag{2.45}$$

Traces of higher powers like $\mathrm{Tr}(U^4)$ and $\mathrm{Tr}(D^4)$ can be reduced to traces of lower powers of U and D [149]. Like the angles of the CKM triangle the four angles of Eqs. (2.44) and (2.45) specify the abstract geometry of flavor and contain the full information of quark mixing. From the defining relation in C_{32} we know that they also determine the square of the Jarlskog determinant [149].

To summarize, there are several very different but equivalent approaches to parametrize flavor (beyond the masses) and CP violation. In the SM with three generations we discussed in this paragraph the following options:

- Three Euler angles and one phase of the CKM matrix, for example in its standard parametrization.

- Four absolute values of CKM matrix elements plus the sign of the Jarlskog determinant.
- Plaquette invariants, *i.e.*, the angles of the unitarity triangles.
- Trace invariant generators of the algebra C_{32}.
- Abstract angles between flavor matrices.

The trace invariants introduced in this section can be used in model building for the construction of a potential of scalar spurion fields [149, 158–160]. The extremization of such a potential is supposed to reproduce the measured Yukawa couplings – for example in the sequential breaking of flavor symmetries [158]. For local flavor symmetries, the latter has in turn implications for phenomenology in form of additional heavy gauge bosons, the modification of flavor observables or the solution of the strong CP problem [158, 161]. Furthermore, abstract angles between NP and SM flavor structures can serve as model-independent covariant measures of misalignment [155–157].

After the overview of possible parametrizations of flavor and CP violation, in the next section we turn to the CP invariant part of the SM and ask about the flavor structure of QCD.

2.2.2. Approximative SU(3)-Flavor Symmetry of QCD

From the perspective of the QCD part of the SM, the only place where the flavor of quarks does appear are their mass terms. The gluon-fermion interaction is flavor-diagonal. For approximately degenerate quark masses as in the case of u and d quark,

$$m_u - m_d \ll \Lambda_{\text{QCD}}\,, \tag{2.46}$$

the QCD Lagrangian is approximately invariant under unitary transformations of these quarks. For u and d this results in the SU(2) isospin symmetry, which is realized very well. The isospin symmetry can be extended to an approximate $\text{SU}(3)_F$ symmetry including also the s quark. However, while $m_{u,d} \ll \Lambda_{QCD}$, the mass of the strange quark m_s is significantly larger and gives a perturbation to the $\text{SU}(3)_F$ symmetry limit $m_u = m_d = m_s$. We expect a perturbation of the $\text{SU}(3)_F$ symmetry by the strange quark mass to a generic amount of $\sim 30\%$. One can perform a systematic expansion in this perturbation, see below. Besides isospin (symmetry between $u \Leftrightarrow d$), the $\text{SU}(3)_F$ group has as its subgroups the SU(2) groups U-spin (symmetry between $d \Leftrightarrow s$) and V-spin (symmetry between $u \Leftrightarrow s$).

Historically, the $\text{SU}(3)_F$ symmetry has been found in spectroscopy. In form of the famous "eightfold way" it provided the great simplification that lies in the realization that each member of the zoo of hadronic particles is again composed of even smaller particles, the quarks [162–164]. The latter were in the following regarded elementary. For example,

the group theoretic foundation of the meson octet is the equation

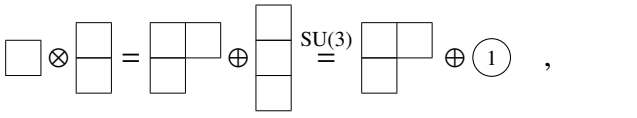

$$\overset{\text{SU(3)}}{=} \oplus (1) \quad , \tag{2.47}$$

i.e. in SU(3): $\Rightarrow \mathbf{3} \otimes \bar{\mathbf{3}} = \mathbf{8} + \mathbf{1}$, (2.48)

where we use the language of the Young tableaux.

A key point in order to benefit from the symmetry is a remarkable theorem by Wigner and Eckart [165–167]. In the notation of de Swart, it reads [168]

$$\left(\phi_{\nu_3}^{(\mu_3)}, T_{\nu_2}^{(\mu_2)} \phi_{\nu_1}^{(\mu_1)}\right) = \sum_{\gamma} \begin{pmatrix} \mu_1 & \mu_2 & \mu_{3\gamma} \\ \nu_1 & \nu_2 & \nu_3 \end{pmatrix} \left\langle \mu_3 \right| T^{(\mu_2)} \left| \mu_1 \right\rangle_{\gamma} , \tag{2.49}$$

with the reduced matrix elements $\left\langle \mu_3 \right| T^{(\mu_2)} \left| \mu_1 \right\rangle_{\gamma}$ that have Clebsch-Gordan coefficients in front of them. Here, $\phi_{\nu_1}^{(\mu_1)}$ is the initial state, $T_{\nu_2}^{(\mu_2)}$ is an irreducible tensor operator and $\phi_{\nu_3}^{(\mu_3)}$ is the final state. ν_i are angular momentum quantum numbers, $\{\mu_i\}$ the corresponding irreducible representations and γ additional quantum numbers belonging to physics outside the considered group. Using Eq. (2.49) one can express amplitudes by reduced matrix elements that do not depend any more on the quantum numbers from angular momentum ν_i, but only on the given representations of initial and final state as well as the tensor operator. In this way the number of parameters compared to using directly the left-hand side of Eq. (2.49) can be reduced and symmetry correlations can be obtained. For details on the proof of the Wigner-Eckart theorem see [168] and also [169].

In order to take SU(3)_F breaking into account, we apply perturbation theory. Considering an operator $O(x)$ between full initial and final states $\left|\tilde{i}\right\rangle$, $\left|\tilde{f}\right\rangle$, respectively, to linear order it is [170]

$$\left\langle \tilde{f} \right| O(0) \left| \tilde{i} \right\rangle = \langle f | O(0) | i \rangle - i \int \mathrm{d}^4 x \, \langle f | T \left[O(0) \mathcal{H}_{\text{break}}(x) \right] | i \rangle \ , \tag{2.50}$$

with a breaking term which for our purposes is given as $\mathcal{H}_{\text{break}} = m_s \, \bar{s} s$. Here, $|i\rangle$ and $|f\rangle$ are SU(3)_F symmetric states. In Eq. (2.50) an analysis of the SU(3)_F structure has to be done and subsequently Eq. (2.49) has to be applied. Then one obtains beyond the reduced SU(3)_F limit matrix elements also the additional SU(3)_F breaking reduced matrix elements.

The systematic expansion in SU(3)_F breaking will be demonstrated to linear order in Ch. 5 for nonleptonic charm meson decays, where we apply Eqs. (2.49) and (2.50) in practice. There, we will also test the amount of SU(3)_F breaking by fits of the reduced matrix elements to data.

2.3. Probing CP Violation in Meson Decays

While in Sec. 2.2.1 we studied the possible parametrizations of flavor and CP violation from the theory side, in this section we inspect the phenomenology and the types of observables in order to probe CP violation.

It turns out that though stemming all from one CP-violating phase of the CKM matrix, three different types of CP violation can be distinguished for the decays of K, D and B mesons. For the definition of these mesons and their antiparticles we use the convention [89]

$$\bar{B} = (b\bar{q}) \qquad B = (\bar{b}q) \tag{2.51}$$

$$\bar{K} = (s\bar{q}) \qquad K = (\bar{s}q) \tag{2.52}$$

$$\bar{D} = (\bar{c}q) \qquad D = (c\bar{q}). \tag{2.53}$$

In order to discuss the different types of CP violation we have to introduce some more notation, following Ref. [89]. For the CP conjugation of a meson $|M\rangle$ we write $\left|\overline{M}\right\rangle$, in the same way we do so for the CP conjugation $\left|\bar{f}\right\rangle$ of a final state $|f\rangle$. We write then the amplitudes of meson decays as [89]

$$\mathcal{A}_f = \mathcal{A}(M \to f), \quad \overline{\mathcal{A}}_f = \mathcal{A}(\overline{M} \to f), \quad \mathcal{A}_{\bar{f}} = \mathcal{A}(M \to \bar{f}), \quad \overline{\mathcal{A}}_{\bar{f}} = \mathcal{A}(\overline{M} \to \bar{f}). \tag{2.54}$$

In the case of neutral mesons, the particle and antiparticle have the same quantum numbers so that the phenomenon of meson-mixing takes place. Due to the long time scales of our measurements in collider physics compared to the ones of QCD we can use the standard non-relativistic quantum mechanics of an approximate two state system, the so-called "Wigner-Weißkopf" approximation, in order to describe the meson oscillations [171, 172]. The mass eigenstates of the mesons can be written in form of the flavor eigenstates as follows:

$$\left|M_{\text{Light}}\right\rangle = p\left|M^0\right\rangle - q\left|\overline{M}^0\right\rangle, \qquad \left|M_{\text{Heavy}}\right\rangle = p\left|M^0\right\rangle + q\left|\overline{M}^0\right\rangle. \tag{2.55}$$

with parameters p and q that fulfill $|p|^2 + |q|^2 = 1$. For example, in the Kaon system it is $\left|K_L\right\rangle \equiv \left|M_{\text{Heavy}}\right\rangle$ and $\left|K_S\right\rangle \equiv \left|M_{\text{Light}}\right\rangle$. In order to get the time dependence of the neutral meson decays one has to solve the Schrödinger equation in the Wigner-Weißkopf approximation:

$$i\frac{\mathrm{d}}{\mathrm{d}t}\begin{pmatrix}\left|M^0(t)\right\rangle \\ \left|\overline{M}^0(t)\right\rangle\end{pmatrix} = \left(\mathbf{M} - \frac{i}{2}\mathbf{\Gamma}\right)\begin{pmatrix}\left|M^0(t)\right\rangle \\ \left|\overline{M}^0(t)\right\rangle\end{pmatrix}, \tag{2.56}$$

with 2×2 matrices $\mathbf{M}$ and $\mathbf{\Gamma}$. The result can be found in the literature [89]. For a more detailed deviation see also [120, 121, 173]. Denoting the eigenvalues of $\mathbf{M} - \frac{i}{2}\mathbf{\Gamma}$ as

	x	y
K	0.946 ± 0.002 [a][89]	0.9965 ± 0.0006 [a][89]
D	$0.0063^{+0.0019}_{-0.0020}$ [63]	0.0075 ± 0.0012 [63]
B_d	0.770 ± 0.008 [b][63]	0.008 ± 0.009 [cd][63]
B_s	26.74 ± 0.22 [63]	0.072 ± 0.011 [cd][63]

Table 2.1.: Comparison of measured x and y for the different meson systems, see text for details. [a]Our calculation from Δm_K, τ_S and τ_L, error obtained by Gaussian error propagation. [b]Assuming $y = 0$. [c]Assuming sign(Reλ_{CP}) $= +1$. [d]Obtained from value for $\Delta\Gamma/\Gamma$ by Eq. (2.57).

$m_{L,H} - \frac{i}{2}\Gamma_{L,H}$ important characteristics of the mixing of K, D, B_d and B_s can be written in form of the parameters

$$x = \frac{\Delta m}{\Gamma} \qquad \text{and} \qquad y = \frac{\Delta\Gamma}{2\Gamma}\,, \tag{2.57}$$

with

$$\Delta m = m_H - m_L\,, \qquad \Delta\Gamma = \Gamma_H - \Gamma_L\,, \qquad \Gamma = \frac{\Gamma_H + \Gamma_L}{2}. \tag{2.58}$$

Here, the subscript "H" stands for the heavier and "L" for the lighter eigenstate. It is *a priori* $-1 \leq y \leq 1$. We compare the values for x and y that are realized in the different meson systems in Table 2.1. It turns out that they differ quite substantially. The mass difference Δm takes the role of the oscillation frequency of the mixing between $\left|M^0\right\rangle$ and $\left|\overline{M}^0\right\rangle$. Consequently, x gives the relative frequency compared to the average decay rate. In the B_s system x has the largest value, *i.e.*, the mixing takes place very fast. In D mixing x and also y are very small, *i.e.*, the mixing is barely visible. This was also one of the reasons why for the D system it took the longest time of all the meson systems shown in Table 2.1 to observe its mixing. Among the remaining features, in the B_d system the width difference $\Delta\Gamma_d$ is negligible with respect to Δm_d. For the B_d and B_s system the SM predicts [174]

$$\Delta\Gamma_d/\Gamma_d = 0.0042 \pm 0.0008 \qquad \Delta\Gamma_s/\Gamma_s = 0.137 \pm 0.027. \tag{2.59}$$

This is in striking contrast to the Kaon system. Here, y is very near to one, *i.e.*, the maximum value, as the lifetimes of K_S and K_L are drastically different, $\tau_S = (8.954 \pm 0.004) \cdot 10^{-11}$s and $\tau_L = (5.116 \pm 0.021) \cdot 10^{-8}$s. Therefore, after a while a kaon beam only consists of K_L states.

We come now to the discussion of the different forms of CP violation. The three different types that one can observe in meson decays are the following:

- (Direct) CP violation in decay $\Leftrightarrow \left|\overline{\mathcal{A}}_{\bar{f}}/\mathcal{A}_f\right| \neq 1$.
- CP violation in mixing $\Leftrightarrow |q/p| \neq 1$.
- CP violation in the interference between decays with/without mixing $\Leftrightarrow \mathrm{Im}\left[(q/p)\left(\overline{\mathcal{A}}_f/\mathcal{A}_f\right)\right] \neq 0$.

We also use the notation $\lambda_f \equiv (q/p)\left(\overline{\mathcal{A}}_f/\mathcal{A}_f\right)$. For the direct CP asymmetry of a decay d we write

$$a_{CP}^{\mathrm{dir}}(d) = \frac{|\mathcal{A}(d)|^2 - |\overline{\mathcal{A}}(d)|^2}{|\mathcal{A}(d)|^2 + |\overline{\mathcal{A}}(d)|^2}. \tag{2.60}$$

In charged meson decays, only direct CP violation is possible. Examples for the occurrence of CP violation in mixing can be found in semileptonic decays of the neutral mesons. The third category comes across in decays of neutral mesons to CP eigenstates.

Additionally, there are time integrated and time dependent measurements of CP violation. In the latter, time-resolved experiments, one can disentangle direct and indirect CP violation. For example for B_d, where $y \ll 1$, one can write the time dependence of a decay amplitude as [89]

$$\mathcal{A}_f(t) = S_f \, \sin(\Delta m t) - C_f \cos(\Delta m t)\,, \tag{2.61}$$

with

$$S_f = \frac{2\mathrm{Im}(\lambda_f)}{1+|\lambda_f|^2}\,, \qquad C_f = \frac{1-|\lambda_f|^2}{1+|\lambda_f|^2}. \tag{2.62}$$

Here, S_f is the contribution to CP violation from interference between decays with/without mixing and C_f is the one from direct CP violation.
An example for a time-integrated CP observable using a semileptonic decay is given in the Kaon system by [89]

$$\delta_L = \frac{\Gamma(K_L \to l^+\nu_l\pi^-) - \Gamma(K_L \to l^-\bar{\nu}_l\pi^+)}{\Gamma(K_L \to l^+\nu_l\pi^-) + \Gamma(K_L \to l^-\bar{\nu}_l\pi^+)} = \frac{2\mathrm{Re}\varepsilon}{1+|\varepsilon|^2} = (3.32 \pm 0.06)\cdot 10^{-3}. \tag{2.63}$$

If we want to extract the direct CP violation of a decay with a neutral Kaon in the final state, we have to subtract the contribution to CP violation from mixing. We do so for example for the decays $D^+ \to K_S K^+$ and $D_s \to K_S \pi^+$, see Ch. 5. It is [175]

$$a_{CP}^{\mathrm{dir}}(D^+ \to K_S K^+) = A_{CP}(D^+ \to K_S K^+) + \delta_L\,, \tag{2.64}$$

$$a_{CP}^{\mathrm{dir}}(D_s \to K_S \pi^+) = A_{CP}(D_s \to K_S \pi^+) - \delta_L\,. \tag{2.65}$$

The sign in front of δ_L depends on a K^0 or a $\bar{K}^0$ being in the final state of the flavor flow, as *e.g.* explained in [176]. The contribution is $-\delta_L$ for a $\bar{K}_0$ and $+\delta_L$ for a K^0.

In the charm system, it holds $x, y \ll 1$. Writing the charm decay amplitude as $A_f = A_f^T e^{i\phi_f^T}\left(1 + r_f e^{i(\delta_f+\phi_f)}\right)$ with a strong phase ϕ_f and a weak phase δ_f it holds furthermore $r_f \ll 1$ [177]. As a consequence, the total time-integrated CP asymmetry a_f of D^0 decays can be written approximately as a sum of a direct (a_f^d), a mixing (a_f^m) and an interference (a_f^i) contribution linear in r_f, y and x, respectively, [177]

$$a_f = a_f^d + a_f^m + a_f^i \,. \tag{2.66}$$

The direct contribution can because of $r_f \ll 1$ approximately be written as [177]

$$a_f^d = 2 r_f \sin\phi_f \sin\delta_f \,. \tag{2.67}$$

From Eq. (2.67) we learn that for $a_f^d \neq 0$ both a nonvanishing weak and strong phase difference is needed. Considering further the features of Eq. (2.66), for example in the decays $D^0 \to K^+K^-$ and $D^0 \to \pi^+\pi^-$ the indirect contributions to CP violation are the same. Consequently, it is very convenient from the experimental point of view to measure the difference of the respective CP asymmetries. In this case the indirect contributions cancel out and we are left (approximately) with the difference of the pure direct CP violation of these channels:

$$\Delta A_{CP} \equiv A_{CP}(D^0 \to K^+K^-) - A_{CP}(D^0 \to \pi^+\pi^-) \tag{2.68}$$

$$\approx \Delta a_{CP}^{\text{dir}} \equiv a_{CP}^{\text{dir}}(D^0 \to K^+K^-) - a_{CP}^{\text{dir}}(D^0 \to \pi^+\pi^-). \tag{2.69}$$

We will come back to this in Sec. 5.

2.4. Flavor and CP Violation beyond the Standard Model

In view of the vast hierarchy between the electroweak and the Planck scale there are several classes of models that try to explain, stabilize or remove this disparity in order to make the theory more natural. Among the most promising candidates are SUSY, additional strong dynamics in composite models or extra dimensional models. In order to calculate the resulting physics in these models an inevitable tool is the effective theory framework that we will briefly discuss in the next section before we give a short overview of SUSY in Sec. 2.4.2. In Ch. 3 we will give then a specific phenomenological application. For a four-dimensional effective theory of a composite Higgs model see [178]. Implications of extra dimensional models on flavor can be found in [179]. For details and further references with respect to the effective field theory description of meson decays see Ref. [180].

2.4.1. Effective Theories

Effective field theories are designed in order to describe physical systems at a certain (low) energy scale. In b physics this is the scale of the mass of the b quark $O(m_b)$ which

is much smaller than the electroweak scale $O(m_W)$. As a nontrivial consequence one can "integrate" out heavy particles from the theory and write down the interplay of short distance physics at the electroweak or a higher energy scale and the long distance physics at a lower energy scale in factorized form. The $\Delta B = 1$ Hamiltonian that we will use in Ch. 3 in order to describe the impact of $\bar{B} \to \bar{K}^{(*)} l^+ l^-$ observables on the SUSY parameter space is given as

$$\mathcal{H}_{\text{eff}} = -\frac{4G_F}{\sqrt{2}} V_{tb} V_{ts}^* \sum_i C_i(\mu) O_i(\mu)\,, \tag{2.70}$$

with the Fermi constant G_F. The analogue for $\Delta C = 1$ transitions will be outlined in Ch. 5. The separation of long and short distance physics is given by the factorization scale μ. The O_i include only the fields of the particles that are not integrated out. The short distance Wilson coefficients C_i contain the high energy scale parameters of the particles that have been integrated out. The concrete operators in Eq. (2.70) can be found in [181]. The most important ones for $\bar{B} \to \bar{K}^{(*)} l^+ l^-$ will be given in Ch. 3. In NP theories can appear on the one hand additional operators O_i and on the other hand additional contributions to the Wilson coefficients. Seeing it from another point of view one can also use the basis of operators of the effective framework in order to do model-independent scans and fit the Wilson coefficients [182–184].

While Eq. (2.70) gives a handle to disentangle short and long distance physics in a factorized form, it is by far not the "solution" to the problem that follows: While the Wilson coefficients can be calculated mostly perturbatively in a given theory, for the long distance physics that governs the hadronic matrix elements $\langle f | O_j | i \rangle$ between initial and final states $|i\rangle$ and $|f\rangle$, respectively, one needs at any rate nonperturbative means. Depending on the problem there are solutions given by lattice QCD, QCD sum rules, chiral perturbation theory, the Heavy Quark Expansion, the Heavy Quark Effective Field Theory (HQET) and several other types of effective theories, see *e.g.* [185].

If these methods work for b physics this does not mean on the other hand that they do likewise for charm physics. The point is that the b quark mass is considerably larger than the scale of QCD Λ_{QCD}, while the charm quark has an intermediate mass not very far away from Λ_{QCD}. We will show in Chs. 5 and 6 how we can nevertheless make progress by the use of the approximate $\text{SU}(3)_F$ symmetry of QCD that was introduced in Sec. 2.2.2.

An interesting property of $\bar{B} \to \bar{K}^{(*)} l^+ l^-$ is that in different kinematic regions distinct theoretical approaches apply. We will come back to this point in Chs. 3 and 4. In the latter we will also elaborate on how we can benefit from the information we can get from the lattice and sum rules.

2.4.2. The Minimal Supersymmetric Standard Model

In this section we give a short introduction to SUSY and the Minimal Supersymmetric Standard Model (MSSM). For more details on the foundations beyond the following synopsis see *e.g.* the reviews in [89, 186–188].

Symmetry of Fermions and Bosons from a Unique Extension of the Poincaré Group

According to the general theorems by Coleman-Mandula [189] and Haag-Lopuszanski-Sohnius [190] SUSY is under some very generic assumptions the unique extension of the Poincaré symmetry. SUSY relates on a fundamental level the fermionic and bosonic degrees of freedom of a theory [191–194]. The usual space-time with Poincaré symmetry is extended by an N-dimensional superspace. The incorporation of SUSY into quantum field theory has been given in [195, 196]. In minimal versions of SUSY one uses an $N = 1$ dimensional superspace, as is the case in the MSSM [197, 198].

A direct prediction of SUSY are many additional particles that have the same mass as the particle content of the SM but differ in spin: Fermionic and bosonic degrees of freedom correspond to each other. None of these particles have up to now been observed, *i.e.*, assuming SUSY exists, it must be broken. An obvious idea to implement this into a quantum field theory is to construct a mechanism inspired from the Higgs mechanism for electroweak symmetry breaking in the SM, *i.e.*, the spontaneous breaking of SUSY [199–201]. In the MSSM one parametrizes the breaking of SUSY as a global symmetry. In supergravity theories, where SUSY is connected to a theory of gravity, SUSY is broken as a local symmetry [202–205].

From the theoretical perspective the mathematical uniqueness of SUSY with respect to the Poincaré group gives already a strong motivation to search for the additional "sparticles" predicted in SUSY. Unfortunately, the Haag-Lopuszanski-Sohnius theorem does not give a mass scale for SUSY breaking, being a completely general mathematical result. But indeed there are also reasons to expect the observation of SUSY particles at the "low" energy scales available right at the LHC, *i.e.*, at the terascale. The reason lies in important features, that SUSY has only at the terascale, in addition to the unique group theoretic and algebraic conjunction with the Poincaré symmetry which is completely general.

Firstly, at the terascale SUSY could solve the gauge hierarchy problem by removing the fine tuning problem between the Higgs mass and its radiative corrections from Planck scale physics which leads to quadratic divergencies [206–211]. This hierarchy problem of the SM viewed as an effective theory is special to scalar particles because the fermion masses renormalize only logarithmically and are protected by a chiral symmetry. Thus a small fermion mass is natural, but a small scalar mass is not – hence the special role of the Higgs which is the only scalar particle in the SM [212–216].
The Higgs mass gets the strongest loop corrections from the heaviest particles that are contained in the theory and couple to it. As the SM does not contain gravitation, at the latest at the Planck scale there is physics beyond the SM that will then give huge corrections to the mass of the Higgs. The solution of SUSY is provided by adding more (scalar) particles to the theory that have just the right properties, *i.e.* couplings and masses, to cancel these divergencies. In unbroken SUSY the scalar partners of the fermions cancel exactly the divergencies coming from the SM fermions. If SUSY is not broken with too heavy sparticles, this can still be provided approximately. The correction to the Higgs mass is then proportional to the size of the splitting between fermion and sfermion masses

[187]. As long as this result is of the order of the Higgs mass itself, the theory does not get unnatural again. This is a great motivation that SUSY should be realized at the terascale. If the SUSY scale is too far beyond the terascale, it will not help to solve the hierarchy problem any more and to remove the unnaturalness from the SM.

The second feature of TeV-scale SUSY is the unification of the gauge couplings at $\sim 10^{16}$ GeV which would indicate the existence of a grand unified theory (GUT), *i.e.*, a gauge group that contains all the gauge groups of the SM [217–222]. In these theories at the high scale also a reduction of flavor parameters takes place, as for example in form of the Georgi-Jarlskog mass relations in an SU(5) model: $m_b = m_\tau$, $m_\mu = 3m_s$ and $m_e = \frac{1}{3}m_d$ [223].

Thirdly, an additional motivation for SUSY is that in its framework one can easily provide a dark matter candidate. This is an argument which is in principle independent of the scale of the SUSY particles. However, it happens that the mass of weakly interacting massive particles (WIMPs) should also have a mass of the order of a TeV in order to account for the observed relic density, which is the so called "WIMP miracle" [224]. So if dark matter is made of SUSY particles this is an additional motivation that the mass scale of the SUSY particles should be near the terascale.

In order to account for a dark matter candidate in SUSY one can simply introduce an additional symmetry, the so called R- or matter parity [198, 209, 225–228]. At the same time this symmetry is convenient in order to forbid the proton to decay too fast by baryon and lepton number violating SUSY vertices leading to $p \to l^+\pi^0$. The R-parity quantum number is given as $P_R = (-1)^{3(B-L)+2s}$ so that for all SM particles it follows $P_R = +1$ and for all SUSY partner particles $P_R = -1$. If P_R is conserved, a direct consequence is that the lightest SUSY particle (LSP) cannot decay further and is an obvious dark matter candidate [229, 230]. A typical dark matter candidate in R-parity conserving SUSY is the lightest neutralino. Alternatively, it is also possible that the gravitino takes this role, especially in case of gauge-mediated SUSY breaking [186]. One can also construct viable SUSY models with R-parity violation [231–236]. In this case, the gravitino can also serve as a dark matter candidate [237, 238]. Other options are then given by the axion [239] or its SUSY partner particle, the axino [240].

Soft SUSY Breaking and (S)particle Content of the MSSM

In order to break SUSY there are different approaches proposed in the literature. Examples are minimal supergravity (mSUGRA), gauge mediation and anomaly mediation, for details and further references see [186]. As the breaking mechanism of SUSY is not known, it is convenient to parametrize our lack of knowledge in form of explicit SUSY-breaking terms in the Lagrangian. Modifying SUSY in this way by hand one has to be careful to still ensure the stability of the quantum corrections to the scalar masses, especially to the Higgs mass in order to not reintroduce the fine-tuning whose abolishment is one of the main motivations to introduce low-scale SUSY. Terms fulfilling this criterion

are called *soft* in contrast to *hard* breaking which leads again to too strong divergencies. The property of soft SUSY breaking can be uniquely determined in a formal way, especially excluding operators like $\phi\psi\psi$ with mass dimension ≥ 4. [209, 210, 241, 242]. The explicit soft SUSY-breaking terms form then an effective theory for the spontaneous breaking of SUSY. Especially due to the soft terms the MSSM ends up with a total of ~124 parameters [243, 244]. The soft breaking terms constitute many new sources of flavor violation in SUSY. As SUSY itself does not say anything about the flavor violation in SUSY breaking, SUSY flavor violation is generically large. On the other hand, the flavor-changing neutral current (FCNC) data partly drastically constrains the SUSY flavor violation, so that one needs a non-generic structure [245]. A very interesting example for such constraints will be given in Ch. 3. FCNC bounds lead to the so-called SUSY flavor problem.

The matter content of the MSSM is organized in chiral and vector supermultiplets (ϕ, ψ, F) and (V, λ, D), respectively. The fields in the multiplets are scalars ϕ, fermions ψ, vector gauge bosons V, gauginos λ and auxiliary scalar fields F and D. Following [246] we write the Lagrangian of the MSSM as

$$\mathcal{L} = \mathcal{L}_{\text{SUSY}} + \mathcal{L}_{\text{soft}}\,, \tag{2.71}$$

with [246]

$$\begin{aligned}\mathcal{L}_{\text{SUSY}} = &-\frac{1}{4}\left(F_G^A\right)^{\mu\nu}\left(F_G^A\right)_{\mu\nu} + \overline{\lambda_G^A} i\not{D}_{AB}\lambda_G^B + \left(D^\mu\phi\right)^\dagger\left(D_\mu\phi\right) + \bar{\psi} i\not{D}\psi \\ &-\left[\left(\frac{\mathrm{d}W}{\mathrm{d}\Phi_i}\right)^*\left(\frac{\mathrm{d}W}{\mathrm{d}\Phi_i}\right) + \frac{1}{2}\left(\frac{\partial^2 W}{\partial\Phi_i\partial\Phi_j}\psi_i^T C\psi_j + \text{h.c}\right)\right]_{\Phi\to\phi} \\ &\quad - \sqrt{2}g_G\left[\phi^\dagger T_G^A\left(\lambda_G^A\right)^T C\psi + \text{h.c.}\right] - \frac{1}{2}g_G^2\left(\phi^\dagger T_G^A\phi\right)\left(\phi^\dagger T_G^A\phi\right)\,,\end{aligned} \tag{2.72}$$

and the superpotential

$$W = \mu H_1 H_2 + Y_{ij}^U Q_i U_j^c H_2 + Y_{ij}^D Q_i D_j^c H_1 + Y_{ij}^E L_i E_j^c H_1. \tag{2.73}$$

The additional soft breaking terms are given as [246]

$$\begin{aligned}\mathcal{L}_{\text{soft}} = &-\frac{1}{2}\left(m_{\tilde{g}}\tilde{g}^{a\,T} C\tilde{g}^a + m_{\tilde{W}}\tilde{W}^{iT} C\tilde{W}^i + m_{\tilde{B}}\tilde{B}^T C\tilde{B} + \text{h.c.}\right) \\ &- m_1^2 h_1^\dagger h_1 - m_2^2 h_2^\dagger h_2 - \tilde{q}_i^\dagger\left(M_{\tilde{q}}^2\right)_{ij}\tilde{q}_j - \tilde{u}_i^{c\dagger}\left(M_{\tilde{u}^c}^2\right)_{ij}\tilde{u}_j^c - \tilde{d}_i^{c\dagger}\left(M_{\tilde{d}^c}^2\right)_{ij}\tilde{d}_j^c \\ &- \tilde{l}_i^\dagger\left(M_{\tilde{l}}^2\right)_{ij}\tilde{l}_j - \tilde{e}_i^{c\dagger}\left(M_{\tilde{e}^c}^2\right)_{ij}\tilde{e}_j^c \\ &\quad + \left(A_{ij}^U\tilde{q}_i\tilde{u}_j^c h_2 + A_{ij}^D\tilde{q}_i\tilde{d}_j^c h_1 + A_{ij}^E\tilde{l}_i\tilde{e}_j^c h_1 + B\mu h_1 h_2 + \text{h.c.}\right).\end{aligned} \tag{2.74}$$

The particle content encoded in Eqs. (2.71)-(2.74) is given as follows below, using the generation index i.

- Members of **chiral superfields** $Q_i, U_i^c, D_i^c, L_i, E_i^c, H_1, H_2$
  (1 chiral superfield for each SM fermion and 2 Higgs chiral superfields)

  - **Fermions** (spin 1/2)
    - Left- and right-handed quarks: $q_i = (u_i, d_i)^{\mathrm{T}}$, u_i^c, d_i^c with quantum numbers $(\mathbf{3}, \mathbf{2}, 1/6)$.
    - Left- and right-handed leptons: $l_i = (\nu_i, e_i)^{\mathrm{T}}$, e_i^c with quantum numbers $(\mathbf{1}, \mathbf{2}, -1/2)$
    - 2 Higgsino doublets: $\tilde{h}_1 = (\tilde{h}_1^0, \tilde{h}_1^-)$ and $\tilde{h}_2 = (\tilde{h}_2^+, \tilde{h}_2^0)$ with quantum numbers $(\mathbf{1}, \mathbf{2}, 1/2)$ and $(\mathbf{1}, \mathbf{2}, -1/2)$, respectively.
  - **Scalars** (spin 0) (with quantum numbers as their corresponding supermultiplet-partners)
    - Squarks with left- and right-handed degrees of freedom (*dof*): $\tilde{q}_i = \left(\tilde{u}_i, \tilde{d}_i\right)^{\mathrm{T}}$, $\tilde{u}_i^c$, $\tilde{d}_i^c$.
    - Sleptons with left- and right-handed *dof*: $\tilde{l}_i = (\tilde{\nu}_i, \tilde{e}_i)^{\mathrm{T}}$, $\tilde{e}_i^c$.
    - 2 Higgs doublets: $h_1 = (h_1^{0*}, -h_1^-)$ and $h_2 = (h_2^+, h_2^0)$ 8 *dof* $\Rightarrow$ 3 Goldstone bosons G^0, $G^\pm$ plus 5 physical Higgs fields: h^0, H^0 (neutral, CP-even), A^0 (neutral, CP-odd), $H^\pm$ (charged)

- Members of **vector gauge superfields** V_g^a, V_W^k, V_B (1 vector superfield for each SM gauge boson)
  - **Vector Bosons** (spin 1)
    - Gluons $(\mathbf{8}, \mathbf{1}, 0)$, B^0 boson $(\mathbf{1}, \mathbf{1}, 0)$ and $W^\pm$,W^0 bosons $(\mathbf{1}, \mathbf{3}, 0)$
  - **Gauginos** (spin 1/2) (with quantum numbers as their corresponding supermultiplet-partners)
    - Gluinos $\tilde{g}^a$, bino $\tilde{B}^0$ and winos $\tilde{W}^\pm$, $\tilde{W}^0$

Among the particles manifold mixing takes place: Similarly to the mixing of the SM fields B^0 and W^0 to γ and Z during electroweak symmetry breaking we have also mixing between gauginos and higgsinos:

- Mixing of charged gauginos $\tilde{W}^\pm$ with charged higgsinos $\tilde{h}_1^-$, $\tilde{h}_2^+$ $\Rightarrow$ 2 charginos $\tilde{\chi}^\pm$
- Mixing of neutral gauginos $\tilde{B}^0$, $\tilde{W}^0$ with neutral higgsinos $\tilde{h}_1^0$, $\tilde{h}_2^0$ $\Rightarrow$ 4 neutralinos $\tilde{\chi}^0$

The mass matrix of the charginos can be written as

$$M_{\tilde{\chi}^\pm} = \begin{pmatrix} M_2 & \sqrt{2} m_W \sin\beta \\ \sqrt{2} m_W \cos\beta & \mu \end{pmatrix}. \tag{2.75}$$

As this matrix is neither symmetric nor hermitian in order to diagonalize it one has to perform a general singular value decomposition (SVD) with two different unitary matrices U and V:

$$U^* M_{\tilde{\chi}^\pm} V^\dagger = \mathrm{diag}(m_{\tilde{\chi}_1}, m_{\tilde{\chi}_2}). \tag{2.76}$$

We implement the analytic expressions for a SVD of a 2×2 matrix according to Appendix A of [247]. The part of the Lagrangian that is relevant for $b \to s$ transitions via gluino and chargino interactions can be found in the mass eigenstate basis in [246]. For a complete list of Feynman rules that follow from the MSSM-Lagrangian, see Refs. [248, 249].

For each chirality of a quark there is a scalar partner squark. Consequently there are six up and six down squarks, which also mix with themselves, respectively. The mass matrices of the squarks are therefore 6×6 matrices that are in general not diagonal. A parametrization using the so called "mass insertion parameters" is given in Ch. 3.

The Higgs sector of the MSSM consists of a two Higgs doublet model. The ratio of the two different vevs is measured by $\tan\beta = v_2/v_1$, where $\langle h_1^0 \rangle = v_1/\sqrt{2}$ and $\langle h_2^0 \rangle = v_2/\sqrt{2}$. For their sum we have

$$v_1^2 + v_2^2 = v^2 \sim (246\,\mathrm{GeV})^2\,. \tag{2.77}$$

At tree level the masses of the lightest physical Higgs is given as [186]

$$m^2_{h^0,H^0} = \frac{1}{2}\left(m^2_{A^0} + m_Z^2 \mp \sqrt{(m^2_{A^0} - m_Z^2)^2 + 4 m_Z^2 m^2_{A^0} \sin^2(2\beta)}\right). \tag{2.78}$$

Note that in the so called "decoupling limit", *i.e.*, in the case $m_{A^0} \gg m_Z$, Eq. (2.78) means that at tree level it is $m^2_{h^0} \sim m_Z^2 \cos^2(2\beta)$ [186]. Clearly, in view of the measured Higgs mass, if interpreted within the MSSM, quantum corrections are necessary at any rate in order to get a realistic Higgs mass. Indeed, it turns out that the one- and two-loop corrections are so large that the Higgs mass can be lifted into the physical region. In order to take this effect into account we use the software `FeynHiggs` [250–254], see Ch. 3.

In mSUGRA or the Constrained Minimal Supersymmetric Standard Model (CMSSM) the number of parameters is reduced (quite ad hoc) from the mentioned 124 to only five, specified at the GUT scale. These are given as a unified scalar mass m_0, a unified gaugino mass $m_{1/2}$, a common trilinear coupling A_0 as well as $\tan\beta$ and $\mathrm{sgn}(\mu)$.

SUSY Problems

Although there are many motivations for SUSY there are also several problems that have to be addressed in SUSY model building. There are problems that result from the experimental situation, *i.e.*, we have not found any SUSY signal yet, as well as inherent theoretical issues. An example is the SUSY flavor problem. It originates from the bounds from

FCNCs and additionally also from the requirement of a (meta)stable vacuum [255, 256]. These problems have to be solved by a dedicated model of SUSY breaking.
Furthermore, in simplified models the mass spectrum of SUSY keeps to be pushed up by the results from the LHC [257–264]. The χ^2/dof of global CMSSM fits gets larger taking into account current data, especially also the measured value of the Higgs mass [52, 53, 265]. For the latter quite large A terms are needed. The direct searches cannot exclude SUSY as a whole. However, without a signal at some point SUSY will not solve the hierarchy problem any more. This would remove one of the strongest arguments in favor of SUSY, besides its mathematical elegance. Of course such a situation has by far not yet arrived. But there emerges a "little hierarchy problem" [266–268] if SUSY is broken too much, because one then has to reintroduce some fine tuning in order to get a Higgs mass at the electroweak scale. In extensions of the MSSM this problem can be alleviated, see recently *e.g.* [269, 270].
Another problem is for example to find an explanation for why the higgsino mass parameter μ is of the same order of magnitude as the in principle physically unrelated soft masses, the so-called μ-problem [271, 272].
Continuing with possible sources of phenomenological problems, in the MSSM there are not only many additional new sources of flavor violation but also of both flavor dependent and independent CP violation. All CP phases of the MSSM can be represented in an invariant way by using trace invariants, similar to the one CP violating phase of the SM which can be expressed by the Jarlskog determinant. For the (s)quark sector of the MSSM this is done systematically in Ref. [273], for the (s)leptons in [274]. A generalization of Jarlskog's projector formalism to the MSSM and more examples are given in [275].

2.4.3. Minimal Organizing Principles of Flavor Violation

Models of Flavor and Minimal Ansätze In the literature, many attempts were made for an explanation of the origin of flavor. A promising idea in order to account for the hierarchies is to introduce an additional interaction with a "flavon" field, *e.g.* by a U(1) symmetry. Depending on the charge under the additional symmetry different flavors of quarks and leptons couple to different numbers of the flavon field. When the flavon gets a vev during spontaneous breaking of the U(1) symmetry the values of the elements of the Yukawa matrices can emerge in a natural way [276]. The flavon field itself is usually an effective theory description of heavy fermions at a higher mass scale, for a nice review see Ref. [277]. An alternative is the use of discrete horizontal symmetries [278, 279]. Using the discrete group $\Delta(27)$ one can also account for the CP violating phase of the CKM matrix [280, 281].
A very interesting approach to an organizing principle of flavor is a gauge theory of flavor, as recently considered in Refs. [282–287]. It is an intriguing idea that the gauge principle that is so successful in describing the fundamental interactions could also be the key to flavor.
Regarding models beyond the SM, a *minimal* ansatz for the flavor structure of NP models is the general idea that they could be the same or proportional to the flavor structure known

in the SM. This idea is commonly denoted by Minimal Flavor Violation (MFV) [242, 288–291]. However, the concrete implementation and meaning of this concept varies in the literature.
The most intriguing way in order to implement the minimality principle into a theory is the group theoretic way proposed in Ref. [290]. Here one formally demands invariance under the flavor symmetry group G_F of the SM, see Eq. (2.14). This feature is provided by postulating that the Yukawa matrices of the SM are spurions with nontrivial representations under G_F. Specifically, one uses the assignments

$$Y_u : (\mathbf{3}, \bar{\mathbf{3}}, \mathbf{1}) , \qquad Y_d : (\mathbf{3}, \mathbf{1}, \bar{\mathbf{3}}) \tag{2.79}$$

under the $U(3)_{Q_L} \otimes U(3)_U \otimes U(3)_D$ subgroup of G_F, so that Y_u and Y_d transform as

$$Y_u \mapsto U_L Y_u U_{u_R}^\dagger , \qquad Y_d \mapsto U_L Y_d U_{d_R}^\dagger \tag{2.80}$$

under G_F transformations. Similar expressions can be written down also for the leptons. In this way, the corresponding transformations of the fermion fields are exactly balanced, so that the Lagrangian becomes formally invariant under G_F. The vevs of the Yukawa spurions are the usual Yukawa matrices whose values remain unexplained in the framework of MFV. In the considered NP theory the Yukawa spurions are then postulated to be the only ones that may appear as generators of nontrivial flavor structures. Extended spurion sectors beyond MFV are considered in [292]. One can further differentiate between the case where the expansion in the Yukawa spurions can be truncated after the first orders or where one has to take higher orders into account, depending on the size of the b and t Yukawa couplings. Also then a (different) expansion is nevertheless possible, which is given the name "General" MFV [293]. Furthermore, G_F could be replaced by a discrete symmetry [294].
The MFV-concept is useful in quite different contexts: For example, the group theory of MFV can be used to construct natural dark matter candidates [295, 296]. Furthermore, the assumption of MFV can be used in the MSSM instead of R-parity in order to stabilize the proton [297, 298].
One can also turn the tables and see MFV just as a classification scheme for different theories. For instance, one can classify the anomaly mediated SUSY model in Ref. [299] as MFV and the hybrid gauge gravity model in [300, 301] as non-MFV.

In the MSSM with MFV, one can write the soft squared mass matrices and the trilinear couplings as [290]

$$M_{q_L}^2 = \tilde{m}^2 \left(a_1 \mathbb{1} + b_1 Y_u Y_u^\dagger + b_2 Y_d Y_d^\dagger + \dots \right) , \tag{2.81}$$

$$M_{u_R}^2 = \tilde{m}^2 \left(a_2 \mathbb{1} + b_5 Y_u^\dagger Y_u + \dots \right) , \tag{2.82}$$

$$M_{d_R}^2 = \tilde{m}^2 \left(a_3 \mathbb{1} + b_6 Y_d^\dagger Y_d + \dots \right) , \tag{2.83}$$

$$A_u = A \left(a_4 \mathbb{1} + b_7 Y_d Y_d^\dagger + \dots \right) Y_u , \tag{2.84}$$

$$A_d = A \left(a_5 \mathbb{1} + b_8 Y_u Y_u^\dagger + \dots \right) Y_d . \tag{2.85}$$

But do these expansions actually contain any implications when the coefficients a_i, b_i are arbitrary? Or are they just a way of writing the same thing in a different basis? Reformulating this question, are the SM Yukawa spurions able to account for *arbitrary* flavor structures? And if this is the case, which unique "if-and-only-if" property does guarantee this?

Digression into Matrix Algebra The question if two spurions (from the SM or also NP ones) can account for arbitrary flavor structures can be translated into a mathematical one: "When do two matrices generate the algebra of 3×3 matrices $M_3(\mathbb{C})$?" The latter question is answered in the mathematical literature: Using Shemesh's Theorem [302] the following is found in Ref. [303]:

1. *"The two* 3×3 *matrices A and B generate* M_3 *if and only if both* $\sum_{k,l=1}^{2} \left[A^k, B^l\right]^* \left[A^k, B^l\right]$ *and* $\sum_{k,l=1}^{2} \left[A^k, B^l\right] \left[A^k, B^l\right]^*$ *are invertible."*[1]
2. *"Let* $A, B \in M_2$*. A and B generate* M_2 *if and only if* $[A, B]$ *is invertible."*
3. *"Let* $A,\ B \in M_3$*. If* $[A, B]$ *is invertible, then A and B generate* M_3*."*
4. *"Let* $A,\ B \in M_3$*. Then*

$$\begin{aligned} &\det\left(I, A, A^2, B, B^2, AB, BA, [A, [A, B]], [B, [B, A]]\right) \\ &= 9 \det [A, B]\ H([A, B]), \end{aligned} \tag{2.86}$$

so if $\det [A, B] \neq 0$ *and* $H([A, B]) \neq 0$*, then*

$$\left\{I, A, A^2, B, B^2, AB, BA, [A, [A, B]], [B, [B, A]]\right\} \tag{2.87}$$

form a basis for M_3*."*

Here, it is $H(M) = \frac{1}{2}\left((\mathrm{Tr}M)^2 - \mathrm{Tr}(M^2)\right)$. For hermitian matrices A and B the first item means that the necessary and sufficient condition for two hermitian flavor structures in order to generate arbitrary flavor structures is given as

$$\det\left([A, B]^2 + \left[A^2, B\right]^2 + \left[A, B^2\right]^2 + \left[A^2, B^2\right]^2\right) \neq 0. \tag{2.88}$$

From such hermitian matrices one can also make up a basis of the 3×3 hermitian matrices as a real vector space. Setting $A = U = Y_u Y_u^\dagger$ and $B = D = Y_d Y_d^\dagger$ with the SM Yukawa matrices such a basis can be easily obtained from the basis given in Eq. (2.87). Firstly, we replace DU by $UD + DU$ which does not change the determinant of the 9×9 matrix. Then we replace $UD \mapsto 2i\,UD$ which changes the determinant in Eq. (2.86) to $18i \det [U, D]\ H([U, D])$. Then $2iUD$ is replaced by

$$2iUD \mapsto 2iUD - i\{U, D\} = i[U, D], \tag{2.89}$$

which again does not change the determinant. We arrive then at the basis

$$\left\{\mathbb{1}, U, U^2, D, D^2, \{U, D\}, i[U, D], [U, [U, D]], [D, [D, U]]\right\}. \tag{2.90}$$

[1] The " * " here means complex conjugation and transposition.

Implications of the Matrix Algebra Results for the MFV Expansion What do the theorems of the previous paragraph mean for the MFV expansion? In our interpretation the first two theorems are if-and-only-if criteria, while the third is an if-then statement for the ability to account for arbitrary flavor structures with the SM Yukawa matrices. The latter also agrees with the observation in [304, 305] that this is possible thanks to the Jarlskog determinant being nonzero, *i.e.*, that the SM violates CP.
Here, we want to point out that from the general theorems in [303] we learn that the relation between being able to account for arbitrary flavor structures and CP violation is *not* compulsory. One could in principle also account for arbitrary flavor structures without CP violation as the non-vanishing of the Jarlskog determinant is not contained in the "if-and-only-if" criterion.

Altogether, the Eqs. (2.81)-(2.85) are nothing more than a mere reparametrization as long as one does not demand that the a_i and b_i are natural $O(1)$ parameters [304–307]. The SM Yukawa matrices can account for arbitrary flavor structures at the price of fine-tuned coefficients, a feature which one can use in order to classify NP flavor structures in a geometrical way by projecting given spurions on them [155, 156, 297, 304–307]. As was shown in Refs. [155, 156, 305] one can construct even a metric of flavor space using the Yukawa spurions, obtaining an abstract geometry of flavor.[2] The coordinate system given by the Yukawa matrices can in this way be used as an ordering principle for easier identifying non-SM flavor structures.

[2]Note that speaking of "flavor geometry" is here only meant in an abstract sense, not in the sense of extra space dimensions in Minkowski space.

3. Precision Probes of SUSY Flavor Violation from $\bar{B} \to \bar{K}^{(*)} l^+ l^-$

In this chapter we come to the first application of the general ideas that were developed in Ch. 2. From data on rare exclusive semileptonic decays $\bar{B} \to \bar{K}^{(*)} l^+ l^-$ we derive constraints on SUSY flavor violation. Parts of the results presented here were recently published also in Refs. [308, 309]. In the first section we review observables of the angular analysis of $\bar{B} \to \bar{K}^{(*)} l^+ l^-$.

3.1. Observables of the Angular Analysis of $\bar{B} \to \bar{K}^{(*)} l^+ l^-$

Being a multi-body decay with a vector meson in the final state, $\bar{B} \to \bar{K}^*(\to \bar{K}\pi) l^+ l^-$ possesses a multitude of observables. These depend not only on different angles defined below after Eq. (3.2) but also especially on the invariant mass squared q^2 of the final state lepton pair. The latter is a key variable for both $\bar{B} \to \bar{K}^* l^+ l^-$ and $\bar{B} \to \bar{K} l^+ l^-$ because depending on q^2 different approaches from the theory side have to be taken in order to handle the hadronic effects. At small q^2 the $\bar{K}^{(*)}$ has a large hadronic recoil, *i.e.*, the energy of the $\bar{K}^{(*)}$ is large in the $\bar{B}$ rest frame compared to the scale of QCD. In this case one can apply QCDF [310–314]. For high q^2 on the other side of the spectrum the energy of the $\bar{K}^{(*)}$, having now only a small recoil, is of the order of the scale of QCD. Here a technique different from QCDF is needed. As worked out in Refs. [315, 316] one can make here an operator product expansion (OPE) in $1/Q$, with $Q = \{m_b, \sqrt{q^2}\}$.
The fully differential decay width of semileptonic $\bar{B}$ decays with a $\bar{K}^*$ in the final state decaying on-shell to $\bar{K}\pi$ can be written as [317–320]

$$\frac{\mathrm{d}^4\Gamma(\bar{B} \to \bar{K}^* l^+ l^-)}{\mathrm{d}q^2 \, \mathrm{d}\cos\theta_l \, \mathrm{d}\cos\theta_K \, \mathrm{d}\phi} = \frac{3}{8\pi} J(q^2, \cos\theta_l, \cos\theta_K, \phi). \tag{3.1}$$

The function $J(q^2, \cos\theta_l, \cos\theta_K, \phi)$ depends in general on 12 observables $J_i^{(a)}(q^2)$ that are functions of the invariant mass q^2 of the lepton pair only. It can be written as [321]

$$\begin{aligned} J(q^2, \cos\theta_l, \cos\theta_K, \phi) &= \Big(J_{1s}(q^2) + J_{2s}(q^2)\cos 2\theta_l + J_{6s}(q^2)\cos\theta_l\Big)\sin^2\theta_K \\ &+ \Big(J_{1c}(q^2) + J_{2c}(q^2)\cos 2\theta_l + J_{6c}(q^2)\cos\theta_l\Big)\cos^2\theta_K \\ &+ \Big(J_3(q^2)\cos 2\phi + J_9(q^2)\sin 2\phi\Big)\sin^2\theta_K \sin^2\theta_l \\ &+ \Big(J_4(q^2)\cos\phi + J_8(q^2)\sin\phi\Big)\sin 2\theta_K \sin 2\theta_l \\ &+ \Big(J_5(q^2)\cos\phi + J_7(q^2)\sin\phi\Big)\sin 2\theta_K \sin\theta_l. \end{aligned} \tag{3.2}$$

The angles in Eq. (3.2) are defined as follows:

- $\theta_l = \angle(l^-, \bar{B})$ in lepton pair rest frame.
- $\theta_K = \angle(\bar{K}, \bar{B})$ in $\bar{K}\pi$ rest frame.
- $\phi = \angle$(normal of $\bar{K}\pi$ plane, normal of l^+l^- plane).

The angle between the direction of two particles X and Y is here denoted as $\angle(X, Y)$. The ultimate goal of an experimental analysis of $\bar{B} \to \bar{K}^* l^+ l^-$ is the complete measurement of all the observables $J_i^{(a)}(q^2)$, which is equivalent to a full angular analysis. However, a drawback of the $J_i^{(a)}(q^2)$ is their proportionality to hadronic matrix elements which constitute large theoretical uncertainties. In general, one can write the measured observables as functions of combinations of several $J_i^{(a)}(q^2)$, especially also ratios of them. Exactly here lies the very chance that is given in exploiting the data on observables from the angular analysis: In ratios and clever algebraic combinations of the $J_i^{(a)}(q^2)$, *i.e.*, in "optimized observables" [78, 317, 321–328], there is a reduced or even vanishing dependence on the form factors, which typically dominate the theoretical uncertainty. On the other hand one can also form combinations where in limited kinematic regions the short distance physics cancels out and one can vice versa access the ratios of form factors only. The latter will be further discussed and utilized in Ch. 4. This way one can make much progress in precision compared for example to observables as $\mathrm{d}\mathcal{B}/\,\mathrm{d}q^2$, where the largest error of the theory prediction comes exactly from the form factors. This is a general problem of exclusive meson decays.

It turns out that it is very convenient to express the $J_i^{(a)}(q^2)$ by transversity amplitudes $A_{\perp,\parallel,0}^{L,R}$ [317]. This is especially true at high q^2 because in this kinematic region the transversity amplitudes show a universal short distance behavior [78] that we will further discuss in Ch. 4. In the notation "$A_{\perp,\parallel,0}^{L,R}$" the superscript (L, R) indicates the chirality of the lepton current and the subscript $(\perp, \parallel, 0)$ characterizes the final state angular momentum. The latter can intuitively be constructed by examining the polarization vector of the K^* and the intermediate Z boson, as is explicated in Ref. [319]. Additionally, there is a transversity amplitude A_t that corresponds to a timelike vector boson and only contributes in case of taking $m_l \neq 0$ into account [317]. In the most general case, beyond the SM basis, where also tensor operators are taken into account, there appear six additional transversity amplitudes [321]. Another approach using only helicity amplitudes is given in [329]. The expression of all the $J_i(q^2)$ in transversity amplitudes can be found in [321].

Among the observables that are in the center of interest of the current experimental analysis of $\bar{B} \to \bar{K}^* l^+ l^-$ are the following [78, 321]:

- Differential decay width $\mathrm{d}\Gamma(\bar{B} \to \bar{K}^* l^+ l^-)/\,\mathrm{d}q^2$.
- Lepton pair forward-backward asymmetry

$$A_{\mathrm{FB}} = \frac{1}{\mathrm{d}\Gamma/\,\mathrm{d}q^2}\left(J_{6s} + \frac{1}{2}J_{6c}\right) = \left(\int_0^1 - \int_{-1}^0\right) \mathrm{d}\cos\theta_l \, \frac{\mathrm{d}^2\Gamma}{\mathrm{d}q^2\,\mathrm{d}\cos\theta_l}\Big/\frac{\mathrm{d}\Gamma}{\mathrm{d}q^2}\,. \quad (3.3)$$

  In the SM operator basis A_{FB} is related to the Wilson coefficients of the effective theory as [78]

$$A_{\mathrm{FB}} \propto \mathrm{Re}\left(\left(C_9^{\mathrm{eff}} + \kappa\frac{2m_b m_B}{q^2}C_7^{\mathrm{eff}}\right)C_{10}^*\right), \quad (3.4)$$

  with C_7^{eff} and C_9^{eff} as defined in [78] and $\kappa = 1 - 2\frac{\alpha_s}{3\pi}\log\left(\frac{\mu}{m_b}\right) + O(\alpha_s^2)$ [315]. A special feature of Eq. (3.4) is that depending on the values of C_9^{eff} and C_7^{eff}, *i.e.*, the short distance physics, A_{FB} could have a zero at a specific value of q^2.
- Fraction of longitudinal polarized K^* mesons

$$F_L = \frac{1}{\mathrm{d}\Gamma/\,\mathrm{d}q^2}\left(J_{1c} - \frac{1}{3}J_{2c}\right) = \frac{|A_0^L|^2 + |A_0^R|^2}{\Sigma_{X=L,R}\left(|A_0^X|^2 + |A_\perp^X|^2 + |A_\parallel|^2\right)}\,. \quad (3.5)$$

- Transverse asymmetry

$$A_T^{(2)} = \frac{1}{2}\frac{J_3}{J_{2s}} = \frac{|A_\perp^L|^2 + |A_\perp^R|^2 - |A_\parallel^L|^2 - |A_\parallel^R|^2}{|A_\perp^L|^2 + |A_\perp^R|^2 + |A_\parallel^L|^2 + |A_\parallel^R|^2}\,. \quad (3.6)$$

  In the literature it is also used the corresponding observable S_3 [319, 330, 331] to that $A_T^{(2)}$ is related via

$$S_3 = \frac{1}{2}(1 - F_L)A_T^{(2)}. \quad (3.7)$$

Additionally, also the CP asymmetry A_{CP} between decays $\bar{B}^0 \to \bar{K}^{*0}\mu^+\mu^-$ and $B^0 \to K^{*0}\mu^+\mu^-$ is measured [332].

Note that the measurement of A_{FB} can be defined just by "counting negatively charged muons": In the lepton pair rest frame A_{FB} is equal to the difference between the number of leptons with negative charge that go forward or backward relative to the $\bar{B}$, respectively, normalized to their total number.
It turns out that the zero of the forward-backward asymmetry, *i.e.* the point q_0^2 with $A_{\mathrm{FB}}(q_0^2) = 0$ is an especially clean observable in order to test the short distance physics

encoded in the Wilson coefficients in Eq. (3.4). The zero depends in the large energy limit almost completely on these Wilson coefficients only, besides m_b and m_{K^*} [313, 333–335]. Uncertainties due to form factors arise not before next to leading order (NLO). Consequently, the prediction of q_0^2 is quite precise in the SM, it is given as [184, 314, 336]

$$\left(q_0^2\right)^{\text{SM}} = (4.0 \pm 0.3)\,\text{GeV}. \tag{3.8}$$

In the angular analysis of $\bar{B} \to \bar{K}^{*0}\mu^+\mu^-$ by the LHCb experiment [330, 331, 337, 338] the zero point of A_{FB} has been determined as [331]

$$\left(q_0^2\right)^{\text{exp}} = (4.9 \pm 0.9)\,\text{GeV}^2\,, \tag{3.9}$$

which agrees well with the SM value in Eq. (3.8). Especially, as a consequence of Eq. (3.9) the zero crossing indeed *exists*, which can already exclude several NP models, see *e.g.* Ref. [339].

The fully differential decay width of $\bar{B} \to \bar{K} l^+ l^-$ decays – with a pseudoscalar in the final state – is simpler than the one of $\bar{B} \to \bar{K}^* l^+ l^-$ in Eq. (3.1). It depends besides q^2 on only one angle and reads [340]

$$\frac{\mathrm{d}^2\Gamma(\bar{B} \to \bar{K} l^+ l^-)}{\mathrm{d}q^2\,\mathrm{d}\cos\theta} = a_l(q^2) + b_l(q^2)\cos\theta + c_l(q^2)\cos^2\theta\,, \tag{3.10}$$

with the three q^2-dependent coefficients $a_l(q^2)$, $b_l(q^2)$, $c_l(q^2)$ as given in [340]. The angle is given as $\theta = \angle(\bar{B}, l^-)$ in the rest frame of the lepton pair. Integrating over q^2, from Eq. (3.10) one obtains the angular distribution [340]

$$\frac{1}{\Gamma}\frac{\mathrm{d}\Gamma}{\mathrm{d}\cos\theta} = \frac{3}{4}(1 - F_H)(1 - \cos^2\theta) + \frac{1}{2}F_H + A_{\text{FB}}\cos\theta\,, \tag{3.11}$$

with the forward-backward asymmetry A_{FB} of $\bar{B} \to \bar{K} l^+ l^-$ decays and a flat contribution to the angular distribution, F_H. Note that the SM predicts $A_{\text{FB}}(q^2) \equiv 0$ for the whole q^2 region of $\bar{B} \to \bar{K} l^+ l^-$ up to very small corrections from QED [340]. F_H has a nontrivial dependence on q^2 but is also predicted to be quite small, consistent with the experiment [341].

Model independent analyses of $\bar{B} \to \bar{K}^{(*)} l^+ l^-$ observables and their impact on the short distance physics – parametrized by the Wilson coefficients – have been given in [78, 182–184, 321, 322]. As discussed further in Sec. 3.2, the semileptonic decays of $\bar{B}$ mesons constrain especially the Wilson coefficients of 4-Fermi operators C_9 and C_{10}. The Wilson coefficient of the electromagnetic dipole operator C_7 is constrained heavily from $b \to s\gamma$. We analyze the consequences of these model independent bounds on a specific model, namely the MSSM, that was introduced in Sec. 2.4.2. In order to do so, we use the model independent bounds obtained in [184] taking into account recent data presented in [337, 342].

3.2. Comparison of SUSY Predictions with Data

Firstly, we compare the SUSY predictions with data by studying the spread of SUSY models in the planes of the effective couplings. Then we present improved bounds on squark flavor, specifically the scharm-stop left-right mixing. The bounds have then consequences for SUSY model building and implications for rare top decays.

3.2.1. NP Contributions in the Effective Field Theory Picture

NP Modification of Wilson Coefficients The inevitable tool for the analysis of FCNCs is the effective field theory mechanism that was introduced in Sec. 2.4.1. In the effective $|\Delta B| = |\Delta S| = 1$ Hamiltonian

$$\mathcal{H}_{\text{eff}} = -\frac{4G_F}{\sqrt{2}} V_{tb} V_{ts}^* \sum_i C_i(\mu) O_i(\mu) + \text{h.c.}\,, \tag{3.12}$$

the most important operators for the semileptonic process $b \to s l^+ l^-$ are

$$O_7 = \frac{e}{16\pi^2} m_b \left(\bar{s}_L \sigma_{\mu\nu} b_R\right) F^{\mu\nu}\,, \qquad O_9 = \frac{e^2}{16\pi^2} \left(\bar{s}_L \gamma_\mu b_L\right)\left(\bar{l}\gamma^\mu l\right)\,, \tag{3.13}$$

$$O_{10} = \frac{e^2}{16\pi^2} \left(\bar{s}_L \gamma_\mu b_L\right)\left(\bar{l}\gamma^\mu \gamma_5 l\right). \tag{3.14}$$

In Eq. (3.12) the heavy particles are integrated out and can be found in the expressions for the couplings of the lighter fields only, *i.e.*, in the Wilson coefficients C_i.

In a NP model like SUSY in general not only the Wilson coefficients C_i are modified but also additional operators O_i beyond the SM basis appear. We neglect the operators $O'_{7,9,10}$ which are defined by flipping the chirality in Eqs. (3.13) and (3.14). Their contribution is relatively to them suppressed by m_s/m_b in the SM and MFV SUSY. The latter also holds beyond MFV for the chargino contributions, on that we concentrate here, as will be explained further below in the discussion of different contributions to squark flavor violation. Therefore, we only look at operators including $b_L \to s_L$ and $b_R \to s_L$ transitions here.

Furthermore, we concentrate on low $\tan\beta \lesssim 15$ and can thus neglect the additional scalar operators that could otherwise play an important role [343]. The latter is especially justified having in mind the recent measurement of $\mathcal{B}(B_s \to \mu^+\mu^-)$ [47]. If there were indeed large scalar operators the deviations of its SM value would have been bigger. Consequently, in the part of the parameter space we look at we can confidently stay in the SM operator basis. Switching on SUSY corresponds then to additional contributions to the Wilson coefficients only:

$$C_i \Rightarrow C_i^{\text{SM}} + C_i^{\text{NP}}, \quad \text{here: } i = 7, 9, 10. \tag{3.15}$$

m_t^{pole}	173.3 GeV	[344]
$m_b(m_b)$	4.19 GeV	[345]
m_W	80.399 GeV	[345]
m_Z	91.1876 GeV	[345]
$\alpha_s(m_Z)$	0.1184	[345]
s_W^2	0.23116	[345]

Table 3.1.: Numerical input parameters used for the evaluation of the Wilson coefficients. Table taken from [308].

The two loop results for the SM contributions are given in Ref. [181]. The one loop MSSM results are calculated in Ref. [246]. The MSSM contribution to the other Wilson coefficients $C_{1,\dots,6}$ can be safely neglected [246]. The numerical evaluation of the Wilson coefficients is performed with our MSSM extension of the `EOS` code [346]. For the numerical analysis we use the input values as given in Table 3.1. For the SM values of the Wilson coefficients we obtain, after the renormalization group (RG) running, at the scale $\mu_b = 4.2$ GeV

$$C_7^{\text{SM}}(\mu_b) = -0.33\,, \qquad C_9^{\text{SM}}(\mu_b) = 4.27\,, \qquad C_{10}^{\text{SM}}(\mu_b) = -4.15. \tag{3.16}$$

The MSSM contributions come from different particles in the quantum corrections shown in Fig. 3.1. According to the beyond-SM particles in the loop the different contributions fall into the categories:

- Charged Higgs diagrams
- Chargino diagrams
- Neutralino diagrams
- Gluino diagrams

Charged Higgses, charginos and neutralinos appear in box, penguin and self-energy topologies. Gluinos occur in penguin and self-energy diagrams only because they do not couple directly to (s)leptons. Of these categories only the charged Higgs contributions do not depend on squark flavor. The contributions from chargino, neutralino and gluino diagrams all depend on both the sparticle masses as well as on the unitary matrices that diagonalize the squark mass matrices. The neutralino and gluino contributions both come with off-diagonal elements of the down squark mass matrix. The neutralino contribution with its weak coupling is negligible compared to the one from the gluinos which comes with the

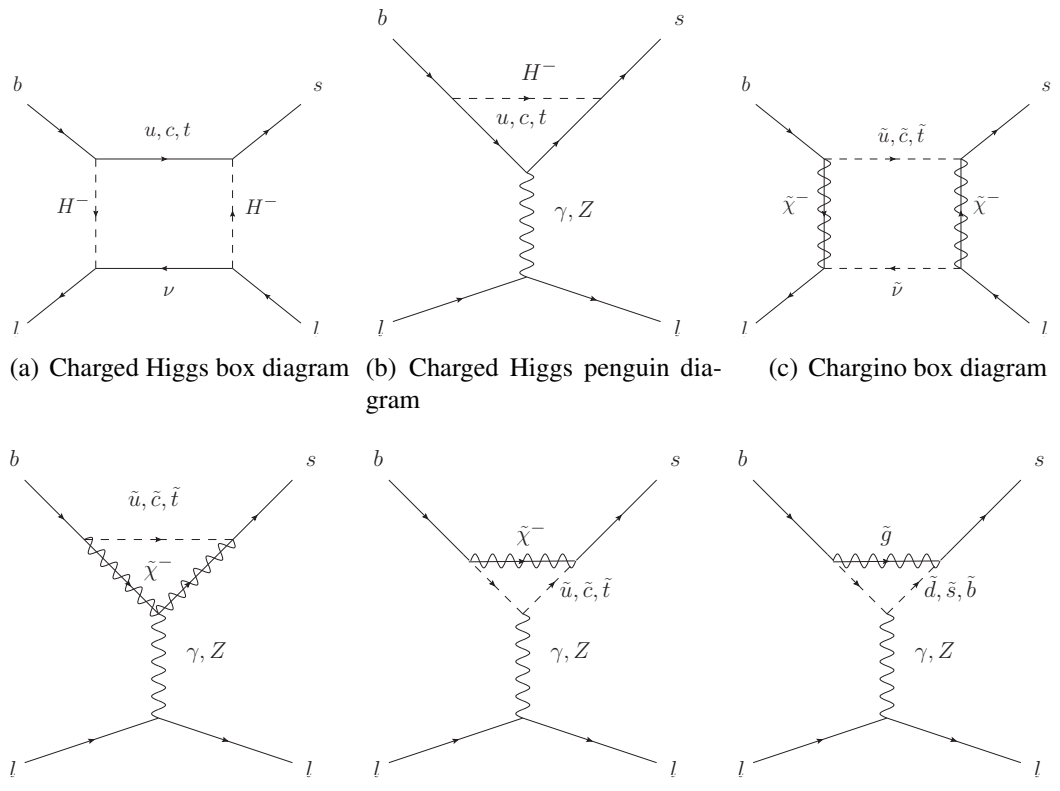

(a) Charged Higgs box diagram (b) Charged Higgs penguin diagram (c) Chargino box diagram

(d) Chargino penguin diagram I (e) Chargino penguin diagram II (f) Gluino penguin diagram

Figure 3.1.: Example Feynman diagrams for $b \to s l^+ l^-$ in the MSSM. For a complete list including self-energy diagrams see Ref. [246].

strong coupling constant. Therefore, the neutralino contribution is not further considered here. In Fig. 3.2 we show a general parametrization of the up squark mass matrix using so-called mass insertions $\left(\Delta^u_{ij}\right)_{AA'}$. Here i, j denote the generation index and A, A' denote the chirality (of the corresponding fermionic quark). Note that the squark mass squared matrices are hermitian, *i.e.*, $\left(\Delta^{u,d}_{ij}\right)_{AA'} = \left(\Delta^{u,d}_{ji}\right)^*_{A'A}$. An analogous matrix with the extra parameters $\left(\Delta^d_{ij}\right)_{AA'}$ is also present for the down squarks. The off-diagonal elements of the squark mass matrices can generically be of the same size as the diagonal ones, which is partially in conflict with FCNC data, as we will demonstrate also in the following. The latter constitutes the SUSY flavor problem, see Sec. 2.4.2.

Mass Insertion Approximation The (exact) one-loop contributions given in Ref. [246] can be expanded in the flavor-off diagonal elements of the squark mass matrices $\left(\Delta^{u,d}_{ij}\right)_{AA'}$ using the so called Mass Insertion Approximation (MIA)

$$C_i^{\mathrm{NP}} \approx C_i^{\mathrm{diag}} + C_i^{\mathrm{MI}}\,, \tag{3.17}$$

where C_i^{diag} only depends on the diagonal elements of the squark mass matrix and C_i^{MI} is at first order MIA linear in the $\left(\Delta^{u,d}_{ij}\right)_{AA'}$. Of course such an expansion in explicit off-

$$
\begin{array}{cc|ccc|ccc}
 & & & L & & & R & \\
 & & \tilde{u} & \tilde{c} & \tilde{t} & \tilde{u} & \tilde{c} & \tilde{t} \\
 & \tilde{u} & m^2_{\tilde{u}_L} & (\Delta^u_{12})_{LL} & (\Delta^u_{13})_{LL} & (\Delta^u_{11})_{LR} & (\Delta^u_{12})_{LR} & (\Delta^u_{13})_{LR} \\
L & \tilde{c} & (\Delta^u_{12})^*_{LL} & m^2_{\tilde{c}_L} & (\Delta^u_{23})_{LL} & (\Delta^u_{21})_{LR} & (\Delta^u_{22})_{LR} & (\Delta^u_{23})_{LR} \\
 & \tilde{t} & (\Delta^u_{13})^*_{LL} & (\Delta^u_{23})^*_{LL} & m^2_{\tilde{t}_L} & (\Delta^u_{31})_{LR} & (\Delta^u_{32})_{LR} & (\Delta^u_{33})_{LR} \\
\hline
 & \tilde{u} & & & & m^2_{\tilde{u}_R} & (\Delta^u_{12})_{RR} & (\Delta^u_{13})_{RR} \\
R & \tilde{c} & & h.c. & & (\Delta^u_{12})^*_{RR} & m^2_{\tilde{c}_R} & (\Delta^u_{23})_{RR} \\
 & \tilde{t} & & & & (\Delta^u_{13})^*_{RR} & (\Delta^u_{23})^*_{RR} & m^2_{\tilde{t}_R}
\end{array}
$$

Figure 3.2.: Parametrization of the up squark mass matrix $M^2_{\tilde{u}}$ in the super-CKM basis with mass insertions $\left(\Delta^u_{ij}\right)_{AA'}$. In $b \to s l^+ l^-$ we are especially sensitive to $(\Delta^u_{23})_{LR}$ (marked in red), see text for details.

diagonal elements is a basis dependent statement. As is common practice, we use the super-CKM basis. In this basis, before the diagonalization of the squark mass matrix the squarks are rotated using the CKM matrix in the same way as the quarks, see *e.g.* [245]. Note that in Ref. [246] the contributions to C_9^{SUSY} and C_{10}^{SUSY} are given in form of Y^{SUSY} and Z^{SUSY} functions with

$$C_9^{\text{SUSY}} = \frac{Y^{\text{SUSY}} - 4\sin^2\theta_W Z^{\text{SUSY}}}{\sin^2\theta_W}, \qquad C_{10}^{\text{SUSY}} = -\frac{Y^{\text{SUSY}}}{\sin^2\theta_W}, \tag{3.18}$$

and the Weinberg angle θ_W. For the numerical evaluation we use the exact one-loop expressions for the Wilson coefficients, diagonalizing the 6×6 squark mass matrix. But as the MIA expressions are quite instructive for an understanding of the different contributions, we derive them nevertheless from the general expressions in [246].

For that, we use the general substitution formula [347, 348]

$$X^\dagger_{ik} f(a_k) X_{kj} \overset{\text{MIA}}{=} \delta_{ij} f(a^0_i) + A^1_{ij} f(a^0_i, a^0_j) + \dots, \tag{3.19}$$

with a loop function

$$f(x, y, z_1, \dots, z_{n-2}) = \frac{f(x, z_1, \dots, z_{n-2}) - f(y, z_1, \dots, z_{n-2})}{x - y}, \tag{3.20}$$

and a unitary matrix X that diagonalizes the matrix $A = A^0 + A^1$. Here, $A^0 = \text{diag}(a^0_1, \dots, a^0_n)$ contains the diagonal elements of A. Its eigenvalues are given as $XAX^\dagger = \text{diag}(a_1, \dots, a_n)$.

Note that by a multiplication $a_k \mapsto \alpha a_k$ Eq. (3.19) changes to

$$X^{\dagger}_{ik} f(\alpha a_k) X_{kj} = \delta_{ij} f(\alpha a^0_i) + \alpha A^1_{ij} f(\alpha a^0_i, \alpha a^0_j) + \dots \tag{3.21}$$

In MIA, we apply the general expansion Eq. (3.19) to the up squark mass squared matrix $M^2_{\tilde{u}}$, *i.e.*, we set $A = M^2_{\tilde{u}}$ therein. In the notation of [246] the matrix $M^2_{\tilde{u}}$ is diagonalized by the unitary matrix Γ^U as

$$\mathrm{diag}\left(M^2_{\tilde{u}}\right) = \Gamma^U M^2_{\tilde{u}} \Gamma^{U\,\dagger}. \tag{3.22}$$

Using Eq. (3.19) we have the expansion

$$\Gamma^{U\,\dagger}_{ik} f\left(m^2_k\right) \Gamma^U_{kj} = \delta_{ij} f\left((m^0_k)^2\right) + \Delta_{ij} f\left((m^0_i)^2, (m^0_j)^2\right) + \dots\,, \tag{3.23}$$

with $i, j, k = 1, \dots, 6$. In Eq. (3.23) Δ_{ij} includes the different chirality combinations, *i.e.*, its indices combine generation and chirality degrees of freedom. Splitting the unitary matrix Γ^U as usual by chirality we write

$$\Gamma^U_{k(j=1,2,3)} = \Gamma^{U_L}_{k(J=1,2,3)}\,, \qquad \Gamma^U_{k(j=4,5,6)} = \Gamma^{U_R}_{k(J=1,2,3)}\,. \tag{3.24}$$

For instance, in the case $i = 2$ and $j = 6$ we have in Eq. (3.23)

$$\begin{aligned}\Gamma^{U\,\dagger}_{2k} f(m^2_k) \Gamma^U_{k6} &= \delta_{26} f\left((m^0_2)^2\right) + \Delta^u_{26} f\left((m^0_2)^2, (m^0_6)^2\right) + \dots = \Gamma^{U_L\,\dagger}_{2k} f(m^2_k) \Gamma^{U_R}_{k3} + \dots \\ &= (\Delta^u_{23})_{LR}\, f\left(m^2_{\tilde{c}_L}, m^2_{\tilde{t}_R}\right) + \dots\,,\end{aligned} \tag{3.25}$$

where the same notation of chirality splitting is adopted for the mass insertions. The same notation was also used in Fig. 3.2. As a measure of flavor violation it is more intuitive to use a dimensionless quantity instead of $\left(\Delta^{u,d}_{ij}\right)_{AA'}$ which has mass dimension two. In order to arrive at such a measure one commonly divides $\left(\Delta^{u,d}_{ij}\right)_{AA'}$ by an average mass scale M^2_{av} of the squark mass matrix. In the literature there are different conventions used for M^2_{av}. In the forthcoming sections we study a hierarchical squark spectrum including a right-handed stop that is considerably lighter than the other squarks. Therefore, for M^2_{av} we choose to take the arithmetic average of the diagonal elements of the squark mass squared matrix, *i.e.*, we define

$$\left(\delta^{u,d}_{ij}\right)_{AA'} \equiv \frac{\left(\Delta^{u,d}_{ij}\right)_{AA'}}{\frac{1}{6}\sum_{i=1}^{6}\left(M^2_{\tilde{u},\tilde{d}}\right)_{ii}}\,. \tag{3.26}$$

Another option would be to take the geometric average of the two diagonal entries that correspond to the indices of the considered parameter $\left(\Delta^{u,d}_{ij}\right)_{AA'}$. In case of the considered hierarchical spectrum this has the disadvantage that *e.g.* $(\delta^u_{23})_{LR}$ is biased towards larger values due to its normalization because the light stop mass enters it multiplicatively in the denominator.

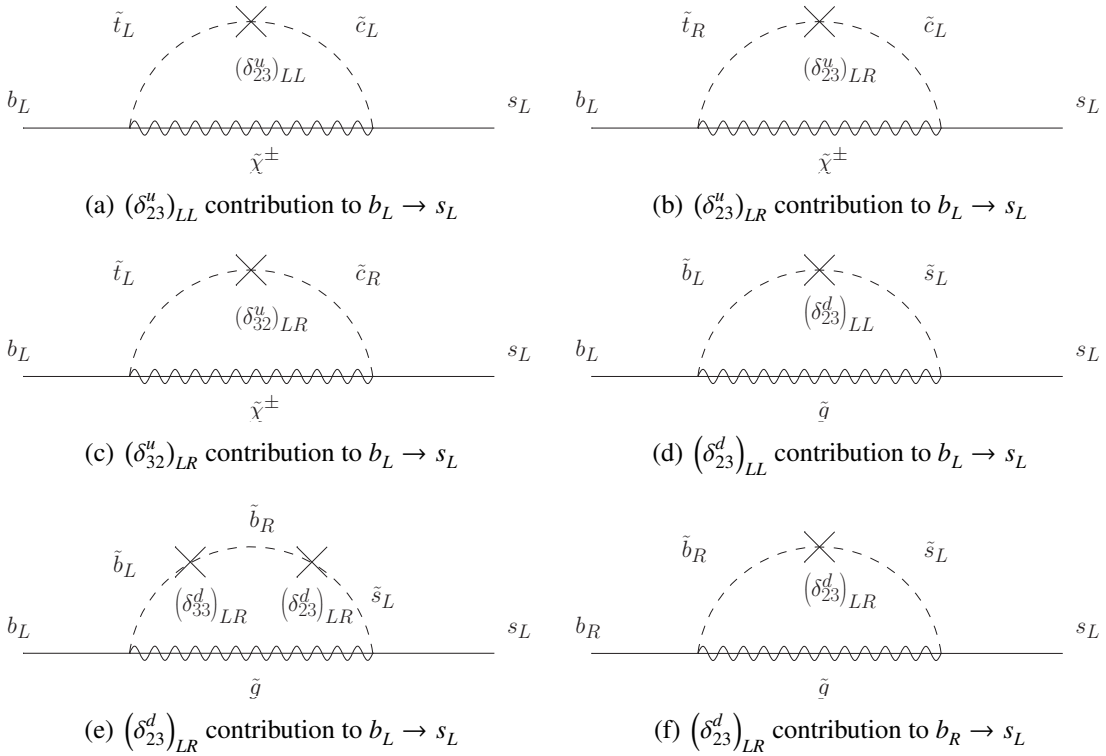

(a) $(\delta^u_{23})_{LL}$ contribution to $b_L \to s_L$

(b) $(\delta^u_{23})_{LR}$ contribution to $b_L \to s_L$

(c) $(\delta^u_{32})_{LR}$ contribution to $b_L \to s_L$

(d) $\left(\delta^d_{23}\right)_{LL}$ contribution to $b_L \to s_L$

(e) $\left(\delta^d_{23}\right)_{LR}$ contribution to $b_L \to s_L$

(f) $\left(\delta^d_{23}\right)_{LR}$ contribution to $b_R \to s_L$

Figure 3.3.: Contributions from different MI parameters to the $b_L \to s_L$ and $b_R \to s_L$ transition, see text for details.

Relative Importance of MI parameters The different mass insertions have quite a distinct importance for $b \to s l^+ l^-$ transitions. We will see in this paragraph that the most important parameter is the scharm-stop left-right mixing $(\delta^u_{23})_{LR}$. Without the new improved bounds from $\bar{B} \to \bar{K}^{(*)} l^+ l^-$ it could be $(\delta^u_{23})_{LR} \sim O(1)$. Besides the flavor bounds on this parameter there is an interesting cross-link to the bounds from the Higgs sector. In the following, we go one by one through the different squark-flavor violating parameters that link the second and third generation in $\bar{B} \to \bar{K}^{(*)} l^+ l^-$. We illustrate the role of the different mass insertions in $b_L \to s_L$ and $b_R \to s_L$ transitions in Fig. 3.3. Chirality flipped transitions are not shown there due to their suppression by m_s/m_b in the chargino contributions, on that we focus in the following, see below.
A notably difference between gluino and chargino diagrams is that in the super-CKM basis MIA framework a change in flavor and chirality in gluino diagrams comes only from the MI parameters. In chargino diagrams it also takes place at the vertex from CKM. The latter situation is illustrated *e.g.* in Fig. 3.3(b). A corresponding diagram for gluinos does *not* exist at first order MIA. We demonstrate this further below.

- Contributions from gluino diagrams to C_9 and C_{10}
  - $\left(\delta^d_{23}\right)_{LR}$ gives only at second order MIA a contribution to $b_L \to s_L$ because in the MIA picture the gluino vertex is chirality and flavor conserving. As can be

$m_{H^\pm}$	$\tan\beta$	M_2	μ	
300 GeV	4	150 GeV	−300 GeV	
$m_{\tilde{t}_R}$	$m_{\tilde{q}}$	A_t	$m_{\tilde{\nu}}$	$m_{\tilde{g}}$
300 GeV	1000 GeV	1000 GeV	100 GeV	700 GeV

Table 3.2.: Example point in the MSSM parameter space at $\mu_0 = 120$ GeV, see text for details. Diagonalizing the squark and chargino mass matrices, we get from this point the mass eigenvalues: $m_{\tilde{t}_1} = 236$ GeV, $m_{\tilde{t}_2} = 1017$ GeV, $m_{\tilde{\chi}_1^\pm} = 150$ GeV and $m_{\tilde{\chi}_2^\pm} = 321$ GeV. Using `FeynHiggs` [250–253] we get for the light Higgs mass the value $m_{h^0} = 117$ GeV. Table adapted from Ref. [308].

seen in Fig. 3.3(e) in order to insert a $\left(\delta^d_{23}\right)_{LR}$ we firstly need a $\left(\delta^d_{33}\right)_{LR}$ insertion for getting a $\tilde{b}_R$ that can then be converted to a $\tilde{s}_L$.
On the other hand, in a $b_R \to s_L$ transition, which is relevant for C_7, $\left(\delta^d_{23}\right)_{LR}$ appears at first order MIA. Here it gives quite a large contribution due to an enhancement factor $m_{\tilde{g}}/m_b$. This can be seen in Table 3.3 where we evaluate the coefficients of the different MI parameters at a SUSY example point which is given in Table 3.2. Due to the enhancement relative to the other MI parameters, $\left(\delta^d_{23}\right)_{LR}$ is quite constrained from $\mathcal{B}(\bar{B} \to X_s\gamma)$, whereas it obviously does not get an additional bound from $\bar{B} \to \bar{K}^{(*)}l^+l^-$.

- $\left(\delta^d_{32}\right)_{LR}$, in that way similar to $\left(\delta^d_{23}\right)_{LR}$, gives only at second oder MIA a contribution to $b_L \to s_L$, because one needs another insertion of $\left(\delta^d_{22}\right)_{LR}$ in order to get the proper chirality for the strange squark $\tilde{s}_L$. Therefore we can neglect this MI parameter in $\bar{B} \to \bar{K}^{(*)}l^+l^-$. In contrast to $\left(\delta^d_{23}\right)_{LR}$ it also enters only at third order MIA in $b_R \to s_L$ transitions, as one needs additional insertions $\left(\delta^d_{33}\right)_{LR}$ and $\left(\delta^d_{22}\right)_{LR}$.
- $\left(\delta^d_{23}\right)_{LL}$ enters at first order MIA as depicted in Fig. 3.3(d). Generally, for chirality conserving mass insertions, the photon penguin dominates the Z penguin for the here considered mass spectrum, *i.e.*, not too heavy squarks of the first and second generation [349]. The photon penguin on the other hand gives only a contribution to C_9. This contribution happens to be numerically small around our SUSY example point because it is proportional to $m_W^2/m_{\tilde{q}}^2$, compare Table 3.3. The contribution of the gluino Z penguin to C_{10} is negligible as it comes with higher orders of mass insertions only.

- Contributions from chargino diagrams to C_9 and C_{10}
  - $(\delta^u_{23})_{LR}$ insertions can appear already at first order MIA, as can be seen in

$C_7^{\mathrm{MI},\tilde{\chi}^\pm}(\mu_0)$	$C_9^{\mathrm{MI},\tilde{\chi}^\pm}(\mu_0)$	$C_{10}^{\mathrm{MI},\tilde{\chi}^\pm}(\mu_0)$
$0.01(\delta^u_{23})_{LR} - 0.38(\delta^u_{23})_{LL}$	$0.21(\delta^u_{23})_{LR} - 0.11(\delta^u_{23})_{LL}$	$-2.68(\delta^u_{23})_{LR} + 0.19(\delta^u_{23})_{LL}$
$C_7^{\mathrm{MI},\tilde{g}}(\mu_0)$	$C_9^{\mathrm{MI},\tilde{g}}(\mu_0)$	$C_{10}^{\mathrm{MI},\tilde{g}}(\mu_0)$
$16.35\,(\delta^d_{23})_{LR} - 0.02(\delta^d_{23})_{LL}$	$0.04\,(\delta^d_{23})_{LL}$	–

Table 3.3.: Hierarchy of the first order MIA contributions to the Wilson coefficients C_7, C_9 and C_{10} at $\mu_0 = 120$ GeV evaluated at the example point specified in Table 3.2. The first row shows the contributions from chargino diagrams stemming from flavor violation in the up squark mass matrix. The second row shows the contributions from gluino diagrams stemming from flavor violation in the down squark mass matrix. Table adapted from Ref. [308].

Fig. 3.3(b). This is in contrast with the $\left(\delta^d_{23}\right)_{LR}$ contribution that is depicted in Fig. 3.3(e). A large contribution comes especially from the Z penguin whose contribution comes without a $m_W^2/m_{\tilde{q}}^2$ suppression factor. No such term on the other hand can be found in the contribution to C_7, *i.e.*, the corresponding coefficient is numerically small and the bound by $\mathcal{B}(\bar{B} \to X_s\gamma)$ not effective. Furthermore, also the contribution to $B_s - \bar{B}_s$ mixing is too small to get a bound from there [350]. This is the reason why from flavor observable constraints $(\delta^u_{23})_{LR} \sim O(1)$ is not excluded (so far).

– $(\delta^u_{32})_{LR}$ insertions come also at first order MIA, as depicted in Fig. 3.3(c). However, they are strongly suppressed by m_c/m_t against the dominating contribution from $(\delta^u_{23})_{LR}$ and therefore negligible.

– $(\delta^u_{23})_{LL}$ also gives first order MIA contributions to $b_L \to s_L$ as can be seen in Fig. 3.3(a). In contrast to $(\delta^u_{23})_{LR}$ it always comes with a factor $m_W^2/m_{\tilde{q}}^2$ and is thus numerically less important than this MI parameter, compare Table 3.3. The situation is the other way around for C_7 and thus the bounds from $\mathcal{B}(\bar{B} \to X_s\gamma)$. The contribution of $(\delta^u_{23})_{LL}$ to C_7 is significantly larger than the one of $(\delta^u_{23})_{LR}$. This is caused by a relative enhancement factor $m_{\tilde{\chi}^\pm}/m_b$ in parts of these contributions.

The most important mass insertion for $b \to s l^+ l^-$ transitions on which bounds we can hope to improve the most is thus the scharm-stop left-right mixing $(\delta^u_{23})_{LR}$ in the chargino contributions.

Parametrization of the Up Squark Mass Squared Matrix Coming from the perspective of the MIA but wanting to take into account the correct treatment of flavor-diagonal

and off-diagonal elements of the up squark mass matrix (as shown in general form in Fig. 3.2) by an appropriate diagonalization we write the up-squark mass matrix as

$$M^2_{\tilde{u}} = \begin{pmatrix} \left(M^2_{\tilde{u}}\right)_{LL} & \left(M^2_{\tilde{u}}\right)_{LR} \\ \left(M^2_{\tilde{u}}\right)^{\dagger}_{LR} & \left(M^2_{\tilde{u}}\right)_{RR} \end{pmatrix}, \tag{3.27}$$

with the submatrices

$$\left(M^2_{\tilde{u}}\right)_{LR} = m^2_{\tilde{q}} \mathbb{1}_{3\times 3}\,, \quad \left(M^2_{\tilde{u}}\right)_{LR} = \begin{pmatrix} 0 & 0 & 0 \\ 0 & 0 & (\Delta^u_{23})_{LR} \\ 0 & 0 & (\Delta^u_{33})_{LR} \end{pmatrix}, \quad \left(M^2_{\tilde{u}}\right)_{RR} = \begin{pmatrix} m^2_{\tilde{q}} & 0 & 0 \\ 0 & m^2_{\tilde{q}} & 0 \\ 0 & 0 & m^2_{\tilde{t}_R} \end{pmatrix}, \tag{3.28}$$

and $(\Delta^u_{33})_{LR} = m_t(A_t - \mu \cot\beta)$. The right-handed stop mass is given as

$$m^2_{\tilde{t}_R} = m^2_{\tilde{t}_R,\text{soft}} + m^2_t + \frac{2}{3} s^2_W m^2_Z \cos 2\beta\,, \tag{3.29}$$

with the soft term $m^2_{\tilde{t}_R,\text{soft}}$. $m^2_{\tilde{q}}$ is the degenerate diagonal element of the first and second generation. With the up squark mass matrix as in Eq. (3.27) the eigenvalues, *i.e.*, the squared masses are given as

$$m^2_{\tilde{t}_{1,2}} = \frac{1}{2}\left(m^2_{\tilde{q}} + m^2_{\tilde{t}_R} \mp \sqrt{\left(m^2_{\tilde{q}} - m^2_{\tilde{t}_R}\right)^2 + 4\,(\Delta^u_{23})^2_{LR} + 4\,(\Delta^u_{33})^2_{LR}} \right) \tag{3.30}$$

for the third generation and $m^2_{\tilde{q}}$ for the first two generations.

Analytical results for the contribution of $(\delta^u_{23})_{LR}$ to C_7, C_9 and C_{10} Our result for the chargino contribution to the Wilson coefficients in the MI approximation proportional to $(\delta^u_{23})_{LR}$ is given as [308]

$$C_7^{\text{MI},\tilde{\chi}^\pm}(\mu_0) = \frac{V^*_{cs}}{V^*_{ts}} \frac{\lambda_t}{g_2} \frac{m^2_W}{m^2_{\tilde{q}}} \times F \times (\delta^u_{23})_{LR}\,, \tag{3.31}$$

$$C_9^{\text{MI},\tilde{\chi}^\pm}(\mu_0) = \frac{V^*_{cs}}{V^*_{ts}} \frac{1}{4s^2_W} \frac{\lambda_t}{g_2} \left((4s^2_W - 1) F^{\text{Z-p}} + 4 s^2_W \frac{m^2_W}{m^2_{\tilde{q}}} F^{\gamma\text{-p}} - \frac{m^2_W}{m^2_{\tilde{q}}} F^{\text{box}} \right) (\delta^u_{23})_{LR}\,, \tag{3.32}$$

$$C_{10}^{\text{MI},\tilde{\chi}^\pm}(\mu_0) = \frac{V^*_{cs}}{V^*_{ts}} \frac{1}{4s^2_W} \frac{\lambda_t}{g_2} \left(F^{\text{Z-p}} + \frac{m^2_W}{m^2_{\tilde{q}}} F^{\text{box}} \right) (\delta^u_{23})_{LR}\,. \tag{3.33}$$

The loop functions are given as follows:

$$F(x_1, x_2, x_{\tilde{t}_R}) = \frac{1}{6}\hat{x}_{av} \sum_{i=1,2} V_{i1} V_{i2}^* x_i^2 \frac{f_1(x_i/x_{\tilde{t}_R}) - f_1(x_i)}{x_i/x_{\tilde{t}_R} - x_i}\,, \tag{3.34}$$

$$\begin{aligned} F^{Z-p}(\hat{x}_1, \hat{x}_2, \hat{x}_{\tilde{t}_R}) = \hat{x}_{av} \sum_{i,j=1,2} V_{j1} V_{i2}^* \Bigg(& U_{j1}^* U_{i1} \sqrt{\hat{x}_i \hat{x}_j} \frac{c_0(\hat{x}_{\tilde{t}_R}, \hat{x}_i, \hat{x}_j) - c_0(1, \hat{x}_i, \hat{x}_j)}{\hat{x}_{\tilde{t}_R} - 1} \\ & - 2 V_{j1}^* V_{i1} \frac{c_2(\hat{x}_{\tilde{t}_R}, \hat{x}_i, \hat{x}_j) - c_2(1, \hat{x}_i, \hat{x}_j)}{\hat{x}_{\tilde{t}_R} - 1} + 2\delta_{ij} \frac{c_2(\hat{x}_j, 1, \hat{x}_{\tilde{t}_R}) - c_2(\hat{x}_j, 1, 1)}{\hat{x}_{\tilde{t}_R} - 1} \Bigg)\,, \end{aligned} \tag{3.35}$$

$$F^{\gamma-p}(\hat{x}_1, \hat{x}_2, \hat{x}_{\tilde{t}_R}) = \frac{1}{9}\hat{x}_{av} \sum_{i=1,2} V_{i1} V_{i2}^* \hat{x}_{\tilde{t}_R} \frac{\hat{x}_i/\hat{x}_{\tilde{t}_R} f_7(\hat{x}_i/\hat{x}_{\tilde{t}_R}) - \hat{x}_i f_7(\hat{x}_i)}{\hat{x}_i/\hat{x}_{\tilde{t}_R} - \hat{x}_i}\,, \tag{3.36}$$

$$F^{box}(\hat{x}_1, \hat{x}_2, \hat{x}_{\tilde{t}_R}, \hat{x}_{\tilde{\nu}_1}) = 4\hat{x}_{av} \sum_{i,j=1,2} V_{i1} V_{i2}^* |V_{j1}|^2 \frac{d_2(\hat{x}_i, \hat{x}_j, \hat{x}_{\tilde{t}_R}, \hat{x}_{\tilde{\nu}_1}) - d_2(\hat{x}_i, \hat{x}_j, 1, \hat{x}_{\tilde{\nu}_1})}{\tilde{x}_{\tilde{t}_R} - 1}\,. \tag{3.37}$$

Here,

$$x_i = \frac{1}{\hat{x}_i} = \frac{m_{\tilde{q}}^2}{m_{\chi_i}^2}, \quad i = 1, 2\,, \qquad x_{\tilde{t}_R} = 1/\hat{x}_{\tilde{t}_R} = \frac{m_{\tilde{q}}^2}{m_{\tilde{t}_R}^2}\,, \tag{3.38}$$

$$x_{\tilde{\nu}_1} = 1/\hat{x}_{\tilde{\nu}_1} = \frac{m_{\tilde{q}}^2}{m_{\tilde{\nu}_1}^2}\,, \qquad \hat{x}_{av} = \frac{1}{6}(5 + \hat{x}_{\tilde{t}_R}). \tag{3.39}$$

The loop functions f_i, c_i, d_2 can be seen in [246]. Note that the loop integrals have numerical singularities at points in the parameter space where it looks like we have to "divide by zero". At these points one has to calculate the different limits of the loop integrals. For the univariate loop functions these limits are

$$f_1(1) = -\frac{5}{12}\,, \qquad f_7(1) = -\frac{7}{4}. \tag{3.40}$$

Exemplary limits of the multivariate integrals are

$$c_0(1,1,1) = -\frac{1}{2}\,, \qquad c_2(1,1,1) = -\frac{1}{4}\log\left(\frac{m_{\tilde{q}}^2}{\mu^2}\right), \qquad d_2(1,1,1,1) = -\frac{1}{12}\,. \tag{3.41}$$

For the difference quotients of the loop functions it holds for example

$$\lim_{x,y\to 1} \frac{f_1(y) - f_1(x)}{y - x} = \frac{1}{5} \qquad \lim_{x,y\to 1} \frac{y f_7(y) - x f_7(x)}{y - x} = -\frac{1}{5}\,. \tag{3.42}$$

In our C++ implementation instead of setting the loop integral discontinuously to the value at its limit in a small interval around the numerical singularity we use for the univariate loop integrals the Padé approximant and for multivariate loop integrals a multivariate Taylor expansion. This way we get smooth numerical representations of the loop integrals.
In Eqs. (3.32) and (3.33) we can read off the most important characteristics of the $(\delta_{23}^u)_{LR}$

contributions to $b \to s l^+ l^-$: $C_9^{\rm NP}$ and $C_{10}^{\rm NP}$ are dominated by the terms that do not come with factors of $m_W^2/m_{\tilde{q}}^2$, *i.e.*, the Z penguin contribution. It follows a strong correlation from the approximate relation

$$\frac{C_{10}^{\rm NP}}{C_9^{\rm NP}} \simeq \frac{1}{(4s_W^2 - 1)} \qquad (Z \text{ penguin dominance}). \tag{3.43}$$

Eq. (3.43) is clearly visible in the figures we show in the next section and causes stronger bounds in the plane of the effective couplings than in the model independent case. A general discussion of NP in Z couplings in $b \to s l^+ l^-$ processes is given in Ref. [351].

3.2.2. The Spread of SUSY Models

With the framework developed in Sec. 3.2.1 at hand, we can compare SUSY predictions including squark flavor violation in the scharm-stop left-right mixing with data. We denote the scenario with a significant $(\delta_{23}^u)_{LR}$ as non-MFV (NMFV). In the MFV scenario, it holds $(\delta_{23}^u)_{LR} \sim y_b^2 V_{cb} V_{tb}^* \frac{m_t}{m_{\tilde{q}}} \ll 1$ [290, 352], see Sec. 3.4, which is below the present experimental precision, *i.e.*, for practical purposes MFV implies $(\delta_{23}^u)_{LR} \simeq 0$.

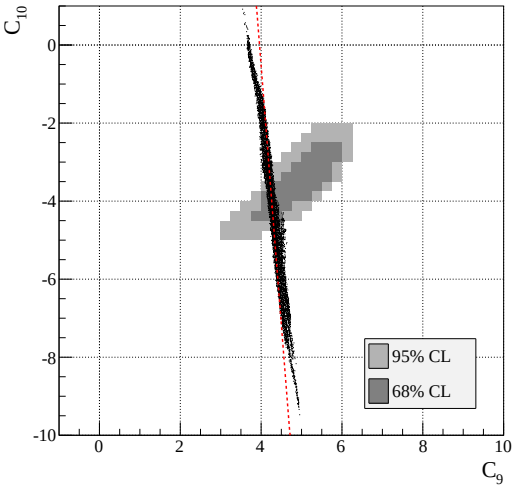

Figure 3.4.: NMFV, including scatter points with largish $(\delta_{23}^u)_{LR}$ without taking Higgs bounds and electroweak precision tests into account. Here, $|A_t|$ is varied up to 5 TeV (which does not have a significant effect for the plot compared to 3 TeV). In gray we show the model independent bounds extracted from rare decays in Ref. [184]. Red dot: SM. Red dashed line: Z penguin dominance. Figure taken from Ref. [309].

In order to explore the SUSY parameter space we take here a bottom-up philosophy and vary the SUSY parameters directly at the electroweak scale. This is in contrast to the top-down strategy where one specifies a certain SUSY model at the GUT scale that is then evolved down to the electroweak scale using the renormalization group equations. We generate scatter points in the ranges given in Table 3.4. These are subsequently overlayed over the improved bounds from $\bar{B} \to \bar{K}^{(*)} l^+ l^-$ in the C_9–C_{10} plane that are obtained model-independently in Refs. [78, 184, 322]. In order to demonstrate the new input of the semileptonic bounds we only draw points in the C_9–C_{10} plane that pass a number of additional constraints. Firstly, the Wilson coefficient C_7 is already heavily constrained by the radiative decay $\bar{B}_d \to X_s \gamma$ to be within the

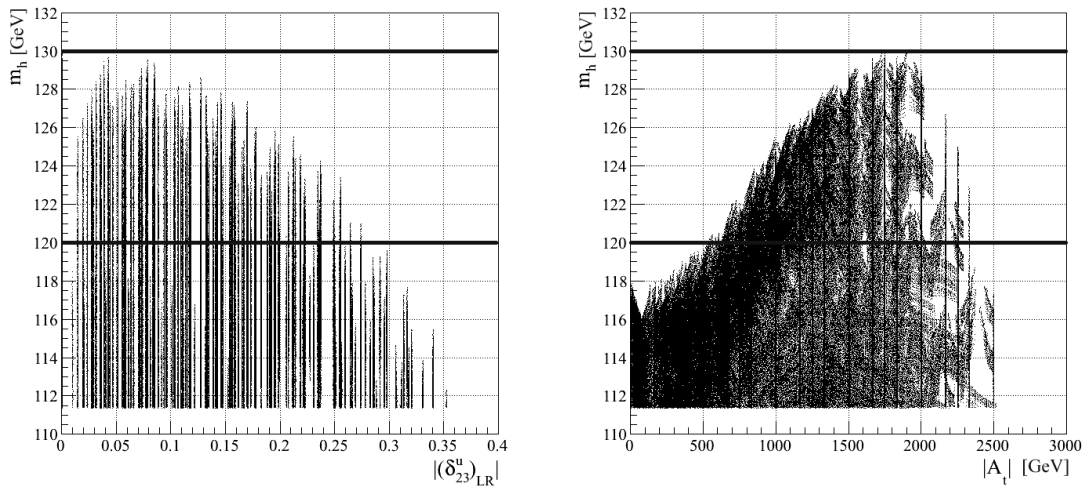

(a) NMFV (b) NMFV

Figure 3.5.: Dependence of m_h on $\left|(\delta^u_{23})_{LR}\right|$ (a) and $|A_t|$ (b), respectively, including the Higgs mass bound in Eq. (3.46). Horizontal black lines: Higgs mass bound Eq. (3.47).

	$\tan\beta$	$m_{H^\pm}$	M_2	$\lvert\mu\rvert$	$m_{\tilde{t}_R}$	A_t	$(\delta^u_{23})_{LR}$
min.	3	300	100	80	170	−3000	−0.85
max.	15	1000	1000	1000	800	3000	0.85

Table 3.4.: SUSY parameters (masses in GeV) and their ranges at $\mu_0 = 120$ GeV used to generate the scatter plots shown in this section. Additionally, we set $m_{\tilde{\nu}} = 100$ GeV and $m_{\tilde{q}} = 1000$ GeV. Table adapted from [308].

range [184]

$$0.3 \leq |C_7| \leq 0.4. \tag{3.44}$$

The 2012 established zero crossing of the forward-backward asymmetry at low q^2, namely $q_0^2 = (4.9 \pm 0.9)\ \text{GeV}^2$ [331], has the consequence that only the sign combinations

$$C_7 < 0\,, C_9 > 0 \qquad \text{and} \qquad C_7 > 0\,, C_9 < 0\,, \quad \textit{i.e.}, \quad C_7 C_9 < 0\,,$$

are allowed [184, 353]. In the MSSM we are bound to $C_9 > 0$ [246] so instead of Eq. (3.44) we use directly the bound

$$-0.4 \leq C_7 \leq -0.3. \tag{3.45}$$

In addition to the flavor bounds we furthermore include the electroweak precision bound $-0.0007 \leq \Delta\rho \leq 0.0017$ [345] and bounds from direct searches for (s)particles that we list below. As we do not specify a certain SUSY model here, we only take bounds into account that are independent of any model assumptions. For example, the recent bounds by ATLAS on the light stop mass excluding $320\,\text{GeV} \leq m_{\tilde{t}_1} \leq 660\,\text{GeV}$ at 95% C.L. [354] using $21\,\text{fb}^{-1}$ depend on such assumptions of simplified models. These are therefore not applied here. The same goes for the ATLAS bound on the light chargino mass $m_{\tilde{\chi}^\pm} \geq 350$ GeV [355] and the analogous results from CMS using $\sim 9\,\text{fb}^{-1}$ [356] and $\sim 10\,\text{fb}^{-1}$ [357] of data, respectively. At CMS, searches for light stop quarks with masses in the region $160\,\text{GeV} \leq m_{\tilde{t}_1} \leq 430$ GeV and for charginos with masses up to ~ 600 GeV have been reported [356, 357]. All these bounds depend especially on the lightest neutralino mass.

Consequently, we apply the following bounds:

- Constraints on the lightest stop mass, $m_{\tilde{t}_1} \geq 100$ GeV [358, 359].
- Constraints on the lightest chargino mass, $m_{\tilde{\chi}^\pm} \geq 94$ GeV [345].
- Constraints on the lightest Higgs mass[1] m_h: In order to have an SM-like lightest SUSY Higgs we demand $m_{A_0} \geq 200$ GeV. With the latter constraint we are in the parameter region of the "decoupling limit" of the other neutral and the charged Higgs bosons, for details see *e.g.* Ref. [186]. In the following we analyze the consequences of the recent observation of a scalar boson that we interpret as a SUSY Higgs. For that, we compare the effects of the following two bounds:

$$\text{(I)} \qquad m_h + 3\,\text{GeV} \geq 114.4\,\text{GeV} \quad [345] \tag{3.46}$$

$$\text{(II)} \qquad 120\,\text{GeV} \leq m_h \leq 130\,\text{GeV}. \tag{3.47}$$

  In both cases we include a theoretical uncertainty of 3 GeV [252] and we are conservative in Eq. (3.47). Recent experimental results for the Higgs mass read, consistent with each other, $m_h = 125.5 \pm 0.2^{+0.5}_{-0.6}$ GeV [12] at ATLAS and $125.8 \pm 0.4 \pm 0.4$ GeV [13] at CMS.

In order to calculate $\Delta\rho$ and m_h we use the `FeynHiggs` [250–253] code.[2] The result of the parameter scan is shown in Figs. 3.4–3.7.

Obviously, with $(\delta^u_{23})_{LR} \sim O(1)$ there is a potential of a huge effect in the C_9–C_{10} plane, as can be seen in Fig. 3.4. We only show solutions with $C_7 < 0$ due to $C_7 > 0$ being disfavored by the zero of A_{FB}, as discussed after Eq. (3.44). The strong correlation of C_9 and C_{10} due to the Z penguin dominance mentioned at the end of Sec. 3.2.1 is clearly visible. As one can see in Fig. 3.6(a) and even more so in Fig. 3.6(b) the application of the Higgs bounds in Eqs. (3.46) and (3.47), respectively, has an effect that is complementary to the

[1] Research was done in the beginning of 2012. The announcement of the Higgs was in July 2012. Since the Higgs bound is not the main point here, but instead the flavor bounds from $\bar{B} \to \bar{K}^{(*)} l^+ l^-$, the plots were not updated. No significant changes are expected.

[2] We thank S. Heinemeyer for trouble-shooting and providing `FeynHiggs` v2.9.0-beta.

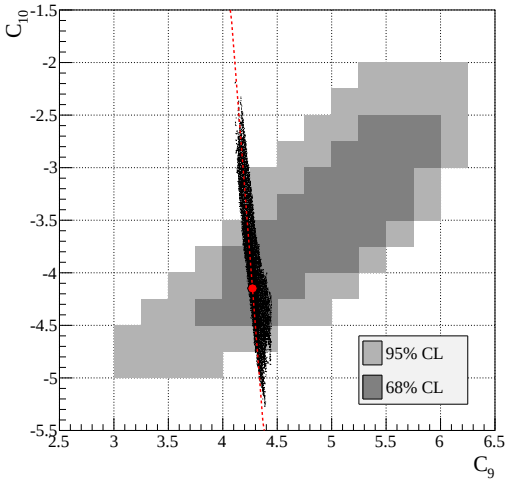

(a) NMFV, Higgs bound Eq. (3.46). Figure taken from Ref. [308]

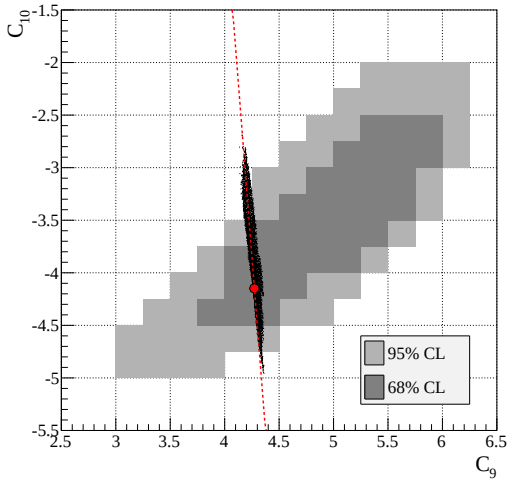

(b) NMFV, Higgs bound Eq. (3.47).

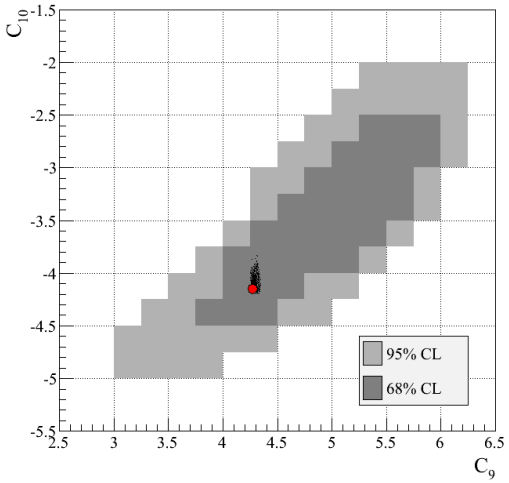

(c) MFV, Higgs bound Eq. (3.47).

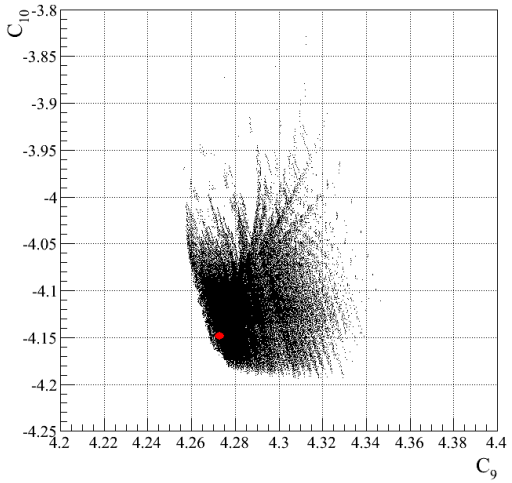

(d) MFV, Higgs bound Eq. (3.47), zoom around SM. Full shown plane allowed at 68% C.L.

Figure 3.6.: Comparison of NMFV and MFV and interplay with Higgs mass bounds in the C_9-C_{10} plane. In gray we show the model independent bounds obtained in Ref. [184]. Red dot: SM. Red dashed line: Z penguin dominance discussed in the text.

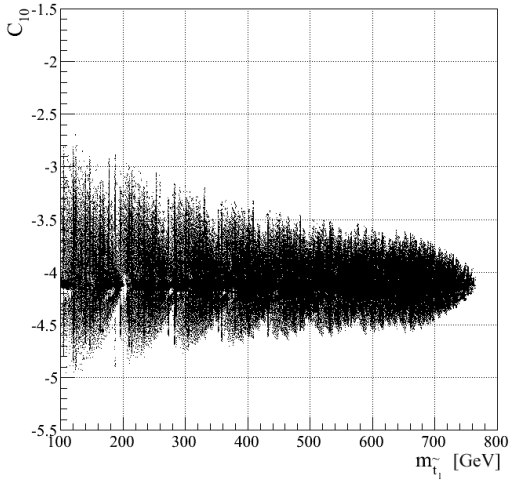

(a) NMFV, Higgs bound Eq. (3.47).

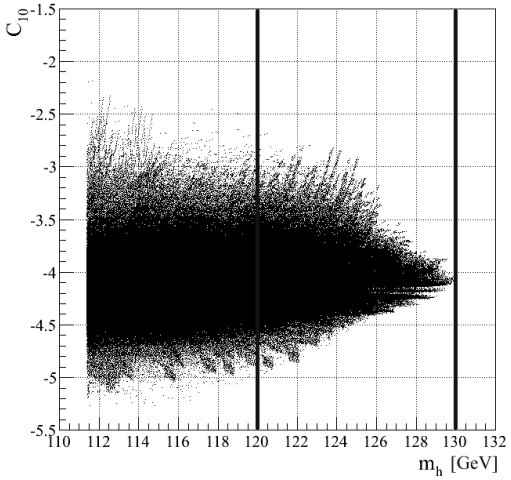

(b) NMFV

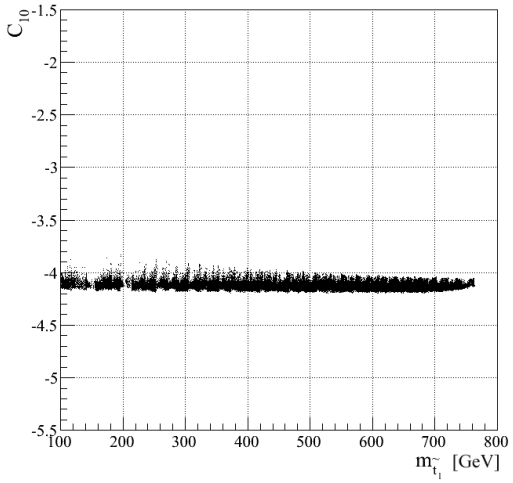

(c) MFV, Higgs bound Eq. (3.47).

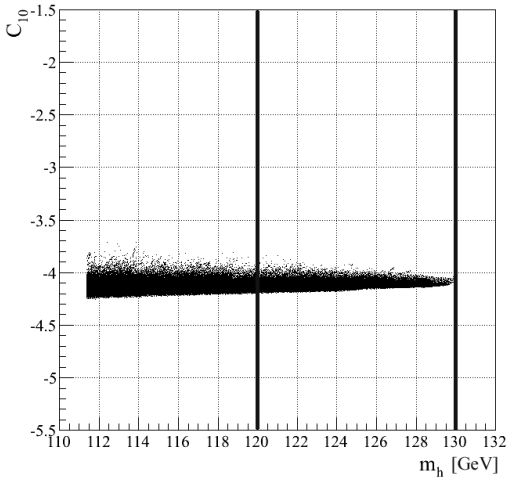

(d) MFV

Figure 3.7.: NMFV and MFV correlation of C_{10} with $m_{\tilde{t}_1}$ and m_h, respectively. Vertical black lines: Higgs mass bound Eq. (3.47).

bounds from the semileptonic decays $\bar{B} \to \bar{K}^{(*)} l^+ l^-$. Due to the substantial correlation of C_9 and C_{10} by the Z penguin dominance the flavor bounds in SUSY are much stronger than in the model independent case.

Many of the SUSY model points are excluded by both the flavor bounds and the Higgs bounds, *i.e.*, both of them cut deeply into the parameter space of the MSSM. The maximal C_{10} range of the scatter point sample shown in Fig. 3.6(a) amounts to

$$\max|C_{10}^{\rm NP}(\mu_b)/C_{10}^{\rm SM}(\mu_b)| \simeq 47\% \qquad \text{(wo. } \bar{B} \to \bar{K}^{(*)} l^+ l^- \text{ bounds)}. \tag{3.48}$$

Applying the semileptonic bounds shown in gray in Fig. 3.6(a) this range reduces at 68% (95%) C.L. to

$$\max|C_{10}^{\rm NP}(\mu_b)/C_{10}^{\rm SM}(\mu_b)| \simeq 16\%\,(28\%) \qquad \text{(with } \bar{B} \to \bar{K}^{(*)} l^+ l^- \text{ bounds)}. \tag{3.49}$$

The complementary effect of the Higgs bounds is illustrated in Fig. 3.5 where we plot the generated scatter points in the $(\delta^u_{23})_{LR}$–m_h and A_t–m_h planes. The correlation and importance of Higgs and b physics constraints has been highlighted recently in [254], where it has been concentrated especially on the SPS [360] MSSM benchmark points. The negative contribution to the Higgs mass at large $(\delta^u_{23})_{LR}$ observed in [254] at the SPS points is also clearly visible in the generic parameter scan in Fig. 3.5 that shows the same tendency as the benchmark points. For that reason, basically all points with $(\delta^u_{23})_{LR} \gtrsim 0.3$ or $A_t \gtrsim 2500$ GeV are excluded by the Higgs bound Eq. (3.47). In order to get the correct Higgs mass $|A_t|$ has to be quite enhanced, as can be read off from Fig. 3.5(b). For m_h fulfilling Eq. (3.47) one needs at least $|A_t| \sim 1$ TeV.

In Figs. 3.6(c) and 3.6(d) (zoom) we show the spread of the flavor-diagonal MSSM (MFV) with $(\delta^u_{23})_{LR} = 0$ in the C_9–C_{10} plane. The maximal enhancement of C_{10} is given as

$$\max|C_{10}^{\rm NP}/C_{10}^{\rm SM}| \simeq 11\% \qquad \text{(MFV, Higgs bound Eq. (3.46).} \tag{3.50}$$

The asymmetric shape of the scatter points around the SM value in Figs. 3.6(c) and 3.6(d) agrees with the general form of the corresponding plot shown in Fig. 12 of Ref. [361], where a plot in the CMSSM has been made.

Obviously, for our scenario the flavor bounds in the C_9–C_{10} plane of $\bar{B} \to \bar{K}^{(*)} l^+ l^-$ are currently far away from being sensitive to the difference between the SM and MFV. However, as was shown in [361], there arises a sensitivity to the CMSSM when one uses an extended operator basis and takes into account large $\tan\beta$.

The dependency of the width of the C_{10} range on $m_{\tilde{t}_1}$ and m_h is an effect that only arises when squark flavor violation is switched on. This is illustrated in Fig. 3.7. An enhancement of C_{10} is especially present for light stop masses. In this part of the parameter space the semileptonic bounds on squark flavor will be consequently especially strong.
The points of our parameter sample above $m_{\tilde{t}_1} \gtrsim 750$ GeV in Figs. 3.7(a) and 3.7(c) are excluded by the Higgs bound Eq. (3.47) as an artifact of our choice for the scan range of $m_{\tilde{t}_R}$, see Table 3.4. From Eq. (3.30) it follows $m_{\tilde{t}_1} \leq m_{\tilde{t}_R}$ and relatively smaller $m_{\tilde{t}_1}$ for larger $(\Delta^u_{23})_{LR}$ and/or $(\Delta^u_{33})_{LR}$. The latter are needed in order to fulfill the Higgs bound, thus at the boundary of the scan range of $m_{\tilde{t}_R}$ no points remain.

3.3. Bounds on Squark Flavor

In Sec. 3.2.2 we have overlayed model independent flavor bounds from $\bar{B} \to \bar{K}^{(*)} l^+ l^-$ with scatter points of SUSY models that violate flavor beyond the SM. We have seen that the bounds deeply cut into the parameter space of the MSSM. This becomes especially visible in the comparison of Eqs. (3.48) and (3.49). How does this translate into bounds on squark flavor violation?

The Higgs bounds give an overall global bound on $(\delta^u_{23})_{LR}$, see Fig. 3.5(a). The strength of the flavor bounds depend strongly on the flavor diagonal SUSY parameters. Thus, in order to exemplify the progress from the semileptonic bounds in parts of the parameter space we study planes around the SUSY example point given in Table 3.2. In order to separately inspect the bounds from flavor physics we disregard here the bounds from electroweak precision and Higgs physics.

In Fig. 3.8 we compare the bounds on the absolute value of the scharm-stop left-right mixing $\left|(\delta^u_{23})_{LR}\right|$ without (Fig. 3.8(a)) and including (Fig. 3.8(b)) the 68% C.L. semileptonic bounds in the $m_{\tilde{t}_R}$–A_t plane around the SUSY example point in Table 3.2. The bounds shown in Fig. 3.8(a) are mainly given by the light stop mass bound $m_{\tilde{t}_1} \geq 100$ GeV and $\mathcal{B}(\bar{B} \to X_s\gamma)$. In part of the parameter space we get in Fig. 3.8(b) significantly improved bounds that go down to $(\delta^u_{23})_{LR} \lesssim 10\%$ for small $m_{\tilde{t}_R}$. These bounds are stronger than the Higgs bounds and also stronger than the corresponding vacuum (meta)stability bounds [255, 256]. The latter give at $m_{\tilde{q}} = m_{\tilde{l}} = 1$ TeV and a light right-handed stop mass $m_{\tilde{t}_R} = 300$ GeV a bound of $(\delta^u_{23})_{LR} \lesssim 30\%$. As the strong bounds on $(\delta^u_{23})_{LR}$ come mainly

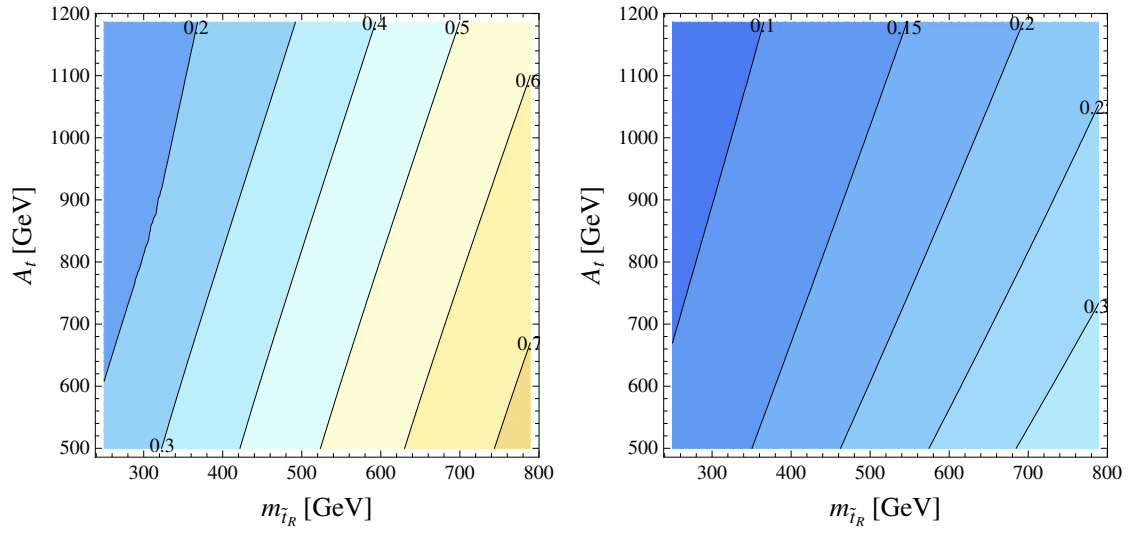

(a) Without $\bar{B} \to \bar{K}^{(*)} l^+ l^-$ bounds.

(b) Including $\bar{B} \to \bar{K}^{(*)} l^+ l^-$ bounds at 68% C.L.

Figure 3.8.: Improvement of the bound on $\left|(\delta^u_{23})_{LR}\right|$ in the $m_{\tilde{t}_R}$–A_t plane around the SUSY example point given in Table 3.2, disregarding the electroweak precision and Higgs bounds. Figures taken from [308].

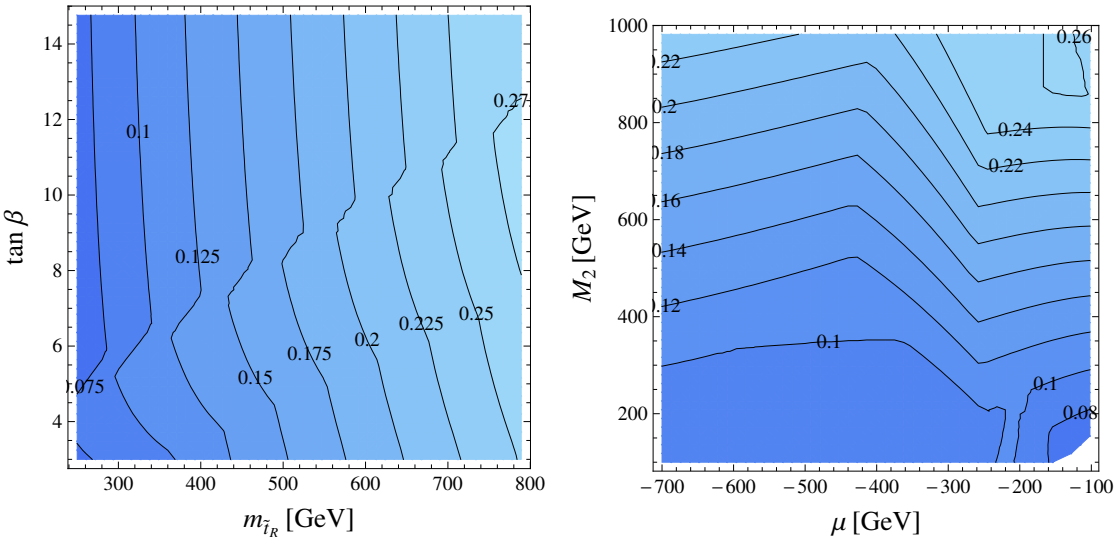

(a) $m_{\tilde{t}_R}$–tanβ plane (b) μ–M_2 plane

Figure 3.9.: Bounds on $\left|(\delta^u_{23})_{LR}\right|$ including the 68% C.L. constraints from $\bar{B} \to \bar{K}^{(*)} l^+ l^-$, disregarding the electroweak precision and Higgs bounds. Figures taken from [308].

from the C_{10} enhancement from the chargino Z diagram, it is interesting to study their dependence on μ, M_2 and tanβ. The latter can be seen in Fig. 3.9. The bounds become stronger for $|\mu| \gg M_2$ and somewhat weaker for larger tanβ, but here the dependence is not really strong.

3.4. Constraints on SUSY Models: Radiative Flavor Violation

In Sec. 3.2.2 and Sec. 3.3 we have investigated a general formulation of the MSSM by varying its parameters at the electroweak scale. We have found in part of the parameter space strong constraints on the scharm-stop left-right mixing $(\delta^u_{23})_{LR}$ from $\bar{B} \to \bar{K}^{(*)} l^+ l^-$. Now we come to the question about the consequences of the new flavor bounds for specific SUSY flavor models. After all, what are actually the generic expectations for the size of $(\delta^u_{23})_{LR}$ in SUSY model building?
As was discussed in Sec. 2.4.3, for example in MFV models one generically expects for the trilinear couplings

$$A_u \simeq A \left(a \mathbb{1} + b Y_d Y_d^\dagger + \dots \right) Y_u \,, \tag{3.51}$$

with $O(1)$-numbers a and b. This results in the approximate relation [290, 352]

$$(\delta^u_{23})_{LR} \sim y_b^2 V_{cb} V_{tb}^* \frac{m_t}{m_{\tilde{q}}} \,, \tag{3.52}$$

with the beauty Yukawa coupling $y_b = \sqrt{2}m_b/v$. Eq. (3.52) indicates a double suppression from V_{cb} and from y_b^2. In models with horizontal flavor symmetries the additional suppression from y_b disappears, $(\delta^u_{23})_{LR} \sim V_{cb}\, m_t/m_{\tilde{q}}$ [362], but we remain still with the suppression from V_{cb}. In both of these model classes the prediction for $(\delta^u_{23})_{LR}$ is consequently order of magnitudes below the current limits and there is no sensitivity.

But there exist also models that make predictions for large values of $(\delta^u_{23})_{LR}$. These are given by models where flavor violation in the quark sector is generated by flavor violation in the SUSY sector, so called Radiative Flavor Violation (RFV) models [363, 364], for previous works see [365–375]. In order to explain the hierarchy in the CKM matrix in this model large trilinear couplings are needed. If these are given, the SM flavor puzzle is traced back to the SUSY flavor puzzle. This is already a great progress in the reduction of complexity. In RFV models, the "bare" CKM matrix takes the most natural form, *i.e.*, the unit matrix [364]. On the contrary, the trilinear SUSY-breaking couplings are not diagonal. Due to the latter, by quantum corrections from SUSY particles of possibly both the down and the up sector the small off-diagonal elements of the CKM matrix are induced. Calculating the corresponding loop diagrams in MIA gives the desired relation between the CKM matrix element $V_{cb} = (40.6 \pm 1.3) \cdot 10^{-3}$ [345] and the trilinear couplings A^u_{23}, A^d_{23}. In the mass insertion approximation holds [363, 364]

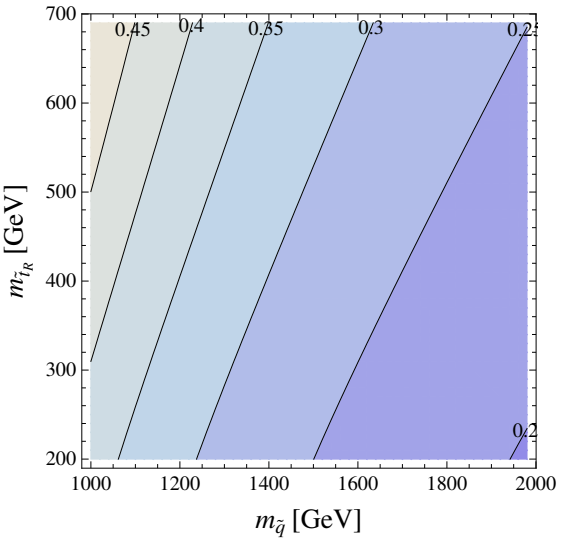

Figure 3.10.: The required value for $(\delta^u_{23})_{LR}$ in the $m_{\tilde{q}}$–$m_{\tilde{t}_R}$ plane in order to generate V_{cb} purely via the up-sector. The gluino mass is fixed to $m_{\tilde{g}} = 1$ TeV.

$$V_{cb} = \frac{2\alpha_s}{3\pi m_{\tilde{g}}} \left(\frac{\left(\Delta^d_{23}\right)_{LR}}{m_b} \tilde{C}_0(x,x) - \frac{(\Delta^u_{23})_{LR}}{m_t} \tilde{C}_0(x,y) \right), \tag{3.53}$$

with the function from the loop calculation

$$\tilde{C}_0(x,y) = \frac{(1-y)x\log(x) + (x-1)y\log y}{(x-1)(y-1)(x-y)}, \tag{3.54}$$

$x = m^2_{\tilde{q}}/m^2_{\tilde{g}}$ and $y = m^2_{\tilde{t}_R}/m^2_{\tilde{g}}$ and $\left(\delta^d_{23}\right)_{LR} = \left(\Delta^d_{23}\right)_{LR}/m^2_{\tilde{q}}$. Eq. (3.53), which we evaluate at the electroweak scale $\mu_0 = 120$ GeV, fixes the requisite values for $(\delta^u_{23})_{LR}$ and/or $\left(\delta^d_{23}\right)_{LR}$ in order to account for V_{cb}.

For simplicity, we look firstly at the case where V_{cb} is purely generated via the up-sector, *i.e.*, with $\left(\delta^d_{23}\right)_{LR} = 0$. In this situation the requisite $(\delta^u_{23})_{LR}$ is shown in Fig. 3.10 in the $m_{\tilde{q}}$–$m_{\tilde{t}_R}$ plane, assuming generically $m_{\tilde{g}} = 1$ TeV. We see that indeed relatively large values of

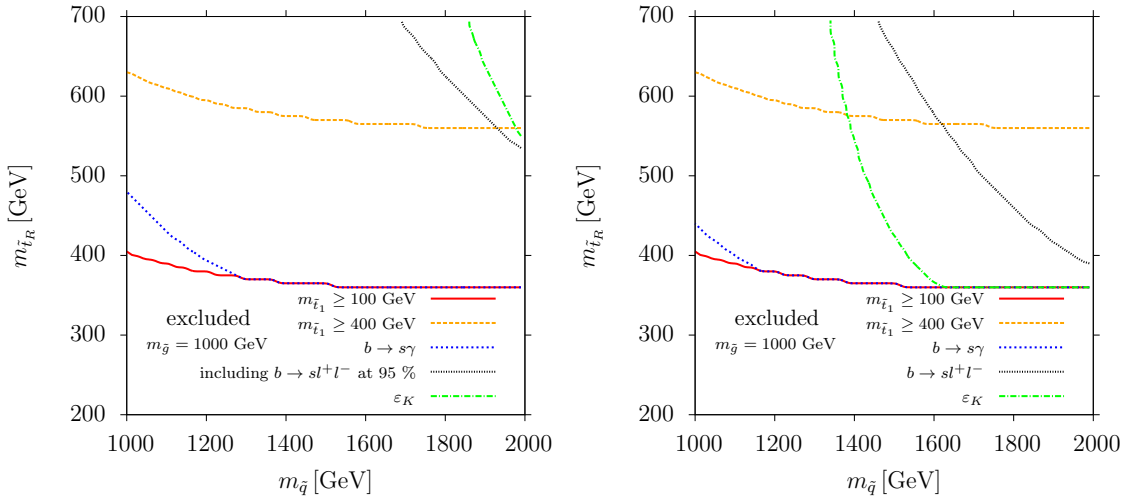

(a) $M_2 = 500$ GeV. Figure taken from [309].

(b) $M_2 = 800$ GeV. Figure taken from [308].

Figure 3.11.: Interplay of the various constraints on the RFV parameter space around the SUSY example point in Table 3.2. Red and orange: Constraints from the mass bound on the light stop mass, in orange a hypothetical future bound on this value. Blue: Bound from $\mathcal{B}(\bar{B} \to X_s\gamma)$. Black: Including additionally the 95% C.L. bound from $\bar{B} \to \bar{K}^{(*)} l^+ l^-$. Green: Bound from ε_K.

$(\delta^u_{23})_{LR}$ are needed in order to account for the measured V_{cb}. Still assuming pure up-sector generation, we translate the value for the scharm-stop left-right mixing into a bound on the RFV parameter space. This is done in the $m_{\tilde{q}}$–$m_{\tilde{t}_R}$ plane around the SUSY example point given in Table 3.2 with the modifications $M_2 = 500$ GeV and $M_2 = 800$, respectively. We show the interplay of the different constraints in Fig. 3.11.

For comparison, we show not only the constraints that we obtain from b physics but also the ones from Kaon physics, namely ε_K, of which the bound has been highlighted already in [364]. The latter bound arises due to a double mass insertion contribution $(\delta^u_{23})^*_{LR}(\delta^u_{13})_{LR}$ which effectively gives a "left first generation"→ "left second generation" transition. Within the RFV model, in the same way as $(\delta^u_{23})_{LR}$ by V_{cb} also $(\delta^u_{13})_{LR}$ is determined by a CKM element that it has to account for, namely V_{ub}. Consequently, $(\delta^u_{13})_{LR}$ acquires a similar sizable phase that can contribute to CP violation in Kaon mixing. The MSSM contribution to the Wilson coefficient $C_1^{\Delta S=2}$ of the operator $(\bar{s}_L\gamma^\mu d_L)(\bar{s}_L\gamma_\mu d_L)$ determining ε_K can be found in Eq. (3.4) of [348]. The right-hand side of this equation has to be multiplied with a correction factor $1/4$ [376][3], *i.e.*, we have altogether [348, 376]

$$C_1^{\Delta S=2} = \frac{1}{4}\frac{G_F^2 m_W^2}{\pi^2} A^d_{ik}\bar{A}^s_{jk}A^d_{jl}\bar{A}^s_{il}\frac{m_W^2}{m^2_{\tilde{u}_k}}k(x_{ik}, x_{jk}, x_{lk}). \tag{3.55}$$

Here, summation over the indices i, j, k, l is implied. The A^d_{ik} and $\bar{A}^s_{jk}$ are composed of the matrices that diagonalize the squark and chargino mass matrices. They as well as the

[3] We thank G. Isidori for pointing this out.

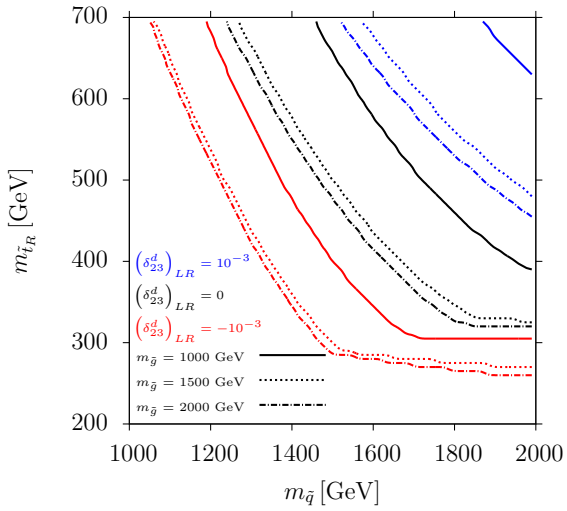

Figure 3.12.: Constraints on the RFV parameter space from $\bar{B} \to \bar{K}^{(*)} l^+ l^-$ at 95% C.L. (including also the weaker bounds by the light stop mass and $\bar{B} \to X_s \gamma$, but disregarding the ones from ε_K) around the SUSY example point in Table 3.2 with $M_2 = 800$ GeV in the case of interference of up- and down-sector generation. Blue: Positive $\left(\delta^d_{23}\right)_{LR} = +10^{-3}$. Red: Negative $\left(\delta^d_{23}\right)_{LR} = -10^{-3}$. For comparison, we show in black the bounds in the case of pure up-sector generation. The solid/dashed/double-dashed lines correspond to different gluino masses. Figure taken from Ref. [308].

loop function $k(x_{ik}, x_{jk}, x_{lk})$ can be found in [348]. The arguments of the loop function are $x_{\{i,j\}k} = m^2_{\tilde{\chi}^\pm_{\{i,j\}}}/m^2_{\tilde{u}_k}$ and $x_{lk} = m^2_{\tilde{u}_l}/m^2_{\tilde{u}_k}$.

Note that in order to use the results given in [348] a basis transformation relative to the super-CKM basis is needed. The conventions are given in Eq. (2.6) of the latter reference and in Eqs. (37)-(39) of Ref. [347]. From $C_1^{\Delta S=2}$ one obtains, after the RG evolution using the factor $\eta \simeq 0.8$ [377, 378] and taking the bag factor $B_K^{\overline{\text{MS}}}(2\,\text{GeV}) = 0.52$ [379] as input, ε_K as described *e.g.* in Refs. [379, 380].
The ε_K bound is implemented as $\varepsilon_K^{\text{RFV}} < 0.6\,\varepsilon_K^{\text{exp}}$ [381], where $\varepsilon_K^{\text{RFV}}$ is the pure RFV contribution to ε_K and $\varepsilon_K^{\text{exp}}$ is the experimental measurement [345].

The relation between Kaon and b physics bounds depends on the flavor-diagonal parameters: For $M_2 = 500$ GeV the bound from ε_K is stronger, *i.e.*, excludes more of the parameter space in the $m_{\tilde{q}}$–$m_{\tilde{t}_R}$ plane than the $\bar{B} \to \bar{K}^{(*)} l^+ l^-$ constraint. This is visible in Fig. 3.11(a). For increasing M_2 this relation is inverted, compare Fig. 3.11(b), where the same plot is shown with $M_2 = 800$ GeV. The bounds are wiped out with rising $m_{\tilde{t}_R}$, which is an effect of the Glashow-Iliopoulos-Maiani (GIM) mechanism. Altogether, the bottom-line of Fig. 3.11 is that in the case of up-sector generation of the CKM matrix the SUSY spectrum has to be $\gtrsim 1$ TeV and that in parts of the parameter space the bounds from $\bar{B} \to \bar{K}^{(*)} l^+ l^-$ are stronger than the ones from Kaon mixing.

Does the conclusion of pushing RFV models beyond the TeV scale also hold when we switch on $\left(\delta^d_{23}\right)_{LR} \neq 0$, *i.e.*, consider an interference of up- and down-sector generation of

the CKM matrix? In order to inspect this question, we compare in Fig. 3.12 the resulting bounds for $\left(\delta^d_{23}\right)_{LR} = \pm 1 \cdot 10^{-3}$.

We only use small values of $\left(\delta^d_{23}\right)_{LR}$ in order not to violate the bound from $\bar{B} \to X_s\gamma$. For the gluino contributions to $C_{7,9,10}$ we use consequently safely the MI expressions that we derive from the formulas given in Ref. [246]. In addition to the dependence on $\left(\delta^d_{23}\right)_{LR}$ we show in Fig. 3.12 also the dependence on the gluino mass.

We observe that for positive $\left(\delta^d_{23}\right)_{LR}$ the constraint on the RFV parameter space gets stronger, while for negative $\left(\delta^d_{23}\right)_{LR}$ it gets weaker. This can easily be understood: For the loop function in Eq. (3.53) it holds $\tilde{C}_0(x, y) < 0$. As $V_{cb} > 0$, it must also be $(\delta^u_{23})_{LR} > 0$. If $\left(\delta^d_{23}\right)_{LR} > 0$, the overall negative contribution of the down sector in Eq. (3.53) has to be compensated by an even larger $(\delta^u_{23})_{LR}$, resulting in a stronger bound on the RFV parameter space from $\bar{B} \to \bar{K}^{(*)} l^+ l^-$. The effect is the other way around for $\left(\delta^d_{23}\right)_{LR} < 0$, then a smaller $(\delta^u_{23})_{LR}$ suffices and the bound on the RFV parameter space is weakened.

3.5. Predictions for Correlated Rare Bottom and Top Decays

Correlation with the rare decay $\bar{B}_s \to \mu^+\mu^-$ Because of the underlying SUSY model we have a link between the constraints on $\bar{B} \to \bar{K}^{(*)} l^+ l^-$ and further rare decays. Firstly, there are possible implications for $\bar{B}_s \to \mu^+\mu^-$ decays. In the low $\tan\beta$ regime that we study here, scalar and pseudoscalar contributions are negligible and the branching ratio $\mathcal{B}(\bar{B}_s \to \mu^+\mu^-)$ only depends on the Wilson coefficient C_{10}, that is,

$$\mathcal{B}(\bar{B}_s \to \mu^+\mu^-) \propto f^2_{B_s} |C_{10}|^2. \tag{3.56}$$

Here, f_{B_s} is the B_s decay constant which is defined by the matrix element [382]

$$\left\langle \bar{B}_s \right| (\bar{b}_\alpha s_\alpha)_{V-A} (\bar{b}_\beta s_\beta)_{V-A} \left| B_s \right\rangle = \frac{8}{3} f^2_{B_s} B_{B_s}(\mu_b) m^2_{B_s}. \tag{3.57}$$

The "bag parameter" $B_{B_s}(\mu) = O(1)$ contains non-perturbative corrections. Using lattice data for f_{B_s} [382, 383] from the allowed range for C_{10} that is implied by Fig. 3.6(a) and accordingly given in Eq. (3.49), we get the allowed range [308]

$$1 \times 10^{-9} \lesssim \mathcal{B}(\bar{B}_s \to \mu^+\mu^-) < 6 \times 10^{-9} \quad \text{(from } \bar{B} \to \bar{K}^{(*)} l^+ l^- \text{ at 95\% C.L.).} \tag{3.58}$$

Here we took the most conservative result that one gets from the different values for f_{B_s} given in [382, 383]. Recently, it has been found evidence for the decay $\bar{B}_s \to \mu^+\mu^-$. Its time integrated (untagged) branching ratio is measured to be [47]

$$\mathcal{B}^{\text{exp}}(\bar{B}_s \to \mu^+\mu^-) = 3.2^{+1.5}_{-1.2} \cdot 10^{-9} \quad \text{(time integrated measurement by LHCb)}, \tag{3.59}$$

which is consistent with the range we obtain from $\bar{B} \to \bar{K}^{(*)} l^+ l^-$ in Eq. (3.58) and also with the recent SM value [384]

$$\mathcal{B}^{\rm SM}(\bar{B}_s \to \mu^+\mu^-) = (3.56 \pm 0.18) \cdot 10^{-9} \quad \text{(time integrated result in the SM)}. \tag{3.60}$$

The latter also includes the effects from the width difference of B_s and $\bar{B}_s$, which is measured as [385]

$$\Delta\Gamma_s = (0.116 \pm 0.018 \pm 0.006)\,\text{ps}^{-1}, \tag{3.61}$$

and gives a correction of up to $\sim 10\%$ [386, 387]. The measurement Eq. (3.59) and its improvement in the future will vice versa further bound the allowed range of C_{10} and has implications for squark flavor and NP models in general. For a recent study of models with NP at the Z vertex see for example Ref. [388]. As discussed in Sec. 3.2.1, at large $\tan\beta$ in the MSSM $\bar{B}_s \to \mu^+\mu^-$ depends also on additional scalar operators. Constraints in this parameter region are studied for MFV-SUSY in [361].

Correlation with Rare Top Decays There is not only an interesting interplay of different b physics channels in constraining the SUSY parameter space, there is furthermore also a link from bottom to top flavor physics: As chargino diagrams of b decays induce FCNCs by up squark loops, the same MI parameters are found in the gluino diagrams of rare top FCNCs $t \to c\gamma, g, Z$. A Feynman diagram showing the gluino loop with the scharm-stop mass insertion $(\delta^u_{23})_{LR}$ is given in Fig. 3.13. The latter MI parameter is also the one that gives the largest contribution to rare top decays [389], so consequently, from the obtained constraints on $(\delta^u_{23})_{LR}$ we can set upper limits on these decays in the MSSM. Due to GIM suppression the SM contribution is negligible [390, 391], *i.e.*, we only take the SUSY contribution into account here. The analytic expressions for $\mathcal{B}(t \to c\gamma, g, Z)$ within SUSY are given in Ref. [392]. We obtain upper bounds by calculating the branching ratios for all generated points shown in Sec. 3.2.2 and applying the therein mentioned bounds including the 68% C.L. bounds from $\bar{B} \to \bar{K}^{(*)} l^+ l^-$. We fix for that the gluino mass to 700 GeV. For larger gluino masses the bounds on the branching ratios will go down even more. As discussed in Sec. 3.2.2, the Higgs bounds are especially important to get a global bound on $(\delta^u_{23})_{LR}$ in addition to the $\bar{B} \to \bar{K}^{(*)} l^+ l^-$ constraints and the bounds on the SUSY spectrum. Our results are given in the last row of Table 3.5 where we compare with the outcome of an MSSM study that was done before LHC started to take data

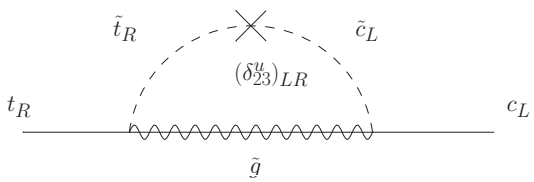

Figure 3.13.: Gluino mediated rare top transition $t_R \to c_L$ from the $(\delta^u_{23})_{LR}$ MI parameter.

[389], the SM prediction [390, 391] and experimental results. The SM prediction is really tiny. The comparison with the 2007 MSSM bounds in [389] shows the significant progress one can make by utilizing the LHC data. The bounds for rare top decays in the MSSM are several orders of magnitude below the prospective sensitivity of both ATLAS [393, 394] and CMS [395]. This is even valid for a future scenario with 100 fb^{-1} at ATLAS. The same is of course even more so true for the current measurements that are with one exception at least one order of magnitude away from the projected sensitivity in the future. In the case of the rare decay $t \to cg$ the current bound at 95% C.L. is even stronger than the requisite branching ratio needed in order to make a 5σ observation.
Altogether, we predict that in foreseeable future we will not observe rare top decays at the LHC if the MSSM is realized.

	$t \to c\gamma$	$t \to cg$	$t \to cZ$
SM prediction [390, 391]	4.6×10^{-14}	4.6×10^{-12}	1×10^{-14}
prospectively needed for 5σ obs. at ATLAS 14 TeV 10 fb^{-1} [393, 394]	$\geq 9.4 \times 10^{-5}$	$\geq 4.3 \times 10^{-3}$	$\geq 4.4 \times 10^{-4}$
prospectively needed for 5σ obs. at ATLAS 14 TeV 100 fb^{-1} [393, 394]	$\geq 3.0 \times 10^{-5}$	$\geq 1.4 \times 10^{-3}$	$\geq 1.4 \times 10^{-4}$
prospectively needed for 5σ obs. at CMS 14 TeV 10 fb^{-1} [395]	$\geq 4.08 \times 10^{-4}$		$\geq 10.4 \times 10^{-4}$
current exp. limit at 95% C.L.	CDF: $< 3.2 \times 10^{-2}$ [397]	ATLAS 7 TeV 2.05 fb^{-1}: $< 2.7 \times 10^{-4}$ [398]	ATLAS 7 TeV 2.1 fb^{-1}: $< 7.3 \times 10^{-3}$ [396] CMS 7 TeV 5.0 fb^{-1}: $< 2.1 \times 10^{-3}$ [399]
MSSM bound pre-LHC [389]	$\lesssim 5.2 \times 10^{-7}$	$\lesssim 3.2 \times 10^{-5}$	$\lesssim 1.8 \times 10^{-6}$
MSSM bound including the 68% C.L. $\bar{B} \to K^{(*)} l^+ l^-$ bounds and the Higgs bound Eq. (3.46)	$\lesssim 2.1 \times 10^{-8}$	$\lesssim 7.2 \times 10^{-7}$	1.0×10^{-7}

Table 3.5.: Branching ratios of rare top decays. 1st row: SM prediction. 2nd and 3rd row: Prospect for sensitivity of ATLAS at 10 fb^{-1} and 100 fb^{-1}, respectively. 4th row: Prospect for sensitivity of CMS at 10 fb^{-1}. 5th row: Current exp. limits. 6th row: Bound in the MSSM before the LHC started taking data. 7th row: The bound we obtain from our parameter scan using the bounds from $\bar{B} \to \bar{K}^{(*)} l^+ l^-$, $\bar{B} \to X_s \gamma$, the EW precision bounds and the constraints on the SUSY spectrum as specified in Sec. 3.2.2 including the Higgs bounds Eq. (3.46), fixing $m_{\tilde{g}} = 700$ GeV. Table adapted and extended from Ref. [308].

4. Improving $\bar{B} \to \bar{K}^*$ Form Factors from Data

In order to benefit the most from the forthcoming data on $\bar{B} \to \bar{K}^* \mu^+ \mu^-$ for future NP studies it is necessary to improve our knowledge of the form factors that are involved in this exclusive decay. This is possible using certain observables at high q^2 as we will explain in the following section. We present in this chapter partly the results of Ref. [400]. A previous study showing for the first time the possibility of the extraction of form factor ratios from data is given in [401].

4.1. Cancellation of Short-distance Physics at Low Recoil

As was mentioned in Sec. 3.1, for the decay $\bar{B} \to \bar{K}^* l^+ l^-$ one can form optimized observables that are especially sensitive to either long or short distance physics, *i.e.*, on the one hand to electroweak physics and on the other hand to nonperturbative QCD effects. As different kind of theories are applicable at high and low invariant dilepton mass q^2, these statements always depend on the region of the considered q^2.

Particularly useful is the universal behavior of the transversity amplitudes of $\bar{B} \to \bar{K}^* l^+ l^-$ at large q^2 [78, 322]

$$A_0^{L,R} = -C^{L,R} f_0 \,, \qquad A_\parallel^{L,R} = -C^{L,R} f_\parallel \,, \qquad A_\perp^{L,R} = +C^{L,R} f_\perp \,. \tag{4.1}$$

These relations are valid at leading order (LO) in the $\Lambda_{\rm QCD}/m_b$ expansion, with universal coefficients $C^{L,R}$ that depend essentially only on the short distance physics and that we specify below in Eq. (4.5). The relations in Eq. (4.1) are the key to the method we describe in the following in order to extract ratios of the form factors at low recoil. The $f_{0,\parallel,\perp}$ are called helicity or transversity form factors, whose relation to the standard heavy-to-light vector and axial vector form factors we give below in Eqs. (4.7)–(4.9). When we insert the expressions for the transversity amplitudes as given in Eq. (4.1) into the observables F_L and $A_T^{(2)}$ defined in Eqs. (3.5) and (3.6) the short distance factors $C^{L,R}$ cancel out [78]

$$F_L = \frac{f_0^2}{f_0^2 + f_\perp^2 + f_\parallel^2} \,, \qquad A_T^{(2)} = \frac{f_\perp^2 - f_\parallel^2}{f_\perp^2 + f_\parallel^2} \,. \tag{4.2}$$

The relations Eq. (4.1) and thus the short-distance independence of F_L and $A_T^{(2)}$ in Eq. (4.2) follow from the Operator Product Expansion (OPE) at high q^2 [315, 316] and improved

Isgur-Wise relations between the form factors [78, 315, 402]. Corrections to Eqs. (4.1), (4.2) are at the percent level, as the ones of the OPE start at $O(\alpha_s \Lambda_{\rm QCD}/m_b, m_c^4/q^4)$ [78, 315] and the ones of the form factor relations at $\sim 2C_7^{\rm eff}/C_9^{\rm eff}\Lambda_{\rm QCD}/m_b$, *i.e.*, the $\Lambda_{\rm QCD}/m_b$ corrections are parametrically suppressed by the Wilson coefficients [78, 315].

Therefore, at high q^2 we can use F_L and $A_T^{(2)}$ in order to probe the ratios of the transversity form factors only, to good approximation without pollution from short distance physics—at least as long as we stay in the SM operator basis. This means at high q^2 it turns out that F_L and $A_T^{(2)}$ are actually optimized observables in order to inspect long distance physics.

Nevertheless, Eq. (4.2) has to be taken with a grain of salt, as NP outside the SM basis of effective operators could modify them. In case of the presence of right-handed currents from chirality flipped operators Eq. (4.2) gets correction factors. In this case, it is not possible to construct optimized observables from where one can extract a ratio that contains $f_\perp$ without a pollution from short distance physics [321]. As demonstrated in [321], from current data it can be inferred that the correction factor in front of $f_\perp/f_\parallel$ can be up to 30% at 2σ. However, one can still extract $f_0/f_\parallel$ from F_L without such a pollution in this case [321].

Another complication arises due to the q^2 binning of the data. While at each single q^2 point the short distance coefficients $C^{L,R}$ cancel out in F_L and $A_T^{(2)}$ this is in principle not the case for the corresponding binned observables. Actually, these are given as

$$\langle F_L \rangle_{\rm bin} = \frac{\int_{\rm bin} \rho_1(q^2) f_0^2 \, {\rm d}q^2}{\int_{\rm bin} \rho_1(q^2) \left(f_0^2 + f_\perp^2 + f_\parallel^2\right) \, {\rm d}q^2} \,, \tag{4.3}$$

$$\langle A_T^{(2)} \rangle_{\rm bin} = \frac{\int_{\rm bin} \rho_1(q^2) \left(f_\perp^2 - f_\parallel^2\right) \, {\rm d}q^2}{\int_{\rm bin} \rho_1(q^2) \left(f_\perp^2 + f_\parallel^2\right) \, {\rm d}q^2} \,. \tag{4.4}$$

Here, $\rho_1 = \frac{1}{2}\left(|C^L|^2 + |C^R|^2\right)$, with [321]

$$C^{L,R} = C_9 + \kappa \frac{2 m_b m_B}{q^2} C_7 + Y(q^2) \mp C_{10} \,, \tag{4.5}$$

where [315]

$$\kappa \overset{O(\alpha_s)}{=} 1 - 2\alpha_s/(3\pi) \log\left(\mu/m_b\right) \,, \tag{4.6}$$

and the function $Y(q^2)$ is defined in [322]. As can be seen from Eqs. (4.3) and (4.4), the dependence on the q^2-dependent coefficients $C^{L,R}$ does not cancel under the integral. As was shown in Ref. [401], due to the slowly varying ρ_1 per bin, this effect is numerically small, especially compared to the precision of current data. However, we take it into account nevertheless.

Altogether, F_L and $A_T^{(2)}$ can be used as model-independent probes of form factor ratios as long as no right-handed currents show up.

Definition of Transversity Form Factors By definition, the transversity form factors $f_{\perp,\parallel,0}$ are related to the vector and axial vector form factors as follows [78]

$$f_\perp = \mathcal{N}\frac{\sqrt{2\hat{s}\hat{\lambda}}}{1+\hat{m}_{K^*}}V\,, \tag{4.7}$$

$$f_\parallel = \mathcal{N}\sqrt{2\hat{s}}(1+\hat{m}_{K^*})A_1\,, \tag{4.8}$$

$$f_0 = \mathcal{N}\frac{(1-\hat{s}-\hat{m}_{K^*}^2)(1+\hat{m}_{K^*})^2A_1-\hat{\lambda}A_2}{2\hat{m}_{K^*}(1+\hat{m}_{K^*})}. \tag{4.9}$$

We used here the following notations and abbreviations:

$$\mathcal{N} = G_F\alpha_e V_{tb}V_{ts}^*\sqrt{\frac{m_B^3\sqrt{\hat{\lambda}}}{3\cdot 2^{10}\pi^5}}\,, \tag{4.10}$$

$$\hat{s} = \frac{q^2}{m_B^2}\,, \qquad \hat{m}_{K^*} = \frac{m_{K^*}}{m_B}\,, \tag{4.11}$$

$$\hat{\lambda} = 1+\hat{s}^2+\hat{m}_{K^*}^4-2(\hat{s}+\hat{s}\hat{m}_{K^*}^2+\hat{m}_{K^*}^2)\,. \tag{4.12}$$

The vector and axial vector form factors in Eqs. (4.7)–(4.9) are given as

$$\langle K^*(k,\epsilon)|\,\bar{s}\gamma_\mu b\,|B(p)\rangle = \frac{2V(q^2)}{m_B+m_{K^*}}\varepsilon_{\mu\rho\sigma\tau}\epsilon^{*\rho}p^\sigma k^\tau\,, \tag{4.13}$$

$$\begin{aligned}\langle K^*(k,\epsilon)|\,\bar{s}\gamma_\mu\gamma_5 b\,|B(p)\rangle = i\epsilon^{*\rho}\Bigg[&2A_0(q^2)m_{K^*}\frac{q_\mu q_\rho}{q^2}\\ &+A_1(q^2)(m_B+m_{K^*})\left(g_{\mu\rho}-\frac{q_\mu q_\rho}{q^2}\right)-A_2(q^2)q_\rho\left(\frac{(p+k)_\mu}{m_B+m_{K^*}}-\frac{m_B-m_{K^*}}{q^2}(p-k)_\mu\right)\Bigg]\,,\end{aligned} \tag{4.14}$$

with the K^* polarization vector ϵ^ρ. Furthermore, the tensor or dipole form factors we write as

$$\langle K^*(k,\epsilon)|\,\bar{s}i\sigma_{\mu\nu}q^\nu b\,|B(p)\rangle = -2T_1(q^2)\,\varepsilon_{\mu\rho\sigma\tau}\epsilon^{*\rho}p^\sigma k^\tau\,, \tag{4.15}$$

$$\begin{aligned}\langle K^*(k,\epsilon)|\,\bar{s}i\sigma_{\mu\nu}\gamma_5 q^\nu b\,|B(p)\rangle = {}&iT_2(q^2)\left(\epsilon_\mu^*(m_B^2-m_{K^*}^2)-(\epsilon^*\cdot q)(p+k)_\mu\right)\\ &+iT_3(q^2)(\epsilon^*\cdot q)\left(q_\mu-\frac{q^2}{m_B^2-m_{K^*}^2}(p+k)_\mu\right).\end{aligned} \tag{4.16}$$

A priori properties of F_L and $A_T^{(2)}$ Inserting the definitions in Eqs. (4.7)–(4.9) into the Eq. (4.2) and evaluating them at the endpoint of the spectrum $q^2_{\text{max}} = (m_B - m_{K^*})^2$ we learn that *a priori* [400]

$$F_L(q^2=q^2_{\text{max}}) = \frac{1}{3}\,, \qquad A_T^{(2)}(q^2=q^2_{\text{max}}) = -1\,, \tag{4.17}$$

where q^2_{max} is the highest invariant mass the lepton pair can have.

4.2. Parametrization of Form Factors by their Series Expansion

QCD motivated parametrization of q^2 shape In order to fit the q^2-dependent form factor ratios $f_\perp/f_\parallel$ and $f_0/f_\parallel$ from high q^2 data on the observables F_L and $A_T^{(2)}$ we use a certain parametrization. We use the so called "Series Expansion" (SE) [403–409] in the variable

$$z(t, t_0) = \frac{\sqrt{t_+ - t} - \sqrt{t_+ - t_0}}{\sqrt{t_+ - t} + \sqrt{t_+ - t_0}}\,. \tag{4.18}$$

In general, $z(t, t_0)$ is complex. The variables in Eq. (4.18) are defined as follows:

- t: analytic continuation of q^2 to the domain of complex numbers.
- $t_+ = (m_B + m_{K^*})^2$: pair production threshold.
- t_0: expansion point of the series expansion, with $0 \le t_0 \le t_+$. For example, one can set $t_0 = 0$ or $t_0 = t_+\sqrt{1 - t_-/t_+}$ [409, 410] with the semileptonic endpoint $t_- = q^2_{\text{max}} = (m_B - m_{K^*})^2$.

The variable z fulfills $z(t_0, t_0) = 0$ and $|z(t, t_0)| \le 1$. The series expansion of the transversity form factors in z is given as

$$f_i(t)/\mathcal{N} = \frac{1}{B(t)\,\phi_T^{V-A}(t)} \left(\sqrt{-z(t,0)}\right)^m \left(\sqrt{z(t,t_-)}\right)^l \sum_k \alpha_{i,k}\, z^k(t, t_0). \tag{4.19}$$

In Eq. (4.19) we used the following assignment of l and m to $f_\perp$, $f_\parallel$ and f_0:

- for $f_\perp$: $l = 1, m = 1$.
- for $f_\parallel$: $l = 0, m = 1$.
- for f_0: $l = 0, m = 0$.

The additional functions are the following:

- $B(t) = z(t, m_R^2)$: Blaschke factor for the off-shell pole of vector or axial vector mesons with mass m_R .
- $\phi_T^{V-A}(t) = \sqrt{\frac{1}{24\pi\chi_f(2)}} \frac{t - t_+}{(t_+ - t_0)^{\frac{1}{4}}} \left(\frac{z(t,0)}{-t}\right)^{\frac{5}{2}} \left(\frac{z(t,t_0)}{t_0 - t}\right)^{-\frac{1}{2}} \left(\frac{z(t,t_-)}{t_- - t}\right)^{-\frac{3}{4}}$ with $\chi_f(2) = \frac{1.2}{100 m_b^2}$.

For details on the series expansion, the Blaschke factor and the function $\phi_T^{V-A}(t)$ see [409, 410]. The parameters we want to determine by a fit from the data are ratios of the coefficients $\alpha_{i,k}$ in Eq. (4.19). These will give us the desired information on the q^2 shape of the ratios of the form factors.
In the following we consider SE1 ($k = 0$) and SE2 (including $k = 1$).

A priori properties of form factors at LO (SE1) At LO Eq. (4.19) gives the following expressions for the transversity form factors [401]

$$f_\perp(t) = \frac{\mathcal{N}}{z(t, m_{1^-}^2)\,\phi_T^{V-A}(t)} \sqrt{-z(t,0)}\,\sqrt{z(t,t_-)} \times \alpha_\perp\,, \tag{4.20}$$

$$f_\parallel(t) = \frac{\mathcal{N}}{z(t, m_{1^+}^2)\,\phi_T^{V-A}(t)} \sqrt{-z(t,0)} \times \alpha_\parallel\,, \tag{4.21}$$

$$f_0(t) = \frac{\mathcal{N}}{z(t, m_{1^+}^2)\,\phi_T^{V-A}(t)} \times \alpha_0\,, \tag{4.22}$$

with $m_{1^-} = 5.42$ GeV and $m_{1^+} = 5.83$ GeV [89]. In Eqs. (4.20)–(4.22) we have written for the leading coefficients of the series expansion

$$\alpha_\perp \equiv \alpha_{\perp,0}\,, \qquad \alpha_\parallel \equiv \alpha_{\parallel,0}\,, \qquad \alpha_0 \equiv \alpha_{0,0}. \tag{4.23}$$

Consequently, at the first order of the series expansion (SE1) there are only three real parameters. Here we only use data on F_L and $A_T^{(2)}$ (at high q^2) and are thus only sensitive to the ratios of these parameters, *e.g.* to $\alpha_\perp/\alpha_\parallel$ and $\alpha_0/\alpha_\parallel$. Only the squares of these ratios appear in the considered observables, see Eq. (4.2). Consequently, we are also not sensitive to their sign and choose without loss of generality $\alpha_\perp/\alpha_\parallel \geq 0$ and $\alpha_0/\alpha_\parallel \geq 0$.

In parametrizing the form factors in SE1 the q^2-shape is very much constrained. For example, there is no dependence on t_0 and there are strong correlations between low and high q^2. We specify these correlations below:

- **Correlation 1:** $\alpha_\perp/\alpha_\parallel$ **and thus** $A_T^{(2)}(q^2)$ **from** $V(0)/A_1(0)$
  Firstly, from the ratio $f_\perp/f_\parallel$ and inserting on the one hand the relation with the vector and axial vector form factors given in Eqs. (4.7)–(4.9) and on the other hand the SE1, we get by solving for $\alpha_\perp/\alpha_\parallel$ [400]

$$\frac{\alpha_\perp}{\alpha_\parallel} = \frac{\sqrt{\hat{\lambda}}}{(1+\hat{m}_{K^*})^2} \frac{z(q^2, m_{1^-}^2)}{z(q^2, m_{1^+}^2)} \frac{1}{\sqrt{z(q^2,t_-)}} \frac{V(q^2)}{A_1(q^2)} \overset{q^2=0}{=} 1.19 \frac{V(0)}{A_1(0)}\,. \tag{4.24}$$

  The latter expression has been numerically evaluated at $q^2 = 0$. Eq. (4.24) implies that the full q^2-shape of $A_T^{(2)}$ is determined by V/A_1 at $q^2 = 0$ (or any other value of q^2) in SE1.

- **Correlation 2:** $\alpha_0/\alpha_\parallel$ **from** $F_L(t_-) = 1/3$
  From the definition of the transversity factors we know that $F_L(t_-) = 1/3$, see Eq. (4.17). This information is however not contained *a priori* in the series expansion, *i.e.*, it will give a constraint on the parameters of the SE. Inserting the SE1 expressions for the f_i into F_L in Eq. (4.17) it follows

$$\frac{\alpha_0}{\alpha_\parallel} = \sqrt{\frac{-z(t_-,0)}{2}} = 0.29. \tag{4.25}$$

In SE1, Eq. (4.25) fixes $\alpha_0/\alpha_\parallel$ from high q^2 information. From the endpoint relation for $A_T^{(2)}$ no such constraint arises, as here the same relation follows not only from the definition of the transversity form factors through the vector and axial form factors, but is also contained in the SE itself. Consequently, no additional information can be obtained from the endpoint relation of $A_T^{(2)}$.

- **Correlation 3: $\alpha_0/\alpha_\parallel$ from $A_2(0)/A_1(0)$**
  On the other hand, the ratio $\alpha_0/\alpha_\parallel$ can also be fixed by yet another form factor ratio at low q^2. Forming the ratio A_2/A_1, inserting the relation to the transversity form factors and subsequently the SE1, we arrive at [400]

$$\frac{A_2(0)}{A_1(0)} = \frac{(1+\hat{m}_{K^*})^2}{(1-\hat{m}_{K^*})^2}\left(1-\hat{m}_{K^*}^2 - 4\sqrt{2}\hat{m}_{K^*}(1+\hat{m}_{K^*})\left(\frac{\alpha_0}{\alpha_\parallel}\right)\right) \tag{4.26}$$

$$= 1.41 - 1.63\left(\frac{\alpha_0}{\alpha_\parallel}\right) \tag{4.27}$$

$$= 0.93. \tag{4.28}$$

  In the last row we inserted the value for $\alpha_0/\alpha_\parallel$ that follows from F_L at high q^2, Eq. (4.25).

The correlations of the SE1 parameters with the form factor ratios V/A_1 and A_2/A_1 open up the opportunity for comparisons with LCSR predictions for these ratios at low q^2 [400], that we give at the end of Sec. 4.3. The value of $\alpha_\perp/\alpha_\parallel$ that can be determined by fits to the data can be used for the extraction of $V(0)/A_1(0)$ via Eq. (4.24). Furthermore, before taking any data into account, from $F_L(t_-) = 1/3$ (Eq. (4.25)) the SE1 determines $A_2(0)/A_1(0)$ *a priori* through Eq. (4.28). Possible disagreements in the comparison of these results with LCSR outcomes could be lead back to several reasons: On the one hand, they can be due to fluctuations of the data. Further options are the possible underestimation of LCSR uncertainties, or the presence of right-handed currents from NP. The latter would spoil our working hypothesis given by the relations Eq. (4.2). On the other hand, a discrepancy between SE1 fits to the data and LCSR results could just mean that the SE1 parametrization itself is not appropriate, because it is too simple and introduces too much bias into the fit. In the case of inconsistencies a combined fit of the data and LCSR input for the form factor ratios at low q^2 will give a large χ^2. We test the interplay of SE1 and LCSR results in Sec. 4.4 and present the outcome of the comparison therein.

Reducing Theoretical Bias by Using the SE at Second Order In the previous paragraph we have shown that the fit using the SE1 is very much constrained already before taking data into account. The ratio $\alpha_0/\alpha_\parallel$ is fixed by an *a priori* relation for the observable F_L at the endpoint, *i.e.*, the only real degree of freedom in the fit is given by $\alpha_\perp/\alpha_\parallel$. We can already overconstrain the fit by taking into account additional theoretical input on V/A_1 and A_2/A_1 at low q^2.

In order to have a parametrization with reduced bias from the theory side, in the following we discuss the second order series expansion (SE2). At this order we write for the

transversity form factors:

$$f_\perp(t) = \frac{\mathcal{N}}{z(t, m_{1^-}^2)\,\phi_T^{V-A}(t)} \sqrt{-z(t,0)}\,\sqrt{z(t,t_-)} \times \alpha_\perp \left(1 + p_\perp\, z(t,t_0)\right) , \tag{4.29}$$

$$f_\parallel(t) = \frac{\mathcal{N}}{z(t, m_{1^+}^2)\,\phi_T^{V-A}(t)} \sqrt{-z(t,0)} \times \alpha_\parallel \left(1 + p_\parallel\, z(t,t_0)\right) , \tag{4.30}$$

$$f_0(t) = \frac{\mathcal{N}}{z(t, m_{1^+}^2)\,\phi_T^{V-A}(t)} \times \alpha_0 \left(1 + p_0\, z(t,t_0)\right) , \tag{4.31}$$

introducing

$$p_\parallel = \alpha_{\parallel,1}/\alpha_{\parallel,0}\,, \qquad p_\perp = \alpha_{\perp,1}/\alpha_{\perp,0}\,, \qquad p_0 = \alpha_{0,1}/\alpha_{0,0}\,. \tag{4.32}$$

In SE2, the fit parameters are extended to five ratios. In addition to $\alpha_\perp/\alpha_\parallel$ and $\alpha_0/\alpha_\parallel$ we have to take into account the three ratios defined in Eq. (4.32). Still, in the considered observables only appear the squares of $\alpha_\perp/\alpha_\parallel$ and $\alpha_0/\alpha_\parallel$, *i.e.*, we can choose without loss of generality $\alpha_\perp/\alpha_\parallel \geq 0$ and $\alpha_0/\alpha_\parallel \geq 0$. However, for the ratios in Eq. (4.32), it is $-\infty \leq p_\parallel, p_\perp, p_0 \leq +\infty$. Furthermore, in contrast to SE1, in Eqs. (4.29)-(4.31) it is introduced an explicit dependence on the expansion point t_0.

Altogether, due to the extended number of parameters the fit of the SE2 contains less *a priori* constraints than the one of SE1. We will recognize this also in the fits presented in Sec. 4.4. Before coming to that, in the next section we present relations for the ratios of form factors at low q^2 that will be used as theoretical input to the fit in addition to the data at high q^2. For that, we will utilize among others the heavy-quark symmetry of QCD that results from $m_b \gg \Lambda_{\rm QCD}$. Subsequently, we analyze the interesting interplay of data and theory input and their effect on the q^2-shape of the form factors.

4.3. Theoretical Input for Form Factors at Low q^2

Large Energy Limit Relations at Leading Order

In Ref. [411] it was proposed to investigate the symmetries that arise for meson decays in the kinematic region of the large energy limit (LEL). Therein, the framework of a Large Energy Effective Theory (LEET) was used. The LEL region of $\bar{B} \to \bar{K}^* l^+ l^-$ is defined as the combination of both the heavy quark limit $m_b \gg \Lambda_{\rm QCD}$ and the kinematic assumption of large hadronic energy $E_{K^*} \gg \Lambda_{\rm QCD}$, corresponding to low q^2. E_{K^*} is the energy of the $\bar{K}^*$ in the $\bar{B}$ rest frame, *i.e.*,

$$E_{K^*} = \frac{m_B^2 + m_{K^*}^2 - q^2}{2m_B}. \tag{4.33}$$

In the LEL by definition the symmetries of the heavy quark limit apply, and possibly further ones are added. Note that the LEET introduced in [411], which systematically

treats the expansion in $1/m_b$ and $1/E_{K^*}$, has shown to be inconsistent as an effective theory of exclusive decays [412–414], see also footnote one in [415]. Nevertheless, the LEL itself can be physically meaning- and useful. Furthermore, unlike the LEET, the Heavy Quark Effective Theory (HQET) [185, 416–422], which uses a systematic expansion in $1/m_b$, indeed gives a consistent effective field theory.

In the heavy quark limit as a consequence of heavy quark spin symmetry the $\bar{B} \to \bar{K}^*$ form factors $V, A_{0,1,2}$ are related to $T_{1,2,3}$, see Eqs. (4)–(6) in [423]. In the LEL, this is of course still true as the heavy quark limit is incorporated therein. On top of that, the form factors reveal several relations that are contained in the expressions [423, 424]

$$V(q^2) = \left(1 + \frac{m_{K^*}}{m_B}\right)\xi_\perp(m_B, E_{K^*})\,, \tag{4.34}$$

$$A_1(q^2) = \frac{2E_{K^*}}{m_B + m_{K^*}}\xi_\perp(m_B, E_{K^*})\,, \tag{4.35}$$

$$A_2(q^2) = \left(1 + \frac{m_{K^*}}{m_B}\right)\left(\xi_\perp(m_B, E_{K^*}) - \frac{m_{K^*}}{E_{K^*}}\xi_\parallel(m_B, E_{K^*})\right), \tag{4.36}$$

$$A_0(q^2) = \left(1 - \frac{m_{K^*}^2}{m_B E_{K^*}}\right)\xi_\parallel(m_B, E_{K^*}) + \frac{m_{K^*}}{m_B}\xi_\perp(m_B, E_{K^*})\,, \tag{4.37}$$

$$T_1(q^2) = \xi_\perp(m_B, E_{K^*})\,, \tag{4.38}$$

$$T_2(q^2) = \left(1 - \frac{q^2}{m_B^2 - m_{K^*}^2}\right)\xi_\perp(m_B, E_{K^*})\,, \tag{4.39}$$

$$T_3(q^2) = \xi_\perp(m_B, E_{K^*}) - \frac{m_{K^*}}{E_{K^*}}\left(1 - \frac{m_{K^*}^2}{m_B^2}\right)\xi_\parallel(m_B, E_{K^*})\,, \tag{4.40}$$

including only two independent form factors $\xi_\perp$ and $\xi_\parallel$ that determine the seven form factors on the left-hand side. On a formal level, in [424] the results Eqs. (4.34)–(4.40) are obtained from the observation that in the LEET the heavy and light fields become approximately two-component spinors. Among the relations that can be derived from the LEL relations Eqs. (4.34)–(4.40) are the following [423, 424]

$$\frac{V(q^2)}{A_1(q^2)} = \frac{(m_B + m_{K^*})^2}{2m_B E_{K^*}} + O(\Lambda_{\text{QCD}}/m_b)\,, \tag{4.41}$$

$$\frac{T_1(q^2)}{T_2(q^2)} = \frac{m_B}{2E_{K^*}} + O(\Lambda_{\text{QCD}}/m_b)\,. \tag{4.42}$$

As will turn out in the calculation of the Λ_{QCD}/m_b-corrections in the next paragraph, it is interesting to consider also the double ratio of Eq. (4.41) and (4.42) [400]. We obtain at $q^2 = 0$

$$\mathcal{R}(q^2 = 0) \equiv \frac{V(0)/A_1(0)}{T_1(0)/T_2(0)} = \frac{V(0)}{A_1(0)} = \frac{m_B + m_{K^*}}{m_B - m_{K^*}} + O(\Lambda_{\text{QCD}}/m_b)\,. \tag{4.43}$$

Note that at $q^2 = 0$ holds $T_1(0) = T_2(0) \equiv T$. It can be shown that Eqs. (4.41), (4.42) and thus also (4.43) follow from helicity conservation (HC) within the perturbative part of QCD [423]. The validity of Eqs. (4.41)–(4.43) coincides with the vanishing of the positive transverse helicity amplitudes of $\bar{B} \to \bar{K}^* l^+ l^-$, whereas the negative transverse helicity amplitudes are induced by the $V - A$ structure of the SM [423]. In the heavy quark limit $m_b \to \infty$ the K^* just takes over the spin of the b quark. A spin flip that would induce corrections to this situation can happen only due to nonperturbative effects. Hence, corrections of Eqs. (4.41)–(4.43) come firstly at $O(\Lambda_{\rm QCD}/m_b)$ and there are no corrections to these relations in the α_s expansion. Putting this into a formal language, in the expansion

$$\mathcal{R} = \mathcal{R}_0 + \mathcal{R}_{\Lambda_{\rm QCD}/m_b} + \mathcal{R}_{\alpha_s} + \mathcal{R}_{\alpha_s \Lambda_{\rm QCD}/m_b} + \mathcal{R}_{\Lambda^2_{\rm QCD}/m_b^2} + \dots , \tag{4.44}$$

where $\mathcal{R}_0$ has been given in Eq. (4.43), all terms $\mathcal{R}_{\alpha_s^n}$ vanish [400]. Despite this feature, without knowing the exact size of the $O(\Lambda_{\rm QCD}/m_b)$ corrections, nevertheless we have to assume an uncertainty of ±30% concerning the value of $\mathcal{R}$ obtained from HC/LEL in order to be conservative. From Eq. (4.41) we obtain altogether

$$\mathcal{R}(0) = \frac{V(0)}{A_1(0)} = 1.33 \pm 0.4 \qquad \text{(HC)}. \tag{4.45}$$

We will utilize Eq. (4.45) as theoretical input for the form factor ratio fits in Sec. 4.4.

$\Lambda_{\rm QCD}/m_b$ Corrections to the Large Energy Limit Relations

The LEL/HC estimate in Eq. (4.45) has a rather large uncertainty. In order to contribute to an improvement on that, we derive in this paragraph the analytic form of the correction term $\mathcal{R}_{\Lambda_{\rm QCD}/m_b}$ in Eq. (4.44). With additional input from LCSRs for the HQET form factors introduced in Eqs. (4.54) and (4.55) below this will give a better control of the theory error.

In order to calculate $\mathcal{R}_{\Lambda_{\rm QCD}/m_b}$, we proceed as follows: We firstly calculate the improved Isgur-Wise [425] relations, *i.e.*, relations between tensor, vector and axial vector form factors *including* corrections of order $\Lambda_{\rm QCD}/m_b$. For that we follow the methodology presented in [315, 402]. From the equations of motion of QCD we obtain

$$i\partial^\nu(\bar{s} i\sigma_{\mu\nu} b) = -(m_b + m_s)(\bar{s}\gamma_\mu b) + i\partial_\mu(\bar{s}b) - 2\bar{s} i\overleftarrow{D}_\mu b\,, \tag{4.46}$$

$$i\partial^\nu(\bar{s} i\sigma_{\mu\nu}\gamma_5 b) = (m_b - m_s)\bar{s}\gamma_\mu\gamma_5 b + i\partial_\mu(\bar{s}\gamma_5 b) - 2\bar{s} i\overleftarrow{D}_\mu\gamma_5 b. \tag{4.47}$$

We take then the hadronic matrix element of the identities Eqs. (4.46) and (4.47) between the states $|B(p)\rangle$ and $\left|K^*(k,\epsilon)\right\rangle$. After that, we insert the definitions of the form factors given in Eqs. (4.13)–(4.16). Concerning the dimension-four QCD operators $\bar{s} i\overleftarrow{D}_\mu b$ and $\bar{s} i\overleftarrow{D}_\mu\gamma_5 b$ we define as follows the form factors $d(q^2)$, $d_1(q^2)$, $d_+(q^2)$ and $d_-(q^2)$ [315]

$$\left\langle K^*(k,\epsilon)\right| \bar{s} i\overleftarrow{D}_\mu b \left|B(p)\right\rangle = d\varepsilon_{\mu\rho\sigma\tau}\epsilon^{*\rho}(p+k)^\sigma(p-k)^\tau\,, \tag{4.48}$$

$$\left\langle K^*(k,\epsilon)\right| \bar{s} i\overleftarrow{D}_\mu\gamma_5 b \left|B(p)\right\rangle = id_1\epsilon^*_\mu + id_+(\epsilon^*\cdot p)(p+k)_\mu + id_-(\epsilon^*\cdot p)(p-k)_\mu\,. \tag{4.49}$$

Note that our definitions in Eqs. (4.48) and (4.49) differ from the ones in [315] by factors of i. The form factors on the right-hand side of Eqs. (4.48) and (4.49) have the disadvantage of having no definite scaling with the beauty quark mass. We can handle the situation nevertheless by matching the dimension-four QCD operators onto HQET [315]

$$\bar{s}i\overleftarrow{D}_\mu b = D_0^{(v)}(\mu) m_b \bar{s}\gamma_\mu b_v + D_1^{(v)}(\mu) m_b \bar{s} v_\mu b_v + \bar{s}i\overleftarrow{D}_\mu b_v + \dots \,, \tag{4.50}$$

$$\bar{s}i\overleftarrow{D}_\mu \gamma_5 b = -D_0^{(v)}(\mu) m_b \bar{s}\gamma_\mu\gamma_5 b_v + D_1^{(v)}(\mu) m_b \bar{s} v_\mu \gamma_5 b_v + \bar{s}i\overleftarrow{D}_\mu \gamma_5 b_v + \dots \,, \tag{4.51}$$

with Wilson coefficients $D_i^{(v)}(\mu)$ and the HQET beauty field b_v that has four-velocity v_μ. The HQET currents $\bar{s}\gamma_\mu b_v$ and $\bar{s} b_v$ in Eq. (4.50) can be related to the quark currents $\bar{s}\gamma_\mu b$ and $\bar{s} b$ via [78]

$$\bar{s}\gamma_\mu b = C_0^{(v)}(\mu)\bar{s}\gamma_\mu b_v + C_1^{(v)}(\mu) v_\mu \bar{s} b_v + \dots \,, \tag{4.52}$$

$$\bar{s} b = C_0^{(s)} \bar{s} b_v + \dots \,, \tag{4.53}$$

with Wilson coefficients $C_i^{(x)}(\mu)$. Similar expressions hold for the currents $\bar{s}\gamma_\mu\gamma_5 b_v$ and $\bar{s}\gamma_5 b_v$. In analogy to the parametrization of the QCD matrix elements of the operators $\bar{s}i\overleftarrow{D}_\mu b$ and $\bar{s}i\overleftarrow{D}_\mu\gamma_5 b$ through the form factors d, d_1, d_+ and d_- in Eqs. (4.48) and (4.49), the matrix elements of the HQET operators $\bar{s}i\overleftarrow{D}_\mu b_v$ and $\bar{s}i\overleftarrow{D}_\mu\gamma_5 b_v$ can be parametrized as

$$\langle K^*(k,\epsilon)\big|\, \bar{s}i\overleftarrow{D}_\mu b_v \,|B(v)\rangle = d^{(0)} \varepsilon_{\mu\rho\sigma\tau}\epsilon^{*\rho}(p+k)^\sigma (p-k)^\tau \,, \tag{4.54}$$

$$\langle K^*(k,\epsilon)\big|\, \bar{s}i\overleftarrow{D}_\mu \gamma_5 b_v \,|B(v)\rangle = i d_1^{(0)}\epsilon_\mu^* + i d_+^{(0)}(\epsilon^*\cdot p)(p+k)_\mu + i d_-^{(0)}(\epsilon^*\cdot p)(p-k)_\mu \,, \tag{4.55}$$

defining the HQET form factors $d^{(0)}$, $d_1^{(0)}$, $d_+^{(0)}$ and $d_-^{(0)}$. The point of using the HQET form factors $d_{(i)}^{(0)}$ for the $\Lambda_{\rm QCD}/m_b$ expansion is that in contrast to the $d_{(i)}$ we know that they fulfill the characteristic scaling laws [315]

$$d^{(0)} \sim m_b^{-1/2} \,, \qquad d_1^{(0)} \sim m_b^{1/2} \,, \tag{4.56}$$

$$d_+^{(0)} - d_-^{(0)} \sim m_b^{-1/2} \,, \qquad d_+^{(0)} + d_-^{(0)} \sim m_b^{-3/2}. \tag{4.57}$$

The scaling of the corresponding $d_{(i)}$ in Eqs. (4.48)–(4.49) is not known.

Consequently, using the HQET form factors $d_{(i)}^{(0)}$ we obtain a systematic $\Lambda_{\rm QCD}/m_b$ expansion. As the first step, for the $d_{(i)}$ one obtains the following expansions in terms of the $d_{(i)}^{(0)}$ [315]

$$d(q^2) = -m_b(\mu)\frac{D_0^{(v)}(\mu)}{C_0^{(v)}(\mu)}\frac{V(q^2)}{m_B + m_{K^*}} + d^{(0)}(q^2) + O\left(\alpha_s\, m_b^{-1/2}, m_b^{-3/2}\right) , \tag{4.58}$$

$$d_1(q^2) = -m_b(\mu)\frac{D_0^{(v)}(\mu)}{C_0^{(v)}(\mu)}(m_B + m_{K^*})A_1(q^2) + d_1^{(0)}(q^2) + O\left(\alpha_s\, m_b^{-1/2}, m_b^{-3/2}\right) , \tag{4.59}$$

$$d_+(q^2) = \quad m_b(\mu)\frac{D_0^{(v)}(\mu)}{C_0^{(v)}(\mu)}\frac{A_2(q^2)}{m_B + m_{K^*}} + d_+^{(0)}(q^2) + O\left(\alpha_s\, m_b^{-1/2}, m_b^{-3/2}\right) , \tag{4.60}$$

$$d_-(q^2) = -m_b(\mu)\frac{D_0^{(v)}(\mu)}{C_0^{(v)}(\mu)}\left(\frac{2m_{K^*}}{q^2}A_0(q^2) - \frac{m_B + m_{K^*}}{q^2}A_1(q^2) + \frac{m_B - m_{K^*}}{q^2}A_2(q^2)\right) + d_-^{(0)}(q^2) + O\left(\alpha_s\, m_b^{-1/2}, m_b^{-3/2}\right). \tag{4.61}$$

The ratio $D_0^{(v)}(\mu)/C_0^{(v)}(\mu)$ is related to $\kappa(\mu)$ as [315]

$$\kappa(\mu) = \left(1 + 2\frac{D_0^{(v)}(\mu)}{C_0^{(v)}(\mu)}\right)\frac{m_b(\mu)}{m_B}, \tag{4.62}$$

where $\kappa(\mu)$ has been given in Eq. (4.6).

Taking everything into account and using the expansions in Eqs. (4.58)–(4.61), we have everything at hand in order to calculate the improved Isgur-Wise relations including the $O(\Lambda_{\rm QCD}/m_b)$ corrections. From the heavy quark expansion of the hadronic matrix element of Eq. (4.46) it follows that [400]

$$T_1 = (m_B\kappa + m_s)\frac{V}{m_B + m_{K^*}} - 2d^{(0)}, \tag{4.63}$$

which is the improved Isgur-Wise relation between T_1 and V including $O(\Lambda_{\rm QCD}/m_b)$ corrections. From the hadronic matrix element of Eq. (4.47) we get three additional relations. They are achieved by equating coefficients of different products of the K^* polarization vector and the momenta. They read as follows [400]

$$T_2 = (m_B\kappa - m_s)\frac{A_1}{m_B - m_{K^*}} - \frac{2d_1^{(0)}}{m_B^2 - m_{K^*}^2}, \tag{4.64}$$

$$T_2 + T_3\frac{q^2}{m_B^2 - m_{K^*}^2} = (m_B\kappa - m_s)\frac{A_2}{m_B + m_{K^*}} + 2d_+^{(0)}, \tag{4.65}$$

$$T_3 = \frac{2m_{K^*}}{q^2}A_0(m_B\kappa - m_s) - \frac{2m_{K^*}}{m_b + m_s}A_0 - \frac{m_B + m_{K^*}}{q^2}A_1(m_B\kappa - m_s) + \frac{m_B - m_{K^*}}{q^2}A_2(\kappa m_B - m_s) - 2d_-^{(0)}. \tag{4.66}$$

Inserting Eq. (4.64) and (4.66) into Eq. (4.65) we obtain equivalently to Eq. (4.66) the relation [400]

$$m_{K^*}A_0\left(\frac{m_B\kappa - m_s}{q^2} - \frac{1}{m_b + m_s}\right) = d_-^{(0)} + \frac{d_1^{(0)}}{q^2} + d_+^{(0)}\frac{m_B^2 - m_{K^*}^2}{q^2}. \tag{4.67}$$

The relations Eq. (4.63) and (4.64) can be used to obtain the ratios V/T_1 and A_1/T_2 including the desired $\Lambda_{\rm QCD}/m_b$ corrections. From these ratios we can form the double ratio $\mathcal{R}$ as $\mathcal{R} = (V/T_1)/(A_1/T_2)$ and finally obtain the result for $\mathcal{R}$ including also the $\Lambda_{\rm QCD}/m_b$-corrections [400]

$$\mathcal{R}(q^2) = \frac{m_B + m_{K^*}}{m_B - m_{K^*}}\left(1 - 2\left[\frac{d_1^{(0)}(q^2)}{(m_B^2 - m_{K^*}^2)T_2(q^2)} - \frac{d^{(0)}(q^2)}{T_1(q^2)} - \frac{2m_s}{\kappa\, m_B}\right]\right) + O\left(\frac{\Lambda_{\rm QCD}^2}{m_b^2}\right). \tag{4.68}$$

Note that for the correct power counting we used here the scaling relations given in Eqs. (4.56) and (4.57). It follows [400]

$$\mathcal{R}(0) = \frac{V(0)}{A_1(0)} \tag{4.69}$$

$$= \frac{m_B + m_{K^*}}{m_B - m_{K^*}} \left(1 - \frac{2}{T}\left(\frac{d_1^{(0)}(0)}{m_B^2 - m_{K^*}^2} - d^{(0)}(0)\right) - \frac{2m_s}{\kappa m_B}\right) + O\left(\frac{\Lambda_{\rm QCD}^2}{m_b^2}, \alpha_s \frac{\Lambda_{\rm QCD}}{m_b}\right). \tag{4.70}$$

Eq. (4.70) contains our analytic result for the corrections to the simple LEL/HC relation for $V(0)/A_1(0)$ in Eq. (4.45). For a numerical evaluation one needs input for the HQET form factors $d^{(0)}$ and $d_1^{(0)}$, *e.g.* from LCSRs. In this way one could obtain an improved theoretical uncertainty of the LEL/HC relation.

The latter task is left for the future. For the numerical studies in Sec. 4.4 we use on the one hand the HC input Eq. (4.45) and on the other hand the update of the well-known LCSR results of [426] that are given in Eq. (4.77) [400] in the next paragraph.

LCSR results

As reviewed in more detail for example in [427–430] the LCSR approach is a further development of the Shifman Vainshtein Zakharov (SVZ) sum rules [431, 432] that uses distribution amplitudes of light mesons on the light-cone. Both the LCSR ansatz and the SVZ sum rules rely on a fundamental level on the same physical principle, *i.e.*, the quark-hadron duality approximation. We briefly sketch here the essentials of the LCSR approach along the lines of Ref. [426], of which the results are updated as given below in Eq. (4.77) from [400]. In order to obtain LCSR results for $\bar{B} \to \bar{K}^*$ form factors one considers the correlation function [426]

$$\Gamma(q^2, p_B^2) = i \int \mathrm{d}^4 x e^{iqx} \left\langle K^*(p) \middle| T J_W(x) j_b^\dagger(0) \middle| 0 \right\rangle , \tag{4.71}$$

with a weak current J_W, a time ordered product T, the off-shell momentum of the B meson p_B and the pseudoscalar current $j_b = m_b \bar{d} i\gamma_5 b$. Γ can be written in two equivalent ways. Following the specific example given in [426], we look at the LCSR for the form factor V. On the one hand, using a dispersion integral over the light-cone expansion, it is [426]

$$\Gamma_V^{\rm LC}(p_B^2, q^2) = \frac{1}{\pi} \int_{m_b^2}^{\infty} \mathrm{d}s \frac{\mathrm{Im}\left(\Gamma_V^{\rm LC}(s, q^2)\right)}{s - p_B^2} , \tag{4.72}$$

where $\mathrm{Im}(\Gamma_V^{\rm LC})$ contains the light-cone distribution amplitudes. On the other hand, one can write the corresponding correlation function using a hadronic dispersion integral [426]

$$\Gamma_V^{\rm had}(p_B^2, q^2) = \int_{m_B^2}^{\infty} \frac{\rho_V^{\rm had}(s, q^2)}{s - p_B^2} , \tag{4.73}$$

where the hadronic spectral density is given as a term containing the form factor V plus another spectral density containing states with higher mass [426]

$$\rho_V^{\text{had}}(s,q^2) = f_{B_d} m_B^2 \frac{2V(q^2)}{m_B + m_{K^*}} \delta(s - m_B^2) + \rho_V^{\text{higher-mass states}}(s,q^2). \tag{4.74}$$

Most importantly, the approximate quark-hadron duality implies [426]

$$\rho_V^{\text{higher-mass states}}(s,q^2) \approx \frac{1}{\pi} \text{Im}\left(\Gamma_V^{\text{LC}}(s,q^2)\right) \theta(s - s_0)\,, \tag{4.75}$$

which together with $\Gamma_V^{\text{had}}(p_B^2, q^2) = \Gamma_V^{\text{LC}}(p_B^2, q^2)$ gives essentially the sum rule for the form factor V. After a subsequent mathematical Borel transformation for suppressing corrections, it is arrived at the LCSR relation [426]

$$e^{-m_B^2/M^2} m_B^2 f_{B_d} \frac{2V(q^2)}{m_B + m_{K^*}} = \frac{1}{\pi} \int_{m_b^2}^{s_0} \text{d}s\, e^{-s/M^2} \text{Im}\left(\Gamma_V^{\text{LC}}(s,q^2)\right). \tag{4.76}$$

The continuum threshold s_0 in Eqs. (4.75) and (4.76) as well as the Borel parameter M^2 in Eq. (4.76) are inherent parameters of the LCSR approach itself. Eq. (4.76) allows the calculation of V from the imaginary part of the light-cone expansion of the correlation function in Eq. (4.71).

The explicit derivation of the numerical LCSR results using Eq. (4.76) and the corresponding analogues for the other form factors lies beyond the scope of this work. Updating [426], the preliminary LCSR results for V/A_1 and A_1/A_2 at $q^2 = 0$ which we utilize in Sec. 4.4 read [400]

$$\frac{V(0)}{A_1(0)} = 1.40 \pm 0.07\,, \qquad \frac{A_1(0)}{A_2(0)} = 1.19 \pm 0.08 \qquad \text{(LCSR)}\,. \tag{4.77}$$

The theoretical uncertainties of $V(0)/A_1(0)$ are much smaller in comparison to the naive power counting estimate by the LEL/HC relation in Eq. (4.45). Note also that the LCSR result is consistent with LEL.

In the following section we will compare the effects which Eqs. (4.45) and (4.77) have on the fits of the form factor ratios to the data.

4.4. Fitting the Form Factor Series Expansion to Data

The currently available high-q^2 data for the observables F_L and $A_T^{(2)}$ is summarized in Table 4.1. In order to compare the influence of the different possible theoretical assumptions on the fit we study the following six configurations:

	BaBar	CDF		LHCb		ATLAS	CMS
q^2 [GeV^2]	F_L	F_L	$A_T^{(2)}$	F_L	$A_T^{(2)}$	F_L	F_L
$[14.18, 16]$	$0.43^{+0.13}_{-0.16}$	$0.40^{+0.12}_{-0.12}$	$0.11^{+0.65}_{-0.65}$	$0.33^{+0.08}_{-0.08}$	$0.07^{+0.26}_{-0.28}$	$0.28^{+0.16}_{-0.16}$	$0.53^{+0.12}_{-0.12}$
$[16, X]$	$0.55^{+0.15}_{-0.17}$	$0.19^{+0.14}_{-0.13}$	$-0.57^{+0.60}_{-0.57}$	$0.38^{+0.09}_{-0.08}$	$-0.71^{+0.36}_{-0.26}$	$0.35^{+0.08}_{-0.08}$	$0.44^{+0.08}_{-0.08}$

Table 4.1.: Summary of the high-q^2 data from BaBar [433], CDF [434], LHCb [331], ATLAS [435] and CMS [436] that is used in the fits of the form factor ratios. Statistical and systematic uncertainties are added in quadrature. The right boundary of the second bin is $X = 19$ for LHCb, ATLAS and CMS and $X = t_-$ otherwise. Table taken from [400].

(a) Plain SE1.

(b) SE1 with the LCSR input Eq. (4.77).

(c) SE1 with the HC input Eq. (4.45).

(d) Plain SE2.

(e) SE2 with the LCSR input Eq. (4.77).

(f) SE2 with the HC input Eq. (4.45).

The fit results including the χ^2 at the best fit points for these configurations are summarized in Table 4.2, except for configuration (b), see below. In Figs. 4.1–4.6 we show the fit results for the observables F_L and $A_T^{(2)}$ as well as for the form factor ratios $f_0/f_\parallel$, $f_\perp/f_\parallel$, V/A_1 and A_2/A_1 as functions of q^2. The labels of the configurations (a)–(f) correspond to the respective subfigure. In the plots of F_L and $A_T^{(2)}$ we overlay the fit result with the data specified in Table 4.1.

The theoretical input from HC and LCSR, respectively, is taken into account using the Rfit scheme [437], see Appendix B for details. Additionally, for the SE2 we demand without loss of generality that $V, A_1, A_2 \geq 0$ in the region $0 < q^2 < 25\,\text{GeV}^2$, *i.e.*, below the first resonance $m_{1^-}^2 = 29.4\,\text{GeV}^2$. For the SE2, we choose $t_0 = 0$. We checked explicitly that the dependence of the quality of the fit on the latter choice is negligible. Further technicalities referring to the fits are given in Appendix B.

As was discussed in Sec. 4.2, in case of the SE1 the fit is very much constrained by the parametrization itself. The only left free fit parameter in SE1 is $\alpha_\perp/\alpha_\parallel$ which is equivalent to the value that $V(0)/A_1(0)$ takes. The corresponding plots in plain SE1 and SE1 including HC input shown in Fig. 4.3 do not differ and have no uncertainties. In contrast to this, in SE2 the ratio $f_0/f_\parallel$ has nonvanishing uncertainties because the fit has more freedom.

Fit	χ^2	$\alpha_\perp/\alpha_\parallel$	$\alpha_0/\alpha_\parallel$	$p_\parallel$	$p_\perp$	p_0	$V(0)/A_1(0)$	$A_2(0)/A_1(0)$
SE1	11	$1.88^{+0.37}_{-0.37}$	[a]0.29	-	-	-	$1.58^{+0.31}_{-0.31}$	[a]0.93
SE1$^{\mathrm{HC}}$	11	$1.88^{+0.18}_{-0.37}$	[a]0.29	-	-	-	$1.58^{+0.15}_{-0.31}$	[a]0.93
SE2	6	$8.52^{+6.83}_{-6.48}$	$0.87^{+0.04}_{-0.40}$	$-5.63^{+8.30}_{-13.66}$	$3.84^{+0.00}_{-15.91}$	$1.90^{+1.71}_{-4.18}$	$7.15^{+5.72}_{-5.37}$	$0.00^{+0.72}_{-0.00}$
SE2$^{\mathrm{LCSR}}$	8	$1.75^{+0.00}_{-0.17}$	$0.38^{+0.00}_{-0.04}$	$3.06^{+0.41}_{-4.55}$	$2.24^{+1.06}_{-5.85}$	$3.67^{+0.08}_{-3.52}$	$1.47^{+0.00}_{-0.14}$	$0.79^{+0.07}_{-0.00}$
SE2$^{\mathrm{HC}}$	7	$2.06^{+0.00}_{-0.95}$	$0.86^{+0.04}_{-0.49}$	$-7.03^{+10.13}_{-17.39}$	$-9.33^{+12.61}_{-42.88}$	$1.40^{+2.28}_{-5.74}$	$1.73^{+0.00}_{-0.80}$	$0.00^{+0.79}_{-0.00}$

Table 4.2.: Fit results for the considered configurations. LCSR and HC input are given in Eqs. (4.77) and (4.45), respectively. The SE1 LCSR fit does not work due to inconsistent input for $A_2(0)/A_1(0)$ and is therefore not shown, see text for details. Table adapted from [400]. [a]Input, resulting from $F_L(t_-) = 1/3$, Eq. (4.17), therefore no uncertainties are given.

The best fit value for $V(0)/A_1(0)$ in plain SE1 is a bit larger than the central value of the HC relation Eq. (4.45). Nevertheless, it is well inside the uncertainties of the latter. As the HC input is taken into account via the Rfit scheme, we obtain thus essentially the same fit as in plain SE1. The main difference lies in the upper uncertainty of $\alpha_\perp/\alpha_\parallel$, which is smaller when the HC input is included. As a result of the Rfit treatment of the HC relation Eq. (4.45) the 68% and 95% C.L. upper uncertainties of $\alpha_\perp/\alpha_\parallel$ coincide. For that reason, in Fig. 4.4(c) and 4.5(c), which show the SE1 HC fit of $f_\perp/f_\parallel$ and V/A_1, respectively, the upper limits of the 68% and 95% C.L. regions agree as well.

The fit of the SE1 including the LCSR results Eq. (4.77) does not work at all. Firstly, the very precise LCSR prediction for $V(0)/A_1(0)$ with an uncertainty of only 5% shifts the value for $\alpha_\perp/\alpha_\parallel$ away from its best fit value. This is due to the LCSR value for $V(0)/A_1(0)$ being smaller than expected from the data—in that way similar to the HC constraint, but with a higher precision. Secondly, the by the parametrization fixed value for $A_2(0)/A_1(0)$ is just outside the 1σ border of the corresponding LCSR value. In the Rfit scheme such an inconsistent situation with contradicting theoretical regions for the same parameter gives a huge contribution to the χ^2, so that the fit is inconsistent and does not make sense at all. Numerically, we obtain $\chi^2_{\mathrm{min}} \sim 870$. Therefore, the SE1 LCSR results are not shown in Table 4.2 and the corresponding plots in Figs. 4.1–4.6 are marked with a gray hatched background. The principally possible conclusions that can be drawn from the SE1 LCSR fit were given after Eq. (4.28).

Turning to SE2, we see firstly from Figs. 4.1 and 4.2 that the high q^2 data is described equally well by SE1 and SE2. The 68% and 95% C.L. regions for F_L and $A_T^{(2)}$ in SE1 and SE2 do not differ very much from each other, regardless of taking into account additional input from theory or not. The shape of the fit to the observables at high q^2 is only marginally influenced by the HC and LCSR input Eq. (4.45) and (4.77), respectively, when we discard the SE1 LCSR fit due to its large χ^2.

On the other hand, for the form factor ratios the predictions of SE1 and SE2 show differences, especially at low q^2. For SE2, the theory input at $q^2 = 0$ has a significant influence on the shape of the form factor ratios for $q^2 \lesssim 14\ \text{GeV}^2$. This is especially visible in Figs. 4.4 and 4.5 which show $f_\perp/f_\parallel$ and V/A_1 against q^2, respectively. In plain SE2, the respective form factor ratios are essentially unconstrained at low q^2. This is because we only take into account high q^2 data, see Table 4.1, in order to be approximately independent of short-distance physics up to right-handed currents as was discussed in Sec. 4.1. Theory input at only one q^2-point, *i.e.*, $q^2 = 0$, suffices to considerably narrow the shape of the bands of $f_\perp/f_\parallel$ and V/A_1 in the region $q^2 \lesssim 14\ \text{GeV}^2$. This is visible in Figs. (4.4) and (4.5). We learn consequently that for a constraint at low q^2 within our approach we need at least some theory input at large recoil. Being approximately independent of short-distance physics has the advantage that our extraction of form factor ratios does not rely on the SM. It is valid also in NP scenarios as long as no right-handed currents are considered.

The results for the form factor ratios can be compared with outcomes from Lattice QCD at high q^2 [438, 439], as was demonstrated in Ref. [401]. Lattice QCD is an approach to QCD that uses a renormalization method that allows to perform nonperturbative calculations of form factors from first principles. In contrast to the LCSR method, which performs well at low q^2, the lattice approach works best at high q^2 for $\bar{B} \to \bar{K}^{(*)} l^+ l^-$. As a matter of fact, these two approaches are thus complementary methods. It was found in [401] that the data is up to now indeed consistent with the Lattice QCD results given in [438, 439].

Altogether, we have shown that using features of $\bar{B} \to \bar{K}^* l^+ l^-$ decays at low recoil we can extract $\bar{B} \to \bar{K}^*$ form factor ratios in a rather model independent way, *i.e.*, in scenarios without right-handed currents, and can give benchmarks for Lattice QCD calculations. Both SE1 and SE2 fits describe the high-q^2 data well and do not differ essentially in this respect. However, SE1 fits introduce a lot of bias into the fit due to the very limited number of parameters. SE2 fits on the other hand need large recoil LCSR or HC input in order to be able to predict form factor ratios at low q^2. The large recoil form factor ratios in plain SE2 are essentially unconstrained, as the second order fit has more freedom due to the larger amount of parameters. Nonetheless, only one anchor point at $q^2 = 0$ already suffices to considerably constrain the shape of the form factor ratios. In this way, with improving data in the future, important consistency checks of the data, LCSR results and Lattice QCD will get feasible.
Future data will not only improve the precision of F_L and $A_T^{(2)}$, important additional information will also come from the measurement of further observables in that the short-distance physics cancels out likewise, see [78]. These will extend our knowledge of the hadronic physics in the different kinematic regions of the $\bar{B} \to \bar{K}^*$ transition and increase the precision of the extracted form factor ratios. Subsequently, the knowledge on form factor ratios obtained in the future by the here demonstrated method [400, 401] will prove invaluable in order to probe for NP in precision studies of $\bar{B} \to \bar{K}^* \mu^+ \mu^-$ decays.

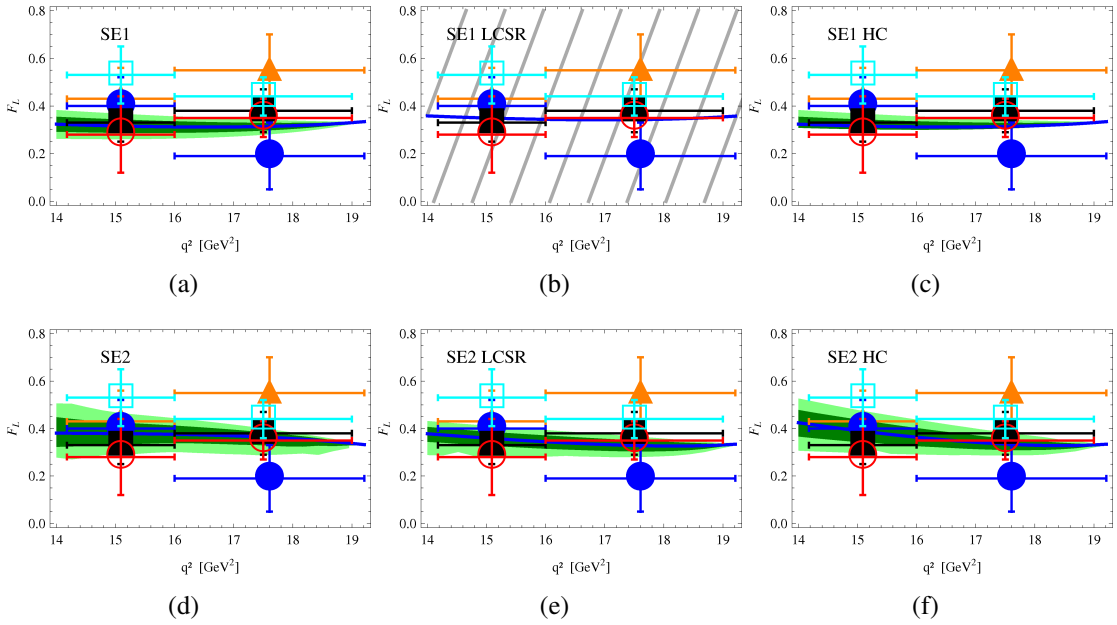

Figure 4.1.: Fit results for F_L against q^2, overlaid with the binned data from BaBar (orange triangles), CDF (blue circles), LHCb (black squares), ATLAS (blue hollow squares) and CMS (red hollow circles). The SE1 LCSR fit is inconsistent, *i.e.*, does not work and is marked with a gray hatched background, see text for details. (Dark) green: (68%) 95% C.L. regions. Blue line: Best fit curve. Plots taken from [400].

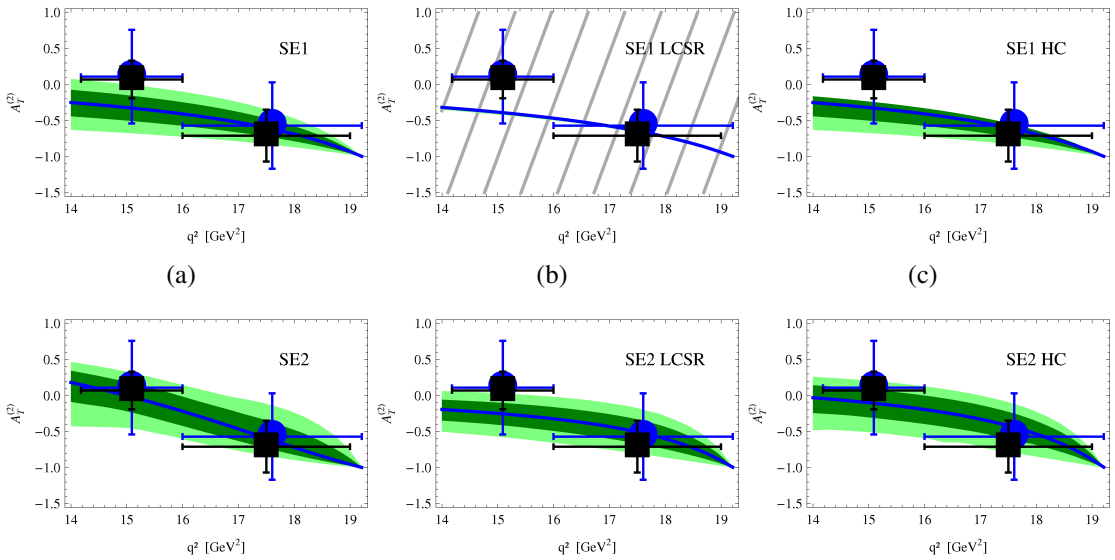

Figure 4.2.: Fit results for $A_T^{(2)}$ against q^2, overlaid with the binned data from CDF (blue circles) and LHCb (black squares). The SE1 LCSR fit is inconsistent, *i.e.*, does not work and is marked with a gray hatched background, see text for details. (Dark) green: (68%) 95% C.L. regions. Blue line: Best fit curve. Plots taken from [400].

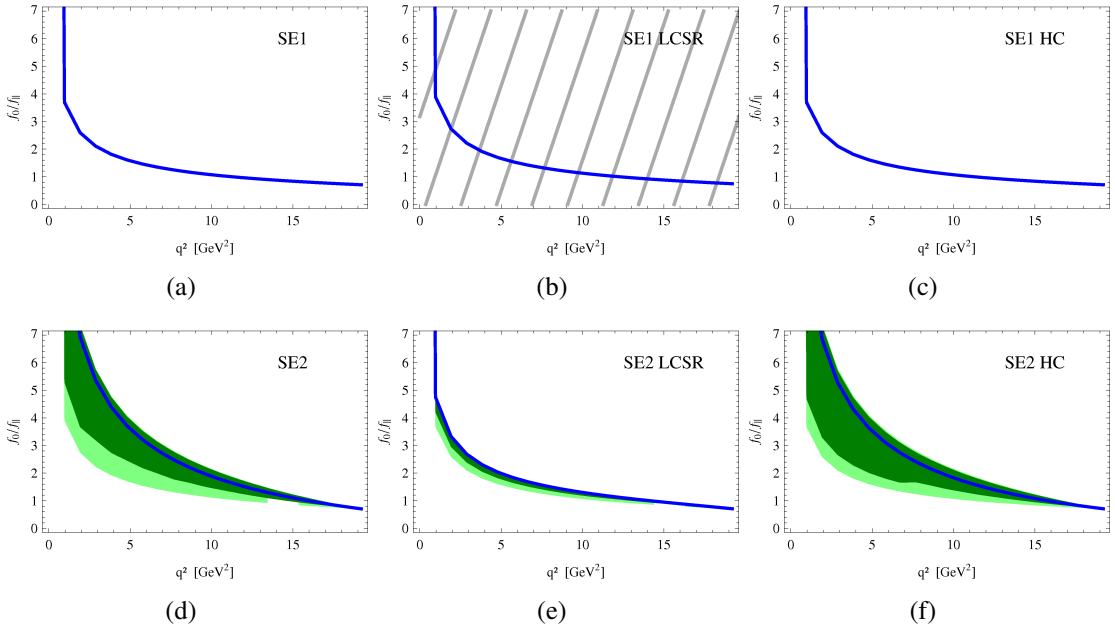

Figure 4.3.: Fit results for $f_0/f_\parallel$ against q^2. The SE1 LCSR fit is inconsistent, *i.e.*, does not work and is marked with a gray hatched background, see text for details. (Dark) green: (68%) 95% C.L. regions. Blue line: Best fit curve. Plots taken from [400].

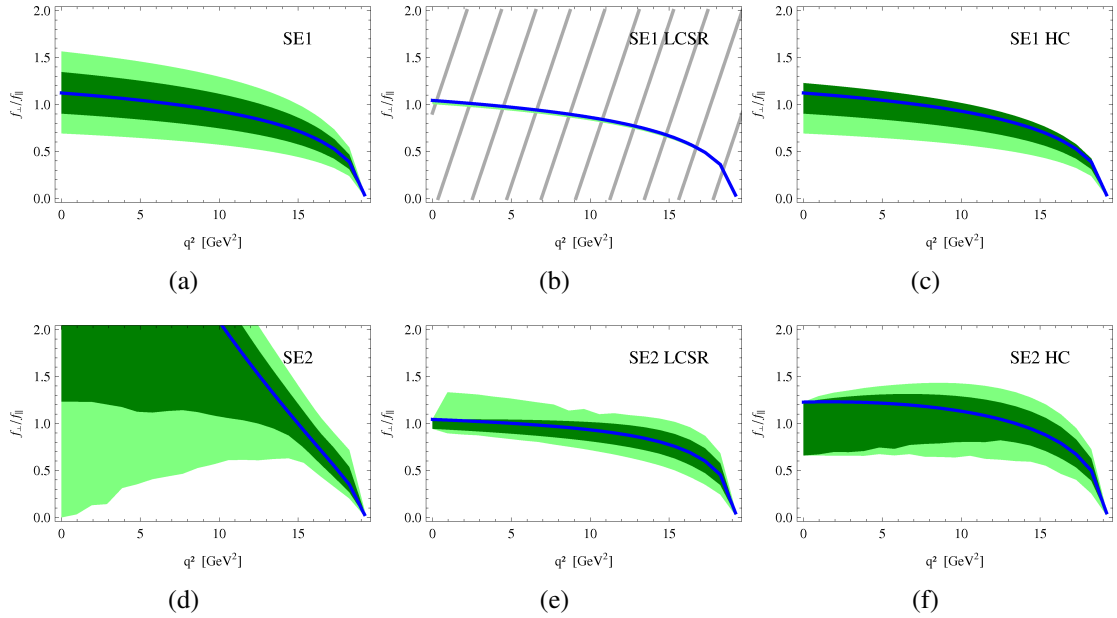

Figure 4.4.: Fit results for $f_\perp/f_\parallel$ against q^2. The SE1 LCSR fit is inconsistent, *i.e.*, does not work and is marked with a gray hatched background, see text for details. (Dark) green: (68%) 95% C.L. regions. Blue line: Best fit curve. Plots taken from [400].

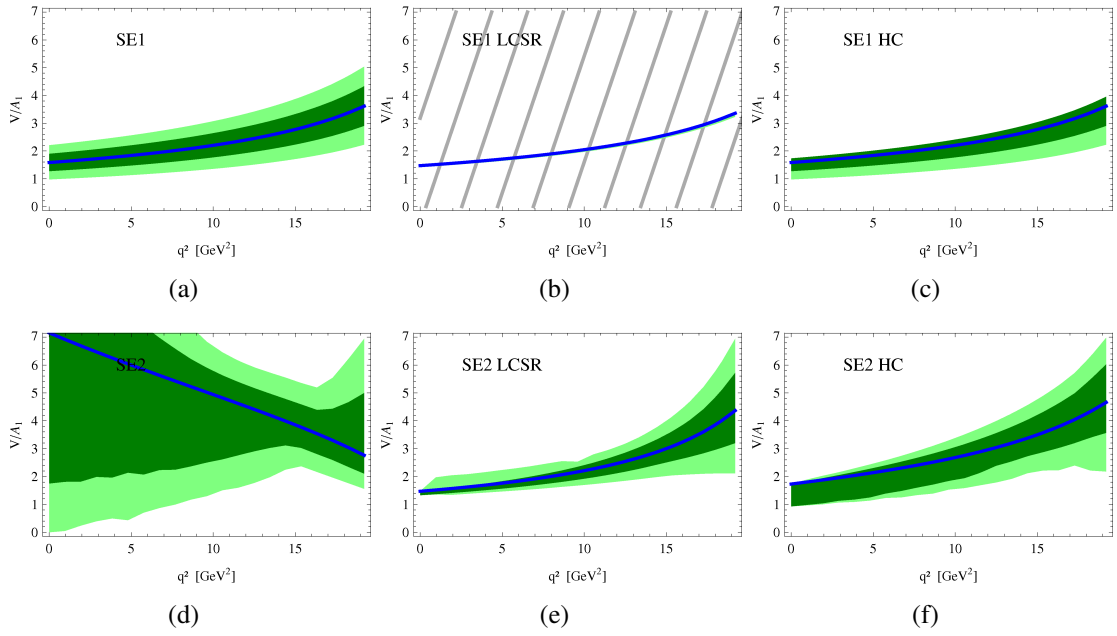

Figure 4.5.: Fit results for V/A_1 against q^2. The SE1 LCSR fit is inconsistent, *i.e.*, does not work and is marked with a gray hatched background, see text for details. (Dark) green: (68%) 95% C.L. regions. Blue line: Best fit curve. Plots taken from [400].

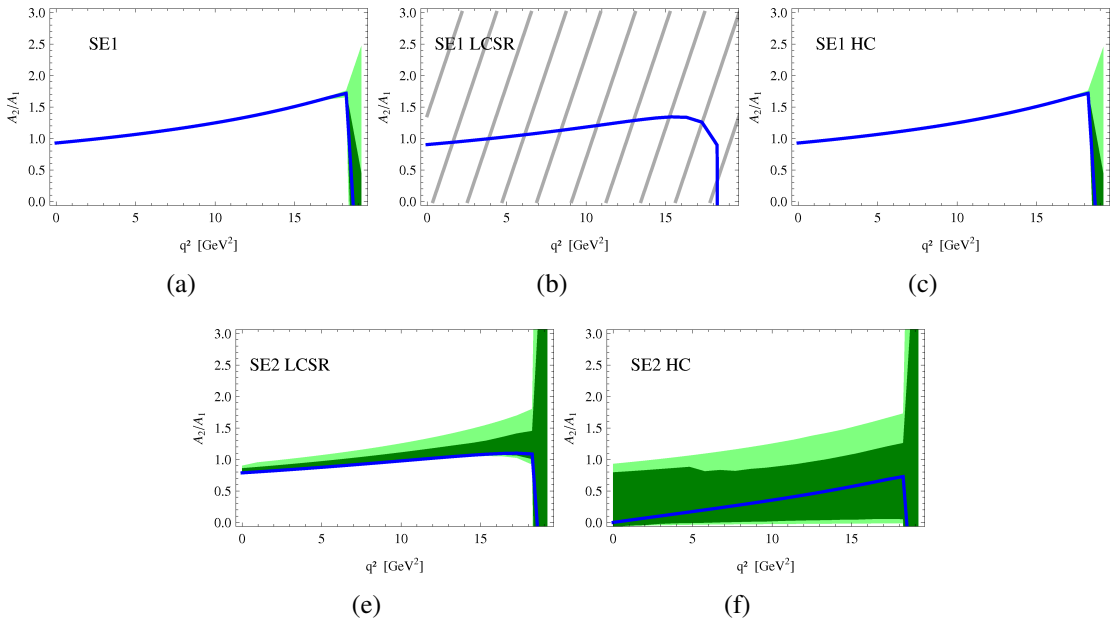

Figure 4.6.: Fit results for A_2/A_1 against q^2. The SE1 LCSR fit is inconsistent, *i.e.*, does not work and is marked with a gray hatched background, see text for details. The plain SE2 fit (d) of A_2/A_1 does not converge due to the lack of input at low q^2 and is therefore not shown. (Dark) green: (68%) 95% C.L. regions. Blue line: Best fit curve. Plots taken from [400].

5. Comprehensive $SU(3)_F$ Breaking in $D \to P_8 P_8$

5.1. CP Violation in Nonleptonic Charm Decays

Charm Physics and Unexpected Data In 2011/2012 spectacular results on direct CP violation in charm decays where observed [60–62]: The difference of the CP asymmetries $a_{CP}^{\text{dir}}(D^0 \to K^+K^-)$ and $a_{CP}^{\text{dir}}(D^0 \to \pi^+\pi^-)$ was found to be sizable [63]

$$\begin{aligned}\Delta a_{CP}^{\text{dir}} &\equiv a_{CP}^{\text{dir}}(D^0 \to K^+K^-) - a_{CP}^{\text{dir}}(D^0 \to \pi^+\pi^-) \\ &= (-0.678 \pm 0.147) \cdot 10^{-2}\,, \end{aligned} \tag{5.1}$$

which is nonzero at 4.6σ. We use here the notation for CP asymmetries that was introduced in Sec. 2.3. The significance of each single measurement is of course smaller, the significance of LHCb alone is 3.5σ [60]. The measurement Eq. (5.1) stimulated much work on the theory side [440–447]. We present here our results that were partly published in Ref. [175]. For the definition and generalities about direct and indirect CP asymmetries of meson decays see Sec. 2.3.

At first glance the number in Eq. (5.1) seems small, however, in comparison to what? The point is here that the SM contribution to $\Delta a_{CP}^{\text{dir}}$ is quite suppressed as well. As was explained in Sec. 2.2.1 CP violation is an effect that only happens with three generations of matter in the SM [17]. The charm system on the other hand is an effectively two-generational system. The third generation and thus CP violation only enters through loops. CP violation is per se suppressed by a factor $\sim 2\,\text{Im}\left(\frac{V_{ub}V_{cb}^*}{V_{us}V_{cs}^*}\right) \sim 10^{-3}$ from the CKM matrix elements. In addition there appears a loop factor which in the SM is naively given as $O(\alpha_s(m_c)/\pi) \sim 0.1$. Consequently, the naive expectation in the SM is that $\Delta a_{CP}^{\text{dir}}$ is below the per mill level.

The problem we are facing here is that we are not able to reliably calculate the loop factor from first principles. This is because the charm quark mass m_c is not much above Λ_{QCD}. The usual techniques used in b physics, like QCDF [310–312] and HQET [185, 416–422], cannot reliably be applied here in a quantitative way, or only to a certain limited extent that we will explore in Ch. 6. As a matter of fact we can thus not tell for sure if the loop factor gives a suppression or on the contrary an enhancement of $\Delta a_{CP}^{\text{dir}}$.

The measurement Eq. (5.1) could be both: a pointer to NP or a nonperturbative QCD effect. Besides, there are also general interesting features incorporated in charm physics

Observable	Measurement	References	Experiments
$\Delta a_{CP}^{\rm dir}(K^+K^-, \pi^+\pi^-)$	-0.00678 ± 0.00147	[60–63, 448, 449]	BaBar, Belle, CDF, LHCb
$\Sigma a_{CP}^{\rm dir}(K^+K^-, \pi^+\pi^-)$	$+0.0014 \pm 0.0039$	†[60–62, 448, 450]	BaBar, Belle, CDF, LHCb
$A_{CP}(D^0 \to K_S K_S)$	-0.23 ± 0.19	[451]	CLEO
$A_{CP}(D^0 \to \pi^0\pi^0)$	$+0.001 \pm 0.048$	[451]	CLEO
$A_{CP}(D^+ \to \pi^0\pi^+)$	$+0.029 \pm 0.029$	[452]	CLEO
$A_{CP}(D^+ \to K_S K^+)$	-0.0011 ± 0.0025	[452–456]	BaBar, Belle, CLEO, FOCUS
$A_{CP}(D_s \to K_S \pi^+)$	$+0.031 \pm 0.015$	†[452, 455, 457]	BaBar, Belle, CLEO
$A_{CP}(D_s \to K^+\pi^0)$	$+0.266 \pm 0.228$	[452]	CLEO

Table 5.1.: CP violation measurements for the 8 SCS decays. †Our average with systematic and statistical error being added quadratically. Table adapted from Ref. [175]. The quoted value for $\Delta a_{CP}^{\rm dir}$ is the one given in [63], online update Sep 2012.

that we should note here. Firstly, it is a complementary tool to the physics of B and K mesons. In the decays of the latter we probe the down quark flavor sector. In the charm system we probe the up quark sector. Furthermore, among the features of charm physics it should be noted that the charm quark is the only up quark with mesons that oscillate and actually indeed large amounts of D mesons are produced at colliders. A large amount of data is already accumulated. We summarize the status quo of the measurements in Tables 5.1, 5.2 and 5.3. In the tables and throughout for the differences and sums of direct CP asymmetries with final states f_1 and f_2 we write

$$\Delta a_{CP}^{\rm dir}(f_1, f_2) = a_{CP}^{\rm dir}(f_1) - a_{CP}^{\rm dir}(f_2)\,, \qquad \Sigma a_{CP}^{\rm dir}(f_1, f_2) = a_{CP}^{\rm dir}(f_1) + a_{CP}^{\rm dir}(f_2). \tag{5.2}$$

Furthermore, we use the common classification scheme of different charm decay channels which is carried out according to their respective Cabibbo suppression. The latter can be read off easily from the underlying quark level process. As examples for the different CKM suppression factors we show in Fig. 5.1 Feynman diagrams with color-favored tree topology. The Cabibbo-favored (CF) decay channels come along with diagonal entries of the CKM matrix. In singly-Cabibbo suppressed (SCS) decays at one of the weak vertices we have a suppression factor $\sim \lambda$. Finally, in doubly-Cabibbo suppressed (DCS) decay modes at both of the weak vertices there can be found factors of the Cabibbo angle, leading to an overall suppression $\sim \lambda^2$. In Feynman diagrams like the ones in Fig. 5.1 the QCD part is depicted in a rough simplification. Consequently, these are not meant as a statement from perturbation theory. On the other hand, the diagrams indeed depict the correct flavor flow of the processes and are useful in this respect. Of course there are

additional, different topologies: Besides the tree diagrams depicted in Fig. 5.1 the most important decay topologies are shown in Figs. 5.2 and 5.3. In Fig. 5.2 we show also the CKM factors.

SCS decays play a special role as only for them there exist penguin topologies as for example the one depicted in Fig. 5.2(b). Here the third generation enters in a loop with a factor of $V_{cb}^* V_{ub}$. The interference of this diagram with the corresponding tree diagram induces CP violation. Penguin contractions of tree operators are most important in this respect [440, 447]. As one can see in Table 5.1 all CP asymmetries in the SCS modes are already measured, although only the measurement of $\Delta a_{CP}^{\text{dir}}$ is significant. Additionally, all branching ratios except for the one of the channel $D_s \to K_L K^+$ are measured. We summarize them in Table 5.2. Furthermore, in Table 5.3 we list the measured indirect CP violation in the charm and kaon system and the relative strong phase of the channels $D^0 \to K^-\pi^+$ and $D^0 \to K^+\pi^-$. Note that the CP asymmetries with a K_S in the final state or a D^0 in the initial state get contributions from indirect CP violation that have to be subtracted in order to extract the pure direct CP violation. This is further described in Sec. 2.3. For the theoretical description of all the different decay channels the starting point is the low energy effective field theory of the weak interaction that was introduced in Sec. 2.4.1 for the B system. The CF, SCS and DCS decays are described by different operators and their respective Wilson coefficients. It is

$$\mathcal{H}_{\text{eff}}^{\Delta C=-1} = \mathcal{H}_{\text{CF}} + \mathcal{H}_{\text{DCS}} + \mathcal{H}_{\text{SCS}}, \tag{5.3}$$

$$\mathcal{H}_{\text{CF}} = \frac{4G_F}{\sqrt{2}} V_{cs}^* V_{ud} \sum_{i=1,2} C_i O_i^{\text{CF}}, \tag{5.4}$$

$$\mathcal{H}_{\text{DCS}} = \frac{4G_F}{\sqrt{2}} V_{cd}^* V_{us} \sum_{i=1,2} C_i O_i^{\text{DCS}}, \tag{5.5}$$

Observable	Measurement	References
SCS branching ratios		
$\mathcal{B}(D^0 \to K^+K^-)$	$(3.96 \pm 0.08) \cdot 10^{-3}$	[89]
$\mathcal{B}(D^0 \to \pi^+\pi^-)$	$(1.401 \pm 0.027) \cdot 10^{-3}$	[89]
$\mathcal{B}(D^0 \to K_S K_S)$	$(0.17 \pm 0.04) \cdot 10^{-3}$	[89]
$\mathcal{B}(D^0 \to \pi^0\pi^0)$	$(0.80 \pm 0.05) \cdot 10^{-3}$	[89]
$\mathcal{B}(D^+ \to \pi^0\pi^+)$	$(1.19 \pm 0.06) \cdot 10^{-3}$	[89]
$\mathcal{B}(D^+ \to K_S K^+)$	$(2.83 \pm 0.16) \cdot 10^{-3}$	[89]
$\mathcal{B}(D_s \to K_S\pi^+)$	$(1.21 \pm 0.08) \cdot 10^{-3}$	[89]
$\mathcal{B}(D_s \to K^+\pi^0)$	$(0.62 \pm 0.21) \cdot 10^{-3}$	[89]
CF* branching ratios		
$\mathcal{B}(D^0 \to K^-\pi^+)$	$(3.88 \pm 0.05) \cdot 10^{-2}$	[89]
$\mathcal{B}(D^0 \to K_S\pi^0)$	$(1.19 \pm 0.04) \cdot 10^{-2}$	[89]
$\mathcal{B}(D^0 \to K_L\pi^0)$	$(1.00 \pm 0.07) \cdot 10^{-2}$	[89]
$\mathcal{B}(D^+ \to K_S\pi^+)$	$(1.47 \pm 0.07) \cdot 10^{-2}$	[89]
$\mathcal{B}(D^+ \to K_L\pi^+)$	$(1.46 \pm 0.05) \cdot 10^{-2}$	[89]
$\mathcal{B}(D_s \to K_S K^+)$	$(1.45 \pm 0.05) \cdot 10^{-2}$	†[89, 458]
DCS branching ratios		
$\mathcal{B}(D^0 \to K^+\pi^-)$	$(1.47 \pm 0.07) \cdot 10^{-4}$	[89]
$\mathcal{B}(D^+ \to K^+\pi^0)$	$(1.83 \pm 0.26) \cdot 10^{-4}$	[89]

Table 5.2.: Branching ratio measurements in the $D \to PP$ system. †Our average with systematic and statistical error being added quadratically. *Decays with a $K_{S,L}$ in the final state, *i.e.*, that have a CF and DCS component from K^0–$\bar{K}^0$ mixing, are assigned to the CF channels. Table adapted from Ref. [175].

and

$$\mathcal{H}_{\text{SCS}} = \frac{4G_F}{\sqrt{2}} \left(\sum_{i=1,2} \sum_{D=d,s} V_{cD}^* V_{uD} C_i O_{i,D}^{\text{SCS}} + V_{cb}^* V_{ub} \sum_{i=3,\ldots,6} C_i O_i \right). \tag{5.6}$$

On the one hand we have the tree operators O^{CF}, O^{SCS} and O^{DCS} that have Wilson coefficients $C_i \sim O(1)$ and on the other hand there are the QCD penguin operators $O_{3,\ldots,6}$ that have Wilson coefficients that are suppressed by $C_i \sim \alpha_s$.

Observable	Measurement	References
Indirect CP Violation		
a_{CP}^{ind}	$(-0.027 \pm 0.163) \cdot 10^{-2}$	[63]
$\delta_L \equiv 2\text{Re}(\varepsilon)/(1+\lvert\varepsilon\rvert^2)$	$(3.32 \pm 0.06) \cdot 10^{-3}$	[89]
$K^+\pi^-$ strong phase difference		
$\delta_{K\pi}$	$21.4^\circ \pm 10.4^\circ$	‡[63]

Table 5.3.: Indirect CP violation and strong phase measurements. ‡Uncertainties calculated by symmetrization of the ones in the literature. Table adapted from Ref. [175].

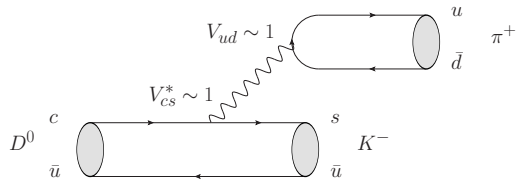

(a) Cabibbo-favored (CF) decay amplitude: $\mathcal{A}(c \to s\bar{d}u) \propto V_{cs}^* V_{ud} \sim 1$

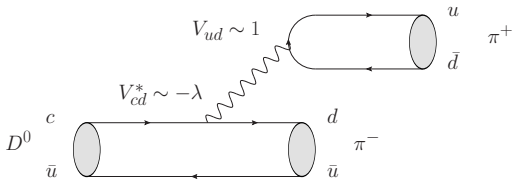

(b) Singly-Cabibbo suppressed (SCS) amplitude: $\mathcal{A}(c \to d\bar{d}u)$ or $\mathcal{A}(c \to s\bar{s}u) \propto V_{cs}^* V_{us} \approx -V_{cd}^* V_{ud} \sim \lambda$

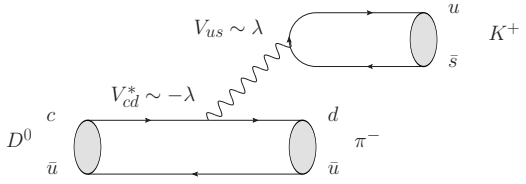

(c) Doubly-Cabibbo suppressed (DCS) amplitude: $\mathcal{A}(c \to d\bar{s}u) \propto V_{cd}^* V_{us} \sim -\lambda^2$

Figure 5.1.: Classification of color-favored tree diagrams in $D \to PP$ according to the Cabibbo suppression of the underlying quark level process, see text for details.

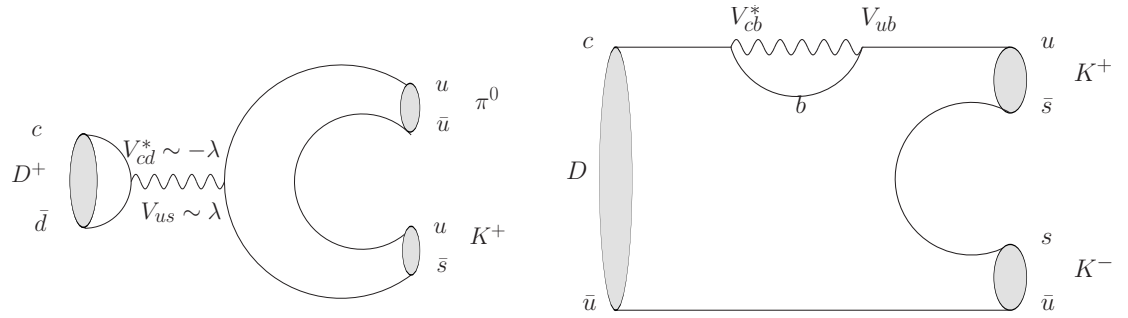

(a) Annihilation diagram for DCS decay with amplitude $\mathcal{A}(D^+ \to \pi^0 K^+) \sim \lambda^2$

(b) CP Violation in SCS decay through penguin topology contribution $\mathcal{A}_P(D^0 \to K^+K^-) \propto V_{cb}^* V_{ub}$

Figure 5.2.: Examples of additional topologies in $D \to PP$.

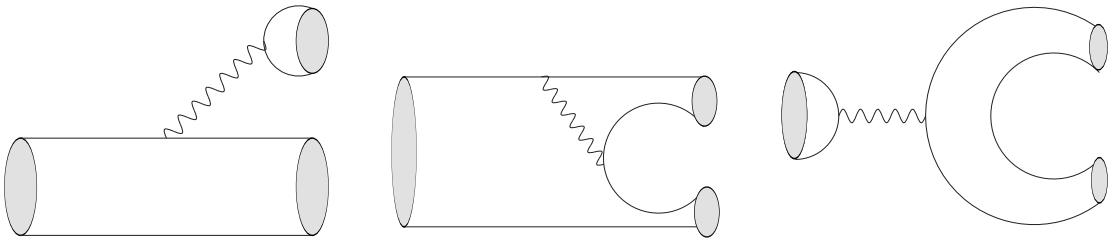

(a) Color-favored tree T with external W emission

(b) Color-suppressed tree C with internal W emission

(c) W-annihilation A

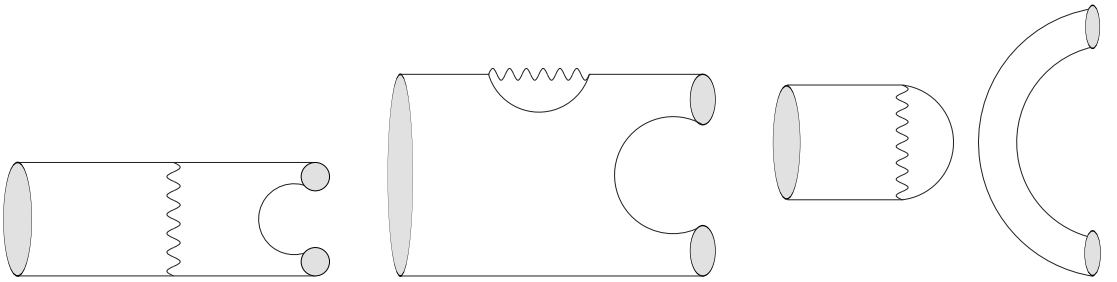

(d) W-exchange E

(e) Penguin topology P

(f) Penguin annihilation PA

Figure 5.3.: Different examples of most important topological Feynman Diagrams, see text for details. For a complete list of all possible topologies see Ref. [442].

Additional operators are omitted in Eqs. (5.3)–(5.6), for an explicit full operator basis see Ref. [459]. For the SU(3) analysis made here, only the flavor structure of the operators is relevant. We discuss this in the next section.

Eqs. (5.4)–(5.6) pose a problem when being confronted with data: The hierarchy that is induced by CKM and the Wilson coefficients is possibly compensated or destroyed by the hadronic matrix elements $\langle f| O_j |i\rangle$ of the operators O_j. The point is that we cannot at present reliably calculate the $\langle f| O_j |i\rangle$.

The best way out of such a problematic situation is to extract the hadronic matrix elements from all the available data using a symmetry that relates several decay amplitudes of $D \to PP$. In the charm system this seems to be possible because there is indeed much data available from the experiments LHCb, CDF, Belle, BaBar, CLEO and FOCUS, see Tables 5.1–5.3.
We fit the degrees of freedom provided by flavor symmetry to the data. We refrain here from taking input from a priori hierarchies between the topological diagrams in Figs. 5.1–5.3. In this process correlations between different channels can emerge that possibly lead to a discrimination of the SM and NP models.

5.2. Exploiting the Approximate SU(3)$_F$ Symmetry of QCD for $D \to P_8 P_8$

In order to tackle the methodology introduced in the previous paragraph we use the approximate SU(3)$_F$ symmetry of QCD that was introduced in Sec. 2.2.2. This symmetry gives us a data-driven way out of the problem of not reliably calculable matrix elements. We start by discussing pure SU(3)$_F$, *i.e.*, the SU(3)$_F$ limit, where $m_s = m_u = m_d$. We examine if one can describe the experimental data using this simplification.

As the charm quark is a singlet from the SU(3)$_F$ point of view the initial states (D^0, D^+, D_s) of the decays $D \to P_8 P_8$ form an antitriplet

$$\bar{\mathbf{3}} = \left(D^0 = -|c\bar{u}\rangle, D^+ = \left|c\bar{d}\right\rangle, D_s = |c\bar{s}\rangle\right). \tag{5.7}$$

Specifically, the quantum numbers of the states are given as

$$\left|D^0\right\rangle = \left|\bar{\mathbf{3}}\right\rangle_{\frac{1}{2},-\frac{1}{2},-\frac{1}{3}}, \qquad \left|D^+\right\rangle = \left|\bar{\mathbf{3}}\right\rangle_{\frac{1}{2},\frac{1}{2},-\frac{1}{3}}, \qquad \left|D_s\right\rangle = \left|\bar{\mathbf{3}}\right\rangle_{0,0,\frac{2}{3}}. \tag{5.8}$$

Here we use the notation $|\mu\rangle_{I,I_3,Y}$ for an SU(3)$_F$ state with the representation μ, isospin I, third component of the isospin I_3 and hypercharge Y. The SU(3)$_F$ quantum numbers of the quarks u, d and s are given in Table 5.4.

In the final state we consider pions and kaons which belong to the octet of pseudoscalars and have the following quantum numbers:

$$\left|\pi^+\right\rangle = |\mathbf{8}\rangle_{1,1,0}, \quad \left|\pi^0\right\rangle = |\mathbf{8}\rangle_{1,0,0}, \quad \left|\pi^-\right\rangle = |\mathbf{8}\rangle_{1,-1,0}, \tag{5.9}$$

$$\left|K^+\right\rangle = |\mathbf{8}\rangle_{\frac{1}{2},\frac{1}{2},1}, \quad \left|K^-\right\rangle = |\mathbf{8}\rangle_{\frac{1}{2},-\frac{1}{2},-1}, \quad \left|K^0\right\rangle = |\mathbf{8}\rangle_{\frac{1}{2},-\frac{1}{2},1}, \quad \left|\bar{K}^0\right\rangle = |\mathbf{8}\rangle_{\frac{1}{2},\frac{1}{2},-1}. \tag{5.10}$$

	I	I_3	Y
u	1/2	1/2	1/3
d	1/2	−1/2	1/3
s	0	0	−2/3

Table 5.4.: SU(3)$_F$ quantum numbers I, I_3 and Y of the quarks u, d and s, see text for details. Note that the hypercharge of SU(3)$_F$ differs from the electroweak hypercharge.

We consider only two-body decays here. From the symmetry point of view two members of the octet are identical particles. Additionally, they are bosons, *i.e.*, the particles in the final state obey Bose statistics. In order to account for this property the final state has to be properly symmetrized. This leads to a reduction of the final representations in the tensor product

$$(\mathbf{8}) \otimes (\mathbf{8}) = (\mathbf{1}) \oplus (\mathbf{8}) \oplus (\mathbf{8}) \oplus (\mathbf{10}) \oplus (\overline{\mathbf{10}}) \oplus (\mathbf{27}) \,, \tag{5.11}$$

where after symmetrization remains

$$[(\mathbf{8}) \otimes (\mathbf{8})]_S = (\mathbf{1}) \oplus (\mathbf{8}) \oplus (\mathbf{27}). \tag{5.12}$$

The Clebsch-Gordan coefficients are calculated with the program [460] or retrieved from the tables in Refs. [168, 461].

The symmetrized two body final states are in detail given as follows:

- Kaon-Kaon final states:

$$\left|K^- K^+\right\rangle = \frac{1}{2}\,|\mathbf{1}\rangle_{0,0,0} + \frac{1}{\sqrt{10}}\,|\mathbf{8}\rangle_{0,0,0} - \sqrt{\frac{3}{10}}\,|\mathbf{8}\rangle_{1,0,0} + \frac{1}{2}\sqrt{\frac{3}{5}}\,|\mathbf{27}\rangle_{0,0,0} + \frac{1}{\sqrt{5}}\,|\mathbf{27}\rangle_{1,0,0} \,, \tag{5.13}$$

$$\left|\bar{K}^0 K^0\right\rangle = -\frac{1}{2}\,|\mathbf{1}\rangle_{0,0,0} - \frac{1}{\sqrt{10}}\,|\mathbf{8}\rangle_{0,0,0} - \sqrt{\frac{3}{10}}\,|\mathbf{8}\rangle_{1,0,0} - \frac{1}{2}\sqrt{\frac{3}{5}}\,|\mathbf{27}\rangle_{0,0,0} + \frac{1}{\sqrt{5}}\,|\mathbf{27}\rangle_{1,0,0} \,, \tag{5.14}$$

$$\left|\bar{K}^0 K^+\right\rangle = -\sqrt{\frac{3}{5}}\,|\mathbf{8}\rangle_{1,1,0} + \sqrt{\frac{2}{5}}\,|\mathbf{27}\rangle_{1,1,0} \,, \tag{5.15}$$

$$\left|K^0 K^+\right\rangle = |\mathbf{27}\rangle_{1,0,2} \,. \tag{5.16}$$

- Pion-Pion final states:

$$\left|\pi^+\pi^-\right\rangle = \frac{1}{2}\,|\mathbf{1}\rangle_{0,0,0} - \sqrt{\frac{2}{5}}\,|\mathbf{8}\rangle_{0,0,0} - \frac{1}{2\sqrt{15}}\,|\mathbf{27}\rangle_{0,0,0} + \frac{1}{\sqrt{3}}\,|\mathbf{27}\rangle_{2,0,0}\ , \tag{5.17}$$

$$\left|\pi^0\pi^0\right\rangle = \sqrt{\frac{2}{3}}\,|\mathbf{27}\rangle_{2,0,0} + \frac{1}{2\sqrt{30}}\,|\mathbf{27}\rangle_{0,0,0} + \frac{1}{\sqrt{5}}\,|\mathbf{8}\rangle_{0,0,0} - \frac{1}{2\sqrt{2}}\,|\mathbf{1}\rangle_{0,0,0}\ , \tag{5.18}$$

$$\left|\pi^0\pi^+\right\rangle = |\mathbf{27}\rangle_{2,1,0}\ . \tag{5.19}$$

- Kaon-Pion final states:

$$\left|K^-\pi^+\right\rangle = \sqrt{\frac{3}{5}}\,|\mathbf{8}\rangle_{\frac{1}{2},\frac{1}{2},-1} + \frac{1}{\sqrt{15}}\,|\mathbf{27}\rangle_{\frac{1}{2},\frac{1}{2},-1} + \frac{1}{\sqrt{3}}\,|\mathbf{27}\rangle_{\frac{3}{2},\frac{1}{2},-1}\ , \tag{5.20}$$

$$\left|\bar{K}^0\pi^0\right\rangle = -\sqrt{\frac{3}{10}}\,|\mathbf{8}\rangle_{\frac{1}{2},\frac{1}{2},-1} - \frac{1}{\sqrt{30}}\,|\mathbf{27}\rangle_{\frac{1}{2},\frac{1}{2},-1} + \sqrt{\frac{2}{3}}\,|\mathbf{27}\rangle_{\frac{3}{2},\frac{1}{2},-1}\ , \tag{5.21}$$

$$\left|\pi^-K^+\right\rangle = \sqrt{\frac{3}{5}}\,|\mathbf{8}\rangle_{\frac{1}{2},-\frac{1}{2},1} + \frac{1}{\sqrt{15}}\,|\mathbf{27}\rangle_{\frac{1}{2},-\frac{1}{2},1} + \frac{1}{\sqrt{3}}\,|\mathbf{27}\rangle_{\frac{3}{2},-\frac{1}{2},1}\ , \tag{5.22}$$

$$\left|\pi^0K^0\right\rangle = -\sqrt{\frac{3}{10}}\,|\mathbf{8}\rangle_{\frac{1}{2},-\frac{1}{2},1} - \frac{1}{\sqrt{30}}\,|\mathbf{27}\rangle_{\frac{1}{2},-\frac{1}{2},1} + \sqrt{\frac{2}{3}}\,|\mathbf{27}\rangle_{\frac{3}{2},-\frac{1}{2},1}\ , \tag{5.23}$$

$$\left|\bar{K}^0\pi^+\right\rangle = |\mathbf{27}\rangle_{\frac{3}{2},\frac{3}{2},-1}\ , \tag{5.24}$$

$$\left|\pi^0K^+\right\rangle = \sqrt{\frac{3}{10}}\,|\mathbf{8}\rangle_{\frac{1}{2},\frac{1}{2},1} + \frac{1}{\sqrt{30}}\,|\mathbf{27}\rangle_{\frac{1}{2},\frac{1}{2},1} + \sqrt{\frac{2}{3}}\,|\mathbf{27}\rangle_{\frac{3}{2},\frac{1}{2},1}\ , \tag{5.25}$$

$$\left|\pi^+K^0\right\rangle = -\sqrt{\frac{3}{5}}\,|\mathbf{8}\rangle_{\frac{1}{2},\frac{1}{2},1} - \frac{1}{\sqrt{15}}\,|\mathbf{27}\rangle_{\frac{1}{2},\frac{1}{2},1} + \frac{1}{\sqrt{3}}\,|\mathbf{27}\rangle_{\frac{3}{2},\frac{1}{2},1}\ , \tag{5.26}$$

$$\left|\bar{K}^0K^+\right\rangle = -\sqrt{\frac{3}{5}}\,|\mathbf{8}\rangle_{1,1,0} + \sqrt{\frac{2}{5}}\,|\mathbf{27}\rangle_{1,1,0}\ , \tag{5.27}$$

$$\left|\pi^+K^0\right\rangle = -\sqrt{\frac{3}{5}}\,|\mathbf{8}\rangle_{\frac{1}{2},\frac{1}{2},1} - \frac{1}{\sqrt{15}}\,|\mathbf{27}\rangle_{\frac{1}{2},\frac{1}{2},1} + \frac{1}{\sqrt{3}}\,|\mathbf{27}\rangle_{\frac{3}{2},\frac{1}{2},1}\ . \tag{5.28}$$

Note that in the literature different conventions are used for the initial and final states. The quark triplet is given as (u, d, s). An ambiguity lies in if one writes the minus sign in front of $\bar{u}$ in the antitriplet $(-\bar{u}, \bar{d}, \bar{s})$ explicitly or absorbs it into the states. We follow the latter approach [462] and use in this way directly the representations of SU(3)$_F$ as states. This implies possible sign differences in the states with an $\bar{u}$ in comparison to the literature. Further differences arise in the treatment of factors of $\sqrt{2}$ that come from the

symmetrization. For instance, our states relate to the ones in Ref. [463] as follows:

$$\left|D^0\right\rangle = -\left|D^0\right\rangle_{\text{previous}}\,, \qquad \left|K^-\pi^+\right\rangle = -\left|K^-\pi^+\right\rangle_{\text{previous}}\,, \tag{5.29}$$

$$\left|K^-K^+\right\rangle = -\left|K^-K^+\right\rangle_{\text{previous}}\,, \qquad \left|\bar{K}^0\pi^0\right\rangle = -\left|\bar{K}^0\pi^0\right\rangle_{\text{previous}}\,, \tag{5.30}$$

$$\left|\pi^+\pi^-\right\rangle = -\left|\pi^+\pi^-\right\rangle_{\text{previous}}\,, \qquad \left|\pi^-K^+\right\rangle = -\left|\pi^-K^+\right\rangle_{\text{previous}}\,, \tag{5.31}$$

$$\left|\pi^0\pi^0\right\rangle = \sqrt{2}\left|\pi^0\pi^0\right\rangle_{\text{previous}}\,, \qquad \left|\pi^0K^0\right\rangle = -\left|\pi^0K^0\right\rangle_{\text{previous}}\,, \tag{5.32}$$

$$\left|\pi^0\pi^+\right\rangle = -\left|\pi^0\pi^+\right\rangle_{\text{previous}}\,, \qquad \left|\pi^0K^+\right\rangle = -\left|\pi^0K^+\right\rangle_{\text{previous}}\,. \tag{5.33}$$

By "previous" we indicate here the states as used in Ref. [463]. The interaction that takes place between initial and final state is governed by the four quark operators of the Hamiltonian Eq. (5.3). In order to match the Hamiltonian on the SU(3)$_F$ ansatz we have to analyze its flavor structure. Depicting only the flavor structure the different parts of the Hamiltonian are given as follows:

$$\mathcal{H}_{\text{eff}} \sim \frac{4G_F}{\sqrt{2}}\left(\underbrace{V_{ud}V_{cs}^*(\bar{u}d)(\bar{s}c)}_{\text{CF}} + \underbrace{V_{us}V_{cs}^*(\bar{u}s)(\bar{s}c) + V_{ud}V_{cd}^*(\bar{u}d)(\bar{d}c)}_{\text{SCS}} + \underbrace{V_{us}V_{cd}^*(\bar{u}s)(\bar{d}c)}_{\text{DCS}}\right). \tag{5.34}$$

In order to make the CKM hierarchy of CP violation visible, the SCS part is most conveniently written as

$$\mathcal{H}_{\text{eff}}^{\text{SCS}} = \frac{4G_F}{\sqrt{2}}\left(\Sigma\left((\bar{u}s)(\bar{s}c) - (\bar{u}d)(\bar{d}c)\right) + \Delta\left((\bar{u}s)(\bar{s}c) + (\bar{u}d)(\bar{d}c)\right)\right). \tag{5.35}$$

Here,

$$\Sigma = \frac{V_{cs}^*V_{us} - V_{cd}^*V_{ud}}{2} \sim \lambda\,, \tag{5.36}$$

$$\Delta = \frac{V_{cs}^*V_{us} + V_{cd}^*V_{ud}}{2} = -\frac{V_{cb}^*V_{ub}}{2} \sim -\frac{A^2}{2}\lambda^5\left(\rho - i\eta\right)\,, \tag{5.37}$$

where in Eq. (5.37) we used the unitarity of the CKM matrix. The ratio of the CKM-suppressed over the CKM-leading part is given by

$$\tilde{\Delta} = \Delta/\Sigma \sim \lambda^4 \sim 10^{-3}. \tag{5.38}$$

Since the charm quark is a singlet under SU(3)$_F$, the structure of all the four quark operators in Eq. (5.34) is given by the tensor product

$$\mathbf{3}\otimes\bar{\mathbf{3}}\otimes\mathbf{3} = \mathbf{3_1}\oplus\mathbf{3_2}\oplus\bar{\mathbf{6}}\oplus\mathbf{15}. \tag{5.39}$$

Inserting this into Eq. (5.34), we obtain:

$$\mathcal{H}_{\text{eff}}^{\text{CF}} = V_{ud}V_{cs}^*\left(-\frac{1}{\sqrt{2}}\bar{\mathbf{6}}_{1,1,-\frac{2}{3}} + \frac{1}{\sqrt{2}}\mathbf{15}_{1,1,-\frac{2}{3}}\right), \tag{5.40}$$

$$\begin{aligned}\mathcal{H}_{\text{eff}}^{\text{SCS}} &= \Sigma\left(\sqrt{\frac{2}{3}}\,\mathbf{15}_{\frac{1}{2},\frac{1}{2},\frac{1}{3}} - \frac{1}{\sqrt{3}}\,\mathbf{15}_{\frac{3}{2},\frac{1}{2},\frac{1}{3}} - \bar{\mathbf{6}}_{\frac{1}{2},\frac{1}{2},\frac{1}{3}}\right)\\ &\quad + \Delta\left(-\sqrt{\frac{3}{2}}\,\mathbf{3}_{\frac{1}{2},\frac{1}{2},\frac{1}{3}} + \frac{1}{\sqrt{6}}\,\mathbf{15}_{\frac{1}{2},\frac{1}{2},\frac{1}{3}} + \frac{1}{\sqrt{3}}\,\mathbf{15}_{\frac{3}{2},\frac{1}{2},\frac{1}{3}}\right),\end{aligned} \tag{5.41}$$

$$\mathcal{H}_{\text{eff}}^{\text{DCS}} = V_{us}V_{cd}^*\left(\frac{1}{\sqrt{2}}\bar{\mathbf{6}}_{0,0,\frac{4}{3}} + \frac{1}{\sqrt{2}}\mathbf{15}_{1,0,\frac{4}{3}}\right). \tag{5.42}$$

By examining the CKM hierarchies in Eq. (5.41) one can as of now infer that in the fit, the matrix elements of the **15** and $\bar{\mathbf{6}}$ representation will be fixed already by the branching ratios as the contribution of the **3** is suppressed by $\tilde{\Delta}$. The only degree of freedom that remains in order to explain a sizable CP violation is precisely this **3**. This means from Eq. (5.41) we can already learn that we will need a triplet enhancement.
Furthermore, we see that in our framework there is a priori no CP violation in CF and DCS decays. If significant CP violation would be measured in one of these decays, we would have to rethink our model. As this is not the case, the corresponding measured values of the CP asymmetries give just a (small) overall constant offset in our χ^2 that does not change the fit result. Therefore, we neglect these observables in the fit.

How do the parametrizations of the Hamiltonian, the initial and the final states relate different decay channels? This is provided by the Wigner-Eckart theorem that was introduced in Sec. 2.2.2. In brief, it tells us that all the matrix elements of different initial and final states with the operators of the Hamiltonian only depend on the representations. The matrix elements do not depend on the additional quantum numbers, here I, I_3 and Y. But the "information" contained in these quantum numbers is not lost: It goes into the Clebsch-Gordan coefficients of the reduced matrix elements.

We apply the Wigner-Eckart theorem to the initial states in Eq. (5.8), the final states in Eqs. (5.13)-(5.28) and the Hamiltonian in Eqs. (5.40)-(5.42). The result is given in Table 5.5.

With the Clebsch-Gordan coefficients in Table 5.5, the amplitude of a given decay d is given as

$$\mathcal{A}_0(d) = \Sigma \sum_{i,k} c_{d;ik} A_i^k\,, \qquad \text{(SCS)} \tag{5.43}$$

$$\mathcal{A}_0(d) = V_{cs}^* V_{ud} \sum_{i,k} c_{d;ik} A_i^k\,, \qquad \text{(CF)} \tag{5.44}$$

$$\mathcal{A}_0(d) = V_{cd}^* V_{us} \sum_{i,k} c_{d;ik} A_i^k\,, \qquad \text{(DCS)} \tag{5.45}$$

where the CKM prefactor depends on the amount of Cabibbo suppression that is present in the considered channel. Our SU(3)$_F$ limit expressions agree with Ref. [463]. Note that

Decay d	A_{27}^{15}	A_8^{15}	$A_8^{\bar{6}}$	A_1^3	A_8^3
SCS					
$D^0 \to K^+K^-$	$\frac{3\tilde{\Delta}+4}{10\sqrt{2}}$	$\frac{\tilde{\Delta}-2}{5\sqrt{2}}$	$\frac{1}{\sqrt{5}}$	$\frac{\tilde{\Delta}}{2\sqrt{2}}$	$\frac{\tilde{\Delta}}{\sqrt{10}}$
$D^0 \to \pi^+\pi^-$	$\frac{3\tilde{\Delta}-4}{10\sqrt{2}}$	$\frac{\tilde{\Delta}+2}{5\sqrt{2}}$	$-\frac{1}{\sqrt{5}}$	$\frac{\tilde{\Delta}}{2\sqrt{2}}$	$\frac{\tilde{\Delta}}{\sqrt{10}}$
$D^0 \to \bar{K}^0K^0$	$\frac{\tilde{\Delta}}{10\sqrt{2}}$	$\frac{\sqrt{2}\tilde{\Delta}}{5}$	0	$-\frac{\tilde{\Delta}}{2\sqrt{2}}$	$\sqrt{\frac{2}{5}}\tilde{\Delta}$
$D^0 \to \pi^0\pi^0$	$\frac{7\tilde{\Delta}-6}{20}$	$-\frac{\tilde{\Delta}+2}{10}$	$\frac{1}{\sqrt{10}}$	$-\frac{\tilde{\Delta}}{4}$	$-\frac{\tilde{\Delta}}{2\sqrt{5}}$
$D^+ \to \pi^0\pi^+$	$\frac{\tilde{\Delta}-1}{2}$	0	0	0	0
$D^+ \to \bar{K}^0K^+$	$\frac{\tilde{\Delta}+3}{5\sqrt{2}}$	$-\frac{\tilde{\Delta}-2}{5\sqrt{2}}$	$\frac{1}{\sqrt{5}}$	0	$\frac{3\tilde{\Delta}}{\sqrt{10}}$
$D_s \to K^0\pi^+$	$\frac{\tilde{\Delta}-3}{5\sqrt{2}}$	$-\frac{\tilde{\Delta}+2}{5\sqrt{2}}$	$-\frac{1}{\sqrt{5}}$	0	$\frac{3\tilde{\Delta}}{\sqrt{10}}$
$D_s \to K^+\pi^0$	$\frac{2\tilde{\Delta}-1}{5}$	$\frac{\tilde{\Delta}+2}{10}$	$\frac{1}{\sqrt{10}}$	0	$-\frac{3\tilde{\Delta}}{2\sqrt{5}}$
CF					
$D^0 \to K^-\pi^+$	$\frac{\sqrt{2}}{5}$	$-\frac{\sqrt{2}}{5}$	$\frac{1}{\sqrt{5}}$	0	0
$D^0 \to \bar{K}^0\pi^0$	$\frac{3}{10}$	$\frac{1}{5}$	$-\frac{1}{\sqrt{10}}$	0	0
$D^+ \to \bar{K}^0\pi^+$	$\frac{1}{\sqrt{2}}$	0	0	0	0
$D_s \to \bar{K}^0K^+$	$\frac{\sqrt{2}}{5}$	$-\frac{\sqrt{2}}{5}$	$-\frac{1}{\sqrt{5}}$	0	0
DCS					
$D^0 \to K^+\pi^-$	$\frac{\sqrt{2}}{5}$	$-\frac{\sqrt{2}}{5}$	$\frac{1}{\sqrt{5}}$	0	0
$D^0 \to K^0\pi^0$	$\frac{3}{10}$	$\frac{1}{5}$	$-\frac{1}{\sqrt{10}}$	0	0
$D^+ \to K^0\pi^+$	$\frac{\sqrt{2}}{5}$	$-\frac{\sqrt{2}}{5}$	$-\frac{1}{\sqrt{5}}$	0	0
$D^+ \to K^+\pi^0$	$\frac{3}{10}$	$\frac{1}{5}$	$\frac{1}{\sqrt{10}}$	0	0
$D_s \to K^0K^+$	$\frac{1}{\sqrt{2}}$	0	0	0	0

Table 5.5.: Result of the application of the Wigner-Eckart theorem to $D \to P_8 P_8$ decays in the SU(3)$_F$ limit. The entries in the table are the Clebsch-Gordan coefficients $c_{d;ij}$ of the expressions for the amplitudes in Eqs. (5.43)–(5.45). Table adapted from [175].

the **3** matrix elements in Table 5.5 have only nonvanishing Clebsch-Gordan coefficients for the SCS decay channels. For instance,

$$\mathcal{A}_0(D^0 \to K^-\pi^+) = V_{cs}^* V_{ud}\left(\frac{\sqrt{2}}{5}A_{27}^{15} - \frac{\sqrt{2}}{5}A_8^{15} + \frac{1}{\sqrt{5}}A_8^{\bar{6}}\right). \tag{5.46}$$

The amplitudes are normalized such that for a decay d with amplitude $\mathcal{A}(d)$ the branching ratio is given as

$$\mathcal{B}(D \to P_1 P_2) = \tau_D \mathcal{P}(d) \left|\mathcal{A}(d)\right|^2, \tag{5.47}$$

with lifetime τ_D of the initial D meson and the phase space factor

$$\mathcal{P}(d) = \frac{\sqrt{(m_D^2 - (m_1 - m_2)^2)(m_D^2 - (m_1 + m_2)^2)}}{16\pi m_D^3}. \tag{5.48}$$

m_D is the mass of the initial D meson and $m_{1,2}$ are the masses of the kaon or pion mesons in the final state. As one can see from Table 5.5 it turns out that the 17 decay channels are described by only five matrix elements. Obviously, a lot of correlations between channels arise. For example, strict SU(3)$_F$ symmetry predicts that

$$\frac{\mathcal{B}(D^0 \to K^+K^-)}{\mathcal{B}(D^0 \to \pi^+\pi^-)} = 1\,, \qquad \frac{\mathcal{B}(D^0 \to K^+\pi^-)}{\lambda^4 \mathcal{B}(D^0 \to K^-\pi^+)} = 1 \qquad \text{(strict SU(3)}_F\text{-limit)}. \tag{5.49}$$

Also, the amplitude

$$\mathcal{A}(D^0 \to \bar{K}^0 K^0)_{\text{SU(3)}_F\text{-limit}} \sim \lambda^5 \tag{5.50}$$

is predicted to be strongly CKM suppressed. For the direct CP asymmetries we have furthermore the following relations:

$$\frac{\Gamma(D^0 \to K^+K^-)}{\Gamma(D^0 \to \pi^+\pi^-)} = -\frac{a_{CP}^{\text{dir}}(D^0 \to \pi^+\pi^-)}{a_{CP}^{\text{dir}}(D^0 \to K^+K^-)}\,, \tag{5.51}$$

$$\frac{\Gamma(D^+ \to \bar{K}^0 K^+)}{\Gamma(D_s \to K^0\pi^+)} = -\frac{a_{CP}^{\text{dir}}(D_s \to K^0\pi^+)}{a_{CP}^{\text{dir}}(D^+ \to K^0 K^+)}\,, \tag{5.52}$$

$$a_{CP}^{\text{dir}}(D^0 \to K^0\bar{K}^0) = 0\,, \tag{5.53}$$

$$a_{CP}^{\text{dir}}(D^+ \to \pi^+\pi^0) = 0. \tag{5.54}$$

From Eqs. (5.51) and (5.52), which are exact in the SU(3)$_F$ limit, follow the approximate relations

$$a_{CP}^{\text{dir}}(D^0 \to K^+K^-) + a_{CP}^{\text{dir}}(D^0 \to \pi^+\pi^-) = O(\text{Re}\tilde{\Delta}\text{Im}\tilde{\Delta})\,, \tag{5.55}$$

$$a_{CP}^{\text{dir}}(D^+ \to \bar{K}^0 K^+) + a_{CP}^{\text{dir}}(D_s \to K^0\pi^+) = O(\text{Re}\tilde{\Delta}\text{Im}\tilde{\Delta})\,. \tag{5.56}$$

It turns out that most of the predictions in the SU(3)$_F$ limit are not fulfilled by the data, for example,

$$\frac{\mathcal{B}(D^0 \to K^+K^-)}{\mathcal{B}(D^0 \to \pi^+\pi^-)} = 2.83 \pm 0.08\,, \qquad \frac{\mathcal{B}(D^0 \to K^+\pi^-)}{\lambda^4 \mathcal{B}(D^0 \to K^-\pi^+)} = 1.47 \pm 0.07\,, \tag{5.57}$$

where we used Gaussian error propagation in order to calculate the uncertainties. Additionally, $\mathcal{B}(D^0 \to K_S K_S)$ is not as suppressed as expected by SU(3)$_F$. A fit of all 25 observables to the five matrix elements in Table 5.5 in the SU(3)$_F$ limit results in $\chi^2/dof \sim 100$. If one fits the branching ratios of CF and DCS decays only, one still has $\chi^2/dof \sim 9$.

We conclude that the SU(3)$_F$-limit description of $D \to P_8 P_8$ does not even work for the branching ratios. It is all the worse for the full set of observables. Consequently, the SU(3)$_F$ ansatz has to be amended by the inclusion of breaking terms. In the next section we show how to include linear SU(3)$_F$ breaking in order to include the corrections from $m_s \neq m_{u,d}$.

5.3. Breaking SU(3)$_F$

Taking into account $m_s \neq m_{u,d}$ As explained in Sec. 5.2 we are forced by the data to include SU(3)$_F$ breaking effects. The approximate SU(3)$_F$ symmetry of the QCD-Lagrangian is broken by the non-vanishing mass terms of the quarks, *i.e.*, the bilinear terms

$$\mathcal{H} \supsetneq m_s\, \bar{s}s + m_d\, \bar{d}d + m_u\, \bar{u}u. \tag{5.58}$$

However, the three SU(2)$_F$ subgroups of SU(3)$_F$ are broken with different amounts. The isospin symmetry $m_u = m_d$ is realized with great precision: the mass difference between m_u and m_d compared to Λ_{QCD} is tiny. Therefore, we assume isospin is not broken. We only take into account the corrections stemming from $m_s \neq m_{u,d}$. The size of these corrections should *a priori* be of the order $\varepsilon \sim m_s/\Lambda_{\text{QCD}} \sim 30\%$ which we take as generic size of the SU(3)$_F$ expansion parameter, and which is absorbed into the SU(3)$_F$-breaking matrix elements as an overall factor. We quantitatively confirm that the data can be described with this nominal SU(3)$_F$ breaking in Sec. 5.4.1.
Perturbation theory tells us to take into account the corrections of the non-perturbed operators given in Eqs. (5.40)-(5.42) by the tensor product with the perturbation, *i.e.*, with the octet stemming from the operator $\bar{s}s$. Thus, SU(3)$_F$ breaking is described by the tensor products

$$\mathbf{15} \otimes \mathbf{8} = \mathbf{42} \oplus \mathbf{24} \oplus \mathbf{15_1} \oplus \mathbf{15_2} \oplus \mathbf{15'} \oplus \bar{\mathbf{6}} \oplus \mathbf{3}\,, \tag{5.59}$$

$$\bar{\mathbf{6}} \otimes \mathbf{8} = \mathbf{24} \oplus \mathbf{15} \oplus \bar{\mathbf{6}} \oplus \mathbf{3}\,, \tag{5.60}$$

$$\mathbf{3} \otimes \mathbf{8} = \mathbf{15} \oplus \bar{\mathbf{6}} \oplus \mathbf{3}. \tag{5.61}$$

Obviously, the result does not only contain small representations like the **3** and $\bar{\mathbf{6}}$ but also higher ones as a **24** and a **42**. There is however no reason for an *a priori* hierarchy between different representations.[1] Calculating the Clebsch-Gordan coefficients of the tensor products in Eqs. (5.59)-(5.61), the Hamiltonian is amended by the following SU(3)-breaking terms:

$$\begin{aligned}\mathcal{H}_{\text{eff}}^{\text{CF,X}} = &-\frac{1}{\sqrt{10}}\overline{\mathbf{6}}^{\mathbf{1}}{}_{1,1,-\frac{2}{3}} - \frac{1}{2\sqrt{5}}\overline{\mathbf{6}}^{\mathbf{2}}{}_{1,1,-\frac{2}{3}} \\ &+ \frac{7}{2\sqrt{366}}\mathbf{15}^{\mathbf{1}}{}_{1,1,-\frac{2}{3}} + \frac{1}{\sqrt{122}}\mathbf{15}^{\mathbf{2}}{}_{1,1,-\frac{2}{3}} + \frac{1}{2}\mathbf{15}^{\mathbf{3}}{}_{1,1,-\frac{2}{3}} - \frac{1}{2\sqrt{2}}\mathbf{15}'{}_{1,1,-\frac{2}{3}} \\ &- \frac{1}{\sqrt{15}}\mathbf{24}^{\mathbf{1}}{}_{1,1,-\frac{2}{3}} - \frac{1}{\sqrt{5}}\mathbf{24}^{\mathbf{2}}{}_{1,1,-\frac{2}{3}} + \frac{1}{\sqrt{6}}\mathbf{42}_{1,1,-\frac{2}{3}}\,,\end{aligned} \tag{5.62}$$

$$\begin{aligned}\mathcal{H}_{\text{eff}}^{\text{SCS,X}} = &-\frac{1}{2}\sqrt{\frac{3}{10}}\mathbf{3}^{\mathbf{1}}{}_{\frac{1}{2},\frac{1}{2},\frac{1}{3}} - \frac{\sqrt{3}}{4}\mathbf{3}^{\mathbf{2}}{}_{\frac{1}{2},\frac{1}{2},\frac{1}{3}} \\ &- \frac{1}{2\sqrt{5}}\overline{\mathbf{6}}^{\mathbf{1}}{}_{\frac{1}{2},\frac{1}{2},\frac{1}{3}} + \frac{1}{2\sqrt{10}}\overline{\mathbf{6}}^{\mathbf{2}}{}_{\frac{1}{2},\frac{1}{2},\frac{1}{3}} \\ &- \frac{2}{3}\sqrt{\frac{2}{61}}\mathbf{15}^{\mathbf{1}}{}_{\frac{1}{2},\frac{1}{2},\frac{1}{3}} + \frac{5}{12\sqrt{61}}\mathbf{15}^{\mathbf{1}}{}_{\frac{3}{2},\frac{1}{2},\frac{1}{3}} - \frac{11}{2\sqrt{366}}\mathbf{15}^{\mathbf{2}}{}_{\frac{1}{2},\frac{1}{2},\frac{1}{3}} - \frac{4}{\sqrt{183}}\mathbf{15}^{\mathbf{2}}{}_{\frac{3}{2},\frac{1}{2},\frac{1}{3}} \\ &+ \frac{\sqrt{3}}{4}\mathbf{15}^{\mathbf{3}}{}_{\frac{1}{2},\frac{1}{2},\frac{1}{3}} + \frac{1}{4}\mathbf{15}'{}_{\frac{3}{2},\frac{1}{2},\frac{1}{3}} \\ &- \frac{2}{3\sqrt{5}}\overline{\mathbf{24}}^{\mathbf{1}}{}_{\frac{1}{2},\frac{1}{2},\frac{1}{3}} + \frac{1}{3}\overline{\mathbf{24}}^{\mathbf{1}}{}_{\frac{3}{2},\frac{1}{2},\frac{1}{3}} - \sqrt{\frac{3}{5}}\overline{\mathbf{24}}^{\mathbf{2}}{}_{\frac{1}{2},\frac{1}{2},\frac{1}{3}} + \frac{4}{3\sqrt{5}}\mathbf{42}_{\frac{1}{2},\frac{1}{2},\frac{1}{3}} - \frac{1}{6}\sqrt{\frac{5}{2}}\mathbf{42}_{\frac{3}{2},\frac{1}{2},\frac{1}{3}}\,,\end{aligned} \tag{5.63}$$

$$\begin{aligned}\mathcal{H}_{\text{eff}}^{\text{DCS,X}} = &-\frac{1}{\sqrt{5}}\overline{\mathbf{6}}^{\mathbf{2}}{}_{0,0,\frac{4}{3}} - \frac{7}{\sqrt{366}}\mathbf{15}^{\mathbf{1}}{}_{1,0,\frac{4}{3}} - \sqrt{\frac{2}{61}}\mathbf{15}^{\mathbf{2}}{}_{1,0,\frac{4}{3}} \\ &- \frac{1}{\sqrt{6}}\overline{\mathbf{24}}^{\mathbf{1}}{}_{1,0,\frac{4}{3}} + \sqrt{\frac{3}{10}}\overline{\mathbf{24}}^{\mathbf{2}}{}_{0,0,\frac{4}{3}} + \frac{1}{\sqrt{6}}\mathbf{42}_{1,0,\frac{4}{3}}\,.\end{aligned} \tag{5.64}$$

Note that in the SU(3)$_F$ breaking we have neglected the contributions from the tensor product $\mathbf{3} \otimes \mathbf{8}$. These terms only appear with a factor Δ in front, *i.e.*, they have a double suppression $\Delta \times \varepsilon$ and are thus higher order in our power counting. With the present measurements of CP asymmetries we are not sensitive to these corrections anyway.

In order to obtain the reduced matrix elements we apply the Wigner-Eckart theorem in the same way as in Sec. 5.2 for the SU(3)$_F$ limit. The resulting Clebsch-Gordan coefficients are given in Table 5.6. The result is in agreement with the result that is obtained by the authors of Ref. [441].[2]

[1] Likewise, the "$\Delta I = 1/2$ rule", while being true for the kaon sector, is found not to be valid for charm in Ref. [464].

[2] The slight disagreements with [441] that we note in [175] are due to typos in the former reference [465].

Note that in Table 5.6 the $\mathbf{15}'$ representation does not contribute at all because all its Clebsch-Gordan coefficients therein vanish. Using the coefficients from Table 5.6 the SU(3)-breaking part of the amplitudes $\mathcal{A}(d) = \mathcal{A}_0(d) + \mathcal{A}_X(d)$ can be written as

$$\mathcal{A}_X(d) = \Sigma \sum_{i,j} c_{d;ij} B_i^j \,, \qquad \text{(SCS)} \tag{5.65}$$

$$\mathcal{A}_X(d) = V_{cs}^* V_{ud} \sum_{i,j} c_{d;ij} B_i^j \,, \qquad \text{(CF)} \tag{5.66}$$

$$\mathcal{A}_X(d) = V_{cd}^* V_{us} \sum_{i,j} c_{d;ij} B_i^j \,. \qquad \text{(DCS)} \tag{5.67}$$

Counting parameters Not all of the matrix elements in Table 5.6 are physical degrees of freedom. Altogether, we have at this stage five SU(3)$_F$ limit matrix elements, where two of them come only with a factor of Δ. As we are only sensitive to relative phases we have thus nine real-valued SU(3)$_F$ limit parameters. In addition to these there are 15 complex matrix elements from the breaking in Table 5.6. Altogether, for the 17 decay channels we have thus 20 matrix elements. But the 17×20 matrix of Clebsch-Gordan coefficients does not have full rank. For calculating the rank of the matrix we have to consider terms coming only with Δ, *i.e.*, the SU(3)$_F$ limit $\mathbf{3}$ matrix elements separately as they have a different order in the power counting.

The 17×18 matrix of Clebsch-Gordan coefficients of matrix elements without factors of Δ has rank 11. This means that only 13 out of 20 matrix elements are physical degrees of freedom. The others can be absorbed by redefinitions. For example, the first and most obvious redefinition is the absorption of the $\mathbf{3^2}$ into the $\mathbf{3^1}$. This redefinition could even be done already on the level of the Hamiltonian. The reason is that the two triplets appear only together and with the same quantum numbers and are thus indistinguishable.

On the matrix element level we replace

$$B_{1,8}^{3_1} \mapsto \sqrt{\frac{7}{2}} B_{1,8}^{3_1} - \sqrt{\frac{5}{2}} B_{1,8}^{3_2}. \tag{5.68}$$

By further similar replacements we eliminate the matrix elements $B_8^{\bar{6}_2}$, $B_8^{15_3}$, $B_{27}^{15_3}$, $B_{27}^{24_2}$ and B_{27}^{42}. The redefinitions in order to do so can be found by Gaussian elimination. During this process we absorb also parts of the SU(3)$_F$ breaking amplitudes into the SU(3)$_F$ limit ones. However, in order to keep the relative normalization of the SU(3)$_F$ limit and breaking amplitudes $\mathcal{A}_0(d)$ and $\mathcal{A}_X(d)$, respectively, for the redefined physical matrix elements we use the normalization $\sqrt{\Sigma_i |c_i|^2} B^{\text{phys}} = \Sigma_i c_i B_i^{\text{SU(3)}}$. The normalization of the SU(3)$_F$ limit matrix elements on the other hand is not touched and no SU(3)$_F$ limit matrix element is absorbed into another one. Hence, the Clebsch-Gordan coefficients of the redefined matrix elements are in the SU(3)$_F$ limit just the same as in Table 5.5. Specifically,

the applied redefinitions that follow the ones in Eq. (5.68) read as follows:

$$A_{27}^{15} \mapsto A_{27}^{15} - \frac{\sqrt{2}}{3} B_{27}^{15_3} + \frac{1}{6} B_{27}^{24_2}\,, \tag{5.69}$$

$$A_{8}^{15} \mapsto A_{8}^{15} - \frac{\sqrt{2}}{3} B_{8}^{15_3} + \frac{3}{8} B_{27}^{24_2}\,, \tag{5.70}$$

$$A_{8}^{\bar{6}} \mapsto A_{8}^{\bar{6}} + \sqrt{\frac{2}{5}} B_{8}^{\bar{6}_2} - \frac{3}{4\sqrt{10}} B_{27}^{24_2}\,, \tag{5.71}$$

$$B_{1}^{3} \mapsto \frac{\sqrt{421}}{14} B_{1}^{3} - \frac{3}{2}\sqrt{\frac{5}{14}} B_{27}^{24_2} + \frac{3}{14}\sqrt{\frac{15}{2}} B_{27}^{42}\,, \tag{5.72}$$

$$B_{8}^{3} \mapsto \frac{\sqrt{3937}}{56} B_{8}^{3} + \frac{15}{8\sqrt{14}} B_{27}^{24_2} + \frac{3}{56}\sqrt{\frac{3}{2}} B_{27}^{42}\,, \tag{5.73}$$

$$B_{8}^{\bar{6}_1} \mapsto \frac{1}{8}\sqrt{\frac{2869}{7}} B_{8}^{\bar{6}_1} - \frac{3}{\sqrt{2}} B_{8}^{\bar{6}_2} + \frac{9}{8\sqrt{2}} B_{27}^{24_2} + \frac{9}{8}\sqrt{\frac{3}{14}} B_{27}^{42}\,, \tag{5.74}$$

$$B_{8}^{15_1} \mapsto \frac{1}{24}\sqrt{\frac{1330969}{854}} B_{8}^{15_1} + \frac{23}{3\sqrt{122}} B_{8}^{15_3} - \frac{69}{16\sqrt{61}} B_{27}^{24_2} + \frac{3}{16}\sqrt{\frac{183}{7}} B_{27}^{42}\,, \tag{5.75}$$

$$B_{8}^{15_2} \mapsto \frac{1}{2}\sqrt{\frac{871}{61}} B_{8}^{15_2} - 4\sqrt{\frac{6}{61}} B_{8}^{15_3} + \frac{9}{2}\sqrt{\frac{3}{61}} B_{27}^{24_2}\,, \tag{5.76}$$

$$B_{27}^{15_2} \mapsto \frac{1}{2}\sqrt{\frac{5281}{854}} B_{27}^{15_1} + \frac{23}{3\sqrt{122}} B_{27}^{15_3} - \frac{23}{12\sqrt{61}} B_{27}^{24_2} - \frac{3}{4}\sqrt{\frac{3}{427}} B_{27}^{42}\,, \tag{5.77}$$

$$B_{27}^{15_2} \mapsto 2\sqrt{\frac{302}{427}} B_{27}^{15_2} - 4\sqrt{\frac{6}{61}} B_{27}^{15_3} + 2\sqrt{\frac{3}{61}} B_{27}^{24_2} + \frac{5}{\sqrt{427}} B_{27}^{42}\,, \tag{5.78}$$

$$B_{27}^{24_1} \mapsto 2\sqrt{\frac{2}{7}} B_{27}^{24_1} - \frac{1}{\sqrt{7}} B_{27}^{42}\,. \tag{5.79}$$

The Clebsch-Gordan coefficients of the redefined matrix elements are given in Table 5.7. In the following we use Eqs. (5.65)-(5.67) only with the Clebsch-Gordan coefficients given in Table 5.7. Note that due to the linear combinations in Eqs. (5.68)–(5.79) the indices of the redefined matrix elements do not correspond anymore to actual representations.

SU(3)$_F$ sum rules Implicitly, the Tables 5.5, 5.6 and 5.7 contain a number of nontrivial sum rules. A comprehensive list of all sum rules for $D \to P_8 P_8$ (and additionally also for $D \to P_1 P_8$, $D \to PV$) that are valid even in the presence of linear breaking terms can be found in [466], see also [447, 467, 468]. As the 17×11 matrix of Clebsch-Gordan coefficients composed of Tables 5.5 and 5.7 has maximal rank (namely 11) we know a priori that there must be six nontrivial sum rules between the amplitudes. The underlying mathematical reason for this is the equality of row and column rank.

Decay d	$B_1^{3_1}$	$B_1^{3_2}$	$B_8^{3_1}$	$B_8^{3_2}$	$B_8^{\bar{6}_1}$	$B_8^{\bar{6}_2}$	$B_8^{15_1}$	$B_8^{15_2}$	$B_8^{15_3}$	$B_{27}^{15_1}$	$B_{27}^{15_2}$	$B_{27}^{15_3}$	$B_{27}^{24_1}$	$B_{27}^{24_2}$	B_{27}^{42}
SCS															
$D^0 \to K^+K^-$	$\frac{1}{4\sqrt{10}}$	$\frac{1}{8}$	$\frac{1}{10\sqrt{2}}$	$\frac{1}{4\sqrt{5}}$	$\frac{1}{10}$	$-\frac{1}{10\sqrt{2}}$	$-\frac{7}{10\sqrt{122}}$	$\frac{\sqrt{\frac{3}{122}}}{5}$	$-\frac{1}{20}$	$-\frac{31}{20\sqrt{122}}$	$-\frac{17}{20\sqrt{366}}$	$\frac{7}{40}$	$-\frac{1}{10\sqrt{6}}$	$\frac{1}{10\sqrt{2}}$	$-\frac{13}{20\sqrt{42}}$
$D^0 \to \pi^+\pi^-$	$\frac{1}{4\sqrt{10}}$	$\frac{1}{8}$	$\frac{1}{10\sqrt{2}}$	$\frac{1}{4\sqrt{5}}$	$-\frac{1}{10}$	$\frac{1}{10\sqrt{2}}$	$-\frac{11}{10\sqrt{122}}$	$-\frac{2\sqrt{\frac{2}{183}}}{5}$	$\frac{3}{20}$	$-\frac{23}{20\sqrt{122}}$	$\frac{11}{20\sqrt{366}}$	$-\frac{1}{40}$	$\frac{1}{10\sqrt{6}}$	$-\frac{1}{10\sqrt{2}}$	$\frac{\sqrt{\frac{7}{6}}}{20}$
$D^0 \to \bar{K}^0K^0$	$-\frac{1}{4\sqrt{10}}$	$-\frac{1}{8}$	$\frac{1}{5\sqrt{2}}$	$\frac{1}{2\sqrt{5}}$	0	0	$-\frac{9}{5\sqrt{122}}$	$-\frac{1}{5\sqrt{366}}$	$\frac{1}{10}$	$-\frac{9}{20\sqrt{122}}$	$-\frac{1}{20\sqrt{366}}$	$\frac{1}{40}$	$-\frac{1}{2\sqrt{6}}$	$-\frac{1}{2\sqrt{2}}$	$\frac{19}{20\sqrt{42}}$
$D^0 \to \pi^0\pi^0$	$-\frac{1}{8\sqrt{5}}$	$-\frac{1}{8\sqrt{2}}$	$-\frac{1}{20}$	$-\frac{1}{4\sqrt{10}}$	$\frac{1}{10\sqrt{2}}$	$-\frac{1}{20}$	$\frac{11}{20\sqrt{61}}$	$\frac{2}{5\sqrt{183}}$	$-\frac{3}{20\sqrt{2}}$	$-\frac{57}{40\sqrt{61}}$	$\frac{7}{20\sqrt{183}}$	$\frac{1}{40\sqrt{2}}$	$\frac{1}{5\sqrt{3}}$	$\frac{1}{20}$	$-\frac{1}{20\sqrt{21}}$
$D^+ \to \pi^0\pi^+$	0	0	0	0	0	0	0	0	0	$-\frac{2(1-\tilde{\Delta})}{\sqrt{61}}$	$\frac{5(1-\tilde{\Delta})}{8\sqrt{183}}$	0	$\frac{1-\tilde{\Delta}}{4\sqrt{3}}$	0	$\frac{1-\tilde{\Delta}}{8\sqrt{21}}$
$D^+ \to \bar{K}^0K^+$	0	0	$\frac{3}{10\sqrt{2}}$	$\frac{3}{4\sqrt{5}}$	$\frac{1}{10}$	$-\frac{1}{10\sqrt{2}}$	$\frac{7}{10\sqrt{122}}$	$-\frac{\sqrt{\frac{3}{122}}}{5}$	$\frac{1}{20}$	$-\frac{3\sqrt{\frac{2}{61}}}{5}$	$-\frac{23}{20\sqrt{366}}$	$\frac{1}{5}$	$-\frac{1}{10\sqrt{6}}$	$-\frac{\sqrt{2}}{5}$	$-\frac{19}{20\sqrt{42}}$
$D_s \to K^0\pi^+$	0	0	$\frac{3}{10\sqrt{2}}$	$\frac{3}{4\sqrt{5}}$	$-\frac{1}{10}$	$\frac{1}{10\sqrt{2}}$	$\frac{11}{10\sqrt{122}}$	$\frac{2\sqrt{\frac{2}{183}}}{5}$	$-\frac{3}{20}$	$-\frac{3}{5\sqrt{122}}$	$\frac{19}{20\sqrt{366}}$	$-\frac{1}{10}$	$-\frac{\sqrt{\frac{2}{3}}}{5}$	$-\frac{1}{10\sqrt{2}}$	$-\frac{19}{20\sqrt{42}}$
$D_s \to K^+\pi^0$	0	0	$-\frac{3}{20}$	$-\frac{3}{4\sqrt{10}}$	$\frac{1}{10\sqrt{2}}$	$-\frac{1}{20}$	$-\frac{11}{20\sqrt{61}}$	$-\frac{2}{5\sqrt{183}}$	$\frac{3}{20\sqrt{2}}$	$-\frac{17}{10\sqrt{61}}$	$\frac{\sqrt{\frac{3}{61}}}{20}$	$\frac{1}{10\sqrt{2}}$	$-\frac{\sqrt{3}}{10}$	$\frac{1}{20}$	$-\frac{\sqrt{\frac{3}{7}}}{20}$
CF															
$D^0 \to K^-\pi^+$	0	0	0	0	$\frac{1}{5}$	$\frac{1}{5\sqrt{2}}$	$-\frac{\sqrt{\frac{2}{61}}}{5}$	$-\frac{7}{5\sqrt{366}}$	$-\frac{1}{5}$	$\frac{\sqrt{\frac{2}{61}}}{5}$	$\frac{7}{5\sqrt{366}}$	$\frac{1}{5}$	$\frac{1}{20\sqrt{6}}$	$\frac{1}{20\sqrt{2}}$	$-\frac{1}{2\sqrt{42}}$
$D^0 \to \bar{K}^0\pi^0$	0	0	0	0	$-\frac{1}{5\sqrt{2}}$	$-\frac{1}{10}$	$\frac{1}{5\sqrt{61}}$	$\frac{7}{10\sqrt{183}}$	$\frac{1}{5\sqrt{2}}$	$\frac{3}{10\sqrt{61}}$	$\frac{7\sqrt{\frac{3}{61}}}{20}$	$\frac{3}{10\sqrt{2}}$	$-\frac{\sqrt{3}}{20}$	$-\frac{3}{20}$	0
$D^+ \to \bar{K}^0\pi^+$	0	0	0	0	0	0	0	0	0	$\frac{1}{\sqrt{122}}$	$\frac{7}{2\sqrt{366}}$	$\frac{1}{2}$	$-\frac{1}{4\sqrt{6}}$	$-\frac{1}{4\sqrt{2}}$	$-\frac{1}{2\sqrt{42}}$
$D_s \to \bar{K}^0K^+$	0	0	0	0	$-\frac{1}{5}$	$-\frac{1}{5\sqrt{2}}$	$-\frac{\sqrt{\frac{2}{61}}}{5}$	$-\frac{7}{5\sqrt{366}}$	$-\frac{1}{5}$	$\frac{\sqrt{\frac{2}{61}}}{5}$	$\frac{7}{5\sqrt{366}}$	$\frac{1}{5}$	$\frac{1}{5\sqrt{6}}$	$\frac{1}{5\sqrt{2}}$	$\frac{1}{\sqrt{42}}$
DCS															
$D^0 \to K^+\pi^-$	0	0	0	0	0	$-\frac{\sqrt{2}}{5}$	$\frac{2\sqrt{\frac{2}{61}}}{5}$	$\frac{7\sqrt{\frac{2}{183}}}{5}$	0	$-\frac{2\sqrt{\frac{2}{61}}}{5}$	$-\frac{7\sqrt{\frac{2}{183}}}{5}$	0	$-\frac{1}{4\sqrt{6}}$	$\frac{3}{20\sqrt{2}}$	$-\frac{1}{2\sqrt{42}}$
$D^0 \to K^0\pi^0$	0	0	0	0	0	$\frac{1}{5}$	$-\frac{2}{5\sqrt{61}}$	$-\frac{7}{5\sqrt{183}}$	0	$-\frac{3}{5\sqrt{61}}$	$-\frac{7\sqrt{\frac{3}{61}}}{10}$	0	$-\frac{\sqrt{3}}{8}$	$-\frac{3}{40}$	0
$D^+ \to K^0\pi^+$	0	0	0	0	0	$\frac{\sqrt{2}}{5}$	$\frac{2\sqrt{\frac{2}{61}}}{5}$	$\frac{7\sqrt{\frac{2}{183}}}{5}$	0	$-\frac{2\sqrt{\frac{2}{61}}}{5}$	$-\frac{7\sqrt{\frac{2}{183}}}{5}$	0	$-\frac{1}{4\sqrt{6}}$	$-\frac{3}{20\sqrt{2}}$	$-\frac{1}{2\sqrt{42}}$
$D^+ \to K^+\pi^0$	0	0	0	0	0	$-\frac{1}{5}$	$-\frac{2}{5\sqrt{61}}$	$-\frac{7}{5\sqrt{183}}$	0	$-\frac{3}{5\sqrt{61}}$	$-\frac{7\sqrt{\frac{3}{61}}}{10}$	0	$-\frac{\sqrt{3}}{8}$	$\frac{3}{40}$	0
$D_s \to K^0K^+$	0	0	0	0	0	0	0	0	0	$-\sqrt{\frac{2}{61}}$	$-\frac{7}{\sqrt{366}}$	0	$\frac{1}{2\sqrt{6}}$	0	$\frac{1}{\sqrt{42}}$

Table 5.6.: Result of the application of the Wigner-Eckart theorem to $D \to P_8P_8$ decays for the SU(3)$_F$ breaking part. The entries in the table are the Clebsch-Gordan coefficients $c_{d;ij}$ of the expressions for the amplitudes in Eqs. (5.65)–(5.67). Here, no reparametrizations are applied yet. Table adapted from [175].

Decay d	B_1^3	B_8^3	$B_8^{\bar{6}_1}$	$B_8^{15_1}$	$B_8^{15_2}$	$B_{27}^{15_1}$	$B_{27}^{15_2}$	$B_{27}^{24_1}$
SCS								
$D^0 \to K^+K^-$	$\frac{\sqrt{\frac{421}{35}}}{16}$	$\frac{\sqrt{\frac{3937}{7}}}{160}$	$\frac{\sqrt{\frac{2869}{7}}}{80}$	$-\frac{\sqrt{9316783}}{29280}$	$\frac{\sqrt{\frac{2613}{2}}}{610}$	$-\frac{31\sqrt{\frac{5281}{7}}}{4880}$	$-\frac{17\sqrt{\frac{151}{21}}}{610}$	$-\frac{1}{5\sqrt{21}}$
$D^0 \to \pi^+\pi^-$	$\frac{\sqrt{\frac{421}{35}}}{16}$	$\frac{\sqrt{\frac{3937}{7}}}{160}$	$-\frac{\sqrt{\frac{2869}{7}}}{80}$	$-\frac{11\sqrt{\frac{1330969}{7}}}{29280}$	$-\frac{\sqrt{\frac{1742}{3}}}{305}$	$-\frac{23\sqrt{\frac{5281}{7}}}{4880}$	$\frac{11\sqrt{\frac{151}{21}}}{610}$	$\frac{1}{5\sqrt{21}}$
$D^0 \to \bar{K}^0K^0$	$-\frac{\sqrt{\frac{421}{35}}}{16}$	$\frac{\sqrt{\frac{3937}{7}}}{80}$	0	$-\frac{3\sqrt{\frac{1330969}{7}}}{4880}$	$-\frac{\sqrt{\frac{871}{6}}}{610}$	$-\frac{9\sqrt{\frac{5281}{7}}}{4880}$	$-\frac{\sqrt{\frac{151}{21}}}{610}$	$-\frac{1}{\sqrt{21}}$
$D^0 \to \pi^0\pi^0$	$-\frac{\sqrt{\frac{421}{70}}}{16}$	$-\frac{\sqrt{\frac{3937}{14}}}{160}$	$\frac{\sqrt{\frac{2869}{14}}}{80}$	$\frac{11\sqrt{\frac{1330969}{14}}}{29280}$	$\frac{\sqrt{\frac{871}{3}}}{305}$	$-\frac{57\sqrt{\frac{5281}{14}}}{4880}$	$\frac{\sqrt{\frac{1057}{6}}}{305}$	$\frac{2\sqrt{\frac{2}{21}}}{5}$
$D^+ \to \pi^0\pi^+$	0	0	0	0	0	$-\frac{\sqrt{\frac{5281}{14}}(1-\tilde{\Delta})}{61}$	$\frac{5\sqrt{\frac{151}{42}}(1-\tilde{\Delta})}{122}$	$\frac{1-\tilde{\Delta}}{\sqrt{42}}$
$D^+ \to \bar{K}^0K^+$	0	$\frac{3\sqrt{\frac{3937}{7}}}{160}$	$\frac{\sqrt{\frac{2869}{7}}}{80}$	$\frac{\sqrt{9316783}}{29280}$	$-\frac{\sqrt{\frac{2613}{2}}}{610}$	$-\frac{3\sqrt{\frac{5281}{7}}}{610}$	$-\frac{23\sqrt{\frac{151}{21}}}{610}$	$-\frac{1}{5\sqrt{21}}$
$D_s \to K^0\pi^+$	0	$\frac{3\sqrt{\frac{3937}{7}}}{160}$	$-\frac{\sqrt{\frac{2869}{7}}}{80}$	$\frac{11\sqrt{\frac{1330969}{7}}}{29280}$	$\frac{\sqrt{\frac{1742}{3}}}{305}$	$-\frac{3\sqrt{\frac{5281}{7}}}{1220}$	$\frac{19\sqrt{\frac{151}{21}}}{610}$	$-\frac{4}{5\sqrt{21}}$
$D_s \to K^+\pi^0$	0	$-\frac{3\sqrt{\frac{3937}{14}}}{160}$	$\frac{\sqrt{\frac{2869}{14}}}{80}$	$-\frac{11\sqrt{\frac{1330969}{14}}}{29280}$	$-\frac{\sqrt{\frac{871}{3}}}{305}$	$-\frac{17\sqrt{\frac{5281}{14}}}{1220}$	$\frac{\sqrt{\frac{453}{14}}}{305}$	$-\frac{\sqrt{\frac{6}{7}}}{5}$
CF								
$D^0 \to K^-\pi^+$	0	0	$\frac{\sqrt{\frac{2869}{7}}}{40}$	$-\frac{\sqrt{\frac{1330969}{7}}}{7320}$	$-\frac{7\sqrt{\frac{871}{6}}}{610}$	$\frac{\sqrt{\frac{5281}{7}}}{610}$	$\frac{2\sqrt{\frac{1057}{3}}}{305}$	$\frac{1}{10\sqrt{21}}$
$D^0 \to \bar{K}^0\pi^0$	0	0	$-\frac{\sqrt{\frac{2869}{14}}}{40}$	$\frac{\sqrt{\frac{1330969}{14}}}{7320}$	$\frac{7\sqrt{\frac{871}{3}}}{1220}$	$\frac{3\sqrt{\frac{5281}{14}}}{1220}$	$\frac{\sqrt{\frac{3171}{2}}}{305}$	$-\frac{\sqrt{\frac{3}{14}}}{5}$
$D^+ \to \bar{K}^0\pi^+$	0	0	0	0	0	$\frac{\sqrt{\frac{5281}{7}}}{244}$	$\frac{\sqrt{\frac{1057}{3}}}{61}$	$-\frac{1}{2\sqrt{21}}$
$D_s \to \bar{K}^0K^+$	0	0	$-\frac{\sqrt{\frac{2869}{7}}}{40}$	$-\frac{\sqrt{\frac{1330969}{7}}}{7320}$	$-\frac{7\sqrt{\frac{871}{6}}}{610}$	$\frac{\sqrt{\frac{5281}{7}}}{610}$	$\frac{2\sqrt{\frac{1057}{3}}}{305}$	$\frac{2}{5\sqrt{21}}$
DCS								
$D^0 \to K^+\pi^-$	0	0	0	$\frac{\sqrt{\frac{1330969}{7}}}{3660}$	$\frac{7\sqrt{\frac{871}{6}}}{305}$	$-\frac{\sqrt{\frac{5281}{7}}}{305}$	$-\frac{4\sqrt{\frac{1057}{3}}}{305}$	$-\frac{1}{2\sqrt{21}}$
$D^0 \to K^0\pi^0$	0	0	0	$-\frac{\sqrt{\frac{1330969}{14}}}{3660}$	$-\frac{7\sqrt{\frac{871}{3}}}{610}$	$-\frac{3\sqrt{\frac{5281}{14}}}{610}$	$-\frac{\sqrt{6342}}{305}$	$-\frac{\sqrt{\frac{3}{14}}}{2}$
$D^+ \to K^0\pi^+$	0	0	0	$\frac{\sqrt{\frac{1330969}{7}}}{3660}$	$\frac{7\sqrt{\frac{871}{6}}}{305}$	$-\frac{\sqrt{\frac{5281}{7}}}{305}$	$-\frac{4\sqrt{\frac{1057}{3}}}{305}$	$-\frac{1}{2\sqrt{21}}$
$D^+ \to K^+\pi^0$	0	0	0	$-\frac{\sqrt{\frac{1330969}{14}}}{3660}$	$-\frac{7\sqrt{\frac{871}{3}}}{610}$	$-\frac{3\sqrt{\frac{5281}{14}}}{610}$	$-\frac{\sqrt{6342}}{305}$	$-\frac{\sqrt{\frac{3}{14}}}{2}$
$D_s \to K^0K^+$	0	0	0	0	0	$-\frac{\sqrt{\frac{5281}{7}}}{122}$	$-\frac{2\sqrt{\frac{1057}{3}}}{61}$	$\frac{1}{\sqrt{21}}$

Table 5.7.: The Clebsch-Gordan coefficients $c_{d;ij}$ of the redefined physical matrix elements which are obtained from Table 5.6 after applying the redefinitions given in Eqs. (5.68)–(5.79), see text for details. Table adapted from [175].

The six SU(3)$_F$-breaking sum rules for $D \to P_8 P_8$ given in Ref. [466] translate to our normalization of states as given below in Eqs. (5.80)–(5.85) [469]. Among the subset of SCS decays there is only one such sum rule as the corresponding 8×11 submatrix has rank seven. It is given as

- Pure SCS sum rule from isospin

$$\mathcal{A}(D^0 \to \pi^0\pi^0) + \frac{1}{\sqrt{2}}\mathcal{A}(D^0 \to \pi^+\pi^-) - \mathcal{A}(D^+ \to \pi^0\pi^+) = 0. \tag{5.80}$$

The other five sum rules are [466]

- Pure CF sum rule from isospin

$$\mathcal{A}(D^0 \to \bar{K}^0\pi^0) + \frac{1}{\sqrt{2}}\mathcal{A}(D^0 \to K^-\pi^+) - \frac{1}{\sqrt{2}}\mathcal{A}(D^+ \to \bar{K}^0\pi^+) = 0. \tag{5.81}$$

- Pure DCS sum rule from isospin

$$\begin{aligned}&\sqrt{2}\mathcal{A}(D^0 \to \pi^0 K^0) + \mathcal{A}(D^0 \to \pi^- K^+)\\ &\quad - \sqrt{2}\mathcal{A}(D^+ \to \pi^0 K^+) - \mathcal{A}(D^+ \to \pi^+ K^0) = 0.\end{aligned} \tag{5.82}$$

- Mixed CF, SCS, DCS sum rule from U-spin

$$\begin{aligned}&\frac{1}{\Sigma}\mathcal{A}(D^0 \to K^-K^+) - \frac{1}{V_{cd}^* V_{us}}\mathcal{A}(D^0 \to \pi^-K^+)\\ &\quad - \frac{1}{V_{cs}^* V_{ud}}\mathcal{A}(D^0 \to K^-\pi^+) - \frac{1}{\Sigma}\mathcal{A}(D^0 \to \pi^+\pi^-) = 0.\end{aligned} \tag{5.83}$$

- Mixed CF, SCS, DCS sum rule

$$\begin{aligned}&\frac{1}{V_{cs}^* V_{ud}}\mathcal{A}(D^+ \to \bar{K}^0\pi^+) - \frac{1}{V_{cs}^* V_{ud}}\mathcal{A}(D_s \to \bar{K}^0K^+) - \frac{1}{\Sigma}\mathcal{A}(D^+ \to \bar{K}^0K^+)\\ &\quad + \frac{1}{\Sigma}\mathcal{A}(D_s \to \pi^+K^0) - \frac{1}{V_{cd}^* V_{us}}\mathcal{A}(D^+ \to \pi^+K^0) + \frac{1}{V_{cd}^* V_{us}}\mathcal{A}(D_s \to K^0K^+) = 0.\end{aligned} \tag{5.84}$$

- Mixed CF, SCS, DCS sum rule

$$\begin{aligned}&\sqrt{2}\frac{1}{V_{cd}^* V_{us}}\mathcal{A}(D^+ \to \pi^0K^+) - \frac{1}{\Sigma}\mathcal{A}(D^+ \to \bar{K}^0K^+) + \sqrt{2}\frac{1}{\Sigma}\mathcal{A}(D^+ \to \pi^0\pi^+)\\ &\quad + \frac{1}{V_{cs}^* V_{ud}}\mathcal{A}(D^+ \to \bar{K}^0\pi^+) - \sqrt{2}\frac{1}{\Sigma}\mathcal{A}(D_s \to \pi^0K^+) - \frac{1}{V_{cs}^* V_{ud}}\mathcal{A}(D_s \to \bar{K}^0K^+) = 0.\end{aligned} \tag{5.85}$$

Apart from these exact sum rules one could ask also if there are any approximate sum rules that are broken only by a few matrix elements. Such relations indeed exist, as one can show by calculating the rank of submatrices omitting the columns corresponding to the Clebsch-Gordan coefficients of the considered matrix elements. Among the SCS decays with redefined matrix elements as in Table 5.7 there is only one relation where only one breaking matrix element appears, namely the (quasi-)triangle relation

$$\mathcal{A}(D^+ \to \pi^+\pi^0) - \frac{1}{\sqrt{2}}\mathcal{A}(D_s \to K^0\pi^+) - \mathcal{A}(D_s \to K^+\pi^0) = \Sigma\sqrt{\frac{3}{14}}B_{27}^{24_1}. \tag{5.86}$$

It was already found in [468] that Eq. (5.86) gives an exact sum rule when only triplet matrix elements are considered in the SU(3)$_F$ breaking as an however ad hoc assumption. In the non-redefined system on the right-hand side of Eq. (5.86) there would appear two matrix elements, see Eq. (5.79). However, in the system of matrix elements before redefinitions there is no approximate sum rule that involves only one breaking matrix element in the destruction of the exact rule.

The test of the SU(3)$_F$ sum rules with future data will probe on the one hand NP and on the other hand the validity of the SU(3)$_F$ expansion itself. The latter is also provided by global fits to current data which we present in Sec. 5.4.1. The experimental sum rule test is an ambitious task, as one needs measurements of the strong phases of all concerned amplitudes. For this reason, in Ref. [466] there are also constructed decay rate sum rules. In order to test these, no information on the strong phases is needed.

5.4. Answering Questions in Charm Physics without Prejudice

After setting up our framework in Secs. 5.2 and 5.3 we can pose questions that we can answer by fitting the 13 independent complex SU(3)$_F$ matrix elements to the data of 25 observables. Firstly, is after all the SU(3)$_F$ expansion working? That means, can we describe all the different charm decay channels with a reasonable size of SU(3)$_F$ breaking? If the SU(3)$_F$-breaking terms are larger than the leading ones the whole series expansion would not make sense. In this case we would have to stop and have to think about a different approach to charm decays.

Note that in the description of SU(3)$_F$ breaking we are conservative in a maximal way: In order to avoid all prejudices we only use the SU(3)$_F$ symmetry group and do not assume any further dynamical understanding of QCD. For example we do not assume that certain diagrams in Figs. 5.1–5.3 are enhanced or suppressed. Consequently, we especially do not assume that certain matrix elements are more important than others. Also every matrix element can have a complex (CP-conserving) phase.

In the case that the SU(3)$_F$ expansion works we can go on to the next questions: How large is the enhancement of the hadronic matrix elements of the **3** in the Hamiltonian in

Eq. (5.41) in order to account for the measured CP violation in charm decays? And finally, are there any patterns of NP that are distinguishable from the SM, or more generally, SM extensions with MFV?
We will discuss these questions now one after the other.

5.4.1. How Large is the SU(3)$_F$ Breaking?

In order to evaluate the size of SU(3)$_F$ breaking we define two complementary measures. On the one hand we look at the ratio of the maximal SU(3)$_F$ breaking matrix element over the maximal SU(3)$_F$ limit matrix element:

$$\delta_X = \frac{\max_{ij}|B_i^j|}{\max\left(|A_{27}^{15}|, |A_8^{\bar{6}}|, |A_8^{15}|\right)} . \quad (5.87)$$

On the other hand we study the maximal ratio of the breaking part of all amplitudes over the respective complete amplitude:

$$\delta'_X = \max_d \left|\frac{\mathcal{A}_X(d)}{\mathcal{A}(d)}\right| . \quad (5.88)$$

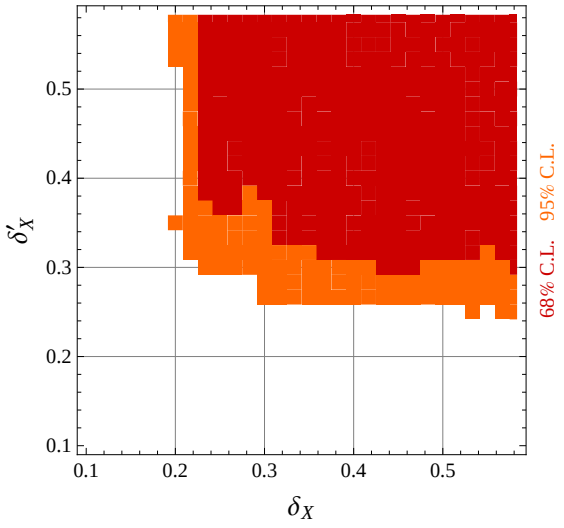

Figure 5.4.: Regions in the δ_X-δ'_X plane that are allowed at 68% (red) and 95% (orange) C.L. Figure taken from [175].

In Eq. (5.88) we take the maximum over all decays d without taking the mode $D^0 \to K_S K_S$ into account. The SU(3)$_F$ limit amplitude of this channel is CKM suppressed by $\tilde{\Delta}$, the CKM leading part firstly arises at linear SU(3)$_F$ breaking. Thus, the contribution of $D^0 \to K_S K_S$ would give δ'_X a bias towards large values. Both of the measures in Eqs. (5.87) and (5.88) have their advantages and disadvantages. The first one in Eq. (5.87) does not account for possible hierarchies in the Clebsch-Gordan coefficients that could destroy the hierarchy of the matrix elements in the amplitudes. The second one in Eq. (5.88) does not contain information on possible cancellations of large matrix elements. So in order to have a comprehensive understanding we plot the correlation of both measures δ_X, δ'_X against each other. The result is shown in Fig. 5.4 where we show the 68% and 95% C.L. contour lines with respect to the best fit point. The shaded areas are allowed regions. At the best fit point we have $\chi^2 = 1$ because in the SM we cannot account for the 1σ measurement of a nonvanishing CP asymmetry in $D^+ \to \pi^0\pi^+$ decays, see Sec. 5.4.4 below. Fig. 5.4 contains the important information that the data can be described already by an SU(3)$_F$ breaking of $\delta_X^{(\prime)} \sim 30\%$. If the shown area had been shifted towards much larger values that would have meant that the SU(3)$_F$ expansion in $\varepsilon \sim m_s/\Lambda_{\text{QCD}}$ did not make sense. But this is not the case, so that we can go on and look at the further phenomenological

implications of the approximate SU(3)$_F$ symmetry of QCD being confronted with the data.

5.4.2. Can we Exclude Scenarios of SU(3)$_F$ Breaking from Data?

Our parametrization of the linear breaking of the SU(3)$_F$ symmetry is completely general. But can we also say something about the detailed anatomy of the SU(3)$_F$ breaking? The answer is yes. The different configurations of SU(3)$_F$ breaking can be tested in a systematic way by taking into account subsets of matrix elements only, while setting all other to zero.

Using this procedure, we learn that for a reasonable fit at least two nonzero SU(3)$_F$ breaking matrix elements are needed. These two are again restricted: It does not suffice to take the triplet matrix elements B_1^3 and B_8^3. The corresponding fit gives $\chi^2/dof = 8.6$. It is clear from Table 5.7 that such a fit can not work because the SU(3)$_F$ breaking triplet matrix elements appear in the SCS decay modes only. They can thus not explain the SU(3)$_F$ violation in the branching ratios of the CF and DCS channels. As a curiosity, a fit only with the B_1^3 and B_8^3 to the SCS charm decays would work, it gives $\chi^2/dof = 1$. But this does not help us here as we want to get a consistent description for all $D \to P_8 P_8$ charm decays.

If one takes higher representations into account, such as in the configuration B_1^3 and $B_{27}^{15_2}$ with all others vanishing, one obtains a nicer fit with $\chi^2/dof = 1.3$. Demanding that the SU(3)$_F$ breaking stays below a sensible value, *i.e.*, imposing $\delta_X^{(\prime)} \leq 50\%$ the fit gets slightly worse to $\chi^2/dof = 1.6$. Keeping $\delta_X^{(\prime)} \leq 50\%$ and systematically performing fits with three nonvanishing matrix elements we find that for example the configurations

- B_1^3, $B_8^{15_2}$, $B_{27}^{24_1}$ and
- B_1^3, $B_{27}^{15_1}$, $B_{27}^{15_2}$

give each $\chi^2/dof = 1.0$. However, without having a dynamical theory that would argue in the direction of one such specific configuration, these observations are of little help. In the following therefore always all matrix elements are taken into account.

5.4.3. How Large is the Triplet Enhancement?

In order to analyze the triplet (penguin) enhancement in charm, we define two complementary measures in complete analogy to the ones for SU(3)$_F$ breaking in Eqs. (5.87) and (5.88). The first one is a measure on the matrix element level:

$$\delta_3 = \frac{\max\left(|A_1^3|, |A_8^3|\right)}{\max\left(|A_{27}^{15}|, |A_8^{\bar{6}}|, |A_8^{15}|\right)} \,. \tag{5.89}$$

Similar to δ_X, this measure ignores a possible enhancement or suppression from the Clebsch-Gordan coefficients. In order to account for this we define a second measure from the fraction that the triplet matrix elements contribute to the amplitudes. As the ratio is intended to be a measure of the QCD part only, we divide out the CKM matrix elements from the amplitudes. We define $\delta_3' = \max_d \delta_3'(d)$ with

$$\delta_3'(d) = \left| \frac{\Sigma\times \text{ total amplitude by } A_1^3,\, A_8^3}{\Delta\times \text{ total amplitude by } A_{27}^{15},\, A_8^{\bar{6}},\, A_8^{15}} \right| = \left| \frac{c_{d;1\,3} A_1^3 + c_{d;8\,3} A_8^3}{c_{d;27\,15} A_{27}^{15} + c_{d;8\,\bar{6}} + c_{d;8\,15} A_8^{15}} \right| . \tag{5.90}$$

In the last equation we have written the expression using symbolically the Clebsch-Gordan coefficients given in Table 5.5. In taking the maximum over all decays d in $\max_d \delta_3'(d)$ we exclude the decay $D^0 \to K_S K_S$ due to its CKM suppressed $SU(3)_F$ limit amplitude, as was discussed after Eq. (5.88) for δ_X'. The correlation plot of δ_3 and δ_3' from the fit to data is shown in Fig. 5.5. We see that enhanced triplets $\delta_3 \sim 2$ and $\delta_3' \sim 7$ are needed in order to account for the data at 95% C.L. Also, the 68% C.L. region is shifted to extremely large values. The plot in Fig. 5.5 is extremely unexpected. As was explained in Sec. 5.1, in the SM we would naively expect $\delta_3^{(\prime)} \sim 0.1$ and would conceive already $\delta_3^{(\prime)} \sim 1$ as an enhancement. $\delta_3^{(\prime)} \sim 5$–$10$ is therefore quite unlikely, on the other hand we can also not exclude such a behavior without having a dynamical theory at hand. Besides the enhancement we can also recognize that there are regions where large cancellations take place, *i.e.*, for fixed δ_3' one can go along the δ_3 axis to also very large values and vice versa.

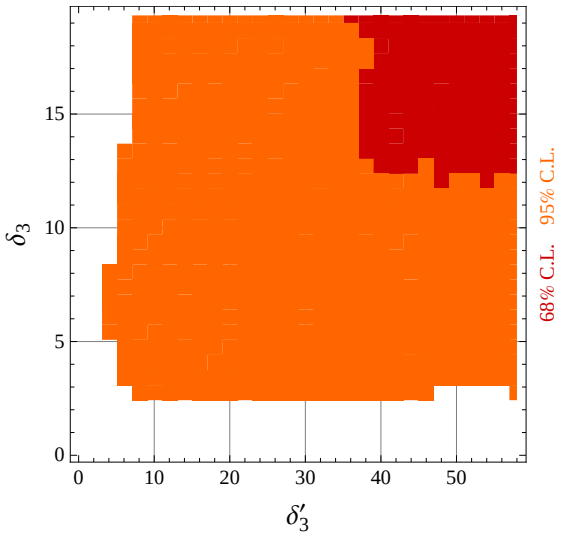

Figure 5.5.: Regions in the δ_3'-δ_3 plane that are allowed at 68% (red) and 95% (orange) C.L. without assumption on $\delta_X^{(\prime)}$. Figure taken from [175].

Which observables drive the triplet matrix elements to such large values? It is not only the quite precise and thus significant measurement of $\Delta a_{CP}^{\text{dir}}(K^+K^-, \pi^+\pi^-)$. There are also other CP asymmetries that are measured with largish central values, although the uncertainty is quite large (compare also Table 5.1):

$$A_{CP}(D^0 \to K_S K_S) = -0.23 \pm 0.19\,, \tag{5.91}$$
$$A_{CP}(D_s \to K_S \pi^+) = 0.031 \pm 0.015\,, \tag{5.92}$$
$$A_{CP}(D_s \to K^+ \pi^0) = 0.266 \pm 0.228\,. \tag{5.93}$$

The statistical significance of each individual one of these CP asymmetries is not large, between 1 and 2σ. Together they can be however quite powerful. We analyze the effect

of the observables Eqs. (5.91)–(5.93) quantitatively in Fig. 5.6, where we exclude them from the fit.

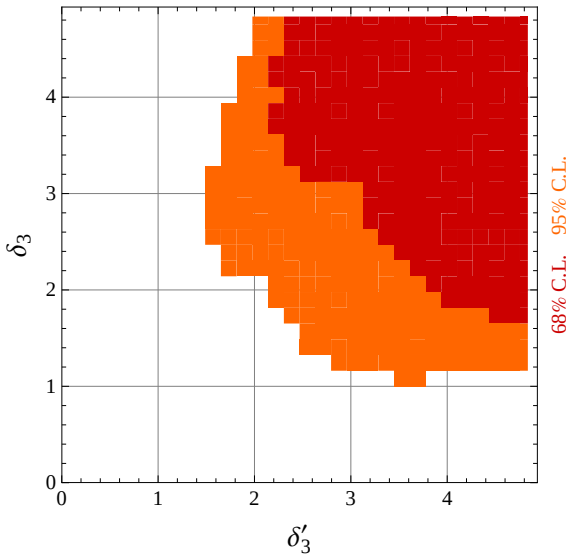

Figure 5.6.: Regions in the δ_3'-δ_3 plane that are allowed at 68% (red) and 95% (orange) C.L. excluding the observables $A_{CP}(D^0 \to K_S K_S)$, $A_{CP}(D_s \to K_S \pi^+)$ and $A_{CP}(D_s \to K^+ \pi^0)$ from the fit. No assumption on $\delta_X^{(\prime)}$ is made. Figure taken from [175].

In this configuration a penguin enhancement of $\delta_3^{(\prime)} \sim 3$ becomes allowed at 68% C.L. This is still a very large value but a bit more sensible from the SM perspective. Furthermore, it is in agreement with previous U-spin analyses [444, 447]. In these works only a smaller subset of observables is taken into account. In particular the ones excluded from the fit shown in Fig. 5.6 have not been considered as well. In order to study how the triplet enhancement depends in detail on the measured value of $\Delta a_{CP}^{\text{dir}}$, we show in Fig. 5.7(a) its correlation with δ_3 when its measurement is taken out of the fit. Here, we include also an overall constraint on the SU(3)$_F$ breaking $\delta_X^{(\prime)} \leq 50\%$. Even in the hypothetical case $\Delta a_{CP}^{\text{dir}} = 0$ the other largish CP asymmetries lead to a penguin enhancement. This points out impressively the need for a more precise measurement of all CP asymmetries.

In Fig. 5.7(b) we also show δ_3 if one additionally excludes the CP asymmetries $A_{CP}(D^0 \to K_S K_S)$, $A_{CP}(D_s \to K_S \pi^+)$ and $A_{CP}(D_s \to K^+ \pi^0)$ from the fit. Then, only $\Delta a_{CP}^{\text{dir}}$ determines the needed value of δ_3 directly. This leads to the coincidence of 68% and 95% C.L. regions and as expected, both triplet matrix elements are allowed to vanish for $\Delta a_{CP}^{\text{dir}} = 0$.

One could ask the question if the 68% C.L. triplet enhancement results perhaps from an intriguing sign combination of the observables in Eqs. (5.91) to (5.93).[3] In order to inspect this issue we show in Fig. 5.8 the correlation of δ_3 and δ_3' in a fictitious scenario where $A_{CP}(D^0 \to K_S K_S) = +0.23 \pm 0.19$, *i.e.*, where the CP asymmetry has a flipped sign. As can be seen, such a sign flip does not have a high impact on the requisite penguin enhancement. The difference between Figs. 5.8 and 5.5 is completely negligible. The explanation lies in the plenty hadronic matrix elements in the SU(3)$_F$ breaking where much freedom exists for an absorption of phases. Consequently, only the absolute value of $A_{CP}(D^0 \to K_S K_S)$ is crucial for the size of $\delta_3^{(\prime)}$.

[3] We thank T. Feldmann and A. Khodjamirian for a useful discussion about this possibility.

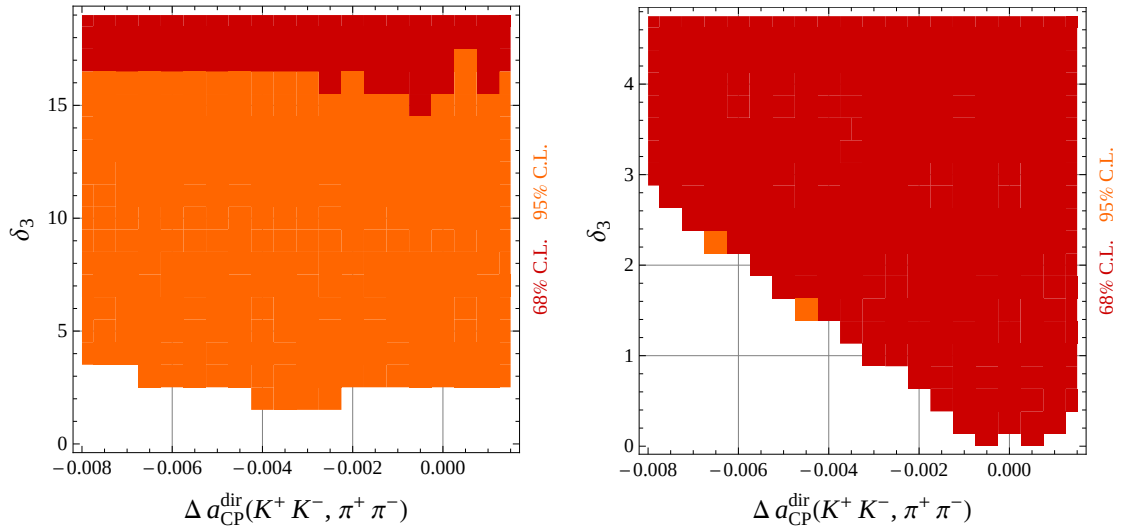

(a) All data.

(b) Excluding $A_{CP}(D^0 \to K_S K_S)$, $A_{CP}(D_s \to K_S\pi^+)$ and $D_s \to K^+\pi^0$.

Figure 5.7.: Penguin enhancement δ_3 against possible values of $\Delta a_{CP}^{\mathrm{dir}}$ (excluding its measurement from the fit) that are allowed at 68% (red) and 95% (orange) C.L., including an overall bound of $\delta_X^{(\prime)} \leq 50\%$.

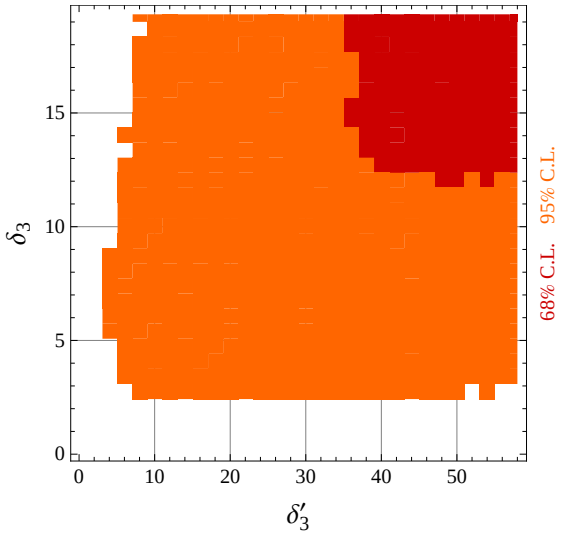

Figure 5.8.: Regions in the δ_3'-δ_3 plane that are allowed at 68% (red) and 95% (orange) C.L. with hypothetical data $A_{CP}(D^0 \to K_S K_S) = +0.23 \pm 0.19$ (flipped sign in comparison with Table 5.1).

5.4.4. Can we Differentiate the SM from Patterns of NP?

In the literature, there are many different possible NP models to explain the measured $\Delta a_{CP}^{\text{dir}}$ [177, 459, 470–473]. In order to incorporate NP models into our ansatz, we have to analyze their SU(3)$_F$ structure. In the SU(3)$_F$ approach the Dirac structure does not appear explicitly any more. Its information only goes into the counting of representations as additional degrees of freedom. For example there may appear representations $\mathbf{15}^{\text{NP}}$ from scalar operators in addition to the SM **15**, the matrix elements of which are independent. The questions is then: Can we recognize traces of the characteristic SU(3)$_F$ structures of specific NP models in correlations and patterns of branching ratios and CP asymmetries of different channels? This is analyzed in the following paragraphs. In order to stay in the physical part of the parameter space we constrain the SU(3)$_F$ breaking as $\delta_X^{(\prime)} \leq 50\%$.

Characteristic SU(3)$_F$ Structures The flavor structure of the SU(3)$_F$ limit SM-Hamiltonian has been given in Eqs. (5.40)-(5.42). The SCS part is schematically given as

$$\mathcal{H}_{\text{SM}}^{\text{SCS}} \sim \underbrace{\lambda(\mathbf{15} + \bar{\mathbf{6}})}_{\mathcal{H}_\Sigma^{\text{SCS}}} + \underbrace{\Delta(\mathbf{15} + \mathbf{3})}_{\mathcal{H}_{\Delta,\text{SM}}^{\text{SCS}}} . \tag{5.94}$$

As discussed in Sec. 5.2, the matrix elements of the operators in $\mathcal{H}_\Sigma^{\text{SCS}}$ are fixed in the fit by the branching ratios whereas the matrix elements of the operators in $\mathcal{H}_\Delta^{\text{SCS}}$ induce CP violation. We consider three specific NP models which have a different flavor structure in the $\mathcal{H}_\Delta^{\text{SCS}}$ part of the Hamiltonian, *i.e.*, we replace $\mathcal{H}_{\Delta,\text{SM}}^{\text{SCS}}$ by different $\mathcal{H}_{\Delta,\text{NP}}^{\text{SCS}}$. We keep the $\mathcal{H}_\Sigma^{\text{SCS}}$ part as well as the Hamiltonians for the CF and DCS decays and study how different representations in $\mathcal{H}_{\Delta,\text{NP}}^{\text{SCS}}$ for distinct NP models change possible resulting patterns of CP asymmetries.
Note that the Wilson coefficients of the operators in the Hamiltonian cannot be disentangled from the hadronic matrix elements in the SU(3)$_F$ approach as they come in products of each other only. This is valid both for the SM and NP models. Consequently, we absorb the Wilson coefficients into the hadronic matrix elements. Furthermore, we are not sensitive to an absolute NP weak phase $\Delta_{\text{NP}} \neq \Delta$ as such can also be absorbed into the unknown NP matrix elements. We choose therefore to have the same overall normalization as in the SM and set $\Delta_{\text{NP}} = \Delta$.

Specifically, we look at the following NP models:

- **"Triplet model"**
  In the triplet model, we replace $\mathcal{H}_{\Delta,\text{SM}}^{\text{SCS}}$ by a pure triplet operator, *i.e.*, by

$$\mathcal{H}_3^{\text{SCS}} = \Delta \sqrt{\frac{3}{2}} \mathbf{3}_{\frac{1}{2},\frac{1}{2},\frac{1}{3}}^{\text{NP}} \sim (\bar{u}c) \sum \bar{q}q \, . \tag{5.95}$$

  Such operators can arise from an enhancement of the chromomagnetic dipole operator or QCD penguin operators in SUSY [177, 470, 471] or models with extra

dimensions [472]. In contrast to the SM, in the triplet model there is no **15** representation in $\mathcal{H}_\Delta^{\text{SCS}}$. However, as in the SM the matrix elements with the **15** are already fixed by the branching ratios, their contribution to CP violation is negligible. Therefore, using nonleptonic charm decays we are not able to disentangle the triplet model from the SM. Nevertheless, this is possible by taking into account radiative D decays [474].

- **"Hochberg-Nir (HN) model"**
  The HN model is a specific Two-Higgs doublet model (2HDM) that connects charm and top physics [473]. It gives rise to the operator

$$\mathcal{H}_{3+15}^{\text{SCS}} = \Delta\left(\mathbf{15}^{\text{NP}}_{\frac{3}{2},\frac{1}{2},\frac{1}{3}} + \frac{1}{\sqrt{2}}\mathbf{15}^{\text{NP}}_{\frac{1}{2},\frac{1}{2},\frac{1}{3}} + \sqrt{\frac{3}{2}}\mathbf{3}^{\text{NP}}_{\frac{1}{2},\frac{1}{2},\frac{1}{3}}\right) \sim (\bar{u}c)(\bar{u}u). \tag{5.96}$$

  The HN model shares with the SM the feature that $\mathcal{H}_\Delta^{\text{SCS}}$ contains the representations **3** + **15** only. However, in case of the SM, the same representations are also contained in $\mathcal{H}_\Sigma^{\text{SCS}}$. This is not true for the HN model, due to the different Dirac structure of the scalar operator $(\bar{u}_R c_L)(\bar{u}_L u_R)$. Especially, the HN model is the only model considered here which contains two independent $\Delta I = 3/2$ operators coming with a relative weak phase: $\mathbf{15}_{\frac{3}{2},\frac{1}{2},\frac{1}{3}}$ and $\mathbf{15}^{\text{NP}}_{\frac{3}{2},\frac{1}{2},\frac{1}{3}}$.

- **"ΔU = 1 model"** The $\Delta U = 1$ model breaks the discrete U-spin symmetry of the Hamiltonian at the operator level by

$$\mathcal{H}_{3+\bar{6}+15}^{\text{SCS}} = \Delta\left(\sqrt{\frac{3}{2}}\mathbf{15}^{\text{NP}}_{\frac{1}{2},\frac{1}{2},\frac{1}{3}} - \bar{\mathbf{6}}^{\text{NP}}_{\frac{1}{2},\frac{1}{2},\frac{1}{3}} - \sqrt{\frac{3}{2}}\mathbf{3}^{\text{NP}}_{\frac{1}{2},\frac{1}{2},\frac{1}{3}}\right) \sim (\bar{s}c)(\bar{u}s)\,, \tag{5.97}$$

  without a corresponding operator $(\bar{d}c)(\bar{u}d)$ being present. It is realized, *e.g.*, in 2HDMs or color octet models, see Ref. [459]. In addition to the **3** and **15** representations there is also a $\bar{\mathbf{6}}$ present in Eq. (5.97).

Note that the relative factors of the representations in Eqs. (5.95)–(5.97) come from the Clebsch-Gordan coefficients of the tensor products. The overall normalization is chosen such that the prefactor of the **3** matrix element has the same absolute value as in the SM Hamiltonian in Eq. (5.41). The resulting Clebsch-Gordan coefficients of the matrix elements of the NP Hamiltonians with the final and initial states of the different decay channels are given in Table 5.8. From the distinct $\text{SU}(3)_F$ decompositions of the models we can already draw several phenomenological conclusions.

Decay d	$\tilde{\Delta}\left(A_{27}^{15}\right)^{\rm NP}$	$\tilde{\Delta}\left(A_{8}^{15}\right)^{\rm NP}$	$\tilde{\Delta}\left(A_{8}^{\bar{6}}\right)^{\rm NP}$	$\tilde{\Delta}\left(A_{1}^{3}\right)^{\rm NP}$	$\tilde{\Delta}\left(A_{8}^{3}\right)^{\rm NP}$
SCS, Triplet model					
$D^0 \to K^+K^-$	0	0	0	$-\frac{1}{2\sqrt{2}}$	$-\frac{1}{\sqrt{10}}$
$D^0 \to \pi^+\pi^-$	0	0	0	$-\frac{1}{2\sqrt{2}}$	$-\frac{1}{\sqrt{10}}$
$D^0 \to \bar{K}^0K^0$	0	0	0	$\frac{1}{2\sqrt{2}}$	$-\sqrt{\frac{2}{5}}$
$D^0 \to \pi^0\pi^0$	0	0	0	$\frac{1}{4}$	$\frac{1}{2\sqrt{5}}$
$D^+ \to \pi^0\pi^+$	0	0	0	0	0
$D^+ \to \bar{K}^0K^+$	0	0	0	0	$-\frac{3}{\sqrt{10}}$
$D_s \to K^0\pi^+$	0	0	0	0	$-\frac{3}{\sqrt{10}}$
$D_s \to K^+\pi^0$	0	0	0	0	$\frac{3}{2\sqrt{5}}$
SCS, HN model					
$D^0 \to K^+K^-$	$\frac{3\sqrt{\frac{3}{2}}}{10}$	$\frac{\sqrt{\frac{3}{2}}}{5}$	0	$-\frac{1}{2\sqrt{2}}$	$-\frac{1}{\sqrt{10}}$
$D^0 \to \pi^+\pi^-$	$\frac{3\sqrt{\frac{3}{2}}}{10}$	$\frac{\sqrt{\frac{3}{2}}}{5}$	0	$-\frac{1}{2\sqrt{2}}$	$-\frac{1}{\sqrt{10}}$
$D^0 \to \bar{K}^0K^0$	$\frac{\sqrt{\frac{3}{2}}}{10}$	$\frac{\sqrt{6}}{5}$	0	$\frac{1}{2\sqrt{2}}$	$-\sqrt{\frac{2}{5}}$
$D^0 \to \pi^0\pi^0$	$\frac{7\sqrt{3}}{20}$	$-\frac{\sqrt{3}}{10}$	0	$\frac{1}{4}$	$\frac{1}{2\sqrt{5}}$
$D^+ \to \pi^0\pi^+$	$\frac{\sqrt{3}}{2}$	0	0	0	0
$D^+ \to \bar{K}^0K^+$	$\frac{\sqrt{\frac{3}{2}}}{5}$	$-\frac{\sqrt{\frac{3}{2}}}{5}$	0	0	$-\frac{3}{\sqrt{10}}$
$D_s \to K^0\pi^+$	$\frac{\sqrt{\frac{3}{2}}}{5}$	$-\frac{\sqrt{\frac{3}{2}}}{5}$	0	0	$-\frac{3}{\sqrt{10}}$
$D_s \to K^+\pi^0$	$\frac{2\sqrt{3}}{5}$	$\frac{\sqrt{3}}{10}$	0	0	$\frac{3}{2\sqrt{5}}$
SCS, $\Delta U = 1$ model					
$D^0 \to K^+K^-$	$\frac{7}{10\sqrt{2}}$	$-\frac{1}{5\sqrt{2}}$	$\frac{1}{\sqrt{5}}$	$\frac{1}{2\sqrt{2}}$	$\frac{1}{\sqrt{10}}$
$D^0 \to \pi^+\pi^-$	$-\frac{1}{10\sqrt{2}}$	$\frac{3}{5\sqrt{2}}$	$-\frac{1}{\sqrt{5}}$	$\frac{1}{2\sqrt{2}}$	$\frac{1}{\sqrt{10}}$
$D^0 \to \bar{K}^0K^0$	$\frac{1}{10\sqrt{2}}$	$\frac{\sqrt{2}}{5}$	0	$-\frac{1}{2\sqrt{2}}$	$\sqrt{\frac{2}{5}}$
$D^0 \to \pi^0\pi^0$	$\frac{1}{20}$	$-\frac{3}{10}$	$\frac{1}{\sqrt{10}}$	$-\frac{1}{4}$	$-\frac{1}{2\sqrt{5}}$
$D^+ \to \pi^0\pi^+$	0	0	0	0	0
$D^+ \to \bar{K}^0K^+$	$\frac{2\sqrt{2}}{5}$	$\frac{1}{5\sqrt{2}}$	$\frac{1}{\sqrt{5}}$	0	$\frac{3}{\sqrt{10}}$
$D_s \to K^0\pi^+$	$-\frac{\sqrt{2}}{5}$	$-\frac{3}{5\sqrt{2}}$	$-\frac{1}{\sqrt{5}}$	0	$\frac{3}{\sqrt{10}}$
$D_s \to K^+\pi^0$	$\frac{1}{5}$	$\frac{3}{10}$	$\frac{1}{\sqrt{10}}$	0	$-\frac{3}{2\sqrt{5}}$

Table 5.8.: Clebsch-Gordan coefficients of the considered NP models, see text for details.

- $a_{CP}^{\text{dir}}(D^+ \to \pi^+\pi^0) \neq 0$ **as a smoking gun for the HN model /**$\Delta I = 3/2$ **NP**
  In the SM, the triplet model and the $\Delta U = 1$ model, all matrix elements in the $\Delta I = 3/2$ transition $D^+ \to \pi^+\pi^0$ come with the same weak phase. In fact, in these models there is only one $\text{SU}(3)_F$ limit matrix element which contributes to $\mathcal{A}_0(D^+ \to \pi^+\pi^0)$, the A_{27}^{15}. It follows that in these models $a_{\text{CP}}^{\text{dir}}(D^+ \to \pi^+\pi^0) = 0$ [467, 475]. In the HN model on the other hand, besides the A_{27}^{15} there contributes the $\left(A_{27}^{15}\right)^{\text{NP}}$, which comes with a relative weak phase. This induces $a_{\text{CP}}^{\text{dir}}(D^+ \to \pi^+\pi^0) \neq 0$ as a smoking gun for the HN model, see also [467]. Currently, the experimental status is $a_{\text{CP}}^{\text{dir}}(D^+ \to \pi^+\pi^0) \neq 0$ at 1σ, see Table 5.1. In the future it is consequently very important to measure this observable with greater precision.

- **U-spin breaking by the** $\Delta U = 1$ **model**
  The breaking of the discrete U-spin symmetry at the operator level by the $\Delta U = 1$ model is reflected by the Clebsch-Gordan coefficients in Table 5.8. In the SM, the high symmetry of the Clebsch-Gordan coefficients for $D^0 \to K^+K^-$, $D^0 \to \pi^+\pi^-$ and $D^+ \to \bar{K}^0K^+$, $D_s \to K^0\pi^+$ lead to the $\text{SU}(3)_F$ limit relations Eqs. (5.51) and (5.52), respectively. From these follow the approximate relations Eqs. (5.55) and (5.56). These sum rules are broken already in the SM by the $\text{SU}(3)_F$-breaking contributions. However, in the $\Delta U = 1$ model they are broken even beyond that at $O(1)$ by the $\text{SU}(3)_F$ limit matrix elements.

- **Enhancement of** $a_{CP}^{\text{dir}}(D^0 \to K_SK_S)$ **in all considered models**
  A general prediction of all considered models including the SM is the enhancement of the CP asymmetry of $D^0 \to K_SK_S$ decays. The reason is that their $\text{SU}(3)_F$ limit contribution is CKM suppressed by Δ and the CKM leading contribution $\propto \Sigma$ arises only with $\text{SU}(3)_F$ breaking. Consequently, $a_{CP}^{\text{dir}}(D^0 \to K_SK_S) \sim O\left(\tilde{\Delta}/\delta_X^{(\prime)}\right)$. The enhancement of $a_{CP}^{\text{dir}}(D^0 \to K_SK_S)$ agrees with similar findings obtained without the context of the $\text{SU}(3)_F$ language [476]. There, also additional decays with vector final states are listed which have similar properties.

With present data and the current theoretical knowledge of $\text{SU}(3)_F$ breaking in nonleptonic charm decays no clear separation of the different NP models is possible. The global minima of all models (including a global bound of $\delta_X^{(\prime)} \leq 50\%$) have $\chi^2_{\text{min}} \sim 1$, except for the HN model which has $\chi^2_{\text{min}} \sim 0$ because it is the only one that can fit the mentioned 1σ measurement of $a_{CP}^{\text{dir}}(D^+ \to \pi^0\pi^+)$. In the next paragraph we analyze if and how one could make progress in the future in order to find out which model is realized.

Consequences of future theoretical and experimental progress In the future, there are in principle two ways in order to make progress. On the one hand, in the future we could gain new theoretical insights in the strong dynamics, especially in the $\text{SU}(3)_F$ breaking where most of the unknown fit parameters stem from. On the other hand, significantly improved data is definitely desirable. For a proof of principle we have designed two benchmark scenarios in order to clarify how far one can get with progress in either of these two directions.

Firstly, let us assume there is an improvement on the theoretical understanding of SU(3)$_F$ breaking without having better data. This could lead for example to the knowledge that only three matrix elements dominate the SU(3)$_F$ breaking. Let us assume for concreteness that these matrix elements are B_1^3, $B_8^{15_2}$ and $B_{27}^{24_1}$ which we know to give a good fit, see Sec. 5.4.2. Including $\delta_X^{(\prime)} \leq 50\%$ we obtain at the best fit points:

$$\begin{aligned}
\chi^2/dof &= 10/10 && \text{(MFV/SM)},\\
\chi^2/dof &= 10/10 && \text{(triplet model)},\\
\chi^2/dof &= 3.2/6 && \text{(HN model)},\\
\chi^2/dof &= 5.4/4 && (\Delta U = 1 \text{ model}).
\end{aligned}$$

As we show in Fig. 5.9, in the triplet model we get in this scenario a correlation between $a_{CP}^{\rm dir}(D^0 \to \pi^0\pi^0)$ and $\Sigma a_{CP}^{\rm dir}(K^+K^-, \pi^+\pi^-)$. The HN and $\Delta U = 1$ model have a quite large number of parameters so that the observables are essentially uncorrelated. The fit mainly just fills the experimentally allowed region for these models.

We can therefore infer that a better understanding of the charm hadronic matrix elements would be of great advantage especially in order to resolve the triplet model from the other ones. Without such further theoretical insights we can only make progress by improving significantly on the precision of the measurements of several direct CP asymmetries. In order to inspect the chances from such an improvement we have designed a future data scenario inside the 2σ region of current data. The assumptions of this scenario are listed in the Table besides Fig. 5.10.

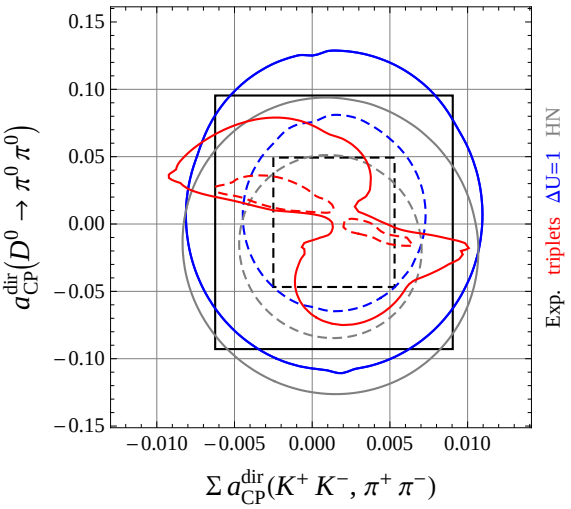

Figure 5.9.: Future *theoretical* improvement: Correlation of observables in NP models at 95% (solid) and 68% (dashed) C.L. with current data and SU(3)$_F$ breaking only from B_1^3, $B_8^{15_2}$ and $B_{27}^{24_1}$ with an upper bound of $\delta_X^{(\prime)} \leq 50\%$. Figure taken from [175].

We assume here that the statistical error of $\Delta a_{CP}^{\rm dir}$ gets so small that it is negligible compared to the systematic one. In addition, we assume the latter to improve by a factor two in comparison to the value that is quoted in [60]. The same uncertainty is also assumed for the CP asymmetries $a_{CP}^{\rm dir}(D^+ \to K_S K^+)$, $a_{CP}^{\rm dir}(D_s \to K_S\pi^+)$ and $a_{CP}^{\rm dir}(D_s \to K^+\pi^0)$. In the triplet model (and analogously in the SM), the latter three CP asymmetries play a special role, because for them the Clebsch-Gordan coefficient in front of the $\left(A_1^3\right)^{\rm NP}$ vanishes. Therefore, these CP asymmetries are controlled by one common parameter only, $\left(B_8^3\right)^{\rm NP}$,

see Table 5.8. For the triplet model it is consequently difficult to create hierarchies in these CP asymmetries. In order to challenge the triplet model we assume for this very reason that $a_{CP}^{\rm dir}(D^+ \to K_S K^+)$, $a_{CP}^{\rm dir}(D_s \to K_S \pi^+)$ are smallish and that $a_{CP}^{\rm dir}(D_s \to K^+\pi^0)$ stays at a large value. The values for $\Delta a_{CP}^{\rm dir}$ and $\Sigma a_{CP}^{\rm dir}(K^+K^-, \pi^+\pi^-)$ are chosen such that $a_{CP}^{\rm dir}(D^0 \to K^+K^-) = -0.0065$ and $a_{CP}^{\rm dir}(D^0 \to \pi^+\pi^-) = 0.0005$, indicating NP from the $(\bar{s}c)(\bar{u}s)$ operator of the $\Delta U = 1$ model. For the same reason $a_{CP}^{\rm dir}(D^+ \to K_S K^+)$ is taken to be larger than currently measured, but not of the same order of magnitude as $D_s \to K^+\pi^0$. Finally, the future error of the strong phase between $\mathcal{A}(D^0 \to K^-\pi^+)$ and $\mathcal{A}(D^0 \to K^+\pi^-)$ is set to the value stated in [477].

On the right-hand side in Fig. 5.10 we show a correlation plot of the observables $a_{CP}^{\rm dir}(D^0 \to \pi^0\pi^0)$ and $\Sigma a_{CP}^{\rm dir}(K^+K^-, \pi^+\pi^-)$ that corresponds to the future data set. No theoretical progress is assumed so that in our comprehensive picture of $\mathrm{SU}(3)_F$ breaking all matrix elements are taken into account. In the future scenario we predict sizable CP violation in the channel $D^0 \to \pi^0\pi^0$ in the triplet model. $a_{CP}^{\rm dir}(D^0 \to \pi^0\pi^0) = 0$ is disfavored, unlike in the other models. This shows that with an improvement in data one could potentially disentangle the triplet model, including the SM, from other NP models.

Observable	Future data
SCS CP asymmetries	
$\Delta a_{CP}^{\rm dir}(K^+K^-, \pi^+\pi^-)$	-0.007 ± 0.0005
$\Sigma a_{CP}^{\rm dir}(K^+K^-, \pi^+\pi^-)$	-0.006 ± 0.0007
$a_{CP}^{\rm dir}(D^+ \to K_S K^+)$	-0.003 ± 0.0005
$a_{CP}^{\rm dir}(D_s \to K_S \pi^+)$	0.0 ± 0.0005
$a_{CP}^{\rm dir}(D_s \to K^+\pi^0)$	0.05 ± 0.0005
$K^+\pi^-$ strong phase difference	
$\delta_{K\pi}$	$21.4^\circ \pm 3.8^\circ$

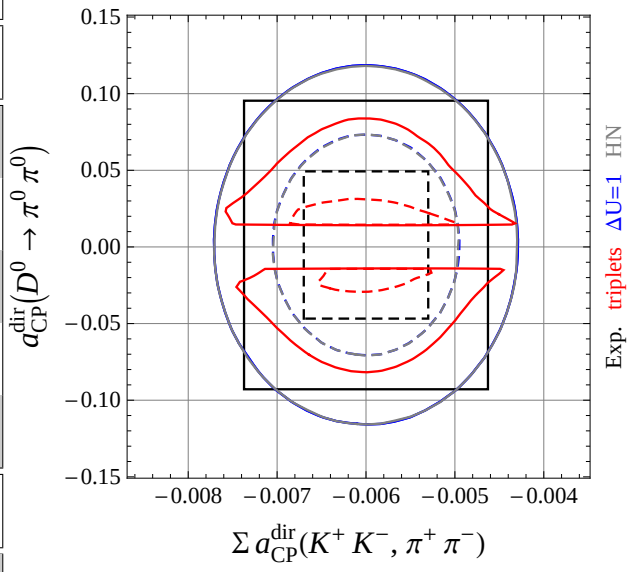

Figure 5.10.: Future *experimental* improvement. Left: Future measurements used for the plot on the right-hand side. All other measurements are taken as in Tables 5.1, 5.2 and 5.3, see text for details. Right: Correlation of observables in NP models at 95% (solid) and 68% (dashed) C.L. in the future data scenario, taking all $\mathrm{SU}(3)_F$-breaking matrix elements into account with an upper bound of $\delta_X^{(\prime)} \leq 50\%$. Note that the curves of the $\Delta U = 1$ and HN model lie on top of each other. Table and Figure taken from [175].

5.5. The Situation after Moriond 2013

At the Moriond conference 2013 new results from LHCb on charm CP violation have been presented. The difference of CP asymmetries $\Delta A_{CP} = A_{CP}(D^0 \to K^+K^-) - A_{CP}(D^0 \to \pi^+\pi^-)$ has been measured for the first time in two different decay channels. The analysis of the D^* channel has been updated [64] and supersedes the former LHCb result [60]. Furthermore, an analysis of the semileptonic B channel has been presented [65]. The results of the separate channels are given as

$$\Delta A_{CP} = -0.0034 \pm 0.0018 \quad \text{(LHCb, } D^* \text{ decay channel [64])}, \tag{5.98}$$

$$\Delta A_{CP} = 0.0049 \pm 0.0033 \quad \text{(LHCb, semileptonic } B \text{ decay channel [65])}, \tag{5.99}$$

where we added statistical and systematic errors quadratically. Between the two results Eqs. (5.98) and (5.99) lies a tension of 2.2σ [65]. This comes from the semileptonic B channel having the opposite sign as the D^* channel. The negative sign of ΔA_{CP} agrees with CDF [61] and Belle [62]. The experimental situation has to be settled in the future. Including Eqs. (5.98) and (5.99) we calculate new world averages for $\Delta a_{CP}^{\text{dir}}$ and $\Sigma\, a_{CP}^{\text{dir}}$. For the latter, our numerical result is not changed compared to Table 5.1. Our result $\Delta a_{CP}^{\text{dir}} = -0.0032 \pm 0.0012$ [469] agrees with the new HFAG world average [63]

$$\Delta a_{CP}^{\text{dir}} = -0.00329 \pm 0.00121 \quad \text{(HFAG, online update March 2013)}. \tag{5.100}$$

The result is 2.7σ away from zero. The new HFAG world average for the indirect CP violation a_{CP}^{ind} is given as [63]

$$a_{CP}^{\text{ind}} = -0.00010 \pm 0.00162 \quad \text{(HFAG, online update March 2013)}. \tag{5.101}$$

The new measurements of LHCb also have consequences for the global fit of D mixing. This affects the strong phase difference of $\mathcal{A}(D^0 \to K^+\pi^-)$ and $\mathcal{A}(D^0 \to K^-\pi^+)$ [63]

$$\delta_{K\pi} = (19.5^{+8.6}_{-11.1})^\circ \quad \text{(HFAG, online update April 2013)}. \tag{5.102}$$

Symmetrizing the uncertainties in Eq. (5.102) we arrive at [469]

$$\delta_{K\pi} = (18.25 \pm 9.85)^\circ \quad \text{(our symmetrization of errors in Eq. (5.102))}. \tag{5.103}$$

Besides ΔA_{CP} after Moriond 2013 LHCb has furthermore measured [478]

$$A_{CP}(D_s \to K_S\pi^+) = 0.0061 \pm 0.0084 \quad \text{(LHCb March 2013)}, \tag{5.104}$$

where we added again statistical and systematic errors quadratically. We obtain as new world average the value [469]

$$A_{CP}(D_s \to K_S\pi^+) = 0.012 \pm 0.007 \quad \text{(our world average)}. \tag{5.105}$$

We summarize all updates in Table 5.9.

Observable	Measurement	References
$\Delta a_{CP}^{\text{dir}}(K^+K^-, \pi^+\pi^-)$	-0.00329 ± 0.00121	[a][63], [60–62, 64, 65, 448, 449]
a_{CP}^{ind}	-0.00010 ± 0.00162	[a][63]
$A_{CP}(D_s \to K_S\pi^+)$	0.012 ± 0.007	[b][452, 455, 457, 478]
$\delta_{K\pi}$	$(18.25 \pm 9.85)^\circ$	[c][63]

Table 5.9.: Updates of charm observable measurements as of May 2013. All other data as in Tables 5.1, 5.2 and 5.3. Table taken from [469].
[a]online update March 2013.
[b]our average.
[c]online update April 2013, our symmetrization of uncertainties.

The general dependence of our analysis on the measurement of $\Delta a_{CP}^{\text{dir}}$ was discussed in Sec. 5.4.3 and is illustrated in Fig. 5.7. In order to demonstrate the impact of the new experimental results we show in Fig. 5.11 the fit of the triplet enhancement in the δ_3'–δ_3 plane including the updates in Table 5.9. In Figs. 5.11(a) and 5.11(b) we use the complete data set, while in Fig. 5.11(c) we exclude $A_{CP}(D^0 \to K_S K_S)$, $A_{CP}(D_s \to K_S\pi^+)$ and $A_{CP}(D_s \to K^+\pi^0)$ from the fit. Fig. 5.11(b) shows a detail from Fig. 5.11(a) with higher resolution for smaller $\delta_3^{(\prime)}$ values. At the best fit points we have for the full data set and the one without $A_{CP}(D^0 \to K_S K_S)$, $A_{CP}(D_s \to K_S\pi^+)$ and $A_{CP}(D_s \to K^+\pi^0)$ still $\chi^2 \sim 1$ due to the 1σ contribution from $A_{CP}(D^+ \to \pi^0\pi^+)$.

In Figs. 5.11(a) and 5.11(b) we observe that including the updates in Table 5.9 after Moriond 2013 still a penguin enhancement is needed. At 95% C.L. $\delta_3^{(\prime)} \gtrsim 1$, as opposed to the naive analysis. At 68% C.L. the triplet matrix elements need to be even larger. Excluding the CP asymmetries with largish measured central values from the fit, as shown in Fig. 5.11(c), $\delta_3^{(\prime)} < 1$ becomes allowed at 95% C.L., while however at 68% C.L. still $\delta_3^{(\prime)} \gtrsim 1$ is necessary.

This highlights the importance of the precise measurement of $A_{CP}(D^0 \to K_S K_S)$, $A_{CP}(D_s \to K_S\pi^+)$ and $A_{CP}(D_s \to K^+\pi^0)$ in the future.

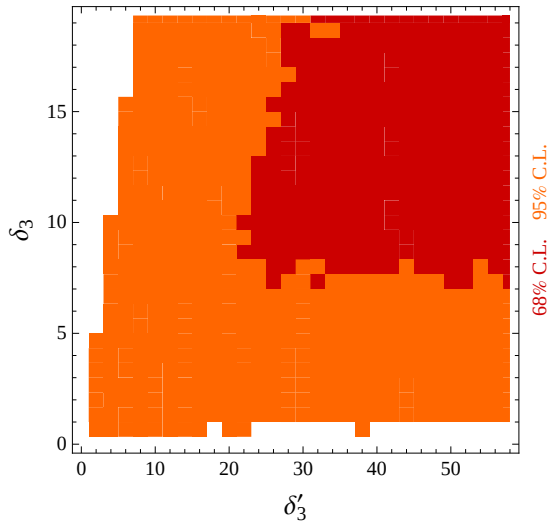

(a) All data.

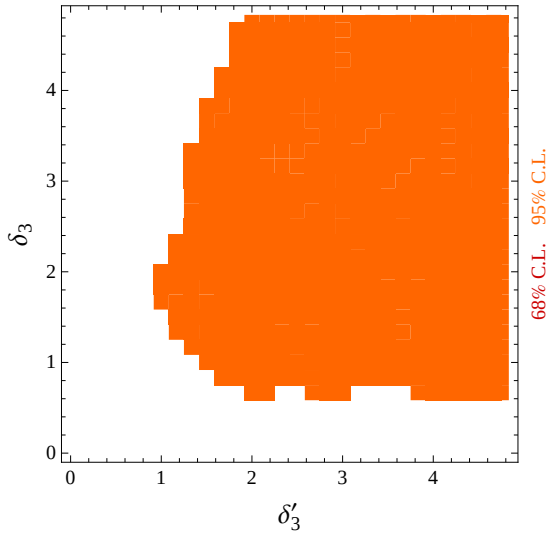

(b) All data, zoom.

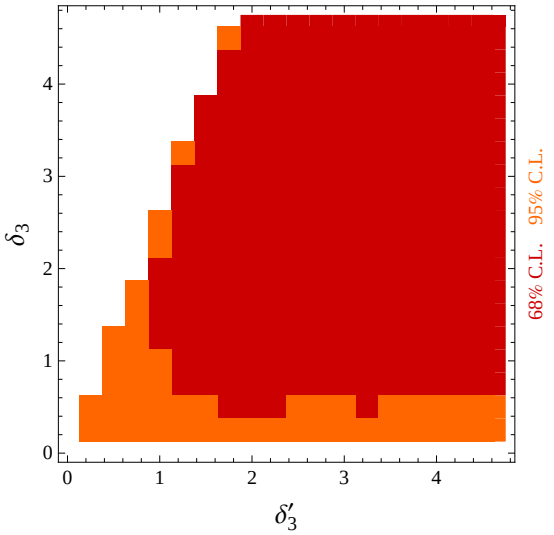

(c) Excluding the observables $A_{CP}(D^0 \to K_S K_S)$, $A_{CP}(D_s \to K_S \pi^+)$ and $A_{CP}(D_s \to K^+ \pi^0)$ from the fit.

Figure 5.11.: Regions in the δ_3'-δ_3 plane that are allowed at 68% (red) and 95% (orange) C.L. including the updates of charm measurements after Moriond 2013 as given in Table 5.9, see text for details. Plots taken from [469].

6. Traces of QCD Factorization in the $SU(3)_F$ Anatomy of $D \to P_8 P_8$

As we learned in Ch. 5, in the pure $SU(3)_F$ symmetry ansatz including linear breaking the SM cannot be distinguished from NP models with present data. In this chapter we look for traces of QCDF [310–312] in charm decays, *i.e.*, relics of the limit $m_c \to \infty$. For previous works discussing QCDF and the $1/m_c$ expansion in the context of the U-spin and $SU(3)_F$ symmetry see *e.g.* [177, 440, 447, 479, 480]. Here, we look for the first time at QCDF in view of comprehensively broken $SU(3)_F$ [469], not relying however on quantitative aspects of QCDF calculations but using sum rules that we derive in Sec. 6.2. As a motivation we compare in Sec. 6.1 QCDF results for the branching ratios in the strict heavy-quark limit to data. The results show that in color-allowed tree dominated channels the QCDF-description is working reasonably well. This leads us to the hypothesis that some information from the $1/m_c$ expansion could be used in the framework of $SU(3)_F$ to assist fits to the data.
We augment therefore the pure $SU(3)_F$ approach from Ch. 5 by reasonable input taken from the general structure of the QCDF expressions only. This helps us to eliminate breaking matrix elements and can sharpen considerably the predictions of the $SU(3)_F$ framework. Parts of the results presented in this chapter are planned to be published in [469].

6.1. QCDF Approach to nonleptonic Charm Decays

QCDF Parametrizations for $D \to P_8 P_8$ In the QCDF framework we can write the amplitudes of $D \to PP$ decays as [177, 310, 312]

$$\langle P_1 P_2 | \mathcal{H}_{\text{eff}} | D \rangle = \langle P_1 P_2 | \mathcal{T}_A + \mathcal{T}_B | D \rangle \,, \tag{6.1}$$

where $\mathcal{T}_A$ contains the contributions where a spectator quark goes into one of the final state mesons and $\mathcal{T}_B$ contains additional annihilation contributions. The different contributions to $\mathcal{T}_A$ can be written as products of form factors, decay constants and kernels that are parametrized by coefficients a_i. The same structure is valid for the annihilation part with corresponding coefficients b_i. The expressions for these coefficients are given in [310–312]. The a_i are composed as [311]

$$a_i^{M_1 M_2} = a_{i,I}^{M_1 M_2} + a_{i,II}^{M_1 M_2}. \tag{6.2}$$

The superscript denotes the dependence on the final state mesons M_1 and M_2. The convention is such that the meson M_1 is the meson that contains the spectator quark [311]. The $a_{i,I}^{M_1M_2}$ contain the naive factorization term and additionally the vertex and penguin corrections. The $a_{i,II}^{M_1M_2}$ comprise in addition to this the hard spectator interaction contributions.

For the physical interpretation, it is instructive to relate the QCDF expressions to topological amplitudes [442],

$$T = i\frac{G_F}{\sqrt{2}} a_1^{M_1M_2} f_{P_2}(m_D^2 - m_{P_1}^2) F_0^{DP_1}(m_{P_2}^2)\,, \tag{6.3}$$

$$C = i\frac{G_F}{\sqrt{2}} a_2^{M_1M_2} f_{P_2}(m_D^2 - m_{P_1}^2) F_0^{DP_1}(m_{P_2}^2)\,, \tag{6.4}$$

$$E = i\frac{G_F}{\sqrt{2}} f_D f_{M_1} f_{M_2} (b_1)_q^{M_1M_2}\,, \tag{6.5}$$

$$A = i\frac{G_F}{\sqrt{2}} f_D f_{M_1} f_{M_2} (b_2)_q^{M_1M_2}\,. \tag{6.6}$$

Here, T, C, E and A are the color allowed tree, color suppressed tree, W-exchange and W-annihilation amplitudes, respectively, f_P are the decay constants and F_0^{DP} the form factors. The index q in $(b_i)_q^{M_1M_2}$ denotes the quark flavor that arises from the vacuum in the annihilation contributions. We assume the conservation of isospin, *i.e.*, $(b_i)_u^{M1M2} = (b_i)_d^{M1M2} \equiv (b_i)^{M1M2}$. Corresponding symbolic Feynman diagrams were shown in Fig. 5.3. For the annihilation contributions proportional to $(b_i)_q^{M_1M_2}$ the convention for the final state mesons is such that M_1 contains the antiquark from the weak vertex [311]. The QCDF parameters in the T and C amplitude can be written as

$$a_{1,I}^{M_1M_2} = C_1 + \frac{C_2}{N_c}\left(1 + \frac{C_F\alpha_s}{4\pi} V_{M_2}\right), \qquad a_{2,I}^{M_1M_2} = C_2 + \frac{C_1}{N_c}\left(1 + \frac{C_F\alpha_s}{4\pi} V_{M_1}\right), \tag{6.7}$$

$$a_{1,II}^{M_1M_2} = \frac{C_2}{N_c}\frac{C_F\pi\alpha_s}{N_c} H_{M_2M_1}\,, \qquad a_{2,II}^{M_1M_2} = \frac{C_1}{N_c}\frac{C_F\pi\alpha_s}{N_c} H_{M_1M_2}\,, \tag{6.8}$$

with Wilson coefficients of the tree operators C_1, C_2, $N_c = 3$ and hadronic parameters V_X, H_X as specified in [311].

Taking only into account the T, C, E and A contributions as given in Eqs. (6.3)–(6.6), the QCDF expressions for the $D \to P_8P_8$ system can be written as follows below in Eqs. (6.9)–(6.25) [469]. Technically, we obtain Eqs. (6.9)–(6.25) by inserting Eqs. (6.3)–(6.6) into the expressions given in Table I of [481]. We disregard here terms that are CKM suppressed by $\Delta = -V_{cb}^* V_{ub}/2$, *i.e.*, in the QCDF approach work in the limit $\Delta = 0$. Therefore, no penguin terms are present in our QCDF expressions. However, in the fit to data in Sec. 6.3 penguins are included by means of SU(3)$_F$-matrix elements, see the discussion at the end of Sec. 6.2 below.

We use the notation $b_i^\pi \equiv b_i^{\pi\pi}$ and $b_i^K \equiv b_i^{KK}$. The form factors are approximated as $F_0^{D\pi}(m_K^2) = F_0^{D\pi}(0)$ and $F_0^{DK}(m_\pi^2) = F_0^{DK}(0)$.

Furthermore, we assume that the parameters $a_1^{M_1M_2}$ and $a_2^{M_1M_2}$ are approximately flavor-universal, *i.e.* that the vertex-corrections as well as the hard-scattering contributions do not introduce a significant flavor-dependence. The latter is subject to current investigation [469]. We express the flavor-universality in the notation by leaving out the superscripts of the a_i. In the next paragraph, after Eqs. (6.9)–(6.25), we show that the flavor-nonuniversality induced by the vertex-corrections is numerically negligible.

CF decays

$$\mathcal{A}^{\text{factor}}(D^0 \to K^-\pi^+) = \left(i\frac{G_F}{\sqrt{2}}\right) V_{cs}^* V_{ud} \left(a_1 f_\pi (m_D^2 - m_K^2) F_0^{DK}(0) + f_D f_K f_\pi (b_1)^{\pi K}\right), \tag{6.9}$$

$$\mathcal{A}^{\text{factor}}(D^0 \to \bar{K}^0\pi^0) = \left(i\frac{G_F}{\sqrt{2}}\right) V_{cs}^* V_{ud} \frac{1}{\sqrt{2}} \left(a_2 f_K (m_D^2 - m_\pi^2) F_0^{D\pi}(0) - f_D f_\pi f_K (b_1)^{\pi K}\right), \tag{6.10}$$

$$\mathcal{A}^{\text{factor}}(D^+ \to \bar{K}^0\pi^+) = \left(i\frac{G_F}{\sqrt{2}}\right) V_{cs}^* V_{ud} \left(a_1 f_\pi (m_D^2 - m_K^2) F_0^{DK}(0) + a_2 f_K (m_D^2 - m_\pi^2) F_0^{D\pi}(0)\right), \tag{6.11}$$

$$\mathcal{A}^{\text{factor}}(D_s^+ \to \bar{K}^0 K^+) = \left(i\frac{G_F}{\sqrt{2}}\right) V_{cs}^* V_{ud} \left(a_2 f_K (m_{D_s}^2 - m_K^2) F_0^{D_s K}(0) + f_{D_s} f_K^2 (b_2)_s^K\right). \tag{6.12}$$

SCS decays

$$\mathcal{A}^{\text{factor}}(D^0 \to K^+K^-) = \left(i\frac{G_F}{\sqrt{2}}\right) \Sigma \left(a_1 f_K (m_D^2 - m_K^2) F_0^{DK}(0) + f_D f_K^2 (b_1)^K\right), \tag{6.13}$$

$$\mathcal{A}^{\text{factor}}(D^0 \to \pi^+\pi^-) = -\left(i\frac{G_F}{\sqrt{2}}\right) \Sigma \left(a_1 f_\pi (m_D^2 - m_\pi^2) F_0^{D\pi}(0) + f_D f_\pi^2 (b_1)^\pi\right), \tag{6.14}$$

$$\mathcal{A}^{\text{factor}}(D^0 \to K^0\bar{K}^0) = \left(i\frac{G_F}{\sqrt{2}}\right) f_D f_K^2 \Sigma \left((b_1)^K - (b_1)_s^K\right), \tag{6.15}$$

$$\mathcal{A}^{\text{factor}}(D^0 \to \pi^0\pi^0) = -\left(i\frac{G_F}{\sqrt{2}}\right) \Sigma \frac{1}{\sqrt{2}} \left(a_2 f_\pi (m_D^2 - m_\pi^2) F_0^{D\pi}(0) - f_D f_\pi^2 (b_1)^\pi\right), \tag{6.16}$$

$$\mathcal{A}^{\text{factor}}(D^+ \to \pi^+\pi^0) = -\left(i\frac{G_F}{\sqrt{2}}\right) \Sigma \frac{1}{\sqrt{2}} f_\pi (m_D^2 - m_\pi^2) F_0^{D\pi}(0) \left(a_1 + a_2\right), \tag{6.17}$$

$$\mathcal{A}^{\text{factor}}(D^+ \to K^+\bar{K}^0) = \left(i\frac{G_F}{\sqrt{2}}\right) \Sigma \left(a_1 f_K (m_D^2 - m_K^2) F_0^{DK}(0) - f_D f_K^2 (b_2)_s^K\right), \tag{6.18}$$

$$\mathcal{A}^{\text{factor}}(D_s^+ \to \pi^+K^0) = \left(i\frac{G_F}{\sqrt{2}}\right) \Sigma \left(f_{D_s} f_K f_\pi (b_2)^{K\pi} - a_1 f_\pi (m_{D_s}^2 - m_K^2) F_0^{D_s K}(0)\right), \tag{6.19}$$

$$\mathcal{A}^{\text{factor}}(D_s^+ \to \pi^0K^+) = -\left(i\frac{G_F}{\sqrt{2}}\right) \Sigma \frac{1}{\sqrt{2}} \left(a_2 f_\pi (m_{D_s}^2 - m_K^2) F_0^{D_s K}(0) + f_{D_s} f_K f_\pi (b_2)^{K\pi}\right). \tag{6.20}$$

DCS decays

$$\mathcal{A}^{\text{factor}}(D^0 \to K^+\pi^-) = \left(i\frac{G_F}{\sqrt{2}}\right) V_{cd}^* V_{us} \left(a_1 f_K (m_D^2 - m_\pi^2) F_0^{D\pi}(0) + f_D f_\pi f_K (b_1)^{K\pi}\right), \tag{6.21}$$

$$\mathcal{A}^{\text{factor}}(D^0 \to K^0\pi^0) = \left(i\frac{G_F}{\sqrt{2}}\right) V_{cd}^* V_{us} \frac{1}{\sqrt{2}} \left(a_2 f_K (m_D^2 - m_\pi^2) F_0^{D\pi}(0) - f_D f_K f_\pi b_1^{K\pi}\right), \tag{6.22}$$

$$\mathcal{A}^{\text{factor}}(D^+ \to K^0\pi^+) = \left(i\frac{G_F}{\sqrt{2}}\right) V_{cd}^* V_{us} \left(a_2 f_K (m_D^2 - m_\pi^2) F_0^{D\pi}(0) + f_D f_K f_\pi (b_2)^{K\pi}\right), \tag{6.23}$$

$$\mathcal{A}^{\text{factor}}(D^+ \to K^+\pi^0) = \left(i\frac{G_F}{\sqrt{2}}\right) V_{cd}^* V_{us} \frac{1}{\sqrt{2}} \left(a_1 f_K (m_D^2 - m_\pi^2) F_0^{D\pi}(0) - f_D f_\pi f_K (b_2)^{K\pi}\right), \tag{6.24}$$

$$\mathcal{A}^{\text{factor}}(D_s^+ \to K^0 K^+) = \left(i\frac{G_F}{\sqrt{2}}\right) V_{cd}^* V_{us} \left((a_1 + a_2)\, f_K (m_{D_s}^2 - m_K^2) F_0^{D_s K}(0)\right). \tag{6.25}$$

Performance Test of QCDF for Charm Decay Branching Ratios In this paragraph we evaluate as a motivation Eqs. (6.9)–(6.25) numerically in the strict heavy quark limit in order to test the performance of QCDF for the branching ratios. For the a_i we take the vertex corrections into account only and neglect the annihilation contributions $(b_i)_q^{M_1 M_2}$.

As we only want to give a motivation, for simplicity, we use the central values of the numerical input given in Table 6.1. Note that the form factor $F_0^{D_s K}(0)$ is not measured yet. For the numerical illustrations presented here we use $F_0^{D_s K}(0) \sim 0.74$, *i.e.* the value of $F_0^{DK}(0)$. Furthermore, we neglect the scale dependence of the Gegenbauer moments α_i^P.

We calculate the Wilson coefficients C_1 and C_2 in Eq. (6.7) following the Eqs. (V.7) and (V.9) in [180].[1] For calculating the α_s running we use the `RunDec` code [482]. At the scale $\mu = 1$ GeV we find:

$$a_1^{M_1\pi}(1\,\text{GeV}) = 1.16 + i\,0.06\,, \qquad a_1^{M_1 K}(1\,\text{GeV}) = 1.16 + i\,0.07\,, \tag{6.26}$$

$$a_2^{\pi M_2}(1\,\text{GeV}) = -0.32 - i\,0.18\,, \qquad a_2^{K M_2}(1\,\text{GeV}) = -0.31 - i\,0.19\,. \tag{6.27}$$

As the vertex corrections give a numerically negligible flavor-nonuniversality we take the flavor average of Eqs. (6.26) and (6.27) for a_1 and a_2, respectively.

We show the results for all measured branching ratios of $D \to P_8 P_8$ in Fig. 6.1, assuming ad hoc a parametric uncertainty of 10%–30% around the central value. From the plots we draw the following conclusions:

- For channels dominated by the color-allowed tree contribution, the QCDF prediction agrees well with the measured values for the branching ratios. Although in some cases the theory band does not touch the experimental 1σ range, in all decays that are mainly described by the T amplitudes the correct order of magnitude is obtained from the QCDF expressions.

[1] Note that our convention for O_1 and O_2 is opposite to the one in [180].

- The branching ratio $\mathcal{B}(D^0 \to K_S K_S)$ can of course not be described at all, as it stems only from annihilation contributions which we have set to zero for our numerical study.
- For the decays whose amplitudes are composed of color-suppressed tree and annihilation contributions still the correct order of magnitude is found. However, not surprisingly, the QCDF predictions deviate significantly from the measurements, as we neglected the annihilation contributions.

Counting Parameters of the QCDF Expressions The numerical illustration for the branching ratios in the last paragraph showed that the effect of the annihilation coefficients $(b_i)_q^{M_1 M_2}$ can be sizable. In contrast to the a_i, for the $(b_i)_q^{M_1 M_2}$ we do not make any assumptions in the following and take them into account in full generality, except for the conservation of isospin.

In the following, we neither use the QCDF expressions for the $(b_i)_q^{M_1 M_2}$ nor for the a_i and treat them as parameters. Our main assumption is the flavor-universality of the a_i. Altogether, the QCDF coefficients that appear in the Eqs. (6.9)–(6.25), where we have taken the $\Delta = 0$ limit, are the following:

$$a_1, a_2, b_1^{K\pi}, b_1^{\pi K}, b_1^K, b_1^\pi, (b_1)_s^K, b_2^{K\pi}, (b_2)_s^K.$$

These are nine complex parameters that we treat as *a priori* unknown. In the next section, we analyze the interrelations of the QCDF approach on the one hand and the application of the SU(3)$_F$ symmetry on the other hand.

6.2. The Interplay of QCDF and SU(3)$_F$

Matching QCDF on SU(3)$_F$ for Charm Decays In order to benefit from the information on the structure of charm decays contained in the QCDF expressions we match the Eqs. (6.9)–(6.25) onto the SU(3)$_F$ ansatz presented in Ch. 5.

In order to do so, we rewrite all SU(3)$_F$-breaking parameters that appear in the QCDF expressions using a reparametrization around the SU(3)$_F$ limit. The latter we define as the arithmetic average

$$X = \frac{1}{N} \sum_{i=1}^{N} X_i \tag{6.28}$$

of a considered group of parameters $\{X_i\}$ that contains N elements. All parameters in the group $\{X_i\}$ can then be written as deviations from the average X using the parameters

$$\delta_i^X = \frac{X_i - X}{X}. \tag{6.29}$$

α_1^K	0.10 ± 0.04	[483]
α_2^K	0.25 ± 0.15	[483]
α_2^π	0.16 ± 0.01	[483]
$\alpha_s(m_Z)$	0.1184 ± 0.0007	[89]
$m_b(\overline{\text{MS}})$	4.18 ± 0.03 GeV	[89]
$m_c(\overline{\text{MS}})$	1.257 ± 0.025 GeV	[89]
m_Z	91.1876 ± 0.0021 GeV	[89]
m_{D^0}	(1864.86 ± 0.13) MeV	[89]
m_{D_s}	(1968.49 ± 0.32) MeV	[89]
m_{π^0}	(134.9766 ± 0.0006) MeV	[89]
m_{K^0}	(497.614 ± 0.024) MeV	[89]
f_D	$(206.7 \pm 8.5 \pm 2.5)$ MeV	[89]
f_{D_s}	(260.0 ± 5.4) MeV	[89]
f_π	$(130.41 \pm 0.03 \pm 0.2)$ MeV	[89]
f_K	$(156.1 \pm 0.2 \pm 0.8 \pm 0.2)$ MeV	[89]
$F_0^{DK}(0)$	0.739(7)(5)(0)	[484]
$F_0^{D\pi}(0)$	0.666(19)(4)(3)	[484]

Table 6.1.: Input values for the numerical calculations. Note that for the numerical calculations we take into account the central values only, see text for details. For additional references with respect to the Gegenbauer moments α_1^K, α_2^K and α_2^π see [483]. Table taken from [469].

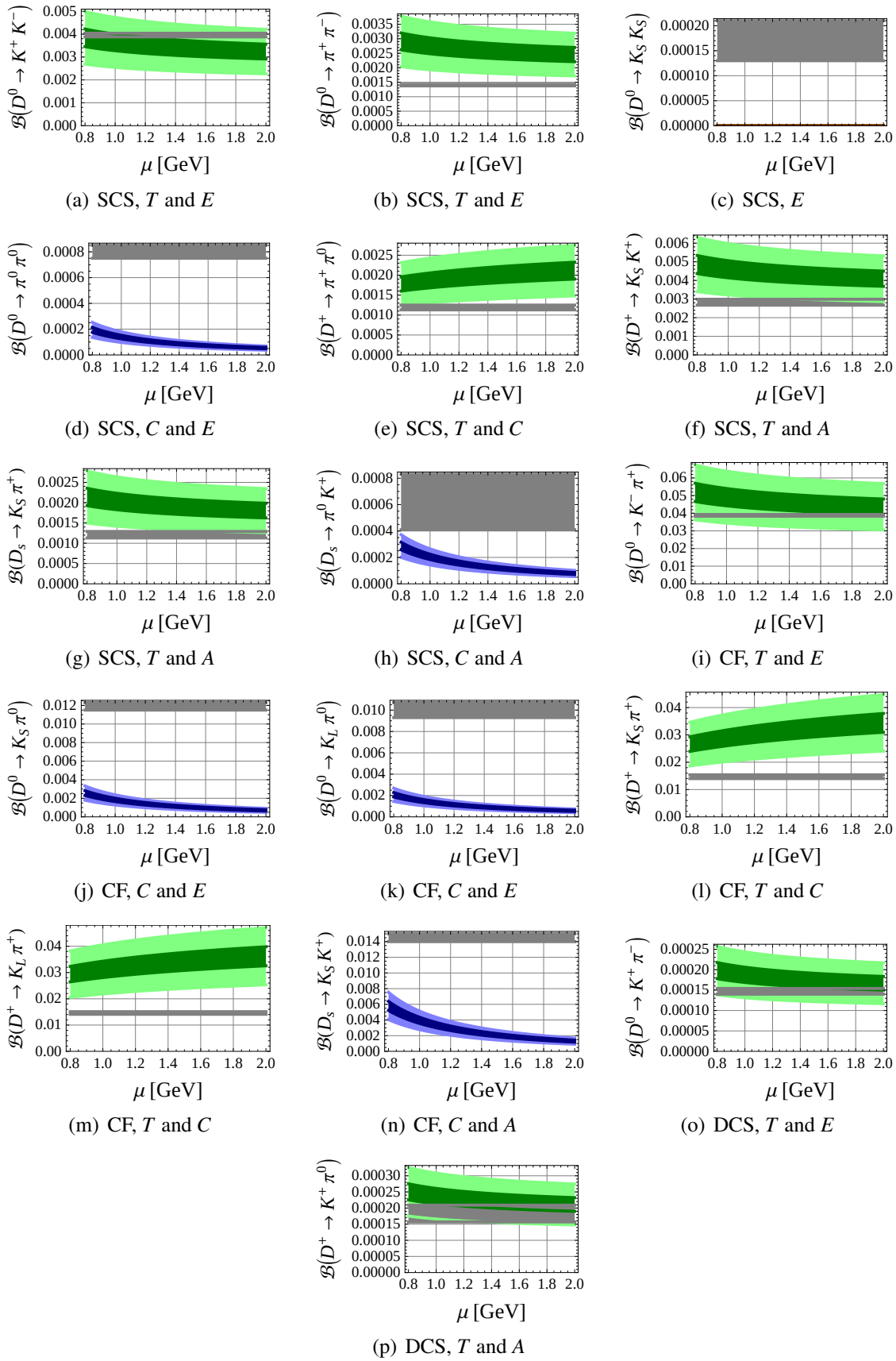

(a) SCS, T and E (b) SCS, T and E (c) SCS, E

(d) SCS, C and E (e) SCS, T and C (f) SCS, T and A

(g) SCS, T and A (h) SCS, C and A (i) CF, T and E

(j) CF, C and E (k) CF, C and E (l) CF, T and C

(m) CF, T and C (n) CF, C and A (o) DCS, T and E

(p) DCS, T and A

Figure 6.1.: Branching ratio predictions of QCDF with $a_{i,II} = b_i = 0$, see text for details. Dark (light) color: 10% (30%) uncertainty around the central value. Green: Amplitude with T dominance . Blue: Amplitude with C dominance. Gray: 1σ range of measurement. Plots of $\mathcal{B}(D^0 \to K^+K^-)$ and $\mathcal{B}(D^0 \to \pi^+\pi^-)$ taken from [469].

Specifically, with the templates of Eqs. (6.28) and (6.29) we rewrite the parameters in the QCDF expressions as follows:

$$m_D^2 - m_K^2 = m_{DP}^2 \left(1 - \delta_1^{m_{DP}^2} - \delta_2^{m_{DP}^2}\right), \tag{6.30}$$

$$m_D^2 - m_\pi^2 = m_{DP}^2 \left(1 + \delta_2^{m_{DP}^2}\right), \tag{6.31}$$

$$m_{D_s}^2 - m_K^2 = m_{DP}^2 \left(1 + \delta_1^{m_{DP}^2}\right), \tag{6.32}$$

$$f_K = f_P \left(1 + \delta^{f_P}\right), \tag{6.33}$$

$$f_\pi = f_P \left(1 - \delta^{f_P}\right), \tag{6.34}$$

$$f_{D_s} = f_d \left(1 + \delta^{f_d}\right), \tag{6.35}$$

$$f_D = f_d \left(1 - \delta^{f_d}\right), \tag{6.36}$$

$$F_0^{DK}(0) = F_0^{DP} \left(1 + \delta_1^{F_0^{DP}}\right), \tag{6.37}$$

$$F_0^{D\pi}(0) = F_0^{DP} \left(1 + \delta_2^{F_0^{DP}}\right), \tag{6.38}$$

$$F_0^{D_s K} = F_0^{DP} \left(1 - \delta_1^{F_0^{DP}} - \delta_2^{F_0^{DP}}\right). \tag{6.39}$$

An analogous reparametrization is used for the QCDF annihilation coefficients:

$$b_1^{K\pi} = b_1 \left(1 + \delta_1^{b_1}\right), \tag{6.40}$$

$$b_1^{K} = b_1 \left(1 + \delta_2^{b_1}\right), \tag{6.41}$$

$$b_1^{\pi} = b_1 \left(1 + \delta_3^{b_1}\right), \tag{6.42}$$

$$(b_s)_1^{K} = b_1 \left(1 - \delta_1^{b_1} - \delta_2^{b_1} - \delta_3^{b_1}\right), \tag{6.43}$$

$$(b_s)_2^{K} = b_2 \left(1 + \delta^{b_2}\right), \tag{6.44}$$

$$b_2^{K\pi} = b_2 \left(1 - \delta^{b_2}\right). \tag{6.45}$$

The SU(3)$_F$ limit is obtained in the limit $\delta^X = 0$. With the still exact reparametrization Eqs. (6.30)–(6.45) we can obtain the linear SU(3)$_F$ expansion of the QCDF amplitudes. We insert the reparametrizations into Eqs. (6.9)–(6.25) and neglect subsequently all powers of δ^X larger than one. The amplitudes have then the form

$$\mathcal{A}^{\text{factor}}(d) = \mathcal{A}_0^{\text{factor}}(d) + \mathcal{A}_X^{\text{factor}}(d) + O(\delta^2), \tag{6.46}$$

where $\mathcal{A}_0^{\text{factor}}(d)$ denotes the SU(3)$_F$ limit amplitude of a decay d and $\mathcal{A}_X^{\text{factor}}(d)$ includes terms linear in δ^X only. Due to the SU(3)$_F$ structure the thus obtained amplitudes must obey the six SU(3)$_F$ sum rules valid to linear SU(3)$_F$ breaking [466] given in Eqs. (5.80)–(5.85). Indeed, they do so, as we explicitly checked, with one important exception where this is not automatically the case. The U-spin sum rule Eq. (5.83) can only be fulfilled if the QCDF parameters obey

$$b_1^{\pi K} = b_1^K + b_1^\pi - b_1^{K\pi}. \tag{6.47}$$

This relation is a prediction of the SU(3)$_F$ approach to linear order in breaking and consequently in the following assumed to hold. The elimination of $b_1^{\pi K}$ by Eq. (6.47) leads to only eight remaining QCDF parameters in the $\Delta = 0$ limit, specifically:

$$a_1, a_2, b_1^{K\pi}, b_1^K, b_1^\pi, (b_1)_s^K, b_2^{K\pi}, (b_2)_s^K.$$

Having only eight parameters describing 17 decay amplitudes, we expect nontrivial relations. We stress that we treat the a_i and $(b_i)_q^{M_1M_2}$ as free parameters.

QCDF Sum Rules Beyond SU(3)$_F$ Actually, from the number of parameters vs. amplitudes we know *a priori* that there have to be nine sum rule relations between the 17 amplitudes. Six of these we have identified in the previous paragraph as the known SU(3)$_F$ sum rules, Eqs. (5.80)–(5.85). But these do of course not give us further information on SU(3)$_F$ matrix elements. On the contrary, these lead to the prediction Eq. (6.47) to linear order in SU(3)$_F$ breaking. But the three additional sum rules do give further dynamical information. We derive in the following these sum rules and show how to benefit from them in order to reduce the degrees of freedom of the plain SU(3)$_F$ parametrization.
In order to derive the additional QCDF sum rules beyond SU(3)$_F$ we proceed as follows: We start with the 17 QCDF amplitudes in Eqs. (6.9)–(6.25) which are not yet expanded to linear order SU(3)$_F$ breaking. We know that at linear order in SU(3)$_F$ we can eliminate six amplitudes in favor of the remaining 11 ones. Without loss of generality we therefore discard the amplitudes

$$\mathcal{A}(D^0 \to \pi^0\pi^0), \mathcal{A}(D^0 \to K^-\pi^+), \mathcal{A}(D^0 \to K^+\pi^-), \mathcal{A}(D^0 \to K^0\pi^0),$$
$$\mathcal{A}(D^+ \to K^0\pi^+), \mathcal{A}(D^+ \to K^+\pi^0).$$

Of course the final result for the SU(3)$_F$ matrix elements will not depend on this choice. The only sum rules that can now remain in the reduced system are the desired additional QCDF sum rules beyond SU(3)$_F$. These can be found by Gaussian elimination of the QCDF parameters a_i and b_i. At this step, the resulting sum rules are valid for the full QCDF expressions in the limit $\Delta = 0$, as given in Eqs. (6.9)–(6.25). They read as follows [469]

$$\sqrt{2}F_0^{D_sK} f_K (m_{D_s}^2 - m_K^2) \frac{\mathcal{A}(D^+ \to \pi^0\pi^+)}{\Sigma} + F_0^{D\pi} f_\pi (m_D^2 - m_\pi^2) \frac{\mathcal{A}(D_s \to K^0K^+)}{V_{cd}^* V_{us}} = 0\,, \tag{6.48}$$

$$\begin{aligned}&\sqrt{2}F_0^{D_sK}(m_{D_s}^2 - m_K^2)\,\mathcal{A}(D^+ \to \pi^0\pi^+)\\ &\quad - F_0^{D\pi}(m_D^2 - m_\pi^2)\Big(\sqrt{2}\mathcal{A}(D_s \to \pi^0K^+) + \mathcal{A}(D_s \to \pi^+K^0)\Big) = 0\,,\end{aligned} \tag{6.49}$$

$$
\begin{aligned}
&F_0^{D\pi} f_K f_\pi (m_D^2 - m_\pi^2) \left(F_0^{DK} f_{D_s} (m_D^2 - m_K^2) - F_0^{D_s K} f_D (m_{D_s}^2 - m_K^2) \right) \frac{\mathcal{A}(D^+ \to \bar{K}^0 \pi^+)}{V_{cs}^* V_{ud}} \\
&+ F_0^{D\pi} f_\pi (m_D^2 - m_\pi^2)^2 \left(-F_0^{DK} f_\pi \frac{m_D^2 - m_K^2}{m_D^2 - m_\pi^2} + F_0^{D\pi} f_K \right) \left(f_D \frac{\mathcal{A}(D_s \to \bar{K}^0 K^+)}{V_{cs}^* V_{ud}} + f_{D_s} \frac{\mathcal{A}(D^+ \to \bar{K}^0 K^+)}{\Sigma} \right) \\
&+ \sqrt{2} F_0^{DK} f_K (m_D^2 - m_K^2) \left(-F_0^{D_s K} f_D f_\pi (m_{D_s}^2 - m_K^2) + F_0^{D\pi} f_{D_s} f_K (m_D^2 - m_\pi^2) \right) \frac{\mathcal{A}(D^+ \to \pi^0 \pi^+)}{\Sigma} = 0 \,.
\end{aligned}
\tag{6.50}
$$

In order to benefit from these sum rules for the full QCDF amplitudes at linear SU(3)$_F$ breaking, firstly we insert our parametrization Eqs. (6.30)-(6.45). Then we neglect coefficients of $O(\delta^2)$ in order to get the linear QCDF sum rule. Inserting the SU(3)$_F$ expressions for the amplitudes that were obtained in Ch. 5 into the expanded QCDF sum rules we extract the following QCDF relations for the SU(3)$_F$ matrix elements [469]

$$
\begin{aligned}
&-\frac{3}{122}\sqrt{\frac{5281}{7}} \times B_{27}^{15_1} - \frac{23}{122}\sqrt{\frac{151}{21}} \times B_{27}^{15_2} + \frac{2}{\sqrt{21}} \times B_{27}^{24_1} \\
&+ \frac{1}{\sqrt{2}} \left(\delta_1^{F_0^{DP}} + 2\delta_2^{F_0^{DP}} - 2\delta^{f_P} - \delta_1^{m_{DP}^2} + \delta_2^{m_{DP}^2} \right) \times A_{27}^{15} = 0 \,,
\end{aligned}
\tag{6.51}
$$

$$
\sqrt{\frac{3}{7}} \times B_{27}^{24_1} + \frac{1}{\sqrt{2}} \left(\delta_1^{F_0^{DP}} + 2\delta_2^{F_0^{DP}} - \delta_1^{m_{DP}^2} + \delta_2^{m_{DP}^2} \right) \times A_{27}^{15} = 0 \,,
\tag{6.52}
$$

$$
\begin{aligned}
&-976 \left(2\delta_1^{F_0^{DP}} - 17\delta_2^{F_0^{DP}} - 10\delta^{f_d} - 24\delta^{f_P} - 2\delta_1^{m_{DP}^2} - 19\delta_2^{m_{DP}^2} \right) \times B_{27}^{24_1} \\
&+ 80\sqrt{151} \left(32\delta_1^{F_0^{DP}} + 25\delta_2^{F_0^{DP}} + 38\delta^{f_d} + 12\delta^{f_P} - 32\delta_1^{m_{DP}^2} - 7\delta_2^{m_{DP}^2} \right) \times B_{27}^{15_2} \\
&+ 80\sqrt{12194} \left(\delta_1^{F_0^{DP}} - \delta_2^{F_0^{DP}} - 2\delta^{f_P} - \delta_1^{m_{DP}^2} - 2\delta_2^{m_{DP}^2} \right) \times B_8^{15_2} \\
&- 183\sqrt{11811} \left(\delta_1^{F_0^{DP}} - \delta_2^{F_0^{DP}} - 2\delta^{f_P} - \delta_1^{m_{DP}^2} - 2\delta_2^{m_{DP}^2} \right) \times B_8^{3} \\
&+ 122\sqrt{8607} \left(\delta_1^{F_0^{DP}} - \delta_2^{F_0^{DP}} - 2\delta^{f_P} - \delta_1^{m_{DP}^2} - 2\delta_2^{m_{DP}^2} \right) \times B_8^{\bar{6}_1} \\
&+ \sqrt{3992907} \left(-\delta_1^{F_0^{DP}} + \delta_2^{F_0^{DP}} + 2\delta^{f_P} + \delta_1^{m_{DP}^2} + 2\delta_2^{m_{DP}^2} \right) \times B_8^{15_1} \\
&- 24\sqrt{15843} \left(2\delta_1^{F_0^{DP}} + 13\delta_2^{F_0^{DP}} + 10\delta^{f_d} + 16\delta^{f_P} - 2\delta_1^{m_{DP}^2} + 11\delta_2^{m_{DP}^2} \right) \times B_{27}^{15_1} = 0 \,.
\end{aligned}
\tag{6.53}
$$

Note that, by construction, in these sum rules the QCDF parameters a_i and $(b_i)_q^{M_1 M_2}$ are not present. Note further that in Eqs. (6.51)–(6.53) we have taken care to retain a consistent power counting. For example we did not keep terms that would have made necessary to go also beyond linear order in the SU(3)$_F$ symmetry approach for consistency

reasons. We use in Eqs. (6.51)–(6.53) directly the redefined SU(3)$_F$ matrix elements introduced in Ch. 5.

Eqs. (6.51) and (6.52) give a nontrivial relation between the SU(3)$_F$ limit matrix element A_{27}^{15} and several breaking matrix elements, namely $B_{27}^{15_1}$, $B_{27}^{15_2}$ and $B_{27}^{24_1}$. They come from amplitudes or their combinations that depend only on (a_1+a_2) from the QCDF perspective. In relation (6.53) all SU(3)$_F$ limit matrix elements cancel out and we obtain a relation between breaking matrix elements only. Altogether we can in this way eliminate three SU(3)$_F$-breaking matrix elements using the information on the structure of the dynamics contained in the QCDF sum rules.

We solve Eqs. (6.51)-(6.53) for the matrix elements $B_{27}^{15_1}$, $B_{27}^{15_2}$, $B_{27}^{24_1}$ and evaluate the result for numerical illustration using the central values given in Table 6.1. We obtain [469]

$$B_{27}^{15_1} = -0.06\, A_{27}^{15} + 0.03\, B_8^{15_1} - 0.14\, B_8^{15_2} + 0.31\, B_8^{3} - 0.18\, B_8^{\bar{6}_1}\,, \tag{6.54}$$

$$B_{27}^{15_2} = -0.24\, A_{27}^{15} - 0.04\, B_8^{15_1} + 0.19\, B_8^{15_2} - 0.42\, B_8^{3} + 0.24\, B_8^{\bar{6}_1}\,, \tag{6.55}$$

$$B_{27}^{24_1} = \quad 0.16\, A_{27}^{15}\,. \tag{6.56}$$

As in Fig. 6.1, for the not measured form factor $F_0^{D_sK}(0)$ we use here $F_0^{D_sK}(0) \sim 0.74$, *i.e.* the value of $F_0^{DK}(0)$. Note that the numbers in Eqs. (6.54)–(6.56) change significantly if one uses instead $F_0^{D_sK}(0) \sim F_0^{D\pi}(0)$.

For consistency, in the amplitudes we do not take into account the isospin-breaking effect from the small mass differences between charged and neutral kaons and pions, respectively, and use everywhere the input values for the masses of the neutral particles. In the phase space we take the effect of the mass differences into account, however.

Note that the sum rules for SU(3)$_F$ matrix elements still remain valid when $\Delta \neq 0$ is taken into account in the QCDF expressions of the amplitudes. As on both sides of the matching equation between SU(3)$_F$ and QCDF we can identify the different contributions, the QCDF sum rules for *amplitudes* then transform into sum rules for *parts of amplitudes*. If we insert into these the corresponding *parts of amplitudes* in the SU(3)$_F$ approach we arrive at the same sum rules for the SU(3)$_F$ matrix elements as in Eqs. (6.51)–(6.53) and (6.54)–(6.56).
As this argument is quite general, it still holds even in the presence of NP. The ability to identify corresponding terms of the QCDF and the SU(3)$_F$ approach is not touched at all by the additional terms considered in the models introduced in Sec. 5.4.4.
Therefore, we can use the sum rules Eqs. (6.51)–(6.53) also in the SU(3)$_F$-fit to CP asymmetries, which we present in the next section.

6.3. Answering Questions in Charm Physics including Traces of QCDF

After deriving the QCDF sum rules in Sec. 6.2 we illustrate their possible implications in this section by fits to the full current data set of charm observables presented in Tables 5.1–5.3 including the recent updates after Moriond 2013 as summarized in Table 5.9. We regard Eqs. (6.51)–(6.53) as reasonable input that relies on the general structure of the QCDF approach only. It does not depend on the details of the calculation of the QCDF parameters a_i and $(b_i)_q^{M_1 M_2}$. Taking this "imprint" of QCDF into account we come back to the questions that we posed in Sec. 5.4. There, we have presented results in plain SU(3)$_F$. Including the additional traces of QCDF we will see that some predictions can be considerably sharpened.

Note that for the numerical illustration of the effect of the QCDF sum rules presented here, in the fit of the remaining 10 SU(3)$_F$ matrix elements, *i.e.* 19 real parameters, we use for the QCDF input directly Eqs. (6.54)–(6.56). We do not take into account the uncertainties of the input parameters in Table 6.1. This includes the used value for $F_0^{D_s K}(0)$, as discussed after Eq. (6.56).

How Large is the SU(3)$_F$ Breaking? The first question we have to account for is how large is the requisite SU(3)$_F$ breaking under the inclusion of the QCDF relations? Firstly, the δ^X from the matching are numerically given as

$$\delta_1^{m_{DP}^2} = 0.06 \qquad \delta_2^{m_{DP}^2} = 0.01 \qquad \delta^{f_P} = 0.09 \tag{6.57}$$

$$\delta^{f_d} = 0.11 \qquad \delta_1^{F_0^{DP}} = 0.03 \qquad \delta_2^{F_0^{DP}} = -0.07. \tag{6.58}$$

As can be seen from Eqs. (6.57)–(6.58), the δ^X are reasonable expansion parameters. For the further investigation of the SU(3)$_F$ breaking we show in Fig. 6.2(a) the two measures of SU(3)$_F$ breaking δ_X and δ'_X defined in Sec. 5.4.1. The result can be compared to the corresponding plot of the plain SU(3)$_F$ analysis shown in Fig. 5.4. We learn that the requisite SU(3)$_F$ breaking in order to obtain a reasonable fit is about 10% larger than in the case of plain SU(3)$_F$. The best fit point has $\chi^2_{\text{min}} = 4.5$ with six degrees of freedom.

In addition to the full fit we present in Fig. 6.2(b) also a fit taking branching ratio measurements into account only. On the theory side we take accordingly the limit $\Delta = 0$. In this case we have two degrees of freedom and $\chi^2 = 1.3$ at the best fit point. The similarity of Figs. 6.2(a) and 6.2(b) shows that the size of SU(3)$_F$ breaking is mainly determined by the branching ratios.

Altogether, we conclude that the SU(3)$_F$ expansion is working fine with or without including QCDF structure in the fit, and we can proceed with our analysis.

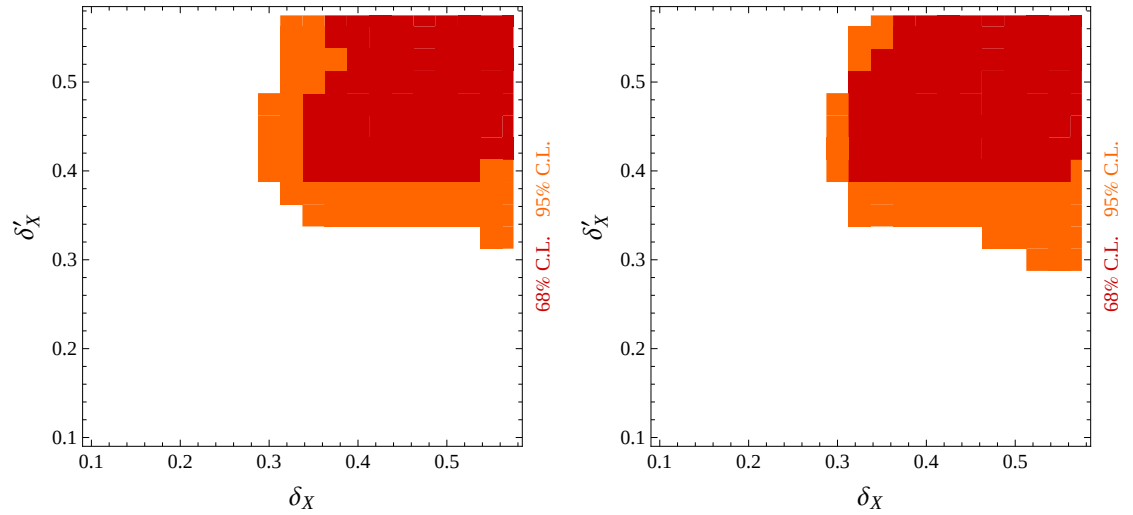

(a) Full fit. (b) Only branching ratios, in the limit $\Delta = 0$.

Figure 6.2.: Regions in the δ_X-δ'_X plane that are allowed at 68% (red) and 95% (orange) C.L. including input from QCDF sum rules and the recent updates after Moriond 2013 as summarized in Table 5.9, see text for details. Plots taken from [469].

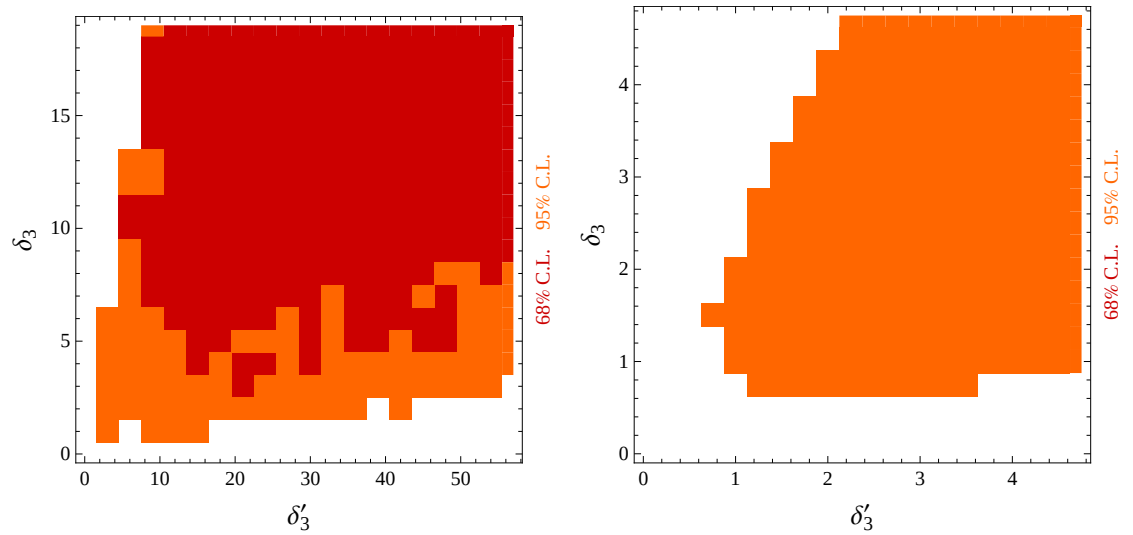

(a) All data (b) All data, zoom

Figure 6.3.: Regions in the δ'_3-δ_3 plane that are allowed at 68% (red) and 95% (orange) C.L. including input from QCDF sum rules and the recent updates after Moriond 2013 as summarized in Table 5.9, see text for details. Figure taken from [469].

How Large are the Triplets? After the validation of the symmetry ansatz, we study the effect of the QCDF input on the size of the triplet matrix elements. In the SM these are the main reason for nonvanishing CP violation in charm. We use for that the measures δ_3 and δ_3' defined in Sec. 5.4.3. The result of the fit to the full data set is shown in Fig. 6.3, which corresponds to the plot in plain SU(3)$_F$ presented in Fig. 5.11(a). No assumption on $\delta_X^{(\prime)}$ is made.

We observe that the 95% C.L. region including the QCDF input has overall not changed much in comparison to plain SU(3)$_F$. However, the 68% C.L. region is extended considerably towards the lower region. The point is that due to the correlation of the breaking matrix elements in Eqs. (6.54)–(6.56) there is significantly less freedom for the arrangement of the strong phases. In this way the fit cannot explain as easily as before the CP asymmetries with largish measured central values. This is exemplified by the observable $A_{CP}(D_s \to K^+\pi^0)$ which gives at the best fit point the largest single contribution to the χ^2, namely $\chi^2\left(A_{CP}(D_s \to K^+\pi^0)\right) = 1.7$. The global minimum is consequently shifted towards somewhat smaller penguins, and the shape of 68% C.L. region behaves accordingly.

Can we Differentiate the SM from Patterns of NP? We come now to the main point, the question if the additional insights from QCDF can help in order to disentangle NP models from the SM. To be specific, we study here the same NP models that were introduced in Sec. 5.4.4. In order to remain in the part of the parameter space where the perturbative expansion in the SU(3)$_F$ breaking does make sense we assume an upper bound $\delta_X^{(\prime)} \leq 50\%$. In plain SU(3)$_F$ we obtained $\chi^2_{\text{min}} = 1.0$ for the SM and the triplet model, $\chi^2_{\text{min}} = 1.0$ for the $\Delta U = 1$ model and $\chi^2_{\text{min}} = 0$ for the HN model.
If we impose additionally the QCDF sum rule relations Eqs. (6.54)–(6.56) we obtain at the best fit points $\chi^2_{\text{min}} = 4.6$ for the SM and the triplet model, $\chi^2_{\text{min}} = 1.1$ for the $\Delta U = 1$ model and $\chi^2_{\text{min}} = 0.6$ for the HN model. In Sec. 5.4.4 we learned that the SM can not be disentangled from the triplet model in plain SU(3)$_F$ using nonleptonic decays only. This is still true including the structure of the QCDF sum rules, as exemplified by the best fit points of the respective models.

In Fig. 6.4 we show the correlation of the CP asymmetry with the branching ratio of the decay $D_s \to K^+\pi^0$ in plain SU(3)$_F$ (Fig. 6.4(a)) and using additionally the QCDF relations Eqs. (6.54)–(6.56) (Fig. 6.4(b)) in fits to the data. In the case of plain SU(3)$_F$, the predictions are inconclusive, *i.e.*, refraining from using any dynamical input one can not disentangle the SM from the other shown NP models with current data. In contrast to that, including the reasonable input from the structure of QCDF, from our numerical illustration in Fig. (6.4(b)) we conclude that we *can* differentiate the SM from the HN model at 68% C.L. As can be seen, for significant progress it would already suffice to have a more precise measurement of the branching ratio $\mathcal{B}(D_s \to K^+\pi^0)$. This could exclude the SM solution with largish $a_{\text{CP}}^{\text{dir}}(D_s \to K^+\pi^0) > 0$. The preference for the other solution with $a_{\text{CP}}^{\text{dir}}(D_s \to K^+\pi^0) < 0$ would at the same time disfavor the HN model at 68% C.L.

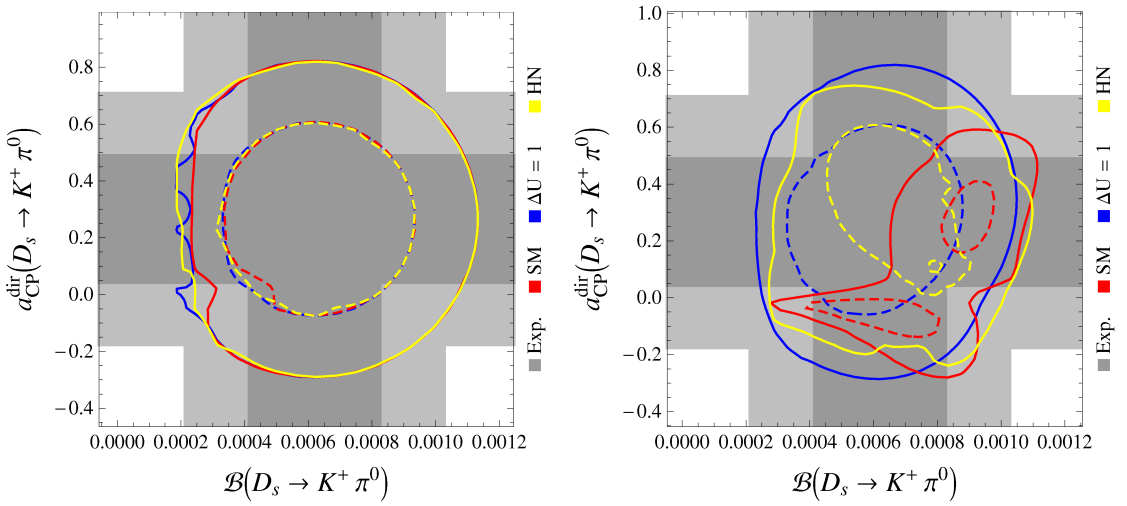

(a) Plain SU(3)$_F$ with $\delta_X^{(\prime)} \leq 50\%$.

(b) Including QCDF sum rules and $\delta_X^{(\prime)} \leq 50\%$.

Figure 6.4.: Correlations of the observables $a_{CP}^{\rm dir}(D_s \to K^+\pi^0)$ and $\mathcal{B}(D_s \to K^+\pi^0)$ at 68% (dashed) and 95% (solid) C.L. in different models, including recent updates after Moriond 2013 as summarized in Table 5.9, see text for details. Red: SM, Blue: $\Delta U = 1$ model, Yellow: HN model. (Dark) Light gray: (1σ) 2σ ranges of experimental measurements.

Note that Fig. 6.4(b) has a dependence on the value that one uses for the not measured form factor $F_0^{D_sK}(0)$, see the note after Eq. (6.56). We checked that using $F_0^{D_sK} \sim F_0^{D\pi}$ instead of $F_0^{D_sK} \sim F_0^{DK}$ does not change our main conclusion, *i.e.*, there remains a 68% C.L. region that is not shared by both the SM and the HN model so that we are still able to disentangle the HN model from the SM.

As the HN model is the only model considered here that could induce $a_{CP}^{\rm dir}(D^+ \to \pi^0\pi^+) \neq 0$, it is interesting to study also the correlation of $a_{CP}^{\rm dir}(D^+ \to \pi^0\pi^+)$ with $a_{CP}^{\rm dir}(D_s \to K^+\pi^0)$ and $\mathcal{B}(D_s \to K^+\pi^0)$ in this model. The results are shown in Fig. 6.5, where we confront fits to current data in plain SU(3)$_F$ with the corresponding ones including the input from QCDF. We observe that although the QCDF sum rules constrain the strong phases considerably, no visible patterns arise between $a_{CP}^{\rm dir}(D^+ \to \pi^0\pi^+)$ and these observables with present data.

Taking everything into account, the new method of using QCDF sum rules, which is independent of specific results for QCDF kernels, can considerably sharpen the predictions of different models for some observables. With future improved data this will bring us into the position to exclude models, maybe the SM or the HN model. As we showed in this section, it is especially important to measure $a_{CP}^{\rm dir}(D_s \to K^+\pi^0)$ and $\mathcal{B}(D_s \to K^+\pi^0)$ with higher precision in order to achieve this goal.

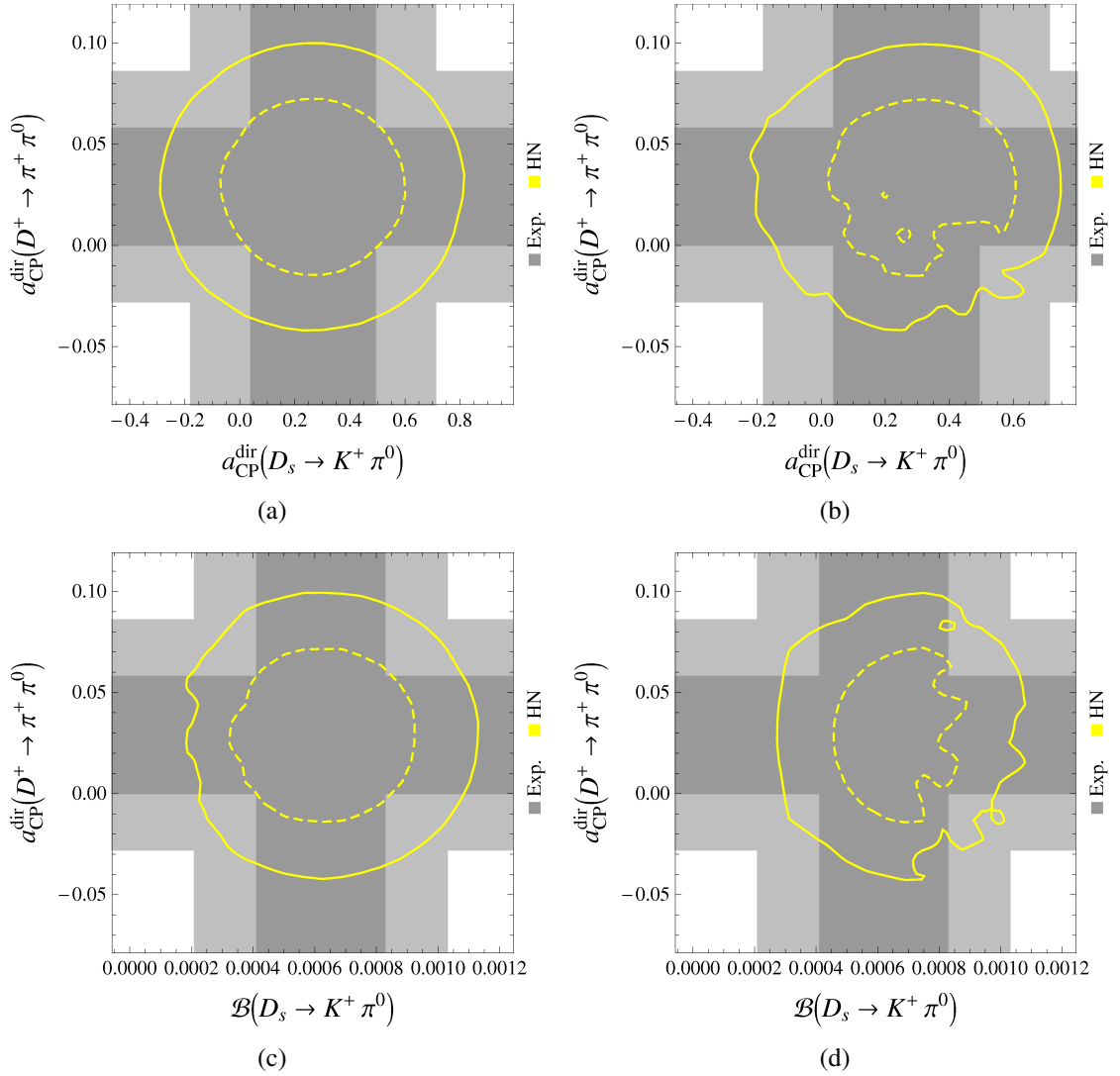

Figure 6.5.: Correlations of $a_{CP}^{\rm dir}(D^+ \to \pi^+\pi^0)$ with $a_{CP}^{\rm dir}(D_s \to K^+\pi^0)$ and $\mathcal{B}(D_s \to K^+\pi^0)$ at 68% (dashed) and 95% (solid) C.L. in the HN model, including recent updates after Moriond 2013 as summarized in Table 5.9. Left (a,c): Plain SU(3)$_F$ with $\delta_X^{(\prime)} \leq 50\%$. Right (b,d): Including input from QCDF sum rules and $\delta_X^{(\prime)} \leq 50\%$, see text for details. Yellow: HN model. (Dark) Light gray: (1σ) 2σ ranges of experimental measurements.

7. Outlook

The decay channels of B and D mesons that were discussed in this work will continue to play an important role in the future.
In the near future, for one of the roadmap channels of LHCb [485], $\bar{B} \to \bar{K}^* \mu^+ \mu^-$, the achievements of the analysis of the 1 fb^{-1} gathered until the end of 2011 will be followed soon by the analysis of the additional data taken in 2012. Prospects for several observables in the more distant future are summarized in Table 7.1. These include perspectives from the upgrade of the LHCb detector [486, 487] that will take place in 2018/19 and data from the future B factory Belle II at the e^+e^- collider SuperKEKB [488, 489].

Belle II is planned to start data taking in 2016 and to collect 50 ab^{-1} until 2023—a huge advance compared to the 1.5 ab^{-1} collected by the former B factories BaBar and Belle [490]. Concerning LHCb, a timeline has recently been presented in [491]. In 2013/14 the long shutdown I takes place, where preparations are made for running at $\sqrt{s} = 13$ TeV in the period from 2015-2018. Until 2018 10 fb^{-1} are planned to be collected [491]. During 2018/19 the long shutdown II takes place. During this time LHCb is upgraded in order to be able to handle an again increased instantaneous luminosity and to run at $\sqrt{s} = 14$ TeV in the years 2019-2022. After that a luminosity upgrade of LHC is planned for 2022-2024. The upgraded LHCb shall collect a total of 50 fb^{-1} in 10 years of data taking [492]. These ambitious experimental physics programs will give invaluable information on the physics at high energy scales and serve as precision probes of NP.

An example par excellence will also in the future be given by the long time goal of a full angular analysis of $\bar{B} \to \bar{K}^* \mu^+ \mu^-$ decays. Still only a small fraction of the full information contained in this decay is unravelled by current data. Future measurements will not only improve on the statistics of the already known observables, but also measure new ones, which will give a litmus test of NP models. As a special example, the bounds on squark flavor presented in Ch. 3 will become increasingly stronger with the improvement of the data. With additional observables we could also probe CP violation of squark flavor, in particular in the scharm-stop left-right mixing. Especially useful for that will be the CP asymmetries A_7^D and $a_{\rm CP}^{(3)}$, as these are sensitive to the phase of the Wilson coefficient C_{10} [183, 308, 318, 322].

In Table 7.1 we summarize the prospects for the future sensitivity in measurements of the zero of the forward-backward asymmetry A_{FB} of $\bar{B} \to \bar{K}^* \mu^+ \mu^-$. While current data on the zero of A_{FB} is consistent with the SM, the prospects for a future precision test look promising. This is the more so true, as the theory uncertainty of this observable is small, the SM prediction has an uncertainty of $\sim 8\%$ [184], see Eq. (3.8). For the Belle II experiment prospects for the sensitivity to the Wilson coefficients $C_{7,9,10}$ are given, assuming

Observable	LHCb current data[a]	LHCb 2018[b]	LHCb 50 fb^{-1} 10 yrs data taking[b]	Belle II 5 ab^{-1}	Belle II 50 ab^{-1} 2023
$S_3(\bar{B} \to \bar{K}^* \mu^+ \mu^-)$ $(1\,\mathrm{GeV}^2 < q^2 < 6\,\mathrm{GeV}^2)$	0.07 [331]	0.025 [486]	0.008 [486]		
zero of $A_{FB}(\bar{B} \to \bar{K}^* \mu^+ \mu^-)$	18% [331]	6% [486]	2% [486]		
C_7/C_9 from $\overline{A}_{FB}(\bar{B} \to \bar{K}^* l^+ l^-)^c$					5% [488]
C_9 from $\overline{A}_{FB}(\bar{B} \to \bar{K}^* l^+ l^-)^c$				11% [488]	4% [488]
C_{10} from $\overline{A}_{FB}(\bar{B} \to \bar{K}^* l^+ l^-)^c$				13% [488]	4% [488]
$\mathcal{B}(B_d \to \mu^+ \mu^-)/\mathcal{B}(B_s \to \mu^+ \mu^-)$	–	~ 100% [486]	~ 35% [486]		
$\Delta A_{CP} \cdot 10^2$	0.18 (D^* ch.) [64] 0.33 (B ch.) [65]	0.065 [486]	0.015 [492]		
$A_{CP}(D^0 \to \pi^+ \pi^-) \cdot 10^2$	–		0.015 [492]		0.07 [477]
$A_{CP}(D^0 \to K^+ K^-) \cdot 10^2$	–		0.01 [492]		0.05 [477]
$A_{CP}(D^+ \to K_S K^+)$	–		0.0001 [492]		0.001 [477]
$A_{CP}(D_s \to K_S \pi^+)$	0.008 [478]				0.003 [477]
$A_{CP}(D^0 \to \pi^0 \pi^0)$	–				$\lesssim 0.01^d$ [493]
$K^+\pi^-$ strong phase difference[e] $\delta_{K\pi}$				6° [488]	3.8° [477]

Table 7.1.: Prospects for sensitivity in selected future measurements and experiments. Numbers given in percent refer to a relative precision, all others to the absolute one.
[a] Statistical and systematic errors are added in quadrature.
[b] Only statistical sensitivity.
[c] Assuming the SM operator basis for $\Delta B = 1$ transitions.
[d] Value that we read off the corresponding plot on slide 20 in [493].
[e] Our symmetrization [469] of the current HFAG average for the strong phase $\delta_{K\pi}$ [63] (online update April 2013) is $\delta_{K\pi} = (18.25 \pm 9.85)^\circ$, Eq. (5.103).

the SM operator basis.
In Ch. 4 the observable $A_T^{(2)}$ has been used to extract the form factor ratio $f_\perp/f_\parallel$ from data at high q^2. This method relies on the abscence of right-handed currents from NP operators, as was discussed there. It is justified by the data, as indeed no right-handed currents have been seen so far. At low q^2, $A_T^{(2)}$ can vice versa be used as an actual probe of NP from chirality flipped operators [494]. As shown in Fig. 2 of [494] in SUSY there could in principle be large deviations from the SM value $A_T^{(2)} \sim 0$ at $q^2 < 4\,\text{GeV}^2$ due to squark flavor violation in gluino diagrams. In Table 7.1 it is given the future sensitivity to the observable S_3, which relates to $A_T^{(2)}$ as $S_3 = \frac{1}{2}(1 - F_L)A_T^{(2)}$. In the future, at low q^2 these observables will give a null test of the SM and improved probes of squark flavor.
The progress in precision will shrink the allowed region in the plane of effective couplings C_9–C_{10} that we overlayed in Fig. 3.6 with SUSY scatter points. If the region is compressed around the SM point, this will give also increasingly strong bounds on squark flavor violation. In addition to $B \to K^*\mu^+\mu^-$, several further decay channels with partonic $b \to s l^+ l^-$ transitions contribute to this progress, as the recently measured decays $B_s \to \phi\mu^+\mu^-$ [495–497] and $\Lambda_b \to \Lambda\mu^+\mu^-$ [496, 498] and the decays $B^+ \to K_1^+\mu^+\mu^-$, $B^0 \to K_2^*\mu^+\mu^-$, which are planned to be measured by LHCb [487]. Furthermore, in addition to $\mu^\pm$ final states, LHCb takes now also first steps to $e^\pm$ final states in $\bar{B} \to \bar{K}^* l^+ l^-$ [499].

Turning from prospects in the down sector to ones in the up sector, a major task for the future will be the measurement of all CP asymmetries in SCS decay channels. As was pointed out in Chs. 5 and 6, besides a clarification of the value of ΔA_{CP} it is especially important to measure the observables $A_{CP}(D^0 \to K_S K_S)$, $A_{CP}(D_s \to K_S\pi^+)$ and $A_{CP}(D_s \to K^+\pi^0)$ with a higher precision as is the case at present. In this way one can determine how large the necessary triplet or penguin enhancement in the charm system really is. As was shown in Ch. 6 also branching ratio measurements can take an important role in this respect, being exemplified by $\mathcal{B}(D_s \to K^+\pi^0)$.
As demonstrated in Table 7.1, there is much progress to expect for the statistical error of ΔA_{CP}. Also the single contributions $A_{CP}(D^0 \to K^+K^-)$ and $A_{CP}(D^0 \to \pi^+\pi^-)$ will be resolved. Belle II will help in an essential way to unravel these asymmetries. As can be seen from Table 7.1, there are also prospects from both LHCb and Belle II for other CP asymmetries of SCS decay modes, *i.e.*, for the ones with a K_S in the final state. Concerning D decays with a π^0 in the final state, these are in general challenging for LHCb. But Belle II can also measure these, for instance it can even perform well for $A_{CP}(D^0 \to \pi^0\pi^0)$ [493]. This measurement will be very interesting in the context of our predictions presented in Figs. 5.9 and 5.10. Furthermore, in [493] the CP asymmetry of the decay $D^+ \to \pi^+\pi^0$ is enumerated in combination with CP asymmetries of other decay modes for that it is stated that *"Belle II is well situated to make many of these measurements, and can make uniquely useful contributions to modes with neutral particles in the final state, complementary to those accessible at LHCb"* [493].
By the measurement of $A_{CP}(D^+ \to \pi^+\pi^0)$ Belle II would be able to make another important null test of the SM, as described in Sec. 5.4.4.

Taking everything into account, in the future we will definitely be able to benefit from the predictions made in this work.

8. Conclusion

In this thesis we have explored topics in the up and down sector of quark flavor physics.

In the down sector we have shown that new theoretical and experimental results on $\bar{B} \to \bar{K}^{(*)} l^+ l^-$ in particular at high q^2 give new constraints on squark flavor violation. The bounds stem from large chargino contributions that lead to a strong correlation of the Wilson coefficients C_9 and C_{10} from the Z penguin. Depending on the parameter space, the bound on the scharm-stop left-right mixing becomes as strong as $(\delta^u_{23})_{LR} \lesssim 0.1$. Assuming the absence of scalar operators, from $\bar{B} \to \bar{K}^{(*)} l^+ l^-$ it follows a lower limit on $\mathcal{B}(\bar{B}_s \to \mu^+ \mu^-)$ that is consistent with the recent evidence for this decay. Using the SUSY link from beauty to top physics we could show that the rare top decays $t \to cV$, $V = \gamma, g, Z$ are too rare to be observed in foreseeable future. For future studies it would also be interesting to further look at the implications of b physics observables on rare $t \to cH$ decays. Moreover, the squark flavor bounds have consequences for SUSY model building. The bounds on Radiative Flavor Violation models become partly even stronger than the ones from ε_K. Generally, they become stronger for lighter stops.

In order to further improve on the interpretation of $\bar{B} \to \bar{K}^* l^+ l^-$ observables a better knowledge of the $\bar{B} \to \bar{K}^*$ form factors is necessary. Therefore we have extracted form factor ratios from observables which are approximately free of short-distance physics at high q^2. We used further theoretical input at low q^2 from Heavy-Quark Symmetry and Light-Cone Sum Rules. These considerably sharpen the fit of the second order series expansion of the form factor ratios to data.

In the up sector we have given the first unbiased comprehensive $\mathrm{SU}(3)_F$ analysis of $D \to P_8 P_8$ decays. We have found that the data can be described with reasonable $\mathrm{SU}(3)_F$ breaking. High and low representations of the $\mathrm{SU}(3)_F$ symmetry both play an important role for that. CP violation indicates strongly enhanced $\mathrm{SU}(3)_F$ limit triplet representations or NP beyond MFV. For a further clarification in the charm sector more precise measurements of all CP asymmetries are desperately needed, besides ΔA_{CP} especially of $A_{CP}(D^+ \to \pi^0 \pi^+)$, $A_{CP}(D^0 \to K_S K_S)$, $A_{CP}(D_s \to K_S \pi^+)$ and $A_{CP}(D_s \to K^+ \pi^0)$.

Current data allows already to exclude various simplified scenarios of $\mathrm{SU}(3)_F$ breaking but not to disentangle the SM or triplet model from other models of NP. We showed as a proof of principle that future theoretical insights into $\mathrm{SU}(3)_F$ breaking or significantly improved data could differentiate the triplet model including the SM from other models with scalar operators.

Improved data not yet being feasible, we improved further from the theory side and explored traces of QCDF that could be left in charm decays. Actually, the quantitative

application of QCDF to charm decays is not suited for precision physics of D decays. The reason lies in the intermediate mass of the charm quark. The latter is problematic for a sensible expansion in $\Lambda_{\rm QCD}/m_c$ in QCDF, *i.e.* the power corrections are too large in order to let the heavy quark expansion converge. Furthermore, for D decays an expansion in α_s is equally doubtful as the strong coupling is evaluated at small energy scales, *i.e.*, it is not small.

Using consequently only structural input from QCDF and no quantitative calculations of the QCDF kernels, we found that reasonable theoretical input can considerably reduce the large number of degrees of freedom that are present in the SU(3)$_F$ analysis. We illustrated that predictions for some D decay observables and their correlations can be sharpened by QCDF sum rules, especially in case of the correlation between $a_{\rm CP}^{\rm dir}(D_s \to K^+\pi^0)$ and $\mathcal{B}(D_s \to K^+\pi^0)$.

In the future, even more precise measurements of the roadmap channel [485] $\bar{B} \to \bar{K}^*\mu^+\mu^-$ are expected at LHCb. New opportunities will show up when we get more statistics and measurements of additional observables. Then, also the sensitivity to $\arg(C_9)$ and $\arg(C_{10})$ will move forwards and one could study SUSY CP violation in $(\delta^u_{23})_{LR}$ which has been assumed real throughout this work. Furthermore, analogous physics programs could be carried out in $b \to dl^+l^-$ transitions. Such a transition has been observed for the first time only very recently [500]. In charm physics we are awaiting likewise landmark results on ΔA_{CP} as well as the other additional SCS CP asymmetries.

The various b and c observables allow to explore flavor physics in and beyond the SM and to test the SM itself. For that a joint effort of precision experiments and theoretical calculations is necessary. Using b physics observables we have reinforced the SUSY flavor problem by limiting further the possible squark flavor violation. We gave additional bounds on the parameter space of SUSY model building. Both of these tasks can be pursued in the future—or if SUSY is found, the SM could be excluded by flavor observables, as well as by direct searches.

Benchmarks on this way will be the more precise measurement of the zero of the forward-backward asymmetry of $\bar{B} \to \bar{K}^*\mu^+\mu^-$ and the transverse asymmetry $A_T^{(2)}$ at low q^2. The latter serves as a null test of the SM [494]. In Ch. 7 we have given a concrete outlook on the sensitivity to these observables with the LHCb upgrade and the future detector Belle II. Further very clean benchmark tests of the SM are possible at high q^2 using the transversity observables $H_T^{(1,3,4,5)}$, see Ref. [321].

In c physics we showed how to unravel different NP models in global fits to $D \to P_8P_8$ data. With precision measurements of nonleptonic D decays in the future we will be able to answer the question for the SU(3)$_F$ anatomy of the Hamiltonian. This will decide if physics with a different flavor structure than the SM is realized.
A null test of the SM is provided by $a_{CP}^{\rm dir}(D^+ \to \pi^+\pi^0)$. It will be an important task of Belle II to measure this quantity in order to find out if NP is present in the $\Delta I = 3/2$ transition. As we illustrated in Ch. 6, the interplay of the CP asymmetry and the branching ratio of the channel $D_s \to K^+\pi^0$ will be a further important building block for the decision on the flavor representations in the CP violating part of the Hamiltonian.

In order to pin down the complete properties of a model, additional information from confronting it with data from other decay modes will also be needed. For example, in the plain $SU(3)_F$ approach, we are not sensitive to the Dirac structure of a given model. But this is *e.g.* the case in radiative D decays where we can probe for NP in the $\Delta C = 1$ dipole operators [474].

In order to establish NP, the direct detection of new particles at ATLAS and CMS is all-important. In the loop corrections of the flavor observables we are able to measure precisely their couplings and perhaps to predict their existence beforehand, as history already has shown. If the mass scale of NP is so high that we are not able to produce the new particles at all, a possibility to probe for NP nevertheless is given by the indirect precision observables.
Besides the b and c observables studied in this thesis, there are a variety of additional examples for such observables. For CP violation, electric dipole moments are important probes, see recently [501] and references therein. The future measurements or limits on the branching ratios of the decays $\mu \to e\gamma$, $\mu \to eee$, $\tau \to \mu\mu\mu$ will reveal invaluable information on lepton flavor violation, see for a recent SUSY study *e.g.* [502]. A very interesting field in the future will also be the precise measurement of the Higgs decays to fermions, specifically in leptonic $H \to \mu\mu$ and $H \to \tau\tau$ decays—and possibly also in flavor violating $H \to \mu\tau$ decays, which would point to NP [106, 503].

Exciting times are lying ahead of us.

Acknowledgments

First of all, I want to thank Gudrun Hiller for suggesting the topic of this work and supervising the whole project. I also thank my second referee Heinrich Päs.

I thank Andreas Crivellin for checks of the numerical calculation of ε_K and Sven Heinemeyer as well as Thomas Hahn for giving advice on the usage of `FeynHiggs`.

For many useful and valuable discussions I thank Arnd Behring, Christoph Bobeth, Christian Gross, Christian Hambrock, Martin Jung, Danny van Dyk and Roman Zwicky.

I gratefully acknowledge support by the *German-Israeli Foundation for Scientific Research and Development (GIF)* and the DFG Research Unit FOR 1873 “Quark Flavour Physics and Effective Field Theories”.

A. Tables for SU(3)$_F$ Analyses including Linear Breaking

In this chapter we demonstrate the universal benefit one can obtain from the SU(3)$_F$ ansatz. Not only can one extend the analysis presented in Chs. 5 and 6 by including η_1 and η_8 final states. The same symmetry-based approach can also be used in B decays.

In order to demonstrate the effectiveness of the SU(3)$_F$ approach we give in the following sections the decompositions needed for phenomenological studies of $D \to PP$ including $P = \eta_1, \eta_8$, $B \to DD$ and $B \to J/\psi P$ including $P = \eta_1, \eta_8$ that we obtain in [504–506].

A.1. Including η_1, η_8 Final States in the Decomposition of $D \to PP$

In the SU(3)$_F$ analysis of charm decays in Chs. 5 and 6 we concentrated on kaon and pion final states only. Here we show how to include also η_1 and η_8 final states. For details on the mixing of η_1 and η_8 to η and η' see [507–509].

In Tables A.1, A.2 and A.3 we list the Clebsch-Gordan coefficients in the SU(3)$_F$ limit as well as including linear breaking of SU(3)$_F$ in full generality. Altogether, including $\eta^{(\prime)}$ leads to 16 additional decay channels, *i.e.*, a total of 33 charm decay channels. In the parameter budget there are four additional SU(3)$_F$ limit matrix elements and nine additional breaking matrix elements.

Decay d	A_{27}^{15}	A_8^{15}	$A_8^{\bar{6}}$	A_1^3	A_8^3	A_8^{15}	$A_8^{\bar{6}}$	A_1^3	A_8^3
SCS									
$D^0 \to \eta_1\pi^0$	0	0	0	0	0	$\frac{2-3\tilde{\Delta}}{2\sqrt{15}}$	$-\frac{1}{\sqrt{6}}$	0	$-\frac{1}{2}\sqrt{3}\tilde{\Delta}$
$D^0 \to \eta_8\pi^0$	$-\frac{1}{5}\sqrt{\frac{3}{2}}\left(\tilde{\Delta}+1\right)$	$\frac{3\tilde{\Delta}-2}{5\sqrt{6}}$	$\frac{1}{\sqrt{15}}$	0	$\sqrt{\frac{3}{10}}\tilde{\Delta}$	0	0	0	0
$D^0 \to \eta_1\eta_1$	0	0	0	0	0	0	0	$\frac{\tilde{\Delta}}{\sqrt{2}}$	0
$D^0 \to \eta_1\eta_8$	0	0	0	0	0	$\frac{1}{\sqrt{5}}$	$-\frac{1}{\sqrt{2}}$	0	0
$D^0 \to \eta_8\eta_8$	$\frac{3}{20}\left(\tilde{\Delta}+2\right)$	$\frac{1}{10}\left(\tilde{\Delta}+2\right)$	$-\frac{1}{\sqrt{10}}$	$-\frac{\tilde{\Delta}}{4}$	$\frac{\tilde{\Delta}}{2\sqrt{5}}$	0	0	0	0
$D^+ \to \eta_1\pi^+$	0	0	0	0	0	$\frac{\tilde{\Delta}-2}{\sqrt{30}}$	$-\frac{1}{\sqrt{3}}$	0	$-\sqrt{\frac{3}{2}}\tilde{\Delta}$
$D^+ \to \eta_8\pi^+$	$-\frac{1}{10}\sqrt{3}\left(\tilde{\Delta}+3\right)$	$-\frac{\tilde{\Delta}-2}{5\sqrt{3}}$	$\sqrt{\frac{2}{15}}$	0	$\sqrt{\frac{3}{5}}\tilde{\Delta}$	0	0	0	0
$D_s \to \eta_1 K^+$	0	0	0	0	0	$\frac{\tilde{\Delta}+2}{\sqrt{30}}$	$\frac{1}{\sqrt{3}}$	0	$-\sqrt{\frac{3}{2}}\tilde{\Delta}$
$D_s \to \eta_8 K^+$	$-\frac{1}{5}\sqrt{3}\left(\tilde{\Delta}+2\right)$	$\frac{\tilde{\Delta}+2}{10\sqrt{3}}$	$\frac{1}{\sqrt{30}}$	0	$-\frac{1}{2}\sqrt{\frac{3}{5}}\tilde{\Delta}$	0	0	0	0
CF									
$D^0 \to \eta_1\bar{K}^0$	0	0	0	0	0	$-\sqrt{\frac{2}{15}}$	$\frac{1}{\sqrt{3}}$	0	0
$D^0 \to \eta_8\bar{K}^0$	$-\frac{\sqrt{3}}{10}$	$-\frac{1}{5\sqrt{3}}$	$\frac{1}{\sqrt{30}}$	0	0	0	0	0	0
$D_s \to \eta_1\pi^+$	0	0	0	0	0	$\sqrt{\frac{2}{15}}$	$\frac{1}{\sqrt{3}}$	0	0
$D_s \to \eta_8\pi^+$	$-\frac{\sqrt{3}}{5}$	$-\frac{2}{5\sqrt{3}}$	$-\sqrt{\frac{2}{15}}$	0	0	0	0	0	0
DCS									
$D^0 \to \eta_1 K^0$	0	0	0	0	0	$-\sqrt{\frac{2}{15}}$	$\frac{1}{\sqrt{3}}$	0	0
$D^0 \to \eta_8 K^0$	$-\frac{\sqrt{3}}{10}$	$-\frac{1}{5\sqrt{3}}$	$\frac{1}{\sqrt{30}}$	0	0	0	0	0	0
$D^+ \to \eta_1 K^+$	0	0	0	0	0	$\sqrt{\frac{2}{15}}$	$\frac{1}{\sqrt{3}}$	0	0
$D^+ \to \eta_8 K^+$	$\frac{\sqrt{3}}{10}$	$\frac{1}{5\sqrt{3}}$	$\frac{1}{\sqrt{30}}$	0	0	0	0	0	0

Table A.1.: Result of the application of the Wigner-Eckart theorem to D decays including η_1 and η_8 in the final state in the SU(3)$_F$ limit. The entries in the table are the Clebsch-Gordan coefficients $c_{d;ij}$ that appear in the expressions for the amplitudes as in Eqs. (5.43)–(5.45). Table taken from [504].

Decay d	$B_1^{3_1}$	$B_1^{3_2}$	$B_8^{3_1}$	$B_8^{3_2}$	$B_8^{\bar{6}_1}$	$B_8^{\bar{6}_2}$	$B_8^{15_1}$	$B_8^{15_2}$	$B_8^{15_3}$	$B_{27}^{15_1}$	$B_{27}^{15_2}$	$B_{27}^{15_3}$	$B_{27}^{24_1}$	$B_{27}^{24_2}$	B_{27}^{42}
SCS															
$D^0 \to \eta_1\pi^0$	0	0	0	0	0	0	0	0	0	0	0	0	0	0	0
$D^0 \to \eta_8\pi^0$	0	0	$\frac{\sqrt{\frac{3}{2}}}{10}$	$\frac{\sqrt{\frac{3}{5}}}{4}$	$\frac{1}{10\sqrt{3}}$	$-\frac{1}{10\sqrt{6}}$	$-\frac{5}{2\sqrt{366}}$	$\frac{\sqrt{\frac{2}{61}}}{15}$	$\frac{1}{20\sqrt{3}}$	$\sqrt{\frac{3}{122}}$	$\frac{9}{20\sqrt{122}}$	$-\frac{\sqrt{3}}{10}$	$\frac{3}{10\sqrt{2}}$	$\frac{\sqrt{\frac{3}{2}}}{5}$	$-\frac{3}{20\sqrt{14}}$
$D^0 \to \eta_1\eta_1$	0	0	0	0	0	0	0	0	0	0	0	0	0	0	0
$D^0 \to \eta_1\eta_8$	0	0	0	0	0	0	0	0	0	0	0	0	0	0	0
$D^0 \to \eta_8\eta_8$	$-\frac{1}{8\sqrt{5}}$	$-\frac{1}{8\sqrt{2}}$	$\frac{1}{20}$	$\frac{1}{4\sqrt{10}}$	$-\frac{1}{10\sqrt{2}}$	$\frac{1}{20}$	$-\frac{11}{20\sqrt{61}}$	$-\frac{2}{5\sqrt{183}}$	$\frac{3}{20\sqrt{2}}$	$-\frac{33}{40\sqrt{61}}$	$-\frac{\sqrt{\frac{3}{61}}}{5}$	$\frac{9}{40\sqrt{2}}$	$\frac{\sqrt{3}}{10}$	$\frac{9}{20}$	$-\frac{2\sqrt{\frac{3}{7}}}{5}$
$D^+ \to \eta_1\pi^+$	0	0	0	0	0	0	0	0	0	0	0	0	0	0	0
$D^+ \to \eta_8\pi^+$	0	0	$\frac{\sqrt{3}}{10}$	$\frac{\sqrt{\frac{3}{10}}}{2}$	$\frac{1}{5\sqrt{6}}$	$-\frac{1}{10\sqrt{3}}$	$\frac{7}{10\sqrt{183}}$	$-\frac{1}{5\sqrt{61}}$	$\frac{1}{10\sqrt{6}}$	$\frac{3\sqrt{\frac{3}{61}}}{5}$	$\frac{23}{40\sqrt{61}}$	$-\frac{\sqrt{\frac{3}{2}}}{5}$	$\frac{1}{20}$	$\frac{\sqrt{3}}{5}$	$\frac{19}{40\sqrt{7}}$
$D_s \to \eta_1 K^+$	0	0	0	0	0	0	0	0	0	0	0	0	0	0	0
$D_s \to \eta_8 K^+$	0	0	$-\frac{\sqrt{3}}{20}$	$-\frac{\sqrt{\frac{3}{10}}}{4}$	$\frac{1}{10\sqrt{6}}$	$-\frac{1}{20\sqrt{3}}$	$-\frac{11}{20\sqrt{183}}$	$-\frac{2}{15\sqrt{61}}$	$\frac{\sqrt{\frac{3}{2}}}{20}$	$\frac{11\sqrt{\frac{3}{61}}}{10}$	$\frac{4}{5\sqrt{61}}$	$-\frac{3\sqrt{\frac{3}{2}}}{10}$	$-\frac{1}{10}$	$-\frac{3\sqrt{3}}{20}$	$-\frac{4}{5\sqrt{7}}$
CF															
$D^0 \to \eta_1\bar{K}^0$	0	0	0	0	0	0	0	0	0	0	0	0	0	0	0
$D^0 \to \eta_8\bar{K}^0$	0	0	0	0	$\frac{1}{5\sqrt{6}}$	$\frac{1}{10\sqrt{3}}$	$-\frac{1}{5\sqrt{183}}$	$-\frac{7}{30\sqrt{61}}$	$-\frac{1}{5\sqrt{6}}$	$-\frac{\sqrt{\frac{3}{61}}}{10}$	$-\frac{7}{20\sqrt{61}}$	$-\frac{\sqrt{\frac{3}{2}}}{10}$	$-\frac{1}{5}$	$-\frac{\sqrt{3}}{5}$	$\frac{1}{2\sqrt{7}}$
$D_s \to \eta_1\pi^+$	0	0	0	0	0	0	0	0	0	0	0	0	0	0	0
$D_s \to \eta_8\pi^+$	0	0	0	0	$-\frac{\sqrt{\frac{2}{3}}}{5}$	$-\frac{1}{5\sqrt{3}}$	$-\frac{2}{5\sqrt{183}}$	$-\frac{7}{15\sqrt{61}}$	$-\frac{\sqrt{\frac{2}{3}}}{5}$	$-\frac{\sqrt{\frac{3}{61}}}{5}$	$-\frac{7}{10\sqrt{61}}$	$-\frac{\sqrt{\frac{3}{2}}}{5}$	$-\frac{1}{10}$	$-\frac{\sqrt{3}}{10}$	$-\frac{1}{2\sqrt{7}}$
DCS															
$D^0 \to \eta_1 K^0$	0	0	0	0	0	0	0	0	0	0	0	0	0	0	0
$D^0 \to \eta_8 K^0$	0	0	0	0	0	$-\frac{1}{5\sqrt{3}}$	$\frac{2}{5\sqrt{183}}$	$\frac{7}{15\sqrt{61}}$	0	$\frac{\sqrt{\frac{3}{61}}}{5}$	$\frac{7}{10\sqrt{61}}$	0	$-\frac{1}{8}$	$-\frac{9\sqrt{3}}{40}$	$\frac{1}{2\sqrt{7}}$
$D^+ \to \eta_1 K^+$	0	0	0	0	0	0	0	0	0	0	0	0	0	0	0
$D^+ \to \eta_8 K^+$	0	0	0	0	0	$-\frac{1}{5\sqrt{3}}$	$-\frac{2}{5\sqrt{183}}$	$-\frac{7}{15\sqrt{61}}$	0	$-\frac{\sqrt{\frac{3}{61}}}{5}$	$-\frac{7}{10\sqrt{61}}$	0	$\frac{1}{8}$	$-\frac{9\sqrt{3}}{40}$	$-\frac{1}{2\sqrt{7}}$

Table A.2.: Result of the application of the Wigner-Eckart theorem to D decays including η_1 and η_8 in the final state for the $\mathrm{SU}(3)_F$-breaking part with **1**, **8** and **27** representations in the final state. The entries in the table are the Clebsch-Gordan coefficients $c_{d;ij}$ that appear in the expressions for the amplitudes as in Eqs. (5.65)–(5.67). Table taken from [504].

Decay d	$B_{\bar{1}}^{3_1}$	$B_{\bar{1}}^{3_2}$	$B_{\bar{8}}^{3_1}$	$B_{\bar{8}}^{3_2}$	$B_{\bar{8}}^{\bar{6}_1}$	$B_{\bar{8}}^{\bar{6}_2}$	$B_{\bar{8}}^{15_1}$	$B_{\bar{8}}^{15_2}$	$B_{\bar{8}}^{15_3}$
SCS									
$D^0 \to \eta_1\pi^0$	0	0	$-\frac{\sqrt{\frac{3}{5}}}{4}$	$-\frac{\sqrt{\frac{3}{2}}}{4}$	$-\frac{1}{2\sqrt{30}}$	$\frac{1}{4\sqrt{15}}$	$\frac{5\sqrt{\frac{5}{183}}}{4}$	$-\frac{1}{3\sqrt{305}}$	$-\frac{1}{4\sqrt{30}}$
$D^0 \to \eta_8\pi^0$	0	0	0	0	0	0	0	0	0
$D^0 \to \eta_1\eta_1$	$\frac{1}{2\sqrt{10}}$	$\frac{1}{4}$	0	0	0	0	0	0	0
$D^0 \to \eta_1\eta_8$	0	0	$\frac{1}{4\sqrt{5}}$	$\frac{1}{4\sqrt{2}}$	$-\frac{1}{2\sqrt{10}}$	$\frac{1}{4\sqrt{5}}$	$-\frac{11}{4\sqrt{305}}$	$-\frac{2}{\sqrt{915}}$	$\frac{3}{4\sqrt{10}}$
$D^0 \to \eta_8\eta_8$	0	0	0	0	0	0	0	0	0
$D^+ \to \eta_1\pi^+$	0	0	$-\frac{\sqrt{\frac{3}{10}}}{2}$	$-\frac{\sqrt{3}}{4}$	$-\frac{1}{2\sqrt{15}}$	$\frac{1}{2\sqrt{30}}$	$-\frac{7}{2\sqrt{1830}}$	$\frac{1}{\sqrt{610}}$	$-\frac{1}{4\sqrt{15}}$
$D^+ \to \eta_8\pi^+$	0	0	0	0	0	0	0	0	0
$D_s \to \eta_1 K^+$	0	0	$-\frac{\sqrt{\frac{3}{10}}}{2}$	$-\frac{\sqrt{3}}{4}$	$\frac{1}{2\sqrt{15}}$	$-\frac{1}{2\sqrt{30}}$	$-\frac{11}{2\sqrt{1830}}$	$-\frac{2\sqrt{\frac{2}{305}}}{3}$	$\frac{\sqrt{\frac{3}{5}}}{4}$
$D_s \to \eta_8 K^+$	0	0	0	0	0	0	0	0	0
CF									
$D^0 \to \eta_1\bar{K}^0$	0	0	0	0	$\frac{1}{\sqrt{15}}$	$\frac{1}{\sqrt{30}}$	$-\sqrt{\frac{2}{915}}$	$-\frac{7}{3\sqrt{610}}$	$-\frac{1}{\sqrt{15}}$
$D^0 \to \eta_8\bar{K}^0$	0	0	0	0	0	0	0	0	0
$D_s \to \eta_1\pi^+$	0	0	0	0	$\frac{1}{\sqrt{15}}$	$\frac{1}{\sqrt{30}}$	$\sqrt{\frac{2}{915}}$	$\frac{7}{3\sqrt{610}}$	$\frac{1}{\sqrt{15}}$
$D_s \to \eta_8\pi^+$	0	0	0	0	0	0	0	0	0
DCS									
$D^0 \to \eta_1 K^0$	0	0	0	0	0	$-\sqrt{\frac{2}{15}}$	$2\sqrt{\frac{2}{915}}$	$\frac{7\sqrt{\frac{2}{305}}}{3}$	0
$D^0 \to \eta_8 K^0$	0	0	0	0	0	0	0	0	0
$D^+ \to \eta_1 K^+$	0	0	0	0	0	$-\sqrt{\frac{2}{15}}$	$-2\sqrt{\frac{2}{915}}$	$-\frac{7\sqrt{\frac{2}{305}}}{3}$	0
$D^+ \to \eta_8 K^+$	0	0	0	0	0	0	0	0	0

Table A.3.: Result of the application of the Wigner-Eckart theorem to D decays including η_1 and η_8 in the final state for the SU(3)$_F$-breaking part with $\tilde{\mathbf{1}}$ and $\tilde{\mathbf{8}}$ representations in the final state. The entries in the table are the Clebsch-Gordan coefficients $c_{d;ij}$ that appear in the expressions for the amplitudes as in Eqs. (5.65)–(5.67). Table taken from [504].

A.2. Decomposition of $B \to DD$

In this work, the $SU(3)_F$ ansatz has so far been applied to charm decays only. The same formalism applies also to nonleptonic B decays. An $SU(3)_F$ analysis of $B \to DD$ including also the recent data [510] is desirable. Therefore, we give here the complete $SU(3)_F$ decomposition of these decay channels [505].

Firstly, we write down the initial and final states. In the initial state we have the following B mesons:

$$\left|\bar{B}^0\right\rangle = \left|\bar{d}b\right\rangle = \left|\bar{\mathbf{3}}\right\rangle_{\frac{1}{2},\frac{1}{2},-\frac{1}{3}} , \quad \left|\bar{B}_s\right\rangle = |\bar{s}b\rangle = \left|\bar{\mathbf{3}}\right\rangle_{0,0,\frac{2}{3}} , \quad \left|B^-\right\rangle = -|\bar{u}b\rangle = \left|\bar{\mathbf{3}}\right\rangle_{\frac{1}{2},-\frac{1}{2},-\frac{1}{3}} . \tag{A.1}$$

In the final state there are the following D mesons:

$$\left|D^0\right\rangle = -|c\bar{u}\rangle = \left|\bar{\mathbf{3}}\right\rangle_{\frac{1}{2},-\frac{1}{2},-\frac{1}{3}} , \qquad \left|\bar{D}^0\right\rangle = |\bar{c}u\rangle = |\mathbf{3}\rangle_{\frac{1}{2},\frac{1}{2},\frac{1}{3}} , \tag{A.2}$$

$$\left|D^+\right\rangle = \left|c\bar{d}\right\rangle = \left|\bar{\mathbf{3}}\right\rangle_{\frac{1}{2},\frac{1}{2},-\frac{1}{3}} , \qquad \left|D^-\right\rangle = |\bar{c}d\rangle = |\mathbf{3}\rangle_{\frac{1}{2},-\frac{1}{2},\frac{1}{3}} , \tag{A.3}$$

$$\left|D_s^+\right\rangle = |c\bar{s}\rangle = \left|\bar{\mathbf{3}}\right\rangle_{0,0,\frac{2}{3}} , \qquad \left|D_s^-\right\rangle = |\bar{c}s\rangle = |\mathbf{3}\rangle_{0,0,-\frac{2}{3}} . \tag{A.4}$$

The considered product final states are given as

$$\left|D^-D^0\right\rangle = |\mathbf{8}\rangle_{1,-1,0} , \quad \left|D_s^-D^0\right\rangle = |\mathbf{8}\rangle_{1/2,-1/2,-1} , \quad \left|D_s^-D^+\right\rangle = |\mathbf{8}\rangle_{1/2,1/2,-1} , \tag{A.5}$$

$$\left|D^-D_s^+\right\rangle = |\mathbf{8}\rangle_{1/2,-1/2,1} , \tag{A.6}$$

$$\left|D^-D^+\right\rangle = -\sqrt{\frac{1}{3}}\,|\mathbf{1}\rangle_{0,0,0} - \sqrt{\frac{1}{6}}\,|\mathbf{8}\rangle_{0,0,0} + \sqrt{\frac{1}{2}}\,|\mathbf{8}\rangle_{1,0,0} , \tag{A.7}$$

$$\left|D_s^-D_s^+\right\rangle = -\sqrt{\frac{1}{3}}\,|\mathbf{1}\rangle_{0,0,0} + \sqrt{\frac{2}{3}}\,|\mathbf{8}\rangle_{0,0,0} , \tag{A.8}$$

$$\left|\bar{D}^0D^0\right\rangle = \sqrt{\frac{1}{3}}\,|\mathbf{1}\rangle_{0,0,0} + \sqrt{\frac{1}{6}}\,|\mathbf{8}\rangle_{0,0,0} + \sqrt{\frac{1}{2}}\,|\mathbf{8}\rangle_{1,0,0} . \tag{A.9}$$

In Eqs. (A.5)–(A.9) no symmetrization is necessary as the final state of triplet and antitriplet does of course not have a Bose symmetry. The flavor structure of the relevant $\Delta B = 1$, $\Delta C = 0$ tree operators is given as [511]

$$\mathcal{H} \sim V_{ub}V_{ud}^*(b\bar{u})(u\bar{d}) + V_{ub}V_{us}^*(b\bar{u})(u\bar{s}) + V_{cb}V_{cd}^*(b\bar{c})(c\bar{d}) + V_{cb}V_{cs}^*(b\bar{c})(c\bar{s}). \tag{A.10}$$

Note that the matrix elements of the additional triplet operators from the penguins can be absorbed into the matrix elements of the tree operators. Furthermore, we absorb global

prefactors into the SU(3)$_F$ matrix elements. The operators in Eq. (A.10) have the following SU(3)$_F$ structure:

$$(b\bar{u})(u\bar{d}) = \frac{1}{2}\sqrt{\frac{3}{2}}\mathbf{3}_{\frac{1}{2},-\frac{1}{2},\frac{1}{3}} - \frac{1}{2}\bar{\mathbf{6}}_{\frac{1}{2},-\frac{1}{2},\frac{1}{3}} + \frac{1}{2\sqrt{6}}\mathbf{15}_{\frac{1}{2},-\frac{1}{2},\frac{1}{3}} + \sqrt{\frac{1}{3}}\mathbf{15}_{\frac{3}{2},-\frac{1}{2},\frac{1}{3}}\,, \tag{A.11}$$

$$(b\bar{u})(u\bar{s}) = \frac{1}{2}\sqrt{\frac{3}{2}}\mathbf{3}_{0,0,-\frac{2}{3}} + \frac{1}{2}\bar{\mathbf{6}}_{1,0,-\frac{2}{3}} + \frac{1}{2\sqrt{2}}\mathbf{15}_{0,0,-\frac{2}{3}} + \frac{1}{2}\mathbf{15}_{1,0,-\frac{2}{3}}\,, \tag{A.12}$$

$$(b\bar{c})(c\bar{d}) = \mathbf{3}_{\frac{1}{2},-\frac{1}{2},\frac{1}{3}}\,, \tag{A.13}$$

$$(b\bar{c})(c\bar{s}) = \mathbf{3}_{0,0,-\frac{2}{3}}. \tag{A.14}$$

The SU(3)$_F$ limit and linear order breaking Clebsch-Gordan coefficients are listed in Tables A.4, A.5 and A.6. In these tables we write for the CKM factors $\lambda_{cd} \equiv V_{cb}V_{cd}^*$, $\lambda_{cs} \equiv V_{cb}V_{cs}^*$, $\lambda_{ud} \equiv V_{ub}V_{ud}^*$ and $\lambda_{us} \equiv V_{ub}V_{us}^*$. Note that in the SU(3)$_F$ breaking we differentiate between representations coming from $\mathbf{8}\otimes\mathbf{3}$, $\mathbf{8}\otimes\bar{\mathbf{6}}$ and $\mathbf{8}\otimes\mathbf{15}$, respectively. We indicate this where necessary *e.g.* by the notation "B_8^{3u3}" for a matrix element with a $\mathbf{3}$ coming from $\mathbf{8}\otimes\mathbf{3}$ and "$B_8^{3u\bar{6}}$" for a matrix element with a $\mathbf{3}$ coming from $\mathbf{8}\otimes\bar{\mathbf{6}}$.

Decay d	A_8^{3c}	A_1^{3c}	A_8^{15u}	$A_8^{\bar{6}u}$	A_8^{3u}	A_1^{3u}
$B^- \to D^- D^0$	λ_{cd}	0	$-\frac{1}{2}\sqrt{\frac{3}{10}}\lambda_{ud}$	$-\frac{\lambda_{ud}}{2\sqrt{3}}$	$\frac{1}{2}\sqrt{\frac{3}{2}}\lambda_{ud}$	0
$B^- \to D_s^- D^0$	λ_{cs}	0	$-\frac{1}{2}\sqrt{\frac{3}{10}}\lambda_{us}$	$-\frac{\lambda_{us}}{2\sqrt{3}}$	$\frac{1}{2}\sqrt{\frac{3}{2}}\lambda_{us}$	0
$\bar{B}^0 \to D_s^- D^+$	λ_{cs}	0	$\frac{\lambda_{us}}{2\sqrt{30}}$	$\frac{\lambda_{us}}{2\sqrt{3}}$	$\frac{1}{2}\sqrt{\frac{3}{2}}\lambda_{us}$	0
$\bar{B}_s \to D^- D_s^+$	λ_{cd}	0	$\frac{\lambda_{ud}}{2\sqrt{30}}$	$\frac{\lambda_{ud}}{2\sqrt{3}}$	$\frac{1}{2}\sqrt{\frac{3}{2}}\lambda_{ud}$	0
$\bar{B}^0 \to D^- D^+$	$\frac{2}{3}\lambda_{cd}$	$-\frac{1}{3}\lambda_{cd}$	$\frac{\lambda_{ud}}{\sqrt{30}}$	0	$\frac{\lambda_{ud}}{\sqrt{6}}$	$-\frac{\lambda_{ud}}{2\sqrt{6}}$
$\bar{B}_s \to D_s^- D_s^+$	$\frac{2}{3}\lambda_{cs}$	$-\frac{1}{3}\lambda_{cs}$	$\frac{\lambda_{us}}{\sqrt{30}}$	0	$\frac{\lambda_{us}}{\sqrt{6}}$	$-\frac{\lambda_{us}}{2\sqrt{6}}$
$\bar{B}^0 \to D_s^- D_s^+$	$-\frac{1}{3}\lambda_{cd}$	$-\frac{1}{3}\lambda_{cd}$	$\frac{\lambda_{ud}}{2\sqrt{30}}$	$-\frac{\lambda_{ud}}{2\sqrt{3}}$	$-\frac{\lambda_{ud}}{2\sqrt{6}}$	$-\frac{\lambda_{ud}}{2\sqrt{6}}$
$\bar{B}_s \to D^- D^+$	$-\frac{1}{3}\lambda_{cs}$	$-\frac{1}{3}\lambda_{cs}$	$\frac{\lambda_{us}}{2\sqrt{30}}$	$-\frac{\lambda_{us}}{2\sqrt{3}}$	$-\frac{\lambda_{us}}{2\sqrt{6}}$	$-\frac{\lambda_{us}}{2\sqrt{6}}$
$\bar{B}^0 \to \bar{D}^0 D^0$	$\frac{1}{3}\lambda_{cd}$	$\frac{1}{3}\lambda_{cd}$	$\frac{1}{2}\sqrt{\frac{3}{10}}\lambda_{ud}$	$-\frac{\lambda_{ud}}{2\sqrt{3}}$	$\frac{\lambda_{ud}}{2\sqrt{6}}$	$\frac{\lambda_{ud}}{2\sqrt{6}}$
$\bar{B}_s \to \bar{D}^0 D^0$	$\frac{1}{3}\lambda_{cs}$	$\frac{1}{3}\lambda_{cs}$	$\frac{1}{2}\sqrt{\frac{3}{10}}\lambda_{us}$	$-\frac{\lambda_{us}}{2\sqrt{3}}$	$\frac{\lambda_{us}}{2\sqrt{6}}$	$\frac{\lambda_{us}}{2\sqrt{6}}$

Table A.4.: The Clebsch-Gordan coefficients of the $SU(3)_F$ limit decomposition of $B \to DD$ decays, including explicitly the CKM factors. Table taken from [505].

Decay d	B_1^{3c}	B_8^{3c}	$B_8^{\bar{6}c}$	B_8^{15c}
$B^- \to D^- D^0$	0	$-\frac{1}{4}\lambda_{cd}$	$-\frac{\lambda_{cd}}{2\sqrt{2}}$	$-\frac{\lambda_{cd}}{4\sqrt{5}}$
$B^- \to D_s^- D^0$	0	$\frac{1}{2}\lambda_{cs}$	0	$-\frac{\lambda_{cs}}{2\sqrt{5}}$
$\bar{B}^0 \to D_s^- D^+$	0	$\frac{1}{2}\lambda_{cs}$	0	$-\frac{\lambda_{cs}}{2\sqrt{5}}$
$\bar{B}_s \to D^- D_s^+$	0	$-\frac{1}{4}\lambda_{cd}$	$\frac{\lambda_{cd}}{2\sqrt{2}}$	$\frac{3\lambda_{cd}}{4\sqrt{5}}$
$\bar{B}^0 \to D^- D^+$	$\frac{1}{12}\lambda_{cd}$	$-\frac{1}{6}\lambda_{cd}$	0	$-\frac{\lambda_{cd}}{2\sqrt{5}}$
$\bar{B}_s \to D_s^- D_s^+$	$-\frac{1}{6}\lambda_{cs}$	$\frac{1}{3}\lambda_{cs}$	0	$\frac{\lambda_{cs}}{\sqrt{5}}$
$\bar{B}^0 \to D_s^- D_s^+$	$\frac{1}{12}\lambda_{cd}$	$\frac{1}{12}\lambda_{cd}$	$-\frac{\lambda_{cd}}{2\sqrt{2}}$	$\frac{3\lambda_{cd}}{4\sqrt{5}}$
$\bar{B}_s \to D^- D^+$	$-\frac{1}{6}\lambda_{cs}$	$-\frac{1}{6}\lambda_{cs}$	0	$-\frac{\lambda_{cs}}{2\sqrt{5}}$
$\bar{B}^0 \to \bar{D}^0 D^0$	$-\frac{1}{12}\lambda_{cd}$	$-\frac{1}{12}\lambda_{cd}$	$-\frac{\lambda_{cd}}{2\sqrt{2}}$	$\frac{\lambda_{cd}}{4\sqrt{5}}$
$\bar{B}_s \to \bar{D}^0 D^0$	$\frac{1}{6}\lambda_{cs}$	$\frac{1}{6}\lambda_{cs}$	0	$\frac{\lambda_{cs}}{2\sqrt{5}}$

Table A.5.: The Clebsch-Gordan coefficients of the linear SU(3)$_F$-breaking decomposition of $B \to DD$ decays coming with λ_{cd} and λ_{cs}, including explicitly the CKM factors. Table taken from [505].

Decay d	B_1^{3u3}	$B_1^{3u\bar{6}}$	B_1^{3u15}	B_8^{3u3}	$B_8^{3u\bar{6}}$	B_8^{3u15}	$B_8^{\bar{6}u3}$	$B_8^{\bar{6}u\bar{6}}$	$B_8^{\bar{6}u15}$	B_8^{15u3}	$B_8^{15u\bar{6}}$	$B_8^{15_1u15}$	$B_8^{15_2u15}$
$B^- \to D^- D^0$	0	0	0	$-\frac{1}{8}\sqrt{\frac{3}{2}}\lambda_{ud}$	$-\frac{1}{8}\sqrt{3}\lambda_{ud}$	$-\frac{1}{8}\sqrt{\frac{3}{10}}\lambda_{ud}$	$-\frac{1}{8}\sqrt{3}\lambda_{ud}$	$\frac{\lambda_{ud}}{4\sqrt{30}}$	$-\frac{\lambda_{ud}}{8\sqrt{15}}$	$-\frac{1}{8}\sqrt{\frac{3}{10}}\lambda_{ud}$	$-\frac{\lambda_{ud}}{8\sqrt{15}}$	$\frac{1}{3}\sqrt{\frac{2}{305}}\lambda_{ud}$	$-\frac{13}{8}\sqrt{\frac{3}{610}}\lambda_{ud}$
$B^- \to D_s^- D^0$	0	0	0	$\frac{1}{4}\sqrt{\frac{3}{2}}\lambda_{us}$	0	$-\frac{1}{4}\sqrt{\frac{3}{10}}\lambda_{us}$	0	$-\frac{\lambda_{us}}{2\sqrt{30}}$	$\frac{\lambda_{us}}{2\sqrt{15}}$	$-\frac{1}{4}\sqrt{\frac{3}{10}}\lambda_{us}$	$\frac{\lambda_{us}}{2\sqrt{15}}$	$-\frac{1}{3}\sqrt{\frac{5}{122}}\lambda_{us}$	$\frac{1}{4}\sqrt{\frac{3}{610}}\lambda_{us}$
$\bar{B}^0 \to D_s^- D^+$	0	0	0	$\frac{1}{4}\sqrt{\frac{3}{2}}\lambda_{us}$	0	$-\frac{1}{4}\sqrt{\frac{3}{10}}\lambda_{us}$	0	$\frac{\lambda_{us}}{2\sqrt{30}}$	$-\frac{\lambda_{us}}{2\sqrt{15}}$	$-\frac{1}{4}\sqrt{\frac{3}{10}}\lambda_{us}$	$-\frac{\lambda_{us}}{2\sqrt{15}}$	$\frac{1}{3}\sqrt{\frac{2}{305}}\lambda_{us}$	$\frac{11\lambda_{us}}{4\sqrt{1830}}$
$\bar{B}_s \to D^- D_s^+$	0	0	0	$-\frac{1}{8}\sqrt{\frac{3}{2}}\lambda_{ud}$	$-\frac{1}{8}\sqrt{3}\lambda_{ud}$	$-\frac{1}{8}\sqrt{\frac{3}{10}}\lambda_{ud}$	$\frac{1}{8}\sqrt{3}\lambda_{ud}$	$-\frac{\lambda_{ud}}{4\sqrt{30}}$	$\frac{\lambda_{ud}}{8\sqrt{15}}$	$\frac{3}{8}\sqrt{\frac{3}{10}}\lambda_{ud}$	$\frac{1}{8}\sqrt{\frac{3}{5}}\lambda_{ud}$	$-\frac{\lambda_{ud}}{3\sqrt{610}}$	$-\frac{11\lambda_{ud}}{8\sqrt{1830}}$
$\bar{B}^0 \to D^- D^+$	$\frac{\lambda_{ud}}{8\sqrt{6}}$	$\frac{\lambda_{ud}}{8\sqrt{3}}$	$\frac{\lambda_{ud}}{8\sqrt{30}}$	$-\frac{\lambda_{ud}}{4\sqrt{6}}$	$-\frac{\lambda_{ud}}{4\sqrt{3}}$	$-\frac{\lambda_{ud}}{4\sqrt{30}}$	0	0	0	$-\frac{1}{4}\sqrt{\frac{3}{10}}\lambda_{ud}$	$-\frac{\lambda_{ud}}{4\sqrt{15}}$	$-\frac{\lambda_{ud}}{3\sqrt{610}}$	$\frac{5}{4}\sqrt{\frac{5}{366}}\lambda_{ud}$
$\bar{B}_s \to D_s^- D_s^+$	$-\frac{\lambda_{us}}{4\sqrt{6}}$	0	$\frac{\lambda_{us}}{4\sqrt{30}}$	$\frac{\lambda_{us}}{2\sqrt{6}}$	0	$-\frac{\lambda_{us}}{2\sqrt{30}}$	0	0	0	$\frac{1}{2}\sqrt{\frac{3}{10}}\lambda_{us}$	0	$\frac{\lambda_{us}}{\sqrt{610}}$	$-\frac{7\lambda_{us}}{2\sqrt{1830}}$
$\bar{B}^0 \to D_s^- D_s^+$	$\frac{\lambda_{ud}}{8\sqrt{6}}$	$\frac{\lambda_{ud}}{8\sqrt{3}}$	$\frac{\lambda_{ud}}{8\sqrt{30}}$	$\frac{\lambda_{ud}}{8\sqrt{6}}$	$\frac{\lambda_{ud}}{8\sqrt{3}}$	$\frac{\lambda_{ud}}{8\sqrt{30}}$	$-\frac{1}{8}\sqrt{3}\lambda_{ud}$	$\frac{\lambda_{ud}}{4\sqrt{30}}$	$-\frac{\lambda_{ud}}{8\sqrt{15}}$	$\frac{3}{8}\sqrt{\frac{3}{10}}\lambda_{ud}$	$\frac{1}{8}\sqrt{\frac{3}{5}}\lambda_{ud}$	$-\frac{\lambda_{ud}}{3\sqrt{610}}$	$-\frac{11\lambda_{ud}}{8\sqrt{1830}}$
$\bar{B}_s \to D^- D^+$	$-\frac{\lambda_{us}}{4\sqrt{6}}$	0	$\frac{\lambda_{us}}{4\sqrt{30}}$	$-\frac{\lambda_{us}}{4\sqrt{6}}$	0	$\frac{\lambda_{us}}{4\sqrt{30}}$	0	$-\frac{\lambda_{us}}{2\sqrt{30}}$	$\frac{\lambda_{us}}{2\sqrt{15}}$	$-\frac{1}{4}\sqrt{\frac{3}{10}}\lambda_{us}$	$-\frac{\lambda_{us}}{2\sqrt{15}}$	$\frac{1}{3}\sqrt{\frac{2}{305}}\lambda_{us}$	$\frac{11\lambda_{us}}{4\sqrt{1830}}$
$\bar{B}^0 \to \bar{D}^0 D^0$	$-\frac{\lambda_{ud}}{8\sqrt{6}}$	$-\frac{\lambda_{ud}}{8\sqrt{3}}$	$-\frac{\lambda_{ud}}{8\sqrt{30}}$	$-\frac{\lambda_{ud}}{8\sqrt{6}}$	$-\frac{\lambda_{ud}}{8\sqrt{3}}$	$-\frac{\lambda_{ud}}{8\sqrt{30}}$	$-\frac{1}{8}\sqrt{3}\lambda_{ud}$	$\frac{\lambda_{ud}}{4\sqrt{30}}$	$-\frac{\lambda_{ud}}{8\sqrt{15}}$	$\frac{1}{8}\sqrt{\frac{3}{10}}\lambda_{ud}$	$\frac{\lambda_{ud}}{8\sqrt{15}}$	$-\frac{1}{3}\sqrt{\frac{2}{305}}\lambda_{ud}$	$\frac{13}{8}\sqrt{\frac{3}{610}}\lambda_{ud}$
$\bar{B}_s \to \bar{D}^0 D^0$	$\frac{\lambda_{us}}{4\sqrt{6}}$	0	$-\frac{\lambda_{us}}{4\sqrt{30}}$	$\frac{\lambda_{us}}{4\sqrt{6}}$	0	$-\frac{\lambda_{us}}{4\sqrt{30}}$	0	$-\frac{\lambda_{us}}{2\sqrt{30}}$	$\frac{\lambda_{us}}{2\sqrt{15}}$	$\frac{1}{4}\sqrt{\frac{3}{10}}\lambda_{us}$	$-\frac{\lambda_{us}}{2\sqrt{15}}$	$\frac{1}{3}\sqrt{\frac{5}{122}}\lambda_{us}$	$-\frac{1}{4}\sqrt{\frac{3}{610}}\lambda_{us}$

Table A.6.: The Clebsch-Gordan coefficients of the linear $SU(3)_F$-breaking decomposition of $B \to DD$ decays coming with λ_{ud} and λ_{us}, including explicitly the CKM factors. Table taken from [505].

A.3. Including η_1, η_8 Final States in the Decomposition of $B \to J/\psi P$

A recent SU(3)$_F$ analysis of $B \to J/\psi P$ decays with P = kaons and pions has been given in [512]. Here, we give the SU(3)$_F$ decomposition including also $P = \eta_1, \eta_8$ in the final state [506]. The initial states of the $B \to J/\psi P$ decay channels are

$$\bar{B}^0 = \left|\bar{d}b\right\rangle = \left|\bar{\mathbf{3}}\right\rangle_{\frac{1}{2},\frac{1}{2},-\frac{1}{3}} , \quad \bar{B}_s = |\bar{s}b\rangle = \left|\bar{\mathbf{3}}\right\rangle_{0,0,\frac{2}{3}} , \quad B^- = -|\bar{u}b\rangle = \left|\bar{\mathbf{3}}\right\rangle_{\frac{1}{2},-\frac{1}{2},-\frac{1}{3}} . \tag{A.15}$$

The product final states (with a trivial product) are given as follows:

$$J/\psi \bar{K}^0 = |\bar{c}c\rangle \left|s\bar{d}\right\rangle = |\mathbf{8}\rangle_{\frac{1}{2},\frac{1}{2},-1} , \tag{A.16}$$

$$J/\psi \pi^0 = |\bar{c}c\rangle \left|\frac{1}{\sqrt{2}}(u\bar{u} - d\bar{d})\right\rangle = |\mathbf{8}\rangle_{1,0,0} , \tag{A.17}$$

$$J/\psi K^- = -|\bar{c}c\rangle\,|s\bar{u}\rangle = |\mathbf{8}\rangle_{\frac{1}{2},-\frac{1}{2},-1} , \tag{A.18}$$

$$J/\psi \pi^- = -|\bar{c}c\rangle\,|d\bar{u}\rangle = |\mathbf{8}\rangle_{1,-1,0} , \tag{A.19}$$

$$J/\psi K^0 = |\bar{c}c\rangle\,|d\bar{s}\rangle = |\mathbf{8}\rangle_{\frac{1}{2},-\frac{1}{2},1} , \tag{A.20}$$

$$J/\psi \eta_1 = |\mathbf{1}\rangle_{0,0,0} , \tag{A.21}$$

$$J/\psi \eta_8 = |\mathbf{8}\rangle_{0,0,0} . \tag{A.22}$$

The Hamiltonian is the same as for $B \to DD$ decays in Eq. (A.10). We give the Clebsch-Gordan coefficients including linear SU(3)$_F$ breaking in the Tables A.7, A.8 and A.9.

Decay d	A_8^{3c}	A_1^{3c}	A_8^{15u}	$A_8^{\bar{6}u}$	A_8^{3u}	A_1^{3u}
$\bar{B}^0 \to J/\psi \bar{K}^0$	λ_{cs}	0	$\frac{\lambda_{us}}{2\sqrt{30}}$	$\frac{\lambda_{us}}{2\sqrt{3}}$	$\frac{1}{2}\sqrt{\frac{3}{2}}\lambda_{us}$	0
$\bar{B}^0 \to J/\psi \pi^0$	$\frac{\lambda_{cd}}{\sqrt{2}}$	0	$\frac{1}{4}\sqrt{\frac{5}{3}}\lambda_{ud}$	$-\frac{\lambda_{ud}}{2\sqrt{6}}$	$\frac{1}{4}\sqrt{3}\lambda_{ud}$	0
$B^- \to J/\psi K^-$	λ_{cs}	0	$-\frac{1}{2}\sqrt{\frac{3}{10}}\lambda_{us}$	$-\frac{\lambda_{us}}{2\sqrt{3}}$	$\frac{1}{2}\sqrt{\frac{3}{2}}\lambda_{us}$	0
$B^- \to J/\psi \pi^-$	λ_{cd}	0	$-\frac{1}{2}\sqrt{\frac{3}{10}}\lambda_{ud}$	$-\frac{\lambda_{ud}}{2\sqrt{3}}$	$\frac{1}{2}\sqrt{\frac{3}{2}}\lambda_{ud}$	0
$\bar{B}_s \to J/\psi \pi^0$	0	0	$\frac{\lambda_{us}}{\sqrt{15}}$	$-\frac{\lambda_{us}}{\sqrt{6}}$	0	0
$\bar{B}_s \to J/\psi K^0$	λ_{cd}	0	$\frac{\lambda_{ud}}{2\sqrt{30}}$	$\frac{\lambda_{ud}}{2\sqrt{3}}$	$\frac{1}{2}\sqrt{\frac{3}{2}}\lambda_{ud}$	0
$\bar{B}^0 \to J/\psi \eta_1$	0	$\frac{\lambda_{cd}}{\sqrt{3}}$	0	0	0	$\frac{\lambda_{ud}}{2\sqrt{2}}$
$\bar{B}^0 \to J/\psi \eta_8$	$-\frac{\lambda_{cd}}{\sqrt{6}}$	0	$\frac{\lambda_{ud}}{4\sqrt{5}}$	$-\frac{\lambda_{ud}}{2\sqrt{2}}$	$-\frac{\lambda_{ud}}{4}$	0
$\bar{B}_s \to J/\psi \eta_1$	0	$\frac{\lambda_{cs}}{\sqrt{3}}$	0	0	0	$\frac{\lambda_{us}}{2\sqrt{2}}$
$\bar{B}_s \to J/\psi \eta_8$	$\sqrt{\frac{2}{3}}\lambda_{cs}$	0	$\frac{\lambda_{us}}{2\sqrt{5}}$	0	$\frac{\lambda_{us}}{2}$	0

Table A.7.: The Clebsch-Gordan coefficients of the $SU(3)_F$ limit decomposition of $B \to J/\psi P$ decays, including explicitly the CKM factors. The results for kaon and pion final states agree with [512]. Table taken from [506].

Decay d	B_1^{3c}	B_8^{3c}	$B_8^{\bar{6}c}$	B_8^{15c}
$\bar{B}^0 \to J/\psi \bar{K}^0$	0	$\frac{\lambda_{cs}}{2}$	0	$-\frac{\lambda_{cs}}{2\sqrt{5}}$
$\bar{B}^0 \to J/\psi \pi^0$	0	$-\frac{\lambda_{cd}}{4\sqrt{2}}$	$-\frac{\lambda_{cd}}{4}$	$-\frac{\lambda_{cd}}{4\sqrt{10}}$
$B^- \to J/\psi K^-$	0	$\frac{\lambda_{cs}}{2}$	0	$-\frac{\lambda_{cs}}{2\sqrt{5}}$
$B^- \to J/\psi \pi^-$	0	$-\frac{\lambda_{cd}}{4}$	$-\frac{\lambda_{cd}}{2\sqrt{2}}$	$-\frac{\lambda_{cd}}{4\sqrt{5}}$
$\bar{B}_s \to J/\psi \pi^0$	0	0	0	0
$\bar{B}_s \to J/\psi K^0$	0	$-\frac{\lambda_{cd}}{4}$	$\frac{\lambda_{cd}}{2\sqrt{2}}$	$\frac{3\lambda_{cd}}{4\sqrt{5}}$
$\bar{B}^0 \to J/\psi \eta_1$	$-\frac{\lambda_{cd}}{4\sqrt{3}}$	0	0	0
$\bar{B}^0 \to J/\psi \eta_8$	0	$\frac{\lambda_{cd}}{4\sqrt{6}}$	$-\frac{1}{4}\sqrt{3}\lambda_{cd}$	$\frac{3}{4}\sqrt{\frac{3}{10}}\lambda_{cd}$
$\bar{B}_s \to J/\psi \eta_1$	$\frac{\lambda_{cs}}{2\sqrt{3}}$	0	0	0
$\bar{B}_s \to J/\psi \eta_8$	0	$\frac{\lambda_{cs}}{\sqrt{6}}$	0	$\sqrt{\frac{3}{10}}\lambda_{cs}$

Table A.8.: The Clebsch-Gordan coefficients of the linear SU(3)$_F$-breaking decomposition of $B \to J/\psi P$ decays coming with λ_{cd} and λ_{cs}, including explicitly the CKM factors. The results for kaon and pion final states agree with [512]. Table taken from [506].

Decay d	B_1^{3u3}	$B_1^{3u\bar{6}}$	B_1^{3u15}	B_8^{3u3}	$B_8^{3u\bar{6}}$	B_8^{3u15}	$B_8^{\bar{6}u3}$	$B_8^{\bar{6}u\bar{6}}$	$B_8^{\bar{6}u15}$	B_8^{15u3}	$B_8^{15u\bar{6}}$	$B_8^{15_1u15}$	$B_8^{15_2u15}$
$\bar{B}^0 \to J/\psi \bar{K}^0$	0	0	0	$\frac{1}{4}\sqrt{\frac{3}{2}}\lambda_{us}$	0	$-\frac{1}{4}\sqrt{\frac{3}{10}}\lambda_{us}$	0	$\frac{\lambda_{us}}{2\sqrt{30}}$	$-\frac{\lambda_{us}}{2\sqrt{15}}$	$-\frac{1}{4}\sqrt{\frac{3}{10}}\lambda_{us}$	$-\frac{\lambda_{us}}{2\sqrt{15}}$	$\frac{1}{3}\sqrt{\frac{2}{305}}\lambda_{us}$	$\frac{11\lambda_{us}}{4\sqrt{1830}}$
$\bar{B}^0 \to J/\psi \pi^0$	0	0	0	$-\frac{1}{16}\sqrt{3}\lambda_{ud}$	$-\frac{1}{8}\sqrt{\frac{3}{2}}\lambda_{ud}$	$-\frac{1}{16}\sqrt{\frac{3}{5}}\lambda_{ud}$	$-\frac{1}{8}\sqrt{\frac{3}{2}}\lambda_{ud}$	$\frac{\lambda_{ud}}{8\sqrt{15}}$	$-\frac{\lambda_{ud}}{8\sqrt{30}}$	$-\frac{1}{16}\sqrt{\frac{3}{5}}\lambda_{ud}$	$-\frac{\lambda_{ud}}{8\sqrt{30}}$	$-\frac{\lambda_{ud}}{2\sqrt{305}}$	$\frac{89\lambda_{ud}}{16\sqrt{915}}$
$B^- \to J/\psi K^-$	0	0	0	$\frac{1}{4}\sqrt{\frac{3}{2}}\lambda_{us}$	0	$-\frac{1}{4}\sqrt{\frac{3}{10}}\lambda_{us}$	0	$-\frac{\lambda_{us}}{2\sqrt{30}}$	$\frac{\lambda_{us}}{2\sqrt{15}}$	$-\frac{1}{4}\sqrt{\frac{3}{10}}\lambda_{us}$	$\frac{\lambda_{us}}{2\sqrt{15}}$	$-\frac{1}{3}\sqrt{\frac{5}{122}}\lambda_{us}$	$\frac{1}{4}\sqrt{\frac{3}{610}}\lambda_{us}$
$B^- \to J/\psi \pi^-$	0	0	0	$-\frac{1}{8}\sqrt{\frac{3}{2}}\lambda_{ud}$	$-\frac{1}{8}\sqrt{3}\lambda_{ud}$	$-\frac{1}{8}\sqrt{\frac{3}{10}}\lambda_{ud}$	$-\frac{1}{8}\sqrt{3}\lambda_{ud}$	$\frac{\lambda_{ud}}{4\sqrt{30}}$	$-\frac{\lambda_{ud}}{8\sqrt{15}}$	$-\frac{1}{8}\sqrt{\frac{3}{10}}\lambda_{ud}$	$-\frac{\lambda_{ud}}{8\sqrt{15}}$	$\frac{1}{3}\sqrt{\frac{2}{305}}\lambda_{ud}$	$-\frac{13}{8}\sqrt{\frac{3}{610}}\lambda_{ud}$
$\bar{B}_s \to J/\psi \pi^0$	0	0	0	0	0	0	0	$-\frac{\lambda_{us}}{2\sqrt{15}}$	$\frac{\lambda_{us}}{\sqrt{30}}$	0	$-\frac{\lambda_{us}}{\sqrt{30}}$	$\frac{7\lambda_{us}}{6\sqrt{305}}$	$\frac{\lambda_{us}}{\sqrt{915}}$
$\bar{B}_s \to J/\psi K^0$	0	0	0	$-\frac{1}{8}\sqrt{\frac{3}{2}}\lambda_{ud}$	$-\frac{1}{8}\sqrt{3}\lambda_{ud}$	$-\frac{1}{8}\sqrt{\frac{3}{10}}\lambda_{ud}$	$\frac{1}{8}\sqrt{3}\lambda_{ud}$	$-\frac{\lambda_{ud}}{4\sqrt{30}}$	$\frac{\lambda_{ud}}{8\sqrt{15}}$	$\frac{3}{8}\sqrt{\frac{3}{10}}\lambda_{ud}$	$\frac{1}{8}\sqrt{\frac{3}{5}}\lambda_{ud}$	$-\frac{\lambda_{ud}}{3\sqrt{610}}$	$-\frac{11\lambda_{ud}}{8\sqrt{1830}}$
$\bar{B}^0 \to J/\psi \eta_1$	$-\frac{\lambda_{ud}}{8\sqrt{2}}$	$-\frac{\lambda_{ud}}{8}$	$-\frac{\lambda_{ud}}{8\sqrt{10}}$	0	0	0	0	0	0	0	0	0	0
$\bar{B}^0 \to J/\psi \eta_8$	0	0	0	$\frac{\lambda_{ud}}{16}$	$\frac{\lambda_{ud}}{8\sqrt{2}}$	$\frac{\lambda_{ud}}{16\sqrt{5}}$	$-\frac{3\lambda_{ud}}{8\sqrt{2}}$	$\frac{\lambda_{ud}}{8\sqrt{5}}$	$-\frac{\lambda_{ud}}{8\sqrt{10}}$	$\frac{9\lambda_{ud}}{16\sqrt{5}}$	$\frac{3\lambda_{ud}}{8\sqrt{10}}$	$-\frac{\lambda_{ud}}{2\sqrt{915}}$	$-\frac{11\lambda_{ud}}{16\sqrt{305}}$
$\bar{B}_s \to J/\psi \eta_1$	$\frac{\lambda_{us}}{4\sqrt{2}}$	0	$-\frac{\lambda_{us}}{4\sqrt{10}}$	0	0	0	0	0	0	0	0	0	0
$\bar{B}_s \to J/\psi \eta_8$	0	0	0	$\frac{\lambda_{us}}{4}$	0	$-\frac{\lambda_{us}}{4\sqrt{5}}$	0	0	0	$\frac{3\lambda_{us}}{4\sqrt{5}}$	0	$\frac{1}{2}\sqrt{\frac{3}{305}}\lambda_{us}$	$-\frac{7\lambda_{us}}{4\sqrt{305}}$

Table A.9.: The Clebsch-Gordan coefficients of the linear $SU(3)_F$-breaking decomposition of $B \to J/\psi P$ decays coming with λ_{ud} and λ_{us}, including explicitly the CKM factors. Table taken from [506].

B. Fits and Technicalities

In order to perform the fits, we use the method of least squares, for a review see *e.g.* [89]. The χ^2 function can schematically be written as

$$\chi^2(\vec{p}) = \sum_{i=1}^{N} \left(\frac{T_i(\vec{p}) - E_i}{\sigma_i} \right)^2 , \tag{B.1}$$

with parameters $\vec{p}$ that give the theoretical values $T_i(\vec{p})$ for experimentally measured observables E_i with uncertainty σ_i. Assuming Gaussian errors for the measurements the minimum of the χ^2 corresponds to the same point in parameter space as determined by the method of maximum likelihood. The corresponding likelihood L is then given as $\chi^2(\vec{p}) = -2 \log L(\vec{p})$. In order to include theoretical uncertainties, we use the Rfit (range fit) scheme [437]. In this scheme, an observable with a pure systematic (or theoretical) uncertainty σ_{syst} is included by [437]

$$\chi^2_{\text{pure syst}}(\vec{p}) = \begin{cases} 0 , & \text{if} \quad |T(\vec{p}) - E| \leq \zeta \sigma_{\text{syst}} \\ \left(\frac{T(\vec{p}) - E}{\kappa \, \sigma_{\text{syst}}} \right)^2 - (\zeta/\kappa)^2 , & \text{if} \quad |T(\vec{p}) - E| > \zeta \sigma_{\text{syst}} \end{cases} , \tag{B.2}$$

where for the Rfit scheme it is $\zeta = 1$ and $\kappa = 0$, see Fig. 4 in [437]. The effect of the contribution $\chi^2_{\text{pure syst}}(\vec{p})$ for the fit is that $T(\vec{p})$ takes values only in a flat range with length $2\sigma_{\text{syst}}$ around E. The combination of statistical and systematic uncertainties gives in the Rfit scheme the contribution [437]

$$\chi^2_{\text{combined stat, syst}}(\vec{p}) = \begin{cases} 0 , & \text{if} \quad |T(\vec{p}) - E| \leq \sigma_{\text{syst}} \\ \left(\frac{|T(\vec{p}) - E| - \sigma_{\text{syst}}}{\sigma_{\text{exp}}} \right)^2 , & \text{if} \quad |T(\vec{p}) - E| > \sigma_{\text{syst}} \end{cases} , \tag{B.3}$$

where by σ_{exp} we denote the Gaussian distributed statistical uncertainty. In Sec. 4.4 we use Eq. (B.2) in order to describe the theoretical uncertainty of the HC and LCSR input, respectively.

In order to minimize the χ^2 we link the `NLopt 2.3` library [513] to our `C++` code. Concretely, for the minimization we use the Sbplx/Subplex algorithms [513, 514]. For the fits presented in Sec. 4.4, we use the `Lucy` code [515], which automatically creates `C++` code from within Mathematica [516] that is subsequently linked to the `NLopt 2.3` library.
For the fits presented in Chs. 5 and 6 we use besides the Sbplx/Subplex algorithm also the augmented Lagrangian method [517, 518] in order to implement non-linear boundary conditions.

The Feynman Diagrams in this thesis are drawn using the Java program `JaxoDraw` [519, 520].

Bibliography

[1] **ATLAS** Collaboration, G. Aad et al., *Observation of a new particle in the search for the Standard Model Higgs boson with the ATLAS detector at the LHC*, *Phys.Lett.B* (2012) [arXiv:1207.7214].

[2] **CMS** Collaboration, S. Chatrchyan et al., *Observation of a new boson at a mass of 125 GeV with the CMS experiment at the LHC*, *Phys.Lett.B* (2012) [arXiv:1207.7235].

[3] F. Englert and R. Brout, *Broken Symmetry and the Mass of Gauge Vector Mesons*, *Phys.Rev.Lett.* **13** (1964) 321–323.

[4] P. W. Higgs, *Broken symmetries, massless particles and gauge fields*, *Phys.Lett.* **12** (1964) 132–133.

[5] P. W. Higgs, *Broken Symmetries and the Masses of Gauge Bosons*, *Phys.Rev.Lett.* **13** (1964) 508–509.

[6] G. Guralnik, C. Hagen, and T. Kibble, *Global Conservation Laws and Massless Particles*, *Phys.Rev.Lett.* **13** (1964) 585–587.

[7] P. W. Higgs, *Spontaneous Symmetry Breakdown without Massless Bosons*, *Phys.Rev.* **145** (1966) 1156–1163.

[8] T. Kibble, *Symmetry breaking in non-Abelian gauge theories*, *Phys.Rev.* **155** (1967) 1554–1561.

[9] Y. Nambu, *Axial vector current conservation in weak interactions*, *Phys.Rev.Lett.* **4** (1960) 380–382.

[10] J. Goldstone, *Field Theories with Superconductor Solutions*, *Nuovo Cim.* **19** (1961) 154–164.

[11] J. Goldstone, A. Salam, and S. Weinberg, *Broken Symmetries*, *Phys.Rev.* **127** (1962) 965–970.

[12] *Combined measurements of the mass and signal strength of the Higgs-like boson with the ATLAS detector using up to 25 fb^{-1} of proton-proton collision data*, Tech. Rep. ATLAS-CONF-2013-014, CERN, Geneva, Mar, 2013.

[13] *Combination of standard model Higgs boson searches and measurements of the properties of the new boson with a mass near 125 GeV*, Tech. Rep. CMS-PAS-HIG-12-045, CERN, Geneva, 2012.

[14] M. Baak, M. Goebel, J. Haller, A. Hoecker, D. Ludwig, et al., *Updated Status of the Global Electroweak Fit and Constraints on New Physics*, *Eur.Phys.J.* **C72** (2012) 2003, [arXiv:1107.0975].

[15] M. Baak, M. Goebel, J. Haller, A. Hoecker, D. Kennedy, et al., *The Electroweak Fit of the Standard Model after the Discovery of a New Boson at the LHC*, *Eur.Phys.J.* **C72** (2012) 2205, [arXiv:1209.2716].

[16] **Planck** Collaboration, P. Ade et al., *Planck 2013 results. I. Overview of products and scientific results*, arXiv:1303.5062.

[17] M. Kobayashi and T. Maskawa, *CP Violation in the Renormalizable Theory of Weak Interaction*, *Prog.Theor.Phys.* **49** (1973) 652–657.

[18] M. Gell-Mann and A. Pais, *Behavior of neutral particles under charge conjugation*, *Phys.Rev.* **97** (1955) 1387–1389.

[19] K. Lande, E. Booth, J. Impeduglia, L. Lederman, and W. Chinowsky, *Observation of Long-Lived Neutral V Particles*, *Phys.Rev.* **103** (1956) 1901–1904.

[20] **ARGUS** Collaboration, H. Albrecht et al., *Observation of B^0 - $\bar{B}^0$ Mixing*, *Phys.Lett.* **B192** (1987) 245.

[21] **CDF** Collaboration, A. Abulencia et al., *Observation of B_s^0 - $\bar{B}_s^0$ Oscillations*, *Phys.Rev.Lett.* **97** (2006) 242003, [hep-ex/0609040].

[22] **BABAR** Collaboration, B. Aubert et al., *Evidence for D^0 - $\bar{D}^0$ Mixing*, *Phys.Rev.Lett.* **98** (2007) 211802, [hep-ex/0703020].

[23] **BABAR** Collaboration, B. Aubert et al., *Measurement of D^0 - $\bar{D}^0$ mixing using the ratio of lifetimes for the decays $D^0 \to K^-\pi^+$, K^-K^+, and $\pi^-\pi^+$*, *Phys.Rev.* **D78** (2008) 011105, [arXiv:0712.2249].

[24] **BABAR** Collaboration, B. Aubert et al., *Measurement of $D^0 - \bar{D}^0$ mixing from a time-dependent amplitude analysis of $D^0 \to K^+\pi^-\pi^0$ decays*, *Phys.Rev.Lett.* **103** (2009) 211801, [arXiv:0807.4544].

[25] **BABAR** Collaboration, B. Aubert et al., *Measurement of D^0 - $\bar{D}^0$ Mixing using the Ratio of Lifetimes for the Decays $D^0 \to K^-\pi^+$ and K^+K^-*, *Phys.Rev.* **D80** (2009) 071103, [arXiv:0908.0761].

[26] **Belle** Collaboration, M. Staric et al., *Evidence for D^0 - $\bar{D}^0$ Mixing*, *Phys.Rev.Lett.* **98** (2007) 211803, [hep-ex/0703036].

[27] **CDF** Collaboration, T. Aaltonen et al., *Evidence for $D^0 - \bar{D}^0$ mixing using the CDF II Detector*, *Phys.Rev.Lett.* **100** (2008) 121802, [arXiv:0712.1567].

[28] **LHCb** Collaboration, R. Aaij et al., *Observation of D^0 - $\bar{D}^0$ oscillations*, *Phys. Rev. Lett. 110,* **101802** (2013) [arXiv:1211.1230].

[29] J. Bjorken and S. Glashow, *Elementary Particles and SU(4)*, *Phys.Lett.* **11** (1964) 255–257.

[30] S. Glashow, J. Iliopoulos, and L. Maiani, *Weak Interactions with Lepton-Hadron Symmetry*, *Phys.Rev.* **D2** (1970) 1285–1292.

[31] **SLAC-SP-017** Collaboration, J. Augustin et al., *Discovery of a Narrow Resonance in e^+e^- Annihilation*, *Phys.Rev.Lett.* **33** (1974) 1406–1408.

[32] **E598** Collaboration, J. Aubert et al., *Experimental Observation of a Heavy Particle J*, *Phys.Rev.Lett.* **33** (1974) 1404–1406.

[33] T. Lee and C.-N. Yang, *Parity Nonconservation and a Two Component Theory of the Neutrino*, *Phys.Rev.* **105** (1957) 1671–1675.

[34] C. Wu, E. Ambler, R. Hayward, D. Hoppes, and R. Hudson, *Experimental Test of Parity Conservation in β Decay*, *Phys.Rev.* **105** (1957) 1413–1414.

[35] J. Christenson, J. Cronin, V. Fitch, and R. Turlay, *Evidence for the 2π Decay of the K_2^0 Meson*, *Phys.Rev.Lett.* **13** (1964) 138–140.

[36] **CPLEAR** Collaboration, A. Angelopoulos et al., *First direct observation of time reversal noninvariance in the neutral kaon system*, *Phys.Lett.* **B444** (1998) 43–51.

[37] **BABAR** Collaboration, J. Lees et al., *Observation of Time Reversal Violation in the B^0 Meson System*, *Phys.Rev.Lett.* **109** (2012) 211801, [arXiv:1207.5832].

[38] G. Luders, *On the Equivalence of Invariance under Time Reversal and under Particle-Antiparticle Conjugation for Relativistic Field Theories*, *Kong.Dan.Vid.Sel.Mat.Fys.Med.* **28N5** (1954) 1–17.

[39] G. Luders, *Proof of the TCP theorem*, *Annals Phys.* **2** (1957) 1–15.

[40] W. Pauli, *Niels Bohr and the development of physics.* McGraw Hill, New York, 1955.

[41] R. Jost, *A remark on the C.T.P. theorem*, *Helv.Phys.Acta* **30** (1957) 409–416.

[42] A. Sakharov, *Violation of CP Invariance, c Asymmetry, and Baryon Asymmetry of the Universe*, *Pisma Zh.Eksp.Teor.Fiz.* **5** (1967) 32–35.

[43] V. Rubakov and M. Shaposhnikov, *Electroweak baryon number nonconservation in the early universe and in high-energy collisions*, *Usp.Fiz.Nauk* **166** (1996) 493–537, [hep-ph/9603208].

[44] S. Herb, D. Hom, L. Lederman, J. Sens, H. Snyder, et al., *Observation of a Dimuon Resonance at 9.5-GeV in 400-GeV Proton-Nucleus Collisions*, *Phys.Rev.Lett.* **39** (1977) 252–255.

[45] **CDF** Collaboration, F. Abe et al., *Observation of top quark production in $\bar{p}p$ collisions*, *Phys.Rev.Lett.* **74** (1995) 2626–2631, [hep-ex/9503002].

[46] **D0** Collaboration, S. Abachi et al., *Observation of the top quark*, *Phys.Rev.Lett.* **74** (1995) 2632–2637, [hep-ex/9503003].

[47] **LHCb** Collaboration, R. Aaij et al., *First evidence for the decay $B_s \to \mu^+\mu^-$*, *Phys.Rev.Lett.* **110** (2013) 021801, [arXiv:1211.2674].

[48] **CMS** Collaboration, S. Chatrchyan et al., *Interpretation of searches for supersymmetry with simplified models*, arXiv:1301.2175.

[49] **ATLAS** Collaboration, *Search for squarks and gluinos with the ATLAS detector using final states with jets and missing transverse momentum and 5.8 fb^{-1} of $\sqrt{s}$=8 TeV proton-proton collision data*, Tech. Rep. ATLAS-CONF-2012-109, 2012.

[50] **ATLAS** Collaboration, *Search for scalar bottom pair production in final states with missing transverse momentum and two b-jets in pp collisions at $\sqrt{s}$=7 TeV with the ATLAS Detector*, Tech. Rep. ATLAS-CONF-2012-106, 2012.

[51] C. Strege, G. Bertone, F. Feroz, M. Fornasa, R. Ruiz de Austri, et al., *Global Fits of the cMSSM and NUHM including the LHC Higgs discovery and new XENON100 constraints*, *JCAP* **1304** (2013) 013, [arXiv:1212.2636].

[52] P. Bechtle, T. Bringmann, K. Desch, H. Dreiner, M. Hamer, et al., *Constrained Supersymmetry after two years of LHC data: a global view with Fittino*, *JHEP* **1206** (2012) 098, [arXiv:1204.4199].

[53] O. Buchmueller, R. Cavanaugh, M. Citron, A. De Roeck, M. Dolan, et al., *The CMSSM and NUHM1 in Light of 7 TeV LHC, $B_s \to \mu^+\mu^-$ and XENON100 Data*, *Eur.Phys.J.* **C72** (2012) 2243, [arXiv:1207.7315].

[54] **CDF** Collaboration, T. Aaltonen et al., *Measurement of the top quark forward-backward production asymmetry and its dependence on event kinematic properties*, *Phys. Rev. D 87,* **092002** (2013) [arXiv:1211.1003].

[55] J. Laiho, E. Lunghi, and R. Van de Water, *Flavor Physics in the LHC era: The Role of the lattice*, *PoS* **LATTICE2011** (2011) 018, [arXiv:1204.0791].

[56] L. Hofer and L. Vernazza, *Status of the $B \to \pi K$ puzzle and its relation to $B_s \to \phi\pi$ and $B_s \to \phi\rho$ decays*, arXiv:1212.4785.

[57] **BaBar** Collaboration, J. Lees et al., *Evidence for an excess of $\bar{B} \to D^{(*)}\tau^-\bar{\nu}_\tau$ decays*, *Phys.Rev.Lett.* **109** (2012) 101802, [arXiv:1205.5442].

[58] **Belle** Collaboration, I. Adachi et al., *Measurement of $B \to D^{(*)}\tau\nu$ using full reconstruction tags*, arXiv:0910.4301.

[59] **Belle** Collaboration, A. Bozek et al., *Observation of $B^+ \to \bar{D}^{0*}\tau^+\nu_\tau$ and Evidence for $B^+ \to \bar{D}^0\tau^+\nu_\tau$ at Belle*, *Phys.Rev.* **D82** (2010) 072005, [arXiv:1005.2302].

[60] **LHCb** Collaboration, R. Aaij et al., *Evidence for CP violation in time-integrated $D^0 \to h^-h^+$ decay rates*, *Phys.Rev.Lett.* **108** (2012) 111602, [arXiv:1112.0938].

[61] **CDF** Collaboration, T. Aaltonen et al., *Measurement of the difference of CP–violating asymmetries in $D^0 \to K^+K^-$ and $D^0 \to \pi^+\pi^-$ decays at CDF*, *Phys.Rev.Lett.* **109** (2012) 111801, [arXiv:1207.2158].

[62] B. R. Ko for the Belle Collaboration, "Direct CP Violation in Charm at Belle." Talk at the 36th International Conference for High Energy Physics (ICHEP), 4-11 July 2012 Melbourne, Australia, arXiv:1212.1975.

[63] **Heavy Flavor Averaging Group** Collaboration, Y. Amhis et al., *Averages of b-hadron, c-hadron, and tau-lepton properties as of early 2012*, arXiv:1207.1158. Online update at http://www.slac.stanford.edu/xorg/hfag/charm/index.html.

[64] *A search for time-integrated CP violation in $D^0 \to K^-K^+$ and $D^0 \to \pi^-\pi^+$ decays*, Tech. Rep. LHCb-CONF-2013-003, Mar, 2013.

[65] **LHCb** Collaboration, R. Aaij et al., *Search for direct CP violation in $D^0 \to h^-h^+$ modes using semileptonic B decays*, arXiv:1303.2614.

[66] *Measurements of the properties of the Higgs-like boson in the two photon decay channel with the ATLAS detector using 25* fb^{-1} *of proton-proton collision data*, Tech. Rep. ATLAS-CONF-2013-012, CERN, Geneva, Mar, 2013.

[67] U. Ellwanger, *Enhanced di-photon Higgs signal in the Next-to-Minimal Supersymmetric Standard Model*, *Phys.Lett.* **B698** (2011) 293–296, [arXiv:1012.1201].

[68] *Updated measurements of the Higgs boson at 125 GeV in the two photon decay channel*, Tech. Rep. CMS-PAS-HIG-13-001, CERN, Geneva, 2013.

[69] D. Hanneke, S. Fogwell Hoogerheide, and G. Gabrielse, *Cavity control of a single-electron quantum cyclotron: Measuring the electron magnetic moment*, *Phys. Rev. A* **83** (May, 2011) 052122.

[70] G. Giudice, P. Paradisi, and M. Passera, *Testing new physics with the electron g-2*, *JHEP* **1211** (2012) 113, [arXiv:1208.6583].

[71] **Muon g-2** Collaboration, G. Bennett et al., *Final Report of the Muon E821 Anomalous Magnetic Moment Measurement at BNL*, *Phys.Rev.* **D73** (2006) 072003, [hep-ex/0602035].

[72] **Muon g-2** Collaboration, G. Bennett et al., *Measurement of the negative muon anomalous magnetic moment to 0.7 ppm*, *Phys.Rev.Lett.* **92** (2004) 161802, [hep-ex/0401008].

[73] **Muon g-2** Collaboration, G. Bennett et al., *Measurement of the positive muon anomalous magnetic moment to 0.7 ppm*, *Phys.Rev.Lett.* **89** (2002) 101804, [hep-ex/0208001].

[74] **Muon g-2** Collaboration, H. Brown et al., *Precise measurement of the positive muon anomalous magnetic moment*, *Phys.Rev.Lett.* **86** (2001) 2227–2231, [hep-ex/0102017].

[75] F. Jegerlehner and A. Nyffeler, *The Muon g-2*, *Phys.Rept.* **477** (2009) 1–110, [arXiv:0902.3360].

[76] K. Hagiwara, R. Liao, A. D. Martin, D. Nomura, and T. Teubner, *$(g\text{-}2)_\mu$ and $\alpha(M_Z^2)$ re-evaluated using new precise data*, *J.Phys.* **G38** (2011) 085003, [arXiv:1105.3149].

[77] M. Davier, A. Hoecker, B. Malaescu, and Z. Zhang, *Reevaluation of the Hadronic Contributions to the Muon g-2 and to $\alpha(M_Z)$*, *Eur.Phys.J.* **C71** (2011) 1515, [arXiv:1010.4180].

[78] C. Bobeth, G. Hiller, and D. van Dyk, *The Benefits of $\bar{B} \to \bar{K}^* l^+ l^-$ Decays at Low Recoil*, *JHEP* **1007** (2010) 098, [arXiv:1006.5013].

[79] S. Glashow, *Partial Symmetries of Weak Interactions*, *Nucl.Phys.* **22** (1961) 579–588.

[80] S. Weinberg, *A Model of Leptons*, *Phys.Rev.Lett.* **19** (1967) 1264–1266.

[81] A. Salam, *Weak and Electromagnetic Interactions*, *Conf.Proc.* **C680519** (1968) 367–377.

[82] G. 't Hooft and M. Veltman, *Regularization and Renormalization of Gauge Fields*, *Nucl.Phys.* **B44** (1972) 189–213.

[83] D. Gross and F. Wilczek, *Ultraviolet Behavior of Nonabelian Gauge Theories*, *Phys.Rev.Lett.* **30** (1973) 1343–1346.

[84] H. D. Politzer, *Reliable Perturbative Results for Strong Interactions?*, *Phys.Rev.Lett.* **30** (1973) 1346–1349.

[85] A. Denner, *Techniques for calculation of electroweak radiative corrections at the one loop level and results for W physics at LEP-200*, *Fortsch.Phys.* **41** (1993) 307–420, [arXiv:0709.1075].

[86] R. K. Ellis, W. J. Stirling, and B. Webber, *QCD and collider physics*, *Camb.Monogr.Part.Phys.Nucl.Phys.Cosmol.* **8** (1996) 1–435.

[87] M. E. Peskin and D. V. Schroeder, *An Introduction to quantum field theory*. 1995.

[88] T. Muta, *Foundations of quantum chromodynamics. Second edition*, *World Sci.Lect.Notes Phys.* **57** (1998) 1–409.

[89] **Particle Data Group** Collaboration, J. Beringer et al., *Review of Particle Physics (RPP)*, *Phys.Rev.* **D86** (2012) 010001.

[90] P. Minkowski, *$\mu \to e\gamma$ at a Rate of One Out of 1-Billion Muon Decays?*, *Phys.Lett.* **B67** (1977) 421.

[91] M. Gell-Mann, P. Ramond, and R. Slansky, *Complex Spinors and Unified Theories*, *Conf.Proc.* **C790927** (1979) 315–321.

[92] T. Yanagida, *Horizontal Symmetry and Masses of Neutrinos*, *Conf.Proc.* **C7902131** (1979) 95.

[93] R. N. Mohapatra and G. Senjanovic, *Neutrino Mass and Spontaneous Parity Violation*, *Phys.Rev.Lett.* **44** (1980) 912.

[94] J. Schechter and J. Valle, *Neutrino Masses in SU(2) x U(1) Theories*, *Phys.Rev.* **D22** (1980) 2227.

[95] W. Konetschny and W. Kummer, *Nonconservation of Total Lepton Number with Scalar Bosons*, *Phys.Lett.* **B70** (1977) 433.

[96] G. Lazarides, Q. Shafi, and C. Wetterich, *Proton Lifetime and Fermion Masses in an SO(10) Model*, *Nucl.Phys.* **B181** (1981) 287.

[97] R. N. Mohapatra and G. Senjanovic, *Neutrino Masses and Mixings in Gauge Models with Spontaneous Parity Violation*, *Phys.Rev.* **D23** (1981) 165.

[98] T. Cheng and L.-F. Li, *Neutrino Masses, Mixings and Oscillations in SU(2) x U(1) Models of Electroweak Interactions*, *Phys.Rev.* **D22** (1980) 2860.

[99] J. Schechter and J. Valle, *Neutrino Decay and Spontaneous Violation of Lepton Number*, *Phys.Rev.* **D25** (1982) 774.

[100] R. Foot, H. Lew, X. He, and G. C. Joshi, *Seesaw Neutrino Masses induced by a Triplet of Leptons*, *Z.Phys.* **C44** (1989) 441.

[101] O. Eberhardt, G. Herbert, H. Lacker, A. Lenz, A. Menzel, et al., *Impact of a Higgs boson at a mass of 126 GeV on the standard model with three and four fermion generations*, *Phys.Rev.Lett.* **109** (2012) 241802, [arXiv:1209.1101].

[102] D. Barducci, A. Belyaev, M. Brown, S. De Curtis, S. Moretti, et al., *The 4-Dimensional Composite Higgs Model (4DCHM) and the 125 GeV Higgs-like signals at the LHC*, arXiv:1302.2371.

[103] G. Panico, M. Redi, A. Tesi, and A. Wulzer, *On the Tuning and the Mass of the Composite Higgs*, *JHEP* **1303** (2013) 051, [arXiv:1210.7114].

[104] B. Bellazzini, C. Csaki, J. Hubisz, J. Serra, and J. Terning, *Composite Higgs Sketch*, *JHEP* **1211** (2012) 003, [arXiv:1205.4032].

[105] *Coupling properties of the new Higgs-like boson observed with the ATLAS detector at the LHC*, Tech. Rep. ATLAS-CONF-2012-127, CERN, Geneva, Sep, 2012.

[106] A. Dery, A. Efrati, Y. Hochberg, and Y. Nir, *What if BR($h \to \mu\mu$)/BR($h \to \tau\tau$) does not equal m_μ^2/m_τ^2?*, arXiv:1302.3229.

[107] *Search for the Standard-Model Higgs boson decaying to tau pairs in proton-proton collisions at $\sqrt{s}$ = 7 and 8 TeV*, Tech. Rep. CMS-PAS-HIG-13-004, CERN, Geneva, 2013.

[108] *Search for the Standard Model Higgs boson in $H \to \tau\tau$ decays in proton-proton collisions with the ATLAS detector*, Tech. Rep. ATLAS-CONF-2012-160, CERN, Geneva, Nov, 2012.

[109] *Study of the spin of the Higgs-like boson in the two photon decay channel using 20.7 fb^{-1} of pp collisions collected at $\sqrt{s}$ = 8 TeV with the ATLAS detector*, Tech. Rep. ATLAS-CONF-2013-029, CERN, Geneva, Mar, 2013.

[110] N. Cabibbo, *Unitary Symmetry and Leptonic Decays*, *Phys.Rev.Lett.* **10** (1963) 531–533.

[111] R. F. Streater and A. S. Wightman, *PCT, spin and statistics, and all that. Classic ed.* Amsterdam: Addison-Wesley. xvi, 207 p., 1989.

[112] M. Dine, *TASI lectures on the strong CP problem*, hep-ph/0011376.

[113] M. D. Swallows, T. H. Loftus, W. C. Griffith, B. R. Heckel, E. N. Fortson, and M. V. Romalis, *Techniques used to search for a permanent electric dipole moment of the ^{199}Hg atom and the implications for CP violation*, *Phys. Rev. A* **87** (Jan, 2013) 012102.

[114] C. Baker, D. Doyle, P. Geltenbort, K. Green, M. van der Grinten, et al., *An Improved experimental limit on the electric dipole moment of the neutron*, *Phys.Rev.Lett.* **97** (2006) 131801, [hep-ex/0602020].

[115] M. Pospelov and A. Ritz, *Theta induced electric dipole moment of the neutron via QCD sum rules*, *Phys.Rev.Lett.* **83** (1999) 2526–2529, [hep-ph/9904483].

[116] R. Peccei and H. R. Quinn, *CP Conservation in the Presence of Instantons*, *Phys.Rev.Lett.* **38** (1977) 1440–1443.

[117] R. Peccei and H. R. Quinn, *Constraints Imposed by CP Conservation in the Presence of Instantons*, *Phys.Rev.* **D16** (1977) 1791–1797.

[118] G. Hiller and M. Schmaltz, *Strong weak CP hierarchy from nonrenormalization theorems*, *Phys.Rev.* **D65** (2002) 096009, [hep-ph/0201251].

[119] C. Jarlskog, (Ed.), *CP Violation*. Singapore, Singapore: World Scientific (1989) 723 p. (Advanced Series on Directions in High Energy Physics, 3).

[120] G. C. Branco, L. Lavoura, and J. P. Silva, *CP Violation*, *Int.Ser.Monogr.Phys.* **103** (1999) 1–536.

[121] I. I. Bigi and A. Sanda, *CP violation*, *Camb.Monogr.Part.Phys.Nucl.Phys.Cosmol.* **9** (2000) 1–382.

[122] A. Santamaria, *Masses, mixings, Yukawa couplings and their symmetries*, *Phys.Lett.* **B305** (1993) 90–97, [hep-ph/9302301].

[123] L.-L. Chau and W.-Y. Keung, *Comments on the Parametrization of the Kobayashi-Maskawa Matrix*, *Phys.Rev.Lett.* **53** (1984) 1802.

[124] L. Wolfenstein, *Parametrization of the Kobayashi-Maskawa Matrix*, *Phys.Rev.Lett.* **51** (1983) 1945.

[125] A. J. Buras, M. E. Lautenbacher, and G. Ostermaier, *Waiting for the top quark mass, $K^+ \to \pi^+ \nu\bar{\nu}$, $B_s^0 - \bar{B}_s^0$ mixing and CP asymmetries in B decays*, *Phys.Rev.* **D50** (1994) 3433–3446, [hep-ph/9403384].

[126] **CKMfitter Group** Collaboration, J. Charles et al., *CP violation and the CKM matrix: Assessing the impact of the asymmetric B factories*, *Eur.Phys.J.* **C41** (2005) 1–131, [hep-ph/0406184].

[127] B. Pontecorvo, *Mesonium and anti-mesonium*, *Sov.Phys.JETP* **6** (1957) 429.

[128] Z. Maki, M. Nakagawa, and S. Sakata, *Remarks on the unified model of elementary particles*, *Prog.Theor.Phys.* **28** (1962) 870–880.

[129] G. Fogli, E. Lisi, A. Marrone, D. Montanino, A. Palazzo, et al., *Global analysis of neutrino masses, mixings and phases: entering the era of leptonic CP violation searches*, *Phys.Rev.* **D86** (2012) 013012, [arXiv:1205.5254].

[130] **DAYA-BAY** Collaboration, F. An et al., *Observation of electron-antineutrino disappearance at Daya Bay*, *Phys.Rev.Lett.* **108** (2012) 171803, [arXiv:1203.1669].

[131] **RENO** Collaboration, J. Ahn et al., *Observation of Reactor Electron Antineutrino Disappearance in the RENO Experiment*, *Phys.Rev.Lett.* **108** (2012) 191802, [arXiv:1204.0626].

[132] P. Harrison, D. Perkins, and W. Scott, *Tri-bimaximal mixing and the neutrino oscillation data*, *Phys.Lett.* **B530** (2002) 167, [hep-ph/0202074].

[133] H. Ishimori and E. Ma, *New Simple A_4 Neutrino Model for Nonzero θ_{13} and Large δ_{CP}*, *Phys.Rev.* **D86** (2012) 045030, [arXiv:1205.0075].

[134] A. de Gouvea and H. Murayama, *Neutrino Mixing Anarchy: Alive and Kicking*, arXiv:1204.1249.

[135] C. Jarlskog, *On Invariants of Quark and Lepton Mass Matrices in the Standard Model*, *Comptes Rendus Physique* **13** (2012) 111–114, [arXiv:1102.2823].

[136] C. Jarlskog, *Ambiguities pertaining to quark-lepton complementarity*, *Phys.Lett.* **B625** (2005) 63–66, [hep-ph/0507212].

[137] J. D. Bjorken and I. Dunietz, *Rephasing Invariant Parametrizations of Generalized Kobayashi-Maskawa Matrices*, *Phys.Rev.* **D36** (1987) 2109.

[138] **CKMfitter** Collaboration. http://ckmfitter.in2p3.fr.

[139] **UTfit** Collaboration. http://utfit.org.

[140] C. Jarlskog, *Commutator of the Quark Mass Matrices in the Standard Electroweak Model and a Measure of Maximal CP Violation*, *Phys. Rev. Lett.* **55** (1985) 1039.

[141] C. Jarlskog, *A Basis Independent Formulation of the Connection Between Quark Mass Matrices, CP Violation and Experiment*, *Z. Phys.* **C29** (1985) 491–497.

[142] C. Jarlskog and A. Kleppe, *Measurables of the Quark Mixing Matrix as Invariant Functions of Mass Matrices*, *Nucl. Phys.* **B286** (1987) 245–252.

[143] C. Jarlskog, *Matrix Representation of Symmetries in Flavor Space, Invariant Functions of Mass Matrices and Applications*, *Phys.Rev.* **D35** (1987) 1685.

[144] C. Jarlskog, *Flavor projection operators and applications to CP violation with any number of families*, *Phys. Rev.* **D36** (1987) 2128.

[145] D.-d. Wu, *The Rephasing Invariants and CP*, *Phys.Rev.* **D33** (1986) 860.

[146] O. Greenberg, *Rephase Invariant Formulation of CP Violation in the Kobayashi-Maskawa Framework*, *Phys.Rev.* **D32** (1985) 1841.

[147] C. Jarlskog and R. Stora, *Unitarity Polygons and CP Violation Areas and Phases in the Standard Electroweak Model*, *Phys. Lett.* **B208** (1988) 268.

[148] E. E. Jenkins and A. V. Manohar, *Rephasing Invariants of Quark and Lepton Mixing Matrices*, *Nucl.Phys.* **B792** (2008) 187–205, [arXiv:0706.4313].

[149] E. E. Jenkins and A. V. Manohar, *Algebraic Structure of Lepton and Quark Flavor Invariants and CP Violation*, *JHEP* **10** (2009) 094, [arXiv:0907.4763].

[150] A. Hanany, E. E. Jenkins, A. V. Manohar, and G. Torri, *Hilbert Series for Flavor Invariants of the Standard Model*, *JHEP* **1103** (2011) 096, [arXiv:1010.3161].

[151] V. Drensky, *Computing with matrix invariants*, math/0506614.

[152] Y. Teranishi, *The ring of invariants of matrices.*, *Nagoya Math. J.* **104** (1986) 149–161.

[153] H. Aslaksen, V. Drensky, and L. Sadikova, *Defining relations of invariants of two* 3×3 *matrices.*, *J. Algebra* **298** (2006), no. 1 41–57.

[154] C. Jarlskog, *Theory of Quark Mixing Matrix and Invariant Functions of Mass Matrices*. Invited plenary Talk given at Int. Symp. on the Production and Decay of Heavy Flavors, Stanford, CA, Sep 1-5, 1987.

[155] O. Gedalia, L. Mannelli, and G. Perez, *Covariant Description of Flavor Violation at the LHC*, *Phys.Lett.* **B693** (2010) 301–304, [arXiv:1002.0778].

[156] O. Gedalia, L. Mannelli, and G. Perez, *Covariant Description of Flavor Conversion at the LHC Era*, *JHEP* **1010** (2010) 046, [arXiv:1003.3869].

[157] O. Gedalia and G. Perez, *TASI 2009 Lectures - Flavor Physics*, arXiv:1005.3106.

[158] T. Feldmann, M. Jung, and T. Mannel, *Sequential Flavour Symmetry Breaking*, *Phys.Rev.* **D80** (2009) 033003, [arXiv:0906.1523].

[159] R. Alonso, M. Gavela, L. Merlo, and S. Rigolin, *On the scalar potential of minimal flavour violation*, *JHEP* **1107** (2011) 012, [arXiv:1103.2915].

[160] R. Alonso, M. Gavela, D. Hernandez, and L. Merlo, *On the Potential of Leptonic Minimal Flavour Violation*, *Phys.Lett.* **B715** (2012) 194–198, [arXiv:1206.3167].

[161] M. Albrecht, T. Feldmann, and T. Mannel, *Goldstone Bosons in Effective Theories with Spontaneously Broken Flavour Symmetry*, *JHEP* **1010** (2010) 089, [arXiv:1002.4798].

[162] M. Gell-Mann, *The Eightfold Way: A Theory of strong interaction symmetry*, 1961. CTSL-20, TID-12608.

[163] M. Gell-Mann, *Symmetries of baryons and mesons*, *Phys.Rev.* **125** (1962) 1067–1084.

[164] Y. Ne'eman, *Derivation of strong interactions from a gauge invariance*, *Nuclear Physics* **26** (1961), no. 2 222–229.

[165] E. Wigner, *Einige Folgerungen aus der Schrödingerschen Theorie für die Termstrukturen.*, *Z. f. Physik* **43** (1927) 624–652.

[166] C. Eckart, *Application of group theory to the quantum dynamics of monatomic systems.*, *Reviews of modern Physics* **2** (1930) 305–380.

[167] E. P. Wigner, *Group theory and its application to the quantum mechanics of atomic spectra. With additions and corrections by Eugene P. Wigner.* Pure and Applied Physics, 5. New York: Academic Press Inc., Publ.; London: Academic Books Ltd. XI, 372 p. , 1959.

[168] J. de Swart, *The Octet model and its Clebsch-Gordan coefficients*, *Rev.Mod.Phys.* **35** (1963) 916–939.

[169] W. Greiner and B. Muller, *Theoretische Physik. Band 5: Quantenmechanik II. Symmetrien. (in German)*. Verlag Harri Deutsch, 2. Auflage, 2005.

[170] M. Jung and T. Mannel, *General Analysis of U-Spin Breaking in B Decays*, *Phys.Rev.* **D80** (2009) 116002, [arXiv:0907.0117].

[171] V. Weisskopf and E. P. Wigner, *Calculation of the natural brightness of spectral lines on the basis of Dirac's theory*, *Z.Phys.* **63** (1930) 54–73.

[172] V. Weisskopf and E. Wigner, *Over the natural line width in the radiation of the harmonius oscillator*, *Z.Phys.* **65** (1930) 18–29.

[173] U. Nierste, *Three Lectures on Meson Mixing and CKM phenomenology*, arXiv:0904.1869.

[174] A. Lenz and U. Nierste, *Numerical Updates of Lifetimes and Mixing Parameters of B Mesons*, arXiv:1102.4274.

[175] G. Hiller, M. Jung, and S. Schacht, *SU(3)-Flavor Anatomy of Non-Leptonic Charm Decays*, *Phys.Rev.* **D87** (2013) 014024, [arXiv:1211.3734].

[176] R. Cenci for the BABAR Collaboration, *Search for CP Violation in the Decays $D^{\pm} \to K^0_S K^{\pm}$, $D^{\pm}_s \to K^0_S K^{\pm}$, and $D^{\pm}_s \to K^0_S \pi^{\pm}$*, arXiv:1209.0138.

[177] Y. Grossman, A. L. Kagan, and Y. Nir, *New physics and CP violation in singly Cabibbo suppressed D decays*, *Phys.Rev.* **D75** (2007) 036008, [hep-ph/0609178].

[178] S. De Curtis, M. Redi, and A. Tesi, *The 4D Composite Higgs*, *JHEP* **1204** (2012) 042, [arXiv:1110.1613].

[179] N. Arkani-Hamed and M. Schmaltz, *Hierarchies without symmetries from extra dimensions*, *Phys.Rev.* **D61** (2000) 033005, [hep-ph/9903417].

[180] G. Buchalla, A. J. Buras, and M. E. Lautenbacher, *Weak decays beyond leading logarithms*, *Rev.Mod.Phys.* **68** (1996) 1125–1144, [hep-ph/9512380].

[181] C. Bobeth, M. Misiak, and J. Urban, *Photonic penguins at two loops and m_t dependence of $BR[B \to X_s l^+ l^-]$*, *Nucl.Phys.* **B574** (2000) 291–330, [hep-ph/9910220].

[182] F. Beaujean, C. Bobeth, D. van Dyk, and C. Wacker, *Bayesian Fit of Exclusive $b \to s\bar{\ell}\ell$ Decays: The Standard Model Operator Basis*, *JHEP* **1208** (2012) 030, [arXiv:1205.1838].

[183] W. Altmannshofer, P. Paradisi, and D. M. Straub, *Model-Independent Constraints on New Physics in $b \to s$ Transitions*, *JHEP* **1204** (2012) 008, [arXiv:1111.1257].

[184] C. Bobeth, G. Hiller, D. van Dyk, and C. Wacker, *The Decay $B \to K l^+ l^-$ at Low Hadronic Recoil and Model-Independent $\Delta B = 1$ Constraints*, *JHEP* **1201** (2012) 107, [arXiv:1111.2558].

[185] A. V. Manohar and M. B. Wise, *Heavy quark physics*, *Camb.Monogr.Part.Phys.Nucl.Phys.Cosmol.* **10** (2000) 1–191.

[186] S. P. Martin, *A Supersymmetry primer*, hep-ph/9709356.

[187] M. Drees, R. Godbole, and P. Roy, *Theory and phenomenology of sparticles: An account of four-dimensional N=1 supersymmetry in high energy physics*. World Scientific Publishing Company, 2004.

[188] D. Chung, L. Everett, G. Kane, S. King, J. D. Lykken, et al., *The Soft supersymmetry breaking Lagrangian: Theory and applications*, *Phys.Rept.* **407** (2005) 1–203, [hep-ph/0312378].

[189] S. R. Coleman and J. Mandula, *All Possible Symmetries of the S Matrix*, *Phys.Rev.* **159** (1967) 1251–1256.

[190] R. Haag, J. T. Lopuszanski, and M. Sohnius, *All Possible Generators of Supersymmetries of the s Matrix*, *Nucl.Phys.* **B88** (1975) 257.

[191] P. Ramond, *Dual Theory for Free Fermions*, *Phys.Rev.* **D3** (1971) 2415–2418.

[192] A. Neveu and J. Schwarz, *Factorizable dual model of pions*, *Nucl.Phys.* **B31** (1971) 86–112.

[193] J.-L. Gervais and B. Sakita, *Field Theory Interpretation of Supergauges in Dual Models*, *Nucl.Phys.* **B34** (1971) 632–639.

[194] Y. Golfand and E. Likhtman, *Extension of the Algebra of Poincare Group Generators and Violation of p Invariance*, *JETP Lett.* **13** (1971) 323–326.

[195] J. Wess and B. Zumino, *Supergauge Transformations in Four-Dimensions*, *Nucl.Phys.* **B70** (1974) 39–50.

[196] A. Salam and J. Strathdee, *Supergauge Transformations*, *Nucl.Phys.* **B76** (1974) 477–482.

[197] P. Fayet, *Supersymmetry and Weak, Electromagnetic and Strong Interactions*, *Phys.Lett.* **B64** (1976) 159.

[198] P. Fayet, *Spontaneously Broken Supersymmetric Theories of Weak, Electromagnetic and Strong Interactions*, *Phys.Lett.* **B69** (1977) 489.

[199] D. Volkov and V. Akulov, *Is the Neutrino a Goldstone Particle?*, *Phys.Lett.* **B46** (1973) 109–110.

[200] L. O'Raifeartaigh, *Spontaneous Symmetry Breaking for Chiral Scalar Superfields*, *Nucl.Phys.* **B96** (1975) 331.

[201] P. Fayet and J. Iliopoulos, *Spontaneously Broken Supergauge Symmetries and Goldstone Spinors*, *Phys.Lett.* **B51** (1974) 461–464.

[202] D. Z. Freedman, P. van Nieuwenhuizen, and S. Ferrara, *Progress Toward a Theory of Supergravity*, *Phys.Rev.* **D13** (1976) 3214–3218.

[203] S. Deser and B. Zumino, *Consistent Supergravity*, *Phys.Lett.* **B62** (1976) 335.

[204] A. H. Chamseddine, R. L. Arnowitt, and P. Nath, *Locally Supersymmetric Grand Unification*, *Phys.Rev.Lett.* **49** (1982) 970.

[205] R. Barbieri, S. Ferrara, and C. A. Savoy, *Gauge Models with Spontaneously Broken Local Supersymmetry*, *Phys.Lett.* **B119** (1982) 343.

[206] S. Dimopoulos and S. Raby, *Supercolor*, *Nucl.Phys.* **B192** (1981) 353.

[207] E. Witten, *Dynamical Breaking of Supersymmetry*, *Nucl.Phys.* **B188** (1981) 513.

[208] M. Dine, W. Fischler, and M. Srednicki, *Supersymmetric Technicolor*, *Nucl.Phys.* **B189** (1981) 575–593.

[209] S. Dimopoulos and H. Georgi, *Softly Broken Supersymmetry and SU(5)*, *Nucl.Phys.* **B193** (1981) 150.

[210] N. Sakai, *Naturalness in Supersymmetric Guts*, *Z.Phys.* **C11** (1981) 153.

[211] R. K. Kaul and P. Majumdar, *Cancellation of Quadratically Divergent Mass Corrections in Globally Supersymmetric Spontaneously Broken Gauge Theories*, *Nucl.Phys.* **B199** (1982) 36.

[212] G. 't Hooft, *Naturalness, chiral symmetry, and spontaneous chiral symmetry breaking*, *NATO Adv.Study Inst.Ser.B Phys.* **59** (1980) 135.

[213] S. Weinberg, *Implications of Dynamical Symmetry Breaking*, *Phys.Rev.* **D13** (1976) 974–996.

[214] S. Weinberg, *Implications of Dynamical Symmetry Breaking: An Addendum*, *Phys.Rev.* **D19** (1979) 1277–1280.

[215] L. Susskind, *Dynamics of Spontaneous Symmetry Breaking in the Weinberg-Salam Theory*, *Phys.Rev.* **D20** (1979) 2619–2625.

[216] E. Gildener, *Gauge Symmetry Hierarchies*, *Phys.Rev.* **D14** (1976) 1667.

[217] H. Georgi and S. Glashow, *Unity of All Elementary Particle Forces*, *Phys.Rev.Lett.* **32** (1974) 438–441.

[218] H. Georgi, H. R. Quinn, and S. Weinberg, *Hierarchy of Interactions in Unified Gauge Theories*, *Phys.Rev.Lett.* **33** (1974) 451–454.

[219] J. R. Ellis, S. Kelley, and D. V. Nanopoulos, *Probing the desert using gauge coupling unification*, *Phys.Lett.* **B260** (1991) 131–137.

[220] U. Amaldi, W. de Boer, and H. Furstenau, *Comparison of grand unified theories with electroweak and strong coupling constants measured at LEP*, *Phys.Lett.* **B260** (1991) 447–455.

[221] P. Langacker and M.-x. Luo, *Implications of precision electroweak experiments for M_t, ρ_0, $\sin^2\theta_W$ and grand unification*, *Phys.Rev.* **D44** (1991) 817–822.

[222] C. Giunti, C. Kim, and U. Lee, *Running coupling constants and grand unification models*, *Mod.Phys.Lett.* **A6** (1991) 1745–1755.

[223] H. Georgi and C. Jarlskog, *A New Lepton - Quark Mass Relation in a Unified Theory*, *Phys.Lett.* **B86** (1979) 297–300.

[224] D. Hooper, *TASI 2008 Lectures on Dark Matter*, `arXiv:0901.4090`.

[225] G. R. Farrar and P. Fayet, *Phenomenology of the Production, Decay, and Detection of New Hadronic States Associated with Supersymmetry*, *Phys.Lett.* **B76** (1978) 575–579.

[226] S. Weinberg, *Supersymmetry at Ordinary Energies. 1. Masses and Conservation Laws*, *Phys.Rev.* **D26** (1982) 287.

[227] N. Sakai and T. Yanagida, *Proton Decay in a Class of Supersymmetric Grand Unified Models*, *Nucl.Phys.* **B197** (1982) 533.

[228] S. Dimopoulos, S. Raby, and F. Wilczek, *Proton Decay in Supersymmetric Models*, *Phys.Lett.* **B112** (1982) 133.

[229] H. Goldberg, *Constraint on the Photino Mass from Cosmology*, *Phys.Rev.Lett.* **50** (1983) 1419.

[230] J. R. Ellis, J. Hagelin, D. V. Nanopoulos, K. A. Olive, and M. Srednicki, *Supersymmetric Relics from the Big Bang*, *Nucl.Phys.* **B238** (1984) 453–476.

[231] C. Aulakh and R. N. Mohapatra, *Neutrino as the Supersymmetric Partner of the Majoron*, *Phys.Lett.* **B119** (1982) 136.

[232] A. Santamaria and J. Valle, *Spontaneous R-Parity Violation in Supersymmetry: A Model for Solar Neutrino Oscillations*, *Phys.Lett.* **B195** (1987) 423.

[233] A. Santamaria and J. Valle, *Supersymmetric Majoron Signatures and Solar Neutrino Oscillations*, *Phys.Rev.Lett.* **60** (1988) 397–400.

[234] A. Santamaria and J. Valle, *Solar Neutrino Oscillation Parameters and the Broken R Parity Majoron*, *Phys.Rev.* **D39** (1989) 1780–1783.

[235] L. J. Hall and M. Suzuki, *Explicit R-Parity Breaking in Supersymmetric Models*, *Nucl.Phys.* **B231** (1984) 419.

[236] J. R. Ellis, G. Gelmini, C. Jarlskog, G. G. Ross, and J. Valle, *Phenomenology of Supersymmetry with Broken R-Parity*, *Phys.Lett.* **B150** (1985) 142.

[237] F. Takayama and M. Yamaguchi, *Gravitino dark matter without R-parity*, *Phys.Lett.* **B485** (2000) 388–392, [hep-ph/0005214].

[238] D. Restrepo, M. Taoso, J. Valle, and O. Zapata, *Gravitino dark matter and neutrino masses with bilinear R-parity violation*, *Phys.Rev.* **D85** (2012) 023523, [arXiv:1109.0512].

[239] B. Feldstein and T. T. Yanagida, *Why is the Supersymmetry Breaking Scale Unnaturally High?*, *Phys.Lett.* **B720** (2013) 166–171, [arXiv:1210.7578].

[240] M. Endo, K. Hamaguchi, S. P. Liew, K. Mukaida, and K. Nakayama, *Axino dark matter with R-parity violation and 130 GeV gamma-ray line*, *Phys.Lett.* **B721** (2013) pp. 111–117, [arXiv:1301.7536].

[241] L. Girardello and M. T. Grisaru, *Soft Breaking of Supersymmetry*, *Nucl.Phys.* **B194** (1982) 65.

[242] L. Hall and L. Randall, *Weak scale effective supersymmetry*, *Phys.Rev.Lett.* **65** (1990) 2939–2942.

[243] S. Dimopoulos and D. W. Sutter, *The Supersymmetric flavor problem*, *Nucl.Phys.* **B452** (1995) 496–512, [hep-ph/9504415].

[244] H. E. Haber, *The Status of the minimal supersymmetric standard model and beyond*, *Nucl.Phys.Proc.Suppl.* **62** (1998) 469–484, [hep-ph/9709450].

[245] M. Misiak, S. Pokorski, and J. Rosiek, *Supersymmetry and FCNC effects*, *Adv.Ser.Direct.High Energy Phys.* **15** (1998) 795–828, [hep-ph/9703442].

[246] P. L. Cho, M. Misiak, and D. Wyler, $K_L \to \pi^0 e^+ e^-$ *and* $B \to X_s l^+ l^-$ *decay in the MSSM*, *Phys.Rev.* **D54** (1996) 3329–3344, [hep-ph/9601360].

[247] S. Choi, D. Choudhury, A. Freitas, J. Kalinowski, J. Kim, et al., *Dirac Neutralinos and Electroweak Scalar Bosons of N=1/N=2 Hybrid Supersymmetry at Colliders*, *JHEP* **1008** (2010) 025, [arXiv:1005.0818].

[248] J. Rosiek, *Complete Set of Feynman Rules for the Minimal Supersymmetric Extension of the Standard Model*, *Phys.Rev.* **D41** (1990) 3464.

[249] J. Rosiek, *Complete set of Feynman rules for the MSSM: Erratum*, hep-ph/9511250.

[250] S. Heinemeyer, W. Hollik, and G. Weiglein, *FeynHiggs: A Program for the calculation of the masses of the neutral CP even Higgs bosons in the MSSM*, *Comput.Phys.Commun.* **124** (2000) 76–89, [hep-ph/9812320].

[251] S. Heinemeyer, W. Hollik, and G. Weiglein, *The Masses of the neutral CP - even Higgs bosons in the MSSM: Accurate analysis at the two loop level*, *Eur.Phys.J.* **C9** (1999) 343–366, [hep-ph/9812472].

[252] G. Degrassi, S. Heinemeyer, W. Hollik, P. Slavich, and G. Weiglein, *Towards high precision predictions for the MSSM Higgs sector*, *Eur.Phys.J.* **C28** (2003) 133–143, [hep-ph/0212020].

[253] M. Frank, T. Hahn, S. Heinemeyer, W. Hollik, H. Rzehak, et al., *The Higgs Boson Masses and Mixings of the Complex MSSM in the Feynman-Diagrammatic Approach*, *JHEP* **0702** (2007) 047, [hep-ph/0611326].

[254] M. Arana-Catania, S. Heinemeyer, M. Herrero, and S. Penaranda, *Higgs Boson masses and B-Physics Constraints in Non-Minimal Flavor Violating SUSY scenarios*, *JHEP* **1205** (2012) 015, [arXiv:1109.6232].

[255] J. Casas and S. Dimopoulos, *Stability bounds on flavor violating trilinear soft terms in the MSSM*, *Phys.Lett.* **B387** (1996) 107–112, [hep-ph/9606237].

[256] J.-h. Park, *Metastability bounds on flavour-violating trilinear soft terms in the MSSM*, *Phys.Rev.* **D83** (2011) 055015, [arXiv:1011.4939].

[257] **CMS** Collaboration, S. Chatrchyan et al., *Interpretation of searches for supersymmetry with simplified models*, arXiv:1301.2175.

[258] **ATLAS** Collaboration, G. Aad et al., *Search for squarks and gluinos with the ATLAS detector in final states with jets and missing transverse momentum using 4.7 fb^{-1} of $\sqrt{s}$ = 7 TeV proton-proton collision data*, *Phys.Rev.* **D87** (2013) 012008, [arXiv:1208.0949].

[259] **ATLAS** Collaboration, G. Aad et al., *Search for top and bottom squarks from gluino pair production in final states with missing transverse energy and at least three b-jets with the ATLAS detector*, *Eur.Phys.J.* **C72** (2012) 2174, [arXiv:1207.4686].

[260] **ATLAS** Collaboration, G. Aad et al., *Search for direct slepton and gaugino production in final states with two leptons and missing transverse momentum with the ATLAS detector in pp collisions at $\sqrt{s}$ = 7 TeV*, *Phys.Lett.* **B718** (2013) 879–901, [arXiv:1208.2884].

[261] **ATLAS** Collaboration, G. Aad et al., *Search for direct production of charginos and neutralinos in events with three leptons and missing transverse momentum in $\sqrt{s}$ = 7 TeV pp collisions with the ATLAS detector*, *Phys.Lett.* **B718** (2013) 841–859, [arXiv:1208.3144].

[262] **ATLAS** Collaboration, G. Aad et al., *Search for supersymmetry in pp collisions at $\sqrt{s}$ = 7 TeV in final states with missing transverse momentum and b^- jets with the ATLAS detector*, *Phys.Rev.* **D85** (2012) 112006, [arXiv:1203.6193].

[263] **ATLAS** Collaboration, G. Aad et al., *Hunt for new phenomena using large jet multiplicities and missing transverse momentum with ATLAS in 4.7 fb^{-1} of $\sqrt{s}$ = 7 TeV proton-proton collisions*, *JHEP* **1207** (2012) 167, [arXiv:1206.1760].

[264] **ATLAS** Collaboration, G. Aad et al., *Further search for supersymmetry at $\sqrt{s}$ = 7 TeV in final states with jets, missing transverse momentum and isolated leptons with the ATLAS detector*, *Phys.Rev.* **D86** (2012) 092002, [arXiv:1208.4688].

[265] **Fittino** Collaboration, X. Prudent, *Constrained Supersymmetry after two years of LHC data: global fits with Fittino*, arXiv:1301.3633.

[266] P. H. Chankowski, J. R. Ellis, and S. Pokorski, *The Fine tuning price of LEP*, *Phys.Lett.* **B423** (1998) 327–336, [hep-ph/9712234].

[267] P. H. Chankowski, J. R. Ellis, M. Olechowski, and S. Pokorski, *Haggling over the fine tuning price of LEP*, *Nucl.Phys.* **B544** (1999) 39–63, [hep-ph/9808275].

[268] G. L. Kane and S. King, *Naturalness implications of LEP results*, *Phys.Lett.* **B451** (1999) 113–122, [hep-ph/9810374].

[269] I. Gogoladze, B. He, and Q. Shafi, *Inverse Seesaw in NMSSM and 126 GeV Higgs Boson*, *Phys.Lett.* **B718** (2013) 1008–1013, [arXiv:1209.5984].

[270] A. Delgado, G. Nardini, and M. Quiros, *A Light Supersymmetric Higgs Sector Hidden by a Standard Model-like Higgs*, arXiv:1303.0800.

[271] J. E. Kim and H. P. Nilles, *The μ-Problem and the Strong CP Problem*, *Phys.Lett.* **B138** (1984) 150.

[272] G. Giudice and A. Masiero, *A Natural Solution to the μ-Problem in Supergravity Theories*, *Phys.Lett.* **B206** (1988) 480–484.

[273] O. Lebedev, *CP violating invariants in supersymmetry*, *Phys.Rev.* **D67** (2003) 015013, [hep-ph/0209023].

[274] H. K. Dreiner, J. S. Kim, O. Lebedev, and M. Thormeier, *Supersymmetric Jarlskog invariants: The Neutrino sector*, *Phys.Rev.* **D76** (2007) 015006, [hep-ph/0703074].

[275] F. Botella, M. Nebot, and O. Vives, *Invariant approach to flavor-dependent CP-violating phases in the MSSM*, *JHEP* **0601** (2006) 106, [hep-ph/0407349].

[276] C. Froggatt and H. B. Nielsen, *Hierarchy of Quark Masses, Cabibbo Angles and CP Violation*, *Nucl.Phys.* **B147** (1979) 277.

[277] K. Babu, *TASI Lectures on Flavor Physics*, arXiv:0910.2948.

[278] M. Leurer, Y. Nir, and N. Seiberg, *Mass matrix models*, *Nucl.Phys.* **B398** (1993) 319–342, [hep-ph/9212278].

[279] M. Leurer, Y. Nir, and N. Seiberg, *Mass matrix models: The Sequel*, *Nucl.Phys.* **B420** (1994) 468–504, [hep-ph/9310320].

[280] G. Bhattacharyya, I. de Medeiros Varzielas, and P. Leser, *A common origin of fermion mixing and geometrical CP violation, and its test through Higgs physics at the LHC*, *Phys.Rev.Lett.* **109** (2012) 241603, [arXiv:1210.0545].

[281] M. Holthausen, M. Lindner, and M. A. Schmidt, *CP and Discrete Flavour Symmetries*, *JHEP* **1304** (2013) 122, [arXiv:1211.6953].

[282] B. Grinstein, M. Redi, and G. Villadoro, *Low Scale Flavor Gauge Symmetries*, *JHEP* **1011** (2010) 067, [arXiv:1009.2049].

[283] T. Feldmann, *See-Saw Masses for Quarks and Leptons in SU(5)*, *JHEP* **1104** (2011) 043, [arXiv:1010.2116].

[284] A. J. Buras, M. V. Carlucci, L. Merlo, and E. Stamou, *Phenomenology of a Gauged $SU(3)^3$ Flavour Model*, *JHEP* **1203** (2012) 088, [arXiv:1112.4477].

[285] D. Guadagnoli, R. N. Mohapatra, and I. Sung, *Gauged Flavor Group with Left-Right Symmetry*, *JHEP* **1104** (2011) 093, [arXiv:1103.4170].

[286] R. T. D'Agnolo and D. M. Straub, *Gauged flavour symmetry for the light generations*, *JHEP* **1205** (2012) 034, [arXiv:1202.4759].

[287] G. Krnjaic and D. Stolarski, *Gauging the Way to MFV*, *JHEP* **JHEP04** (2013) 064, [arXiv:1212.4860].

[288] R. S. Chivukula and H. Georgi, *Composite Technicolor Standard Model*, *Phys.Lett.* **B188** (1987) 99.

[289] A. Buras, P. Gambino, M. Gorbahn, S. Jager, and L. Silvestrini, *Universal unitarity triangle and physics beyond the standard model*, *Phys.Lett.* **B500** (2001) 161–167, [hep-ph/0007085].

[290] G. D'Ambrosio, G. Giudice, G. Isidori, and A. Strumia, *Minimal flavor violation: An Effective field theory approach*, *Nucl.Phys.* **B645** (2002) 155–187, [hep-ph/0207036].

[291] V. Cirigliano, B. Grinstein, G. Isidori, and M. B. Wise, *Minimal flavor violation in the lepton sector*, *Nucl.Phys.* **B728** (2005) 121–134, [hep-ph/0507001].

[292] T. Feldmann and T. Mannel, *Minimal Flavour Violation and Beyond*, *JHEP* **0702** (2007) 067, [hep-ph/0611095].

[293] A. L. Kagan, G. Perez, T. Volansky, and J. Zupan, *General Minimal Flavor Violation*, *Phys.Rev.* **D80** (2009) 076002, [arXiv:0903.1794].

[294] R. Zwicky and T. Fischbacher, *On discrete Minimal Flavour Violation*, *Phys.Rev.* **D80** (2009) 076009, [arXiv:0908.4182].

[295] B. Batell, J. Pradler, and M. Spannowsky, *Dark Matter from Minimal Flavor Violation*, *JHEP* **1108** (2011) 038, [arXiv:1105.1781].

[296] L. Lopez-Honorez and L. Merlo, *Dark matter within the minimal flavour violation ansatz*, *Phys.Lett.* **B722** (2013) 135–143, [arXiv:1303.1087].

[297] E. Nikolidakis and C. Smith, *Minimal Flavor Violation, Seesaw, and R-parity*, *Phys.Rev.* **D77** (2008) 015021, [arXiv:0710.3129].

[298] C. Csaki, Y. Grossman, and B. Heidenreich, *MFV SUSY: A Natural Theory for R-Parity Violation*, *Phys.Rev.* **D85** (2012) 095009, [arXiv:1111.1239].

[299] B. Allanach, G. Hiller, D. Jones, and P. Slavich, *Flavour Violation in Anomaly Mediated Supersymmetry Breaking*, *JHEP* **0904** (2009) 088, [arXiv:0902.4880].

[300] G. Hiller, Y. Hochberg, and Y. Nir, *Flavor Changing Processes in Supersymmetric Models with Hybrid Gauge- and Gravity-Mediation*, *JHEP* **0903** (2009) 115, [arXiv:0812.0511].

[301] G. Hiller, Y. Hochberg, and Y. Nir, *Flavor in Supersymmetry: Anarchy versus Structure*, *JHEP* **1003** (2010) 079, [arXiv:1001.1513].

[302] D. Shemesh, *Common eigenvectors of two matrices.*, *Linear Algebra Appl.* **62** (1984) 11–18.

[303] H. Aslaksen and A. B. Sletsjøe, *Generators of matrix algebras in dimension 2 and 3.*, *Linear Algebra Appl.* **430** (2009), no. 1 1–6.

[304] E. Nikolidakis, *Renormalization Group Equations in the MSSM with Minimal Flavour Violation.* PhD thesis, University of Bern, 2008.

[305] J. Ellis, R. N. Hodgkinson, J. S. Lee, and A. Pilaftsis, *Flavour Geometry and Effective Yukawa Couplings in the MSSM*, *JHEP* **1002** (2010) 016, [arXiv:0911.3611].

[306] G. Colangelo, E. Nikolidakis, and C. Smith, *Supersymmetric models with minimal flavour violation and their running*, *Eur.Phys.J.* **C59** (2009) 75–98, [arXiv:0807.0801].

[307] L. Mercolli and C. Smith, *EDM constraints on flavored CP-violating phases*, *Nucl.Phys.* **B817** (2009) 1–24, [arXiv:0902.1949].

[308] A. Behring, C. Gross, G. Hiller, and S. Schacht, *Squark Flavor Implications from $\bar{B} \to \bar{K}^{(*)} l^+ l^-$*, *JHEP* **1208** (2012) 152, [arXiv:1205.1500].

[309] S. Schacht, *Squark Flavor Implications from $\bar{B} \to \bar{K}^{(*)} l^+ l^-$*, in *Proceedings of the 2nd Workshop on Flavor Symmetries and Consequences in Accelerators and Cosmology (FLASY12)* (I. M. Varzielas, C. Hambrock, G. Hiller, M. Jung, P. Leser, et al., eds.), 2012. arXiv:1210.6239.

[310] M. Beneke, G. Buchalla, M. Neubert, and C. T. Sachrajda, *QCD factorization for exclusive, nonleptonic B meson decays: General arguments and the case of heavy light final states*, *Nucl.Phys.* **B591** (2000) 313–418, [hep-ph/0006124].

[311] M. Beneke, G. Buchalla, M. Neubert, and C. T. Sachrajda, *QCD factorization in $B \to \pi K, \pi\pi$ decays and extraction of Wolfenstein parameters*, *Nucl.Phys.* **B606** (2001) 245–321, [hep-ph/0104110].

[312] M. Beneke and M. Neubert, *QCD factorization for $B \to PP$ and $B \to PV$ decays*, *Nucl.Phys.* **B675** (2003) 333–415, [hep-ph/0308039].

[313] M. Beneke, T. Feldmann, and D. Seidel, *Systematic approach to exclusive $B \to V l^+ l^-, V\gamma$ decays*, *Nucl.Phys.* **B612** (2001) 25–58, [hep-ph/0106067].

[314] M. Beneke, T. Feldmann, and D. Seidel, *Exclusive radiative and electroweak $b \to d$ and $b \to s$ penguin decays at NLO*, *Eur.Phys.J.* **C41** (2005) 173–188, [hep-ph/0412400].

[315] B. Grinstein and D. Pirjol, *Exclusive rare $B \to K^* l^+ l^-$ decays at low recoil: Controlling the long-distance effects*, *Phys.Rev.* **D70** (2004) 114005, [hep-ph/0404250].

[316] M. Beylich, G. Buchalla, and T. Feldmann, *Theory of $B \to K^{(*)} l^+ l^-$ decays at high q^2: OPE and quark-hadron duality*, *Eur.Phys.J.* **C71** (2011) 1635, [arXiv:1101.5118].

[317] F. Kruger and J. Matias, *Probing new physics via the transverse amplitudes of $B^0 \to K^{*0}(\to K^-\pi^+) l^+ l^-$ at large recoil*, *Phys.Rev.* **D71** (2005) 094009, [hep-ph/0502060].

[318] C. Bobeth, G. Hiller, and G. Piranishvili, *CP Asymmetries in $\bar{B} \to \bar{K}^*(\to \bar{K}\pi)\bar{\ell}\ell$ and Untagged $\bar{B}_s$, $B_s \to \phi(\to K^+K^-)\bar{\ell}\ell$ Decays at NLO*, *JHEP* **0807** (2008) 106, [arXiv:0805.2525].

[319] W. Altmannshofer, P. Ball, A. Bharucha, A. J. Buras, D. M. Straub, et al., *Symmetries and Asymmetries of $B \to K^* \mu^+ \mu^-$ Decays in the Standard Model and Beyond*, *JHEP* **0901** (2009) 019, [arXiv:0811.1214].

[320] F. Kruger, L. M. Sehgal, N. Sinha, and R. Sinha, *Angular distribution and CP asymmetries in the decays $\bar{B} \to K^-\pi^+ e^- e^+$ and $\bar{B} \to \pi^-\pi^+ e^- e^+$*, *Phys.Rev.* **D61** (2000) 114028, [hep-ph/9907386].

[321] C. Bobeth, G. Hiller, and D. van Dyk, *General Analysis of $\bar{B} \to \bar{K}^{(*)} \ell^+ \ell^-$ Decays at Low Recoil*, *Phys.Rev.* **D87** (2013) 034016, [arXiv:1212.2321].

[322] C. Bobeth, G. Hiller, and D. van Dyk, *More Benefits of Semileptonic Rare B Decays at Low Recoil: CP Violation*, *JHEP* **1107** (2011) 067, [arXiv:1105.0376].

[323] U. Egede, T. Hurth, J. Matias, M. Ramon, and W. Reece, *New observables in the decay mode $\bar{B}_d \to \bar{K}^{*0} l^+ l^-$*, *JHEP* **0811** (2008) 032, [arXiv:0807.2589].

[324] U. Egede, T. Hurth, J. Matias, M. Ramon, and W. Reece, *New physics reach of the decay mode $\bar{B} \to \bar{K}^{*0} \ell^+ \ell^-$*, *JHEP* **1010** (2010) 056, [arXiv:1005.0571].

[325] D. Becirevic and E. Schneider, *On transverse asymmetries in $B \to K^* l^+ l^-$*, *Nucl.Phys.* **B854** (2012) 321–339, [arXiv:1106.3283].

[326] J. Matias, F. Mescia, M. Ramon, and J. Virto, *Complete Anatomy of $\bar{B}_d \to \bar{K}^{*0}(\to K\pi) l^+ l^-$ and its angular distribution*, *JHEP* **1204** (2012) 104, [arXiv:1202.4266].

[327] S. Descotes-Genon, J. Matias, M. Ramon, and J. Virto, *Implications from clean observables for the binned analysis of $B \to K^* \mu^+ \mu^-$ at large recoil*, *JHEP* **1301** (2013) 048, [arXiv:1207.2753].

[328] S. Descotes-Genon, T. Hurth, J. Matias, and J. Virto, *Optimizing the basis of $B \to K^* ll$ observables in the full kinematic range*, arXiv:1303.5794.

[329] S. Jager and J. M. Camalich, *On $B \to V\, l\, l$ at small dilepton invariant mass, power corrections, and new physics*, arXiv:1212.2263.

[330] LHCb Collaboration, *Differential branching fraction and angular analysis of the $B^0 \to K^{*0} \mu^+ \mu^-$ decay*, Jun, 2012. LHCb-CONF-2012-008.

[331] **LHCb** Collaboration, R. Aaij et al., *Differential branching fraction and angular analysis of the decay $B^0 \to K^{*0} \mu^+ \mu^-$*, arXiv:1304.6325.

[332] **LHCb** Collaboration, R. Aaij et al., *Measurement of the CP asymmetry in $B^0 \to K^{*0} \mu^+ \mu^-$ decays*, *Phys. Rev. Lett. 110,* **031801** (2013) [arXiv:1210.4492].

[333] A. Ali, P. Ball, L. Handoko, and G. Hiller, *A Comparative study of the decays $B \to (K, K^*) \ell^+ \ell^-$ in standard model and supersymmetric theories*, *Phys.Rev.* **D61** (2000) 074024, [hep-ph/9910221].

[334] M. Beneke and T. Feldmann, *Symmetry breaking corrections to heavy to light B meson form-factors at large recoil*, *Nucl.Phys.* **B592** (2001) 3–34, [hep-ph/0008255].

[335] G. Burdman, *Short distance coefficients and the vanishing of the lepton asymmetry in $B \to V \ell^+ \ell^-$*, *Phys.Rev.* **D57** (1998) 4254–4257, [hep-ph/9710550].

[336] A. Ali, G. Kramer, and G.-h. Zhu, *$B \to K^* l^+ l^-$ decay in soft-collinear effective theory*, *Eur.Phys.J.* **C47** (2006) 625–641, [hep-ph/0601034].

[337] LHCb Collaboration, *Angular analysis of $B^0 \to K^{*0} \mu^+ \mu^-$*, Aug, 2011. LHCb-CONF-2011-038.

[338] **LHCb** Collaboration, R. Aaij et al., *Differential branching fraction and angular analysis of the decay $B^0 \to K^{*0} \mu^+ \mu^-$*, *Phys.Rev.Lett.* **108** (2012) 181806, [arXiv:1112.3515].

[339] A. K. Alok, A. Dighe, D. Ghosh, D. London, J. Matias, et al., *New-physics contributions to the forward-backward asymmetry in $B \to K^* \mu^+ \mu^-$*, *JHEP* **1002** (2010) 053, [arXiv:0912.1382].

[340] C. Bobeth, G. Hiller, and G. Piranishvili, *Angular distributions of $\bar{B} \to K \bar{l} l$ decays*, *JHEP* **0712** (2007) 040, [arXiv:0709.4174].

[341] **LHCb** Collaboration, R. Aaij et al., *Differential branching fraction and angular analysis of the $B^+ \to K^+ \mu^+ \mu^-$ decay*, *JHEP* **1302** (2013) 105, [arXiv:1209.4284].

[342] **CDF** Collaboration, T. Aaltonen et al., *Measurements of the Angular Distributions in the Decays $B \to K^{(*)} \mu^+ \mu^-$ at CDF*, *Phys.Rev.Lett.* **108** (2012) 081807, [arXiv:1108.0695].

[343] M. S. Carena, D. Garcia, U. Nierste, and C. E. Wagner, *$b \to s\gamma$ and supersymmetry with large* $\tan\beta$, *Phys.Lett.* **B499** (2001) 141–146, [hep-ph/0010003].

[344] **CDF and D0** Collaboration, T. T. E. W. Group, *Combination of CDF and D0 Results on the Mass of the Top Quark Using Up to 5.6 fb^{-1} of Data*, arXiv:1007.3178.

[345] **Particle Data Group** Collaboration, K. Nakamura et al., *Review of particle physics*, *J.Phys.G* **G37** (2010) 075021.

[346] EOS collaboration, a code for flavor observables. http://project.het.physik.tu-dortmund.de/eos/.

[347] A. J. Buras, A. Romanino, and L. Silvestrini, *$K \to \pi \nu \bar{\nu}$: A Model independent analysis and supersymmetry*, *Nucl.Phys.* **B520** (1998) 3–30, [hep-ph/9712398].

[348] G. Colangelo and G. Isidori, *Supersymmetric contributions to rare kaon decays: Beyond the single mass insertion approximation*, *JHEP* **9809** (1998) 009, [hep-ph/9808487].

[349] E. Lunghi, A. Masiero, I. Scimemi, and L. Silvestrini, $B \to X_s l^+ l^-$ *decays in supersymmetry*, *Nucl.Phys.* **B568** (2000) 120–144, [hep-ph/9906286].

[350] P. Ball, S. Khalil, and E. Kou, B_s^0–$\bar{B}_s^0$ *mixing and the* $B_s \to J/\psi\phi$ *asymmetry in supersymmetric models*, *Phys.Rev.* **D69** (2004) 115011, [hep-ph/0311361].

[351] G. Buchalla, G. Hiller, and G. Isidori, *Phenomenology of nonstandard Z couplings in exclusive semileptonic* $b \to s$ *transitions*, *Phys.Rev.* **D63** (2000) 014015, [hep-ph/0006136].

[352] G. Hiller and Y. Nir, *Measuring Flavor Mixing with Minimal Flavor Violation at the LHC*, *JHEP* **0803** (2008) 046, [arXiv:0802.0916].

[353] G. Hiller, *The Pheno-analysis of* $B \to K^{(*)}\mu^+\mu^-$ *decays in 2011 plus*, arXiv:1106.1547.

[354] *Search for direct production of the top squark in the all-hadronic* $t\bar{t} + E_T^{\text{miss}}$ *final state in 21* fb^{-1} *of p-p collisions at* $\sqrt{s} = 8$ *TeV with the ATLAS detector*, Tech. Rep. ATLAS-CONF-2013-024, CERN, Geneva, Mar, 2013.

[355] *Search for electroweak production of supersymmetric particles in final states with at least two hadronically decaying taus and missing transverse momentum with the ATLAS detector in proton-proton collisions at* $\sqrt{s} = 8$ *TeV*, Tech. Rep. ATLAS-CONF-2013-028, CERN, Geneva, Mar, 2013.

[356] *Search for direct EWK production of SUSY particles in multilepton modes with 8 TeV data*, Tech. Rep. CMS-PAS-SUS-12-022, CERN, Geneva, 2012.

[357] *Search for direct top squark pair production in events with a single isolated lepton, jets and missing transverse energy at* $\sqrt{s} = 8$ *TeV*, Tech. Rep. CMS-PAS-SUS-12-023, CERN, Geneva, 2012.

[358] **D0** Collaboration, V. Abazov et al., *Search for scalar top quarks in the acoplanar charm jets and missing transverse energy final state in* $p\bar{p}$ *collisions at* $\sqrt{s} = 1.96$ *TeV*, *Phys.Lett.* **B665** (2008) 1–8, [arXiv:0803.2263].

[359] LEP2 SUSY Working Group, ALEPH Collaboration, DELPHI Collaboration, L3 Collaboration, OPAL Collaboration, "Combined LEP stop and sbottom Results 183-208 GeV." LEPSUSYWG/04-02.1, http://lepsusy.web.cern.ch/lepsusy/www/squarks_summer04/stop_combi_208_final.html.

[360] B. Allanach, M. Battaglia, G. Blair, M. S. Carena, A. De Roeck, et al., *The Snowmass points and slopes: Benchmarks for SUSY searches*, *Eur.Phys.J.* **C25** (2002) 113–123, [hep-ph/0202233].

[361] F. Mahmoudi, S. Neshatpour, and J. Orloff, *Supersymmetric constraints from* $B_s \to \mu^+\mu^-$ *and* $B \to K^*\mu^+\mu^-$ *observables*, *JHEP* **1208** (2012) 092, [arXiv:1205.1845].

[362] Y. Nir and N. Seiberg, *Should squarks be degenerate?*, *Phys.Lett.* **B309** (1993) 337–343, [hep-ph/9304307].

[363] A. Crivellin and U. Nierste, *Supersymmetric renormalisation of the CKM matrix and new constraints on the squark mass matrices*, *Phys.Rev.* **D79** (2009) 035018, [arXiv:0810.1613].

[364] A. Crivellin, L. Hofer, U. Nierste, and D. Scherer, *Phenomenological consequences of radiative flavor violation in the MSSM*, *Phys.Rev.* **D84** (2011) 035030, [arXiv:1105.2818].

[365] S. Weinberg, *Electromagnetic and weak masses*, *Phys.Rev.Lett.* **29** (1972) 388–392.

[366] L. E. Ibanez, *Radiative Fermion Masses in Grand Unified Theories*, *Nucl.Phys.* **B193** (1981) 317.

[367] A. L. Kagan and C. H. Albright, *Quark and Lepton Masses in Superstring Type Models with Mirror Families*, *Phys.Rev.* **D38** (1988) 917.

[368] A. L. Kagan, *Radiative Quark Mass and Mixing Hierarchies from Supersymmetric Models with a Fourth Mirror Family*, *Phys.Rev.* **D40** (1989) 173.

[369] A. Lahanas and D. Wyler, *Radiative Fermion Masses and Supersymmetry*, *Phys.Lett.* **B122** (1983) 258.

[370] W. Buchmuller and D. Wyler, *CP Violation and R Invariance in Supersymmetric Models of Strong and Electroweak Interactions*, *Phys.Lett.* **B121** (1983) 321.

[371] D. V. Nanopoulos and M. Srednicki, *Fermion Masses from Supergravity*, *Phys.Lett.* **B124** (1983) 37.

[372] A. Masiero, D. V. Nanopoulos, and K. Tamvakis, *Radiative Fermion Masses in Supersymmetric Theories*, *Phys.Lett.* **B126** (1983) 337.

[373] T. Banks, *Supersymmetry and the Quark Mass Matrix*, *Nucl.Phys.* **B303** (1988) 172.

[374] F. Borzumati, G. R. Farrar, N. Polonsky, and S. D. Thomas, *Soft Yukawa couplings in supersymmetric theories*, *Nucl.Phys.* **B555** (1999) 53–115, [hep-ph/9902443].

[375] J. Ferrandis and N. Haba, *Supersymmetry breaking as the origin of flavor*, *Phys.Rev.* **D70** (2004) 055003, [hep-ph/0404077].

[376] A. Buras, G. Colangelo, G. Isidori, A. Romanino, and L. Silvestrini, *Connections between ε'/ε and rare kaon decays in supersymmetry*, *Nucl.Phys.* **B566** (2000) 3–32, [hep-ph/9908371].

[377] M. Ciuchini, V. Lubicz, L. Conti, A. Vladikas, A. Donini, et al., *ΔM_K and ε_K in SUSY at the next-to-leading order*, *JHEP* **9810** (1998) 008, [hep-ph/9808328].

[378] A. J. Buras, S. Jager, and J. Urban, *Master formulae for $\Delta F = 2$ NLO QCD factors in the standard model and beyond*, *Nucl.Phys.* **B605** (2001) 600–624, [hep-ph/0102316].

[379] G. Colangelo, S. Durr, A. Juttner, L. Lellouch, H. Leutwyler, et al., *Review of lattice results concerning low energy particle physics*, *Eur.Phys.J.* **C71** (2011) 1695, [arXiv:1011.4408].

[380] A. J. Buras and D. Guadagnoli, *Correlations among new CP violating effects in $\Delta F = 2$ observables*, *Phys.Rev.* **D78** (2008) 033005, [arXiv:0805.3887].

[381] A. Crivellin and M. Davidkov, *Do squarks have to be degenerate? Constraining the mass splitting with Kaon and D mixing*, *Phys.Rev.* **D81** (2010) 095004, [arXiv:1002.2653].

[382] **HPQCD** Collaboration, E. Gamiz, C. T. Davies, G. P. Lepage, J. Shigemitsu, and M. Wingate, *Neutral B Meson Mixing in Unquenched Lattice QCD*, *Phys.Rev.* **D80** (2009) 014503, [arXiv:0902.1815].

[383] **Fermilab Lattice and MILC** Collaboration, J. Simone et al., *The decay constants f_{D_s}, f_{D^+}, f_{B_s} and f_B from lattice QCD*, *PoS* **LATTICE2010** (2010) 317.

[384] A. J. Buras, R. Fleischer, J. Girrbach, and R. Knegjens, *Probing New Physics with the $B_s \to \mu^+\mu^-$ Time-Dependent Rate*, arXiv:1303.3820.

[385] G. Raven on behalf of the LHCb Collaboration, *Measurement of the CP violation phase ϕ_s in the B_s system at LHCb*, arXiv:1212.4140.

[386] K. De Bruyn, R. Fleischer, R. Knegjens, P. Koppenburg, M. Merk, et al., *Branching Ratio Measurements of B_s Decays*, *Phys.Rev.* **D86** (2012) 014027, [arXiv:1204.1735].

[387] K. De Bruyn, R. Fleischer, R. Knegjens, P. Koppenburg, M. Merk, et al., *Probing New Physics via the $B_s^0 \to \mu^+\mu^-$ Effective Lifetime*, *Phys.Rev.Lett.* **109** (2012) 041801, [arXiv:1204.1737].

[388] D. Guadagnoli and G. Isidori, *$\mathcal{B}(B_s \to \mu^+\mu^-)$ as an electroweak precision test*, arXiv:1302.3909.

[389] J. Cao, G. Eilam, M. Frank, K. Hikasa, G. Liu, et al., *SUSY-induced FCNC top-quark processes at the large hadron collider*, *Phys.Rev.* **D75** (2007) 075021, [hep-ph/0702264].

[390] J. Aguilar-Saavedra and B. Nobre, *Rare top decays $t \to c$ gamma, $t \to cg$ and CKM unitarity*, *Phys.Lett.* **B553** (2003) 251–260, [hep-ph/0210360].

[391] J. Aguilar-Saavedra, *Top flavor-changing neutral interactions: Theoretical expectations and experimental detection*, *Acta Phys.Polon.* **B35** (2004) 2695–2710, [hep-ph/0409342].

[392] G. de Divitiis, R. Petronzio, and L. Silvestrini, *Flavor changing top decays in supersymmetric extensions of the standard model*, *Nucl.Phys.* **B504** (1997) 45–60, [hep-ph/9704244].

[393] **ATLAS** Collaboration, J. Carvalho et al., *Study of ATLAS sensitivity to FCNC top decays*, *Eur.Phys.J.* **C52** (2007) 999–1019, [arXiv:0712.1127].

[394] F. M. A. Veloso, *Study of ATLAS sensitivity to FCNC top quark decays*, 2008. CERN-THESIS-2008-106.

[395] L. Benucci and A. Kyriakis, *CMS sensitivity to top Flavour Changing Neutral Currents*, *Nuclear Physics B Proceedings Supplements* **177** (Mar., 2008) 258–260.

[396] **ATLAS** Collaboration, G. Aad et al., *A search for flavour changing neutral currents in top-quark decays in pp collision data collected with the ATLAS detector at $\sqrt{s} = 7$ TeV*, *JHEP* **1209** (2012) 139, [arXiv:1206.0257].

[397] **CDF** Collaboration, F. Abe et al., *Search for flavor-changing neutral current decays of the top quark in $p\bar{p}$ collisions at $\sqrt{s} = 1.8$ TeV*, *Phys.Rev.Lett.* **80** (1998) 2525–2530.

[398] **ATLAS** Collaboration, G. Aad et al., *Search for FCNC single top-quark production at $\sqrt{s} = 7$ TeV with the ATLAS detector*, *Phys.Lett.* **B712** (2012) 351–369, [arXiv:1203.0529].

[399] **CMS** Collaboration, S. Chatrchyan et al., *Search for flavor changing neutral currents in top quark decays in pp collisions at 7 TeV*, *Phys.Lett.* **B718** (2013) 1252–1272, [arXiv:1208.0957].

[400] C. Hambrock, G. Hiller, S. Schacht and R. Zwicky, *$B \to K^*$ Form Factors from Flavor Data to QCD and Back*. DO-TH 13/13, in preparation.

[401] C. Hambrock and G. Hiller, *Extracting $B \to K^*$ Form Factors from Data*, *Phys.Rev.Lett.* **109** (2012) 091802, [arXiv:1204.4444].

[402] B. Grinstein and D. Pirjol, *Symmetry breaking corrections to heavy meson form-factor relations*, *Phys.Lett.* **B533** (2002) 8–16, [hep-ph/0201298].

[403] M. C. Arnesen, B. Grinstein, I. Z. Rothstein, and I. W. Stewart, *A Precision model independent determination of $|V_{ub}|$ from $B \to \pi l\nu$*, *Phys.Rev.Lett.* **95** (2005) 071802, [hep-ph/0504209].

[404] C. G. Boyd, B. Grinstein, and R. F. Lebed, *Constraints on form-factors for exclusive semileptonic heavy to light meson decays*, *Phys.Rev.Lett.* **74** (1995) 4603–4606, [hep-ph/9412324].

[405] C. G. Boyd and M. J. Savage, *Analyticity, shapes of semileptonic form-factors, and $\bar{B} \to \pi l\bar{\nu}$*, *Phys.Rev.* **D56** (1997) 303–311, [hep-ph/9702300].

[406] I. Caprini, L. Lellouch, and M. Neubert, *Dispersive bounds on the shape of $\bar{B} \to D^{(*)} l\bar{\nu}$ form-factors*, *Nucl.Phys.* **B530** (1998) 153–181, [hep-ph/9712417].

[407] T. Becher and R. J. Hill, *Comment on form-factor shape and extraction of $|V_{ub}|$ from $B \to \pi l\nu$*, *Phys.Lett.* **B633** (2006) 61–69, [hep-ph/0509090].

[408] C. Bourrely, I. Caprini, and L. Lellouch, *Model-independent description of $B \to \pi l \nu$ decays and a determination of $|V_{ub}|$*, *Phys.Rev.* **D79** (2009) 013008, [arXiv:0807.2722].

[409] A. Bharucha, T. Feldmann, and M. Wick, *Theoretical and Phenomenological Constraints on Form Factors for Radiative and Semi-Leptonic B-Meson Decays*, *JHEP* **1009** (2010) 090, [arXiv:1004.3249].

[410] R. J. Hill, *The Modern description of semileptonic meson form factors*, *eConf* **C060409** (2006) 027, [hep-ph/0606023].

[411] M. J. Dugan and B. Grinstein, *QCD basis for factorization in decays of heavy mesons*, *Phys.Lett.* **B255** (1991) 583–588.

[412] U. Aglietti, *Inconsistency of the effective theory for energetic light quarks*, *Phys.Lett.* **B292** (1992) 424–426.

[413] U. Aglietti and G. Corbo, *Factorization in exclusive and semiinclusive decays and effective theories for massless particles*, *Int.J.Mod.Phys.* **A15** (2000) 363–394, [hep-ph/9712242].

[414] U. Aglietti and G. Corbo, *Factorization and effective theories*, *Phys.Lett.* **B431** (1998) 166–172, [hep-ph/9803485].

[415] C. Balzereit, T. Mannel, and W. Kilian, *Evolution of the light cone distribution function for a heavy quark*, *Phys.Rev.* **D58** (1998) 114029, [hep-ph/9805297].

[416] N. Isgur and M. B. Wise, *Weak Decays of Heavy Mesons in the Static Quark Approximation*, *Phys.Lett.* **B232** (1989) 113.

[417] N. Isgur and M. B. Wise, *Weak Transition Form-Factors between Heavy Mesons*, *Phys.Lett.* **B237** (1990) 527.

[418] B. Grinstein, *The Static Quark Effective Theory*, *Nucl.Phys.* **B339** (1990) 253–268.

[419] H. Georgi, *An Effective Field Theory for Heavy Quarks at Low-Energies*, *Phys.Lett.* **B240** (1990) 447–450.

[420] A. F. Falk, B. Grinstein, and M. E. Luke, *Leading mass corrections to the heavy quark effective theory*, *Nucl.Phys.* **B357** (1991) 185–207.

[421] A. F. Falk, H. Georgi, B. Grinstein, and M. B. Wise, *Heavy Meson Form-Factors from QCD*, *Nucl.Phys.* **B343** (1990) 1–13.

[422] T. Mannel, W. Roberts, and Z. Ryzak, *A Derivation of the heavy quark effective Lagrangian from QCD*, *Nucl.Phys.* **B368** (1992) 204–220.

[423] G. Burdman and G. Hiller, *Semileptonic form-factors from $B \to K^* \gamma$ decays in the large energy limit*, *Phys.Rev.* **D63** (2001) 113008, [hep-ph/0011266].

[424] J. Charles, A. Le Yaouanc, L. Oliver, O. Pene, and J. Raynal, *Heavy to light form-factors in the heavy mass to large energy limit of QCD*, *Phys.Rev.* **D60** (1999) 014001, [hep-ph/9812358].

[425] N. Isgur and M. B. Wise, *Relationship between Form-Factors in Semileptonic $\bar{B}$ and D Decays and Exclusive Rare $\bar{B}$ Meson Decays*, *Phys.Rev.* **D42** (1990) 2388–2391.

[426] P. Ball and R. Zwicky, *$B_{(d,s)} \to \rho, \omega, K^*, \phi$ decay form-factors from light-cone sum rules revisited*, *Phys.Rev.* **D71** (2005) 014029, [hep-ph/0412079].

[427] V. M. Braun, *Exclusive semileptonic and rare radiative B decays from QCD sum rules*, hep-ph/9510404.

[428] P. Colangelo and A. Khodjamirian, *QCD sum rules, a modern perspective*, hep-ph/0010175.

[429] P. Ball, *QCD sum rules on the light cone, factorization and SCET*, hep-ph/0308249.

[430] N. Offen, *B-Zerfallsformfaktoren aus QCD-Summenregeln*. PhD thesis, University of Siegen, 2008.

[431] M. A. Shifman, A. Vainshtein, and V. I. Zakharov, *QCD and Resonance Physics. Sum Rules*, *Nucl.Phys.* **B147** (1979) 385–447.

[432] M. A. Shifman, A. Vainshtein, and V. I. Zakharov, *QCD and Resonance Physics: Applications*, *Nucl.Phys.* **B147** (1979) 448–518.

[433] S. Akar for the BaBar Collaboration at the Lake Louise Winter Institute, Canada, February 23, 2012.

[434] H. Miyake, "CDF results on the search for rare $B_{d,s} \to \mu^+\mu^-$ and $X_s\mu^+\mu^-$ decays". Talk presented at the 36th International Conference for High Energy Physics (ICHEP), July 4-11, 2012, Melbourne, Australia.
http://www-cdf.fnal.gov/physics/new/bottom/120628.blessed-b2smumu_96/.

[435] *Angular Analysis of $B_d \to K^{*0}\mu^+\mu^-$ with the ATLAS Experiment*, Tech. Rep. ATLAS-CONF-2013-038, CERN, Geneva, Apr, 2013.

[436] *Angular analysis and branching ratio measurement of the decay $B^0 \to K^{*0}\mu^+\mu^-$*, Tech. Rep. CMS-PAS-BPH-11-009, CERN, Geneva, 2013.

[437] A. Hocker, H. Lacker, S. Laplace, and F. Le Diberder, *A New approach to a global fit of the CKM matrix*, *Eur.Phys.J.* **C21** (2001) 225–259, [hep-ph/0104062].

[438] Z. Liu, S. Meinel, A. Hart, R. R. Horgan, E. H. Muller, et al., *A Lattice calculation of $B \to K^{(*)}$ form factors*, arXiv:1101.2726.

[439] D. Becirevic, V. Lubicz, and F. Mescia, *An Estimate of the $B \to K^*\gamma$ form factor*, *Nucl.Phys.* **B769** (2007) 31–43, [hep-ph/0611295].

[440] J. Brod, A. L. Kagan, and J. Zupan, *Size of direct CP violation in singly Cabibbo-suppressed D decays*, *Phys.Rev.* **D86** (2012) 014023, [arXiv:1111.5000].

[441] D. Pirtskhalava and P. Uttayarat, *CP Violation and Flavor SU(3) Breaking in D-meson Decays*, *Phys.Lett.* **B712** (2012) 81–86, [arXiv:1112.5451].

[442] H.-Y. Cheng and C.-W. Chiang, *Direct CP violation in two-body hadronic charmed meson decays*, *Phys.Rev.* **D85** (2012) 034036, [arXiv:1201.0785].

[443] B. Bhattacharya, M. Gronau, and J. L. Rosner, *CP asymmetries in singly-Cabibbo-suppressed D decays to two pseudoscalar mesons*, *Phys.Rev.* **D85** (2012) 054014, [arXiv:1201.2351].

[444] T. Feldmann, S. Nandi, and A. Soni, *Repercussions of Flavour Symmetry Breaking on CP Violation in D-Meson Decays*, *JHEP* **1206** (2012) 007, [arXiv:1202.3795].

[445] H.-n. Li, C.-D. Lu, and F.-S. Yu, *Branching ratios and direct CP asymmetries in $D \to PP$ decays*, *Phys.Rev.* **D86** (2012) 036012, [arXiv:1203.3120].

[446] E. Franco, S. Mishima, and L. Silvestrini, *The Standard Model confronts CP violation in $D^0 \to \pi^+\pi^-$ and $D^0 \to K^+K^-$*, *JHEP* **1205** (2012) 140, [arXiv:1203.3131].

[447] J. Brod, Y. Grossman, A. L. Kagan, and J. Zupan, *A Consistent Picture for Large Penguins in $D \to \pi^+\pi^-, K^+K^-$*, *JHEP* **1210** (2012) 161, [arXiv:1203.6659].

[448] **BaBar** Collaboration, B. Aubert et al., *Search for CP violation in the decays $D^0 \to K^-K^+$ and $D^0 \to \pi^-\pi^+$*, *Phys.Rev.Lett.* **100** (2008) 061803, [arXiv:0709.2715].

[449] **Belle** Collaboration, M. Staric et al., *Measurement of CP asymmetry in Cabibbo suppressed D^0 decays*, *Phys.Lett.* **B670** (2008) 190–195, [arXiv:0807.0148].

[450] **CDF** Collaboration, T. Aaltonen et al., *Measurement of CP–violating asymmetries in $D^0 \to \pi^+\pi^-$ and $D^0 \to K^+K^-$ decays at CDF*, *Phys.Rev.* **D85** (2012) 012009, [arXiv:1111.5023].

[451] **CLEO** Collaboration, G. Bonvicini et al., *Search for CP violation in $D^0 \to K^0_S\pi^0$ and $D^0 \to \pi^0\pi^0$ and $D^0 \to K^0_S K^0_S$ decays*, *Phys.Rev.* **D63** (2001) 071101, [hep-ex/0012054].

[452] **CLEO** Collaboration, H. Mendez et al., *Measurements of D Meson Decays to Two Pseudoscalar Mesons*, *Phys.Rev.* **D81** (2010) 052013, [arXiv:0906.3198].

[453] B. R. Ko for the Belle Collaboration, "CP violation and mixing in the charm sector at Belle (+current HFAG averages)." Talk at the 7th International Workshop on the CKM Unitarity Triangle, 28 September - 2 October 2012, Cincinnati, Ohio, USA.

[454] **Belle Collaboration** Collaboration, B. Ko et al., *Search for CP Violation in the Decay $D^+ \to K^0_S K^+$*, *JHEP* **1302** (2013) 098, [arXiv:1212.6112].

[455] **BaBar Collaboration** Collaboration, J. Lees et al., *Search for CP violation in the Decays $D^\pm \to K^0_s K^\pm$, $D^\pm_s \to K^0_s K^\pm$, and $D^\pm_s \to K^0_s\pi^\pm$*, *Phys.Rev.* **D87** (2013) 052012, [arXiv:1212.3003].

[456] **FOCUS** Collaboration, J. Link et al., *Search for CP violation in the decays $D^+ \to K_S\pi^+$ and $D^+ \to K_S K^+$*, *Phys.Rev.Lett.* **88** (2002) 041602, [hep-ex/0109022].

[457] **Belle** Collaboration, B. Ko et al., *Search for CP violation in the decays $D^+_{(s)} \to K^0_S\pi^+$ and $D^+_{(s)} \to K^0_S K^+$*, *Phys.Rev.Lett.* **104** (2010) 181602, [arXiv:1001.3202].

[458] M.-Z. Wang for the Belle Collaboration, "Charm decays at Belle." Talk at the 36th International Conference for High Energy Physics (ICHEP), 4-11 July 2012 Melbourne, Australia.

[459] W. Altmannshofer, R. Primulando, C.-T. Yu, and F. Yu, *New Physics Models of Direct CP Violation in Charm Decays*, *JHEP* **1204** (2012) 049, [arXiv:1202.2866].

[460] T. A. Kaeding and H. T. Williams, *Program for generating tables of SU(3) coupling coefficients*, *Comput.Phys.Commun.* **98** (1996) 398–414, [nucl-th/9511025].

[461] T. A. Kaeding, *Tables of SU(3) isoscalar factors*, nucl-th/9502037.

[462] M. Gronau, O. F. Hernandez, D. London, and J. L. Rosner, *Broken SU(3) symmetry in two-body B decays*, *Phys.Rev.* **D52** (1995) 6356–6373, [hep-ph/9504326].

[463] C. Quigg, *Charmed Meson Decays and the Structure of the Charged Weak Current*, *Z.Phys.* **C4** (1980) 55.

[464] L. Abbott, P. Sikivie, and M. B. Wise, *Comment On Cabibbo Suppressed Nonleptonic D Decays*, *Phys.Rev.* **D21** (1980) 768.

[465] Private communication with D. Pirtskhalava and P. Uttayarat.

[466] Y. Grossman and D. J. Robinson, *SU(3) Sum Rules for Charm Decay*, *JHEP* **1304** (2013) 067, [arXiv:1211.3361].

[467] Y. Grossman, A. L. Kagan, and J. Zupan, *Testing for new physics in singly Cabibbo suppressed D decays*, *Phys.Rev.* **D85** (2012) 114036, [arXiv:1204.3557].

[468] W. Kwong and S. P. Rosen, *Minimal breaking of flavor SU(3) in nonleptonic charm decay*, *Phys.Lett.* **B298** (1993) 413–418.

[469] G. Hiller, M. Jung and S. Schacht, *Tracing QCD Factorization in $D \to P_8 P_8$*. in preparation.

[470] G. F. Giudice, G. Isidori, and P. Paradisi, *Direct CP violation in charm and flavor mixing beyond the SM*, *JHEP* **1204** (2012) 060, [arXiv:1201.6204].

[471] G. Hiller, Y. Hochberg, and Y. Nir, *Supersymmetric ΔA_{CP}*, *Phys.Rev.* **D85** (2012) 116008, [arXiv:1204.1046].

[472] L. Da Rold, C. Delaunay, C. Grojean, and G. Perez, *Up Asymmetries From Exhilarated Composite Flavor Structures*, *JHEP* **1302** (2013) 149, [arXiv:1208.1499].

[473] Y. Hochberg and Y. Nir, *Relating direct CP violation in D decays and the forward-backward asymmetry in $t\bar{t}$ production*, *Phys.Rev.Lett.* **108** (2012) 261601, [arXiv:1112.5268].

[474] G. Isidori and J. F. Kamenik, *Shedding light on CP violation in the charm system via $D \to V\gamma$ decays*, *Phys.Rev.Lett.* **109** (2012) 171801, [arXiv:1205.3164].

[475] F. Buccella, M. Lusignoli, G. Mangano, G. Miele, A. Pugliese, et al., *CP Violating asymmetries in charged D meson decays*, *Phys.Lett.* **B302** (1993) 319–325, [hep-ph/9212253].

[476] D. Atwood and A. Soni, *Searching for the Origin of CP violation in Cabibbo Suppressed D-meson Decays*, arXiv:1211.1026.

[477] D. Asner for the Belle II Collaboration, "Prospects for Charm Mixing and CPV at Belle II." Talk at the 7th International Workshop on the CKM Unitarity Triangle, 28 September - 2 October 2012, Cincinnati, Ohio, USA.

[478] **LHCb** Collaboration, R. Aaij et al., *Search for CP violation in $D^+ \to \phi\pi^+$ and $D_s^+ \to K_S^0\pi^+$ decays*, arXiv:1303.4906.

[479] B. Bhattacharya, M. Gronau, and J. L. Rosner, *Direct CP Violation in D Decays in view of LHCb and CDF Results*, arXiv:1207.0761.

[480] H.-Y. Cheng and C.-W. Chiang, *SU(3) symmetry breaking and CP violation in $D \to PP$ decays*, *Phys.Rev.* **D86** (2012) 014014, [arXiv:1205.0580].

[481] H.-Y. Cheng and C.-W. Chiang, *Two-body hadronic charmed meson decays*, *Phys.Rev.* **D81** (2010) 074021, [arXiv:1001.0987].

[482] K. Chetyrkin, J. H. Kuhn, and M. Steinhauser, *RunDec: A Mathematica package for running and decoupling of the strong coupling and quark masses*, *Comput.Phys.Commun.* **133** (2000) 43–65, [hep-ph/0004189].

[483] A. Khodjamirian, C. Klein, T. Mannel, and N. Offen, *Semileptonic charm decays $D \to \pi l \nu_l$ and $D \to K l \nu_l$ from QCD Light-Cone Sum Rules*, *Phys.Rev.* **D80** (2009) 114005, [arXiv:0907.2842].

[484] **CLEO** Collaboration, D. Besson et al., *Improved measurements of D meson semileptonic decays to pi and K mesons*, *Phys.Rev.* **D80** (2009) 032005, [arXiv:0906.2983].

[485] **LHCb** Collaboration, B. Adeva et al., *Roadmap for selected key measurements of LHCb*, arXiv:0912.4179.

[486] **LHCb** Collaboration, *Framework TDR for the LHCb Upgrade: Technical Design Report*, Tech. Rep. CERN-LHCC-2012-007. LHCb-TDR-12, CERN, Geneva, Apr, 2012.

[487] **LHCb** Collaboration, *Letter of Intent for the LHCb Upgrade*, Tech. Rep. CERN-LHCC-2011-001. LHCC-I-018, CERN, Geneva, Mar, 2011.

[488] T. Aushev, W. Bartel, A. Bondar, J. Brodzicka, T. Browder, et al., *Physics at Super B Factory*, arXiv:1002.5012.

[489] T. Abe, I. Adachi, K. Adamczyk, S. Ahn, H. Aihara, K. Akai, M. Aloi, L. Andricek, K. Aoki, Y. Arai, and et al., *Belle II Technical Design Report*, arXiv:1011.0352.

[490] S. Yashchenko for the Belle II Collaboration, "e^+e^- Future B Factory (SuperKEKB/Belle II)." Talk at the 14th International Conference on B-Physics at Hadron Machines (BEAUTY), 8-12 April 2013 Bologna, Italy.

[491] M. Martinelli for the LHCb Collaboration, "The LHCb Upgrade." Talk at the 14th International Conference on B-Physics at Hadron Machines (BEAUTY), 8-12 April 2013 Bologna, Italy.

[492] **LHCb** Collaboration, R. Aaij et al., *Implications of LHCb measurements and future prospects*, *Eur.Phys.J.* **C73** (2013) 2373, [arXiv:1208.3355].

[493] K. Nishimura for the Belle II Collaboration, "New Physics Prospects in Mixing and CP Violation at Belle II." Talk at the 5th International Workshop on Charm Physics (CHARM), 14-17 May 2012, Honolulu, Hawaii, USA, and proceedings arXiv:1212.4112.

[494] E. Lunghi and J. Matias, *Huge right-handed current effects in $B \to K^*(K\pi)l^+l^-$ in supersymmetry*, *JHEP* **0704** (2007) 058, [hep-ph/0612166].

[495] **CDF Collaboration** Collaboration, T. Aaltonen et al., *Measurement of the Forward-Backward Asymmetry in the $B \to K^{(*)}\mu^+\mu^-$ Decay and First Observation of the $B_s^0 \to \phi\mu^+\mu^-$ Decay*, *Phys.Rev.Lett.* **106** (2011) 161801, [arXiv:1101.1028].

[496] **CDF** Collaboration, *Branching ratio measurements of exclusive $b \to s\mu^+\mu^-$ decays and angular analysis in $B^0 \to K^{(*)}\mu^+\mu^-$ decays*, Tech. Rep. CDF public note 10894, 2012.

[497] **LHCb collaboration** Collaboration, R. Aaij et al., *Differential branching fraction and angular analysis of the decay $B_s^0 \to \phi\mu^+\mu^-$*, arXiv:1305.2168.

[498] **CDF Collaboration** Collaboration, T. Aaltonen et al., *Observation of the Baryonic Flavor-Changing Neutral Current Decay $\Lambda_b \to \Lambda\mu^+\mu^-$*, *Phys.Rev.Lett.* **107** (2011) 201802, [arXiv:1107.3753].

[499] **LHCb** Collaboration, R. Aaij et al., *Measurement of the $B^0 \to K^{*0}e^+e^-$ branching fraction at low dilepton mass*, arXiv:1304.3035.

[500] **LHCb** Collaboration, R. Aaij et al., *First observation of the decay $B^+ \to \pi^+\mu^+\mu^-$*, *JHEP* **1212** (2012) 125, [arXiv:1210.2645].

[501] M. Jung, *A robust limit for the electric dipole moment of the electron*, arXiv:1301.1681.

[502] A. Ilakovac, A. Pilaftsis, and L. Popov, *Charged Lepton Flavour Violation in Supersymmetric Low-Scale Seesaw Models*, arXiv:1212.5939.

[503] A. Dery, A. Efrati, G. Hiller, Y. Hochberg, and Y. Nir, *Higgs couplings to fermions: 2HDM with MFV*, arXiv:1304.6727.

[504] G. Hiller, M. Jung, and S. Schacht. in preparation.

[505] M. Jung and S. Schacht, *$B \to DD$ Decays in Broken SU(3)$_F$*. in preparation.

[506] M. Jung and S. Schacht, *$B \to J/\psi P$ Decays in Broken SU(3)$_F$*. in preparation.

[507] T. Feldmann, P. Kroll, and B. Stech, *Mixing and decay constants of pseudoscalar mesons*, *Phys.Rev.* **D58** (1998) 114006, [hep-ph/9802409].

[508] T. Feldmann, P. Kroll, and B. Stech, *Mixing and decay constants of pseudoscalar mesons: The Sequel*, *Phys.Lett.* **B449** (1999) 339–346, [hep-ph/9812269].

[509] T. Feldmann and P. Kroll, *Mixing of pseudoscalar mesons*, *Phys.Scripta* **T99** (2002) 13–22, [hep-ph/0201044].

[510] **LHCb** Collaboration, R. Aaij et al., *First observations of $\bar{B}^0_s \to D^+D^-$, $D^+_s D^-$ and $D^0\bar{D}^0$ decays*, arXiv:1302.5854.

[511] D. Zeppenfeld, *SU(3) Relations for B Meson Decays*, *Z.Phys.* **C8** (1981) 77.

[512] M. Jung, *Determining weak phases from $B \to J/\psi P$ decays*, *Phys.Rev.* **D86** (2012) 053008, [arXiv:1206.2050].

[513] S. G. Johnson, *The nlopt nonlinear-optimization package*. http://ab-initio.mit.edu/nlopt.

[514] T. Rowan, "Functional Stability Analysis of Numerical Algorithms." PhD thesis, Department of Computer Sciences, University of Texas at Austin, 1990.

[515] C. Hambrock, M. Jung, and S. Schacht, *Lucy: A universal code for organizing fits*.

[516] Wolfram Research, Inc., *Mathematica Edition: Version 7.0*, 2008. Champaign, Illinois.

[517] A. Conn, N. Gould, and P. Toint, *A globally convergent augmented lagrangian algorithm for optimization with general constraints and simple bounds*, *SIAM Journal on Numerical Analysis* **28** (1991), no. 2 545–572.

[518] E. Birgin and J. Martínez, *Improving ultimate convergence of an augmented lagrangian method*, *Optimization Methods and Software* **23** (2008), no. 2 177–195.

[519] D. Binosi and L. Theussl, *JaxoDraw: A Graphical user interface for drawing Feynman diagrams*, *Comput.Phys.Commun.* **161** (2004) 76–86, [hep-ph/0309015].

[520] D. Binosi, J. Collins, C. Kaufhold, and L. Theussl, *JaxoDraw: A Graphical user interface for drawing Feynman diagrams. Version 2.0 release notes*, *Comput.Phys.Commun.* **180** (2009) 1709–1715, [arXiv:0811.4113].